Structural and Mechanistic Studies of Bioactive Peptides

A thesis submitted for the Degree of Doctor of Philosophy

by

Tara Louise Pukala B. Sc. (Hons.)

from the

Department of Chemistry, The University of Adelaide

THE UNIVERSITY
OF ADELAIDE
AUSTRALIA

SUB CRUCE LUMEN

August 2006

~ CONTENTS ~

~ AMENDMENTS ~

Page 36, line 5: practise <u>should read</u> practice

Page 62, line 22: <u>insert</u> The helical wheels for caerin 2.6 and 2.7 can be compared with those of more potent antibacterial peptides such as citropin 1.1 and maculatin 1.1 (Section 8.3).

Page 64, line 9: animals <u>should read</u> animal's

Page 76, line 16: relative <u>should read</u> relevant

Page 79, line 4: <u>insert</u> For water-soluble peptides the reference is likely to be trimethylsilylpropionic acid (TSP) or dimethyl-2-silapentane-5-sulphonate (DSS).

Page 84, line 18: residues <u>should read</u> resonances

Page 84, line 16: between <u>should read</u> to

Page 96, line 2: <u>insert</u> and applies only for the same effective τ_c

Page 96, line 7: results <u>should read</u> result

Page 99, line 21: <u>insert</u> Futhermore, internal motions often produce degenerate resonances that cannot be stereospecifically assigned from spectral data alone.

Page 110, line 14: synthesis <u>should read</u> synthesise

Page 125, line 18: <u>insert footnote</u> Uniformly ^{15}N labelled caerin 1.8 was not used, since previous attempts at the biochemical expression of this peptide were unsuccessful [482].

Page 126, line 1: disperse <u>should read</u> dispersed

Page 147, line 10: from <u>should read</u> by

Page 151, Chapter 6 heading: *Crinia* <u>should read</u> Crinia

Page 162, Table 6.2 caption: ^{1}H and ^{13}C chemical shifts <u>should read</u> ^{1}H chemical shifts

Page 163, Table 6.3 caption: ^{1}H and ^{13}C chemical shifts <u>should read</u> ^{1}H chemical shifts

Page 164, line 4: with that of random <u>should read</u> with random

Page 166, line 13: five <u>should read</u> three

Page 167, line 9: <u>insert</u> The majority of NOEs for both signiferin 1 and riparin 1.1 originate from well-defined residues, however, a number of medium- and long-range NOEs observed to the N-terminal residues suggest the differences seen in the resultant structures of each peptide are likely to be significant.

Page 167, line 5: <u>insert footnote</u> Despite the free C-terminal carboxyl groups, the pH difference between signiferin 1.1 and riparin 1.1 is not likely to contribute to the apparent structural differences, given the rigid conformational restraints imparted by the disulphide bridge.

Page 177, line 10: J <u>should read</u> ^{3}J

Page 189, Figure 7.8: <u>should show</u>   (a)   (b)

40   20   0   -20   -40ppm   40   20   0   -20   -40ppm
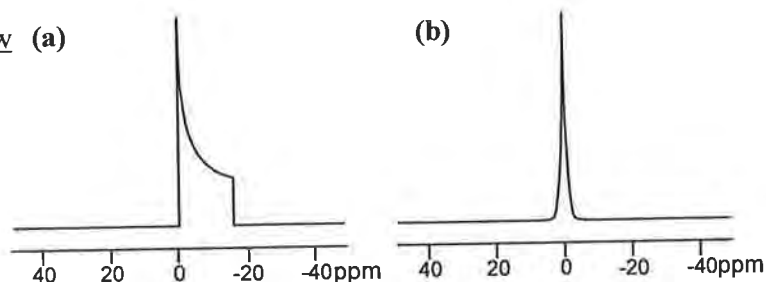
Page 199, line 1: defense <u>should read</u> defence

Page 199, line 4: defense <u>should read</u> defence

Page 218, line 6: in spectrum <u>should read</u> in the spectrum

Page 224, line 12: <u>insert footnote</u> Macroscopic phase transitions in the presence of magainin have also been described [Bechinger, B. (2005) Detergent-like properties of magainin antibiotic peptides: A ^{31}P solid-state NMR spectroscopy study. *Biochim. Biophys. Acta.* 1712:101-108].

Page 225, line 16: <u>insert</u> Furthermore, the ordering observed for d_{54}-DMPC in the presence of citropin 1.1 or maculatin 1.1 could also indicate a lateral separation of d_{54}-DMPC and DMPG, as has been described for in-plane oriented cationic peptides in mixed anionic lipid membranes [Mason, A.J., Martinez, A., Glaubitz, C., Danos, O., Kichler, A. and Bechinger B. (2006) The antibiotic and DNA-transfecting peptide LAH4 selectively associates with, and disorders, anionic lipids in mixed membranes. *FASEB J.* 20:320-2].

Page 247, line 12: is good <u>should read</u> is a good

Page 253, Figure 9.17 caption: bilayers alone (black), and in the presence of cupiennin 1a (blue) <u>should read</u> bilayers alone (blue), and in the presence of cupiennin 1a (red)

Page 254, line 6: <u>insert</u> However, the differences caused by cupiennin 1a are very small, and may not be significant given the errors associated with measurement of the order parameters.

Page 259, line 16: shape <u>should read</u> shapes

Page 265, line 6: were <u>should read</u> was.

Page 272, line 6: Although unstructured <u>should read</u> Although the peptides are unstructured

Page 284, reference 134: Phallagy, P.K. <u>should read</u> Pallaghy, P.K.

Page 319, reference 664: (1986) West Pub. <u>should read</u> (1986) *Microbiology.* West Pub.

Page 323, reference 724: Watts, A. and Norton, R.S. (2003) <u>should read</u> Watts, A., Norton, R.S., and Separovic, F. (2003)

Page 326, Appendix A: Nominal Mass <u>should read</u> Residue Nominal Mass

~ ACKNOWLEDGMENTS ~

~ STATEMENT OF ORIGINALITY ~

This thesis contains no material that has been accepted for the award of any other degree or diploma in any university or other tertiary institution and, to the best of my knowledge and belief, contains no material previously published or written by another person, except where due reference has been made in the text.

I give consent for a copy of this thesis, when deposited in the University Library, to be available for loan and photocopying.

Tara Louise Pukala

August 2nd 2006

~ ABSTRACT ~

Venoms, toxins and host-defence systems constitute rich sources of biologically active molecules, many of which have enormous therapeutic and biotechnological potential. In particular, peptides are often a significant component of these chemical arsenals, and are fundamentally important as biological effector molecules. The research presented in this thesis is centred on the isolation and investigation of peptides from both frogs and spiders, and endeavours to probe the important structural and mechanistic features of these bioactive compounds.

The skin peptide profiles of interspecific hybrids between the green tree frog *Litoria caerulea* and the magnificent tree frog *Litoria splendida* have been investigated in a nine-month survey. Fourteen peptides were characterised primarily using mass spectrometry, of which three had not been identified previously in the skin secretions of either parent. A number of these peptides are antibacterial agents, while others effectively inhibit the formation of nitric oxide by neuronal nitric oxide synthase. Implications for the genetics and expression of amphibian dermal peptides are also discussed.

The majority of frogs of the genus *Litoria* contain at least one peptide in their glandular secretion capable of inhibiting the formation of nitric oxide by the enzyme neuronal nitric oxide synthase. This was proposed to occur by preventing the association of the regulatory cofactor, Ca^{2+}-calmodulin, with its binding site on the enzyme. Non-covalent binding of the amphibian peptides to calmodulin in the presence of Ca^{2+} has been confirmed using electrospray ionisation mass spectrometry, by the observation of complexes in the gas phase with a 1:1:4 calmodulin/peptide/Ca^{2+} stoichiometry. In addition, the structure and binding interactions of caerin 1.8, a potent nitric oxide synthase inhibitor, have been further probed using mass spectrometry and nuclear magnetic resonance spectroscopy techniques.

Recently a number of small, disulfide-containing neuropeptides of the signiferin and riparin families have been characterised from the skin secretion of frogs of the *Crinia* genus. Of these, signiferin 1 and riparin 1.1 are both ten residue peptides with similar primary sequences, however appear to have a significantly different spectrum of bioactivity. Although both act at cholecystokinin-2 receptors, signiferin 1 is smooth muscle active while riparin 1.1 is not, and instead causes proliferation of lymphocytes. The three-dimensional structures of these peptides were determined using nuclear magnetic resonance spectroscopy and restrained molecular dynamics calculations. Both signiferin 1 and riparin 1.1 adopt β-turn type conformations, however differences in these structures may be responsible for the variation in biological activity noted for these peptides.

The dermal secretions of most Australian frogs contain at least one broad-spectrum peptide antibiotic, and often a series of peptides with differing activity to afford greater protection against microbial pathogens. Solid state nuclear magnetic resonance spectroscopy studies were carried out to investigate the interaction of a number of these antibacterial peptides with anionic model membranes, and the results are compared with work previously reported using neutral lipids. It appears the peptides may have a different mode of interaction with the membranes depending upon the charge of the lipid head group.

The cupiennin 1 peptides have been identified in the venom of the neotropical wandering spider, *Cupiennius salei*, and demonstrate potent wide-spectrum antibacterial activity. Primary sequence analysis of these peptides suggests a unique amphipathic structure distinctly different from that of other potentially helical cationic antimicrobial peptides isolated thus far. Using nuclear magnetic resonance spectroscopy and restrained molecular dynamics calculations, cupiennin 1a was found to adopt an α-helical structure with a flexible central hinge region in membrane mimicking solvents. Following this, nuclear magnetic resonance spectroscopy methods were used to further probe the antibacterial and the newly identified neuronal nitric oxide synthase inhibitory activity of this peptide.

~ CHAPTER 1 ~

Naturally Occurring Bioactive Peptides

1.1 Overview

There is a constant struggle throughout nature for each and every species to maximise their survival potential. Since the beginnings of existence, living organisms have continually evolved mechanisms to minimise the hazards of their environment, exploit the resources it offers, and respond to changes that threaten their livelihood. This ongoing drama of intricate measures and countermeasures lends itself to a natural chemical arms race, incorporating an amazing array of remarkable chemistry and biology.

There are endless examples of animals and plants which use a potent chemical arsenal to safeguard themselves against predatory assault. Ranging from the thiols and thioacetates sprayed by the skunk in response to a threat [1], to the catechols produced by poison ivy to deter any disturbing invaders [2], this provides these entities with a significant defensive mechanism against their enemies. Similarly, there are equally as many examples of organisms equipped with a strong offensive chemical front. For instance, few people would be unaware of the potent venoms of many snakes and spiders, which are utilised as part of a prey capture strategy [3,4].

The bioactive nature of these chemicals also makes them interesting to humans who are able to exploit their properties for therapeutic and commercial means. A conventional approach for the development of new pharmaceuticals is the screening of natural products. This can be a result of observing the interesting characteristics of an animal or plant species, or by investigating the use of traditional medicines, and subsequently identifying and purifying the active ingredient in such sources. In this manner an enormous range of novel pharmaceuticals has already been developed.

The science of drugs and their applications has traditionally been based upon structure-activity relationship predictions, derived mainly from the structure of low molecular weight lead compounds. However, with advancing technology it is becoming increasingly apparent that peptides and proteins are at least as important, and possibly much more so, as biological effector molecules [5]. As a result, protein based drug design is amongst the fastest growing sectors within the pharmaceutical industry.

The therapeutic application of peptides and proteins is limited by several problems, such as inherent physical and chemical instability, and the lack of optimal physiochemical properties for adequate transport throughout the body [6]. Thus the challenge remains to formulate these compounds into safe, stable and efficacious drugs. Nevertheless, with progress in biotechnology and research development in this area of study, the clinical applications of peptide mediators should markedly increase.

With such a diverse range of biologically active peptides and proteins apparent in nature, it is necessary to narrow the field of study. This thesis details the isolation and investigation of bioactive peptides from frogs and spiders, in an effort to understand the structure and mechanism of action of such fascinating molecules.

1.2 Peptide Biosynthesis

Peptides consist of a number of amino acids covalently linked by an amide bond between the α-amino and α-carboxyl groups of adjacent residues (Figure 1.1). The distinction between peptides and proteins is subjective, although peptides are generally considered smaller than fifty amino acids in length [5]. The masses and molecular structure of the twenty commonly occurring natural amino acid residues are given in Appendix A.
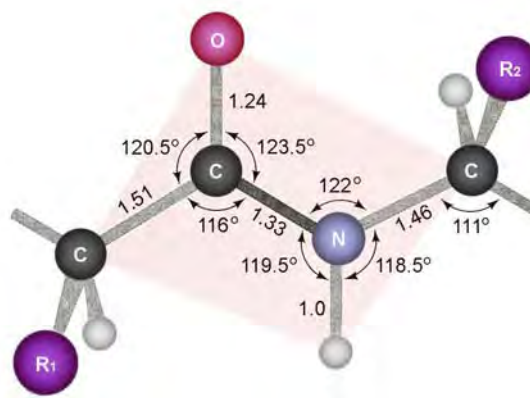
Figure 1.1: Structure of the peptide bond. Bond lengths are given in nanometers.

Peptides and proteins are synthesised in a complex and intricate process involving the transcription of genes encoded in deoxyribonucleic acids (DNA), followed by translation of the resulting messenger ribonucleic acids (mRNA) [7-9]. Biologically active peptides that are destined for release by an endocrine mechanism are initially formed as part of a large precursor protein known as a pre-pro-peptide, which consists of a signal peptide, a spacer region, and one or more active peptides [10]. The signal sequence is involved in the transport of the molecule across cellular membranes, and directs it through the endoplasmic reticulum. Upon reaching the required destination, this segment is removed by specific proteases to give the pro-peptide, which then migrates to the Golgi complex where it can be packaged and stored in secretory granules until required [7].

The spacer region offsets the activity of the mature peptide, and assists with folding to inhibit any enzymatic degradation [11]. This segment must also be cleaved in order to obtain the active peptide, which is typically achieved by endoproteases at some point along the pathway through the endoplasmic reticulum and Golgi complex [10]. Finally, the peptides may undergo post-translational modifications prior to secretion, which are often essential for maximum activity. These can include conversion of N-terminal Glu to pyroglutamate, formation of disulfide bonds, phosphorylation, glycosylation and acetylation, and isomerisation of L-amino acids to the D form [12-14]. The biosynthesis of active peptides is summarised in Figure 1.2.

Pre-pro-peptide

| Signal | Spacer | Peptide |

Proteolytic cleavage of
signal peptide

Pro-peptide

| Spacer | Peptide |

Proteolytic cleavage of
spacer peptide

Unmodified peptide

| Peptide |

Post-translational modification

Active peptide
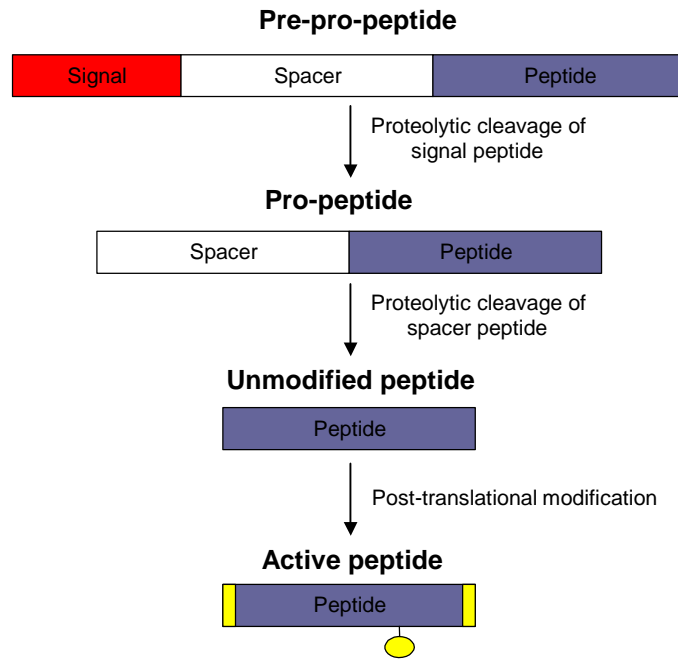
| Peptide |

Figure 1.2: Biosynthesis of biologically active peptides. Initial translation of the mRNA produces a pre-pro-peptide, which is processed in various stages to yield the active peptide.

In some cases the active peptide may be cytotoxic to the host, particularly at the high concentrations present in the storage granules. As a result, there are many examples in which the molecule is stored as the inactive precursor and the spacer segment is only removed upon release of the secretion [15]. The precursor peptides are often co-secreted with the active peptide, raising the possibility that the spacer regions may also have some as yet unidentified activity. For example, the hormone xenopsin is associated with xenopsin precursor fragment (XPF), which was found to possess antibacterial activity [16].

Recently, complementary DNA (cDNA) cloning techniques have been used extensively to characterise precursor proteins, and also to identify new active peptides. By these methods the corresponding cDNA can be synthesised for a given peptide sequence, and used to extract the complete DNA segment coding for the precursor protein in which the peptide is contained [5]. Typically the pre-pro-peptide is approximately 100-250 residues in length, consisting of a hydrophobic signal segment and an anionic spacer region [17,18]. Active peptides are usually bounded by pairs of basic amino acids (Lys-Lys or Lys-Arg), which are the consensus sequences recognised by various trypsin-like proteases that act to liberate the active peptide [10].

4

1.3 Anuran Skin Secretions

One of the most interesting classes of organisms studied to date are the anurans, due to the unparalleled variety of biologically active chemicals contained within the amphibian skin. The therapeutic properties of these dermal compounds have been exploited for thousands of years. Ancient Assyrian, Chinese and Roman cultures employed frogs for the formation of traditional medicines, principally for use as a heart stimulant and also as a diuretic [19,20]. Peruvian Indians took advantage of the stimulant effects which increased physical strength, awareness and resistance to hunger in order to improve their hunting prowess [21,22]. The toxic nature of amphibian glandular contents was also utilised by native Indian tribes of Central and South America, who applied the skin secretion of poison-dart frogs to hunting tools [19,20].

It was not until the 1960s that attempts were made to isolate the biologically active agents from amphibian skin, and began with pioneering work by Vittorio Erspamer and colleagues [23]. Continued investigations over the past five decades has made possible the identification of a vast array of active compounds, including biogenic amines [24], steroidal compounds [25], alkaloids [26] and peptides [27,28]. The toxicity of the poison-dart frog can be attributed to some alkaloids [29], while particular steroid compounds account for the therapeutic effects utilised by the Chinese [25].

Amphibians live and reproduce in stagnant water where numerous microbial pathogens are rife. Despite this, they appear to be essentially immune to infection. This observation led to the discovery of the magainin peptides, isolated from the skin of *Xenopus laevis*, which demonstrate wide-spectrum antibacterial activity [30,31]. Antimicrobial peptides have subsequently been identified in numerous amphibian species, and can often show additional anticancer, antifungal and antiviral activity [28,32,33]. The peptides contained in amphibian skin glands demonstrate a variety of additional biological functions. These can include hormonal, analgesic, and neurotransmitter action [32]. For example, selected peptides can stimulate various types of smooth muscle, allowing for hormone-like control of blood pressure and heart rate, as well as the urinary, reproductive and gastrointestinal systems [20,23].

A number of amphibian skin components have led to the development of pharmaceuticals still in use today for the treatment of various medical conditions including conjunctivitis, gastrointestinal infections, foot ulcers and even cancer [23,34-36]. Epibatidine, an alkaloid identified in the skin of Ecuadorian frogs, represents a major clinical advance in the area of analgesics since it displays potent broad-spectrum antinociceptive action without the side effects associated with traditional opioid painkillers [37]. In addition, the peptide caerulein, isolated from the Australian tree frog *Litoria caerulea*, has found a range of therapeutic applications resulting from its potent stimulation of the gut and gall bladder [20,38]. Finally, antibacterial resistance is a growing problem for the antibiotics currently in clinical use [39]. Exploiting the antibacterial properties of amphibian peptides is particularly promising since it would be difficult for bacteria to acquire resistance to their destructive action on the bacterial cell membrane (Chapter 8) [40].

The unique chemical spectrum of each species is also useful for the purpose of classification, taxonomy and evolutionary studies of amphibians. For example, *L. caerulea* and *L. gilleni* were conclusively shown to be different species on the basis that their peptide profiles were so dissimilar they could not have come from the same species, putting an end to this ongoing debate [41]. In addition, since the time scale of evolutionary change in peptide profiles is short, the differences in skin secretions from animals of the same species sampled from different isolated geographical locations may be taken as a measure of evolutionary divergence [17,42,43]. Similarly, a variety of tissue secretions have been used to determine the evolutionary relationships of frogs and toads, including *Bufo* parotoid gland toxins [44], skin alkaloids [45] and haemoglobin peptides [46].

Research into amphibian skin secretions persists to this day as the isolation, identification and testing of novel components continues to reveal active compounds with valuable biological properties. Only a small fraction of the world's amphibian species has been examined thus far, leaving an abundant resource available for further study.

1.3.1 Collecting the Secretion

The dermal layer of anuran skin contains a distribution of two morphologically distinct glands, namely the mucous and granular glands. The mucous glands are generally smaller and more numerous, and secrete a watery mixture of mucins and mucopolysaccharides over the surface of the body which assist in the control of skin pH, respiration and moisture balance, as well as thermoregulation, adhesion and reproduction [20,47]. In contrast, the granular glands are those principally responsible for synthesis and storage of the toxic or noxious substances secreted by the animal in response to a threat [47].

The granular glands are primarily dispersed along the dorsal surface of the body and are characterised by the presence of a large number of densely packed secretory granules lying in a syncytium, with multiple nuclei located peripherally (Figure 1.3) [48,49]. The gland is surrounded by myoepithelial cells, which contract to force the granules, cytoplasm and other organelles along the gland duct and onto the external surface via a holocrine-type mechanism [50]. Myoepithelial contraction is under the control of the sympathetic nervous system and consequently the secretory contents are expelled in times of stress, for example during predation or infection [51]. Typical activation results in the release of 80-90% of the glandular contents, and regeneration generally occurs over a period ranging from days to several weeks [49].
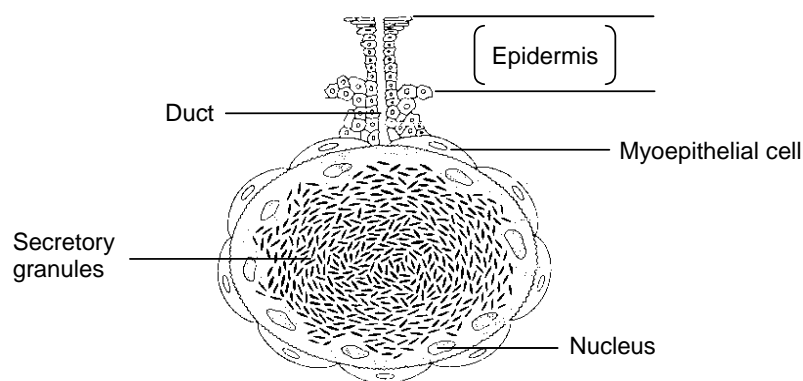
Figure 1.3: Structure of an amphibian granular gland [48].

In the past, collection of amphibian skin secretion samples involved the sacrifice of a number of animals, often over 1,000 specimens for a single study [52,53]. The skins were removed, dried and extracted with an organic solvent in order to obtain the glandular contents [52]. However, due to the significant decline of numerous frog populations noted in recent years, many to the brink of extinction [54], a non-harmful procedure is now essential for obtaining the secretions. This can be achieved by injecting adrenaline or noradrenaline directly into the gland [55]. Although this method is non-fatal, it is still relatively invasive. Another approach involves the surface electrical stimulation (SES) technique, which entails gentle massage of a platinum electrode over the dorsal surface of the animal, applying mild electrical stimulation to the secretory glands [56]. Upon activation, the contents of the gland are exuded onto the skin, where they can be washed from the frog with water and collected for analysis (Figure 1.4). This procedure is rapid, harmless and can be repeated on a monthly basis, thereby being the method of choice for such research.

Figure 1.4: Surface electrical stimulation method for collection of secretory products.

1.3.2 Peptides from Australian Frogs

There are more than 4,000 species of frogs currently described worldwide. Of this number approximately 5% are native to Australia, making this country a rich resource for the study of amphibian skin secretions [57]. The first extensive survey of Australian amphibians was reported by Erspamer and co-workers in 1984, during which the dried skin extracts of over 100 species of frogs from both Australia and Papua New Guinea were subjected to biological screening [52]. Specifically, the effect of peptides on smooth muscle preparations and systemic blood pressure was studied, and the most frequent and abundantly occurring peptides were found to be those of the caerulein, bombesin and tachykinin peptide families.

Since this initial report, a number of Australian frog species have been examined in detail to identify the active peptides contained within their skin glands. More recent work has focussed principally upon species from the *Litoria* genus, although several species from the genera *Limnodynastes*, *Uperoleia* and *Crinia* have also been investigated. The majority of frogs studied from these genera have a range of peptides within the skin glands, generally including a neuropeptide and a powerful broad-spectrum antibiotic. In addition, peptides with anticancer, antiviral and antifungal properties, pheromone activity and neuropeptide functions have also been identified [28,58]. The sequences and activities of selected peptides isolated from these Australian frogs are given in Table 1.1.

Table 1.1: Selected peptides isolated from Australian amphibian skin secretions. Table adapted from [58].

Peptide	Sequence	Species[1]	Activity[2]
Aurein 1.1	GLFDIIKKIAESI-NH$_2$	a	1,2
Aurein 1.2	GLFDIIKKIAESF-NH$_2$	a	1,2
Aurein 2.2	GLFDIVKKVVGALGSL-NH$_2$	a	1,2,3
Aurein 3.1	GLFDIVKKIAGHIAGSI-NH$_2$	a	1,2
Aurein 4.1	GLIQTIKEKLKELAGGLVTGIQS-OH	a	1,2
Aurein 5.2	GLMSSIGKALGGLIVDVLKPKTPAS-OH	a	1,2
Caeridin 1	GLLαDGLLGTGL-NH$_2$	b,c,d,e,f	
Caeridin 1.2	GLLβDGLLGTGL-NH$_2$	d	
Caeridin 1.5	GLLβDGLLGGLGL-NH$_2$	e,f	
Caeridin 2	GLLDVVGNLLGGLGL-NH$_2$	c,d	
Caeridin 3	GLFDAIGNLLGGLGL-NH$_2$	c,d	
Caeridin 4	GLLDVVFNVLHSLGL-NH$_2$	c	
Caerin 1.1	GLLSVLGSVAKHVLPHVVPVIAEHL-NH$_2$	b,c,d	1-5
Caerin 1.1.1	LSVLGSVAKHVLPHVVPVIAEHL-NH$_2$	d	
Caerin 1.3	GLLSVLGSVAQHVLPHVVPVIAEHL-NH$_2$	c	1,2
Caerin 1.9	GLFGVLGSIAKHVLPHVVPVIAEKL-NH$_2$	f	1-5
Caerin 1.11	GLLGAMFKVASKVLPHVVPAITEHF-NH$_2$	g	1
Caerin 2.1	GLVSSIGRALGGLLADVVKSKGQPA-OH	b	1,5
Caerin 2.2	GLVSSIGRALGGLLADVVKSKEQPA-OH	c	1,5
Caerin 2.5	GLVASIGRALGGLLADVVKSKEQPA-OH	d	1,5
Caerin 3.1	GLWQKIKDKASELVSGIVEGVK-NH$_2$	b,c	1
Caerin 3.2	GLWEKIKEKASELVSGIVEGVK-NH$_2$	c	1
Caerin 4.1	GLWQKIKSAAGDLASGIVEGIKS-NH$_2$	c	1
Caerin 4.2	GLWQKIKSAAGDLASGIVEAIKS-NH$_2$	c	1
Caerulein 1.1	pEQDY(SO$_3$)TGWMDF-NH$_2$	h	6
Caerulein 2.1	pEQDY(SO$_3$)TGAHMDF-NH$_2$	b,i	6
Caerulein 3.1	pEQDY(SO$_3$)GTGWMDF-NH$_2$	i	6
Caerulein 4.1	pEQDY(SO$_3$)TGSHMDF-NH$_2$	i	6
Citropin 1.1	GLFDVIKKVASVIGGL-NH$_2$	i	1,2,4,5
Citropin 1.2	GLFDIIKKVASVVGGL-NH$_2$	i,j	1,2,4,5
Dahlein 1.1	GLFDIIKNIVSTL-NH$_2$	k	1
Dahlein 1.2	GLVFDIIKNIFSGL-NH$_2$	k	1
Dahlein 4.1	GLWQLIKDKIKDAATGLVTGIQS-NH$_2$	k	
Dahlein 5.1	GLLGSIGNAIGAFIANKLKP-OH	k	5
Dynastin 1	GLVSNLGI-OH	l	
Dynastin 2	GLLSSLGLNL-OH	m	
Dynastin 3	GLVPNLLNNLGL-OH	n	
Dynastin 4	GLVSNLGI-OH	o	
Electrin 2.1	NEEEKVKWEPDVP-NH$_2$	p	

Table 1.1 (continued):

Peptide	Sequence	Species[1]	Activity[2]
Fletcherin	AGPVSKLVSGIGL-OH	q	
Frenatin 1	GLLDALSGILGL-NH$_2$	r	
Frenatin 2	GLLGTLGNLLNGLGL-NH$_2$	r	
Frenatin 3	GLMSVLGHAVGNVLGGLFKPKS-OH	r	5
Lesueurin	GLLDILKKVGKVA-NH$_2$	s	5
Maculatin 1.1	GLFGVLAKVAAHVVPAIAEHF-NH$_2$	t	1-5
Maculatin 1.3	GLLGLLGSVVSHVVPAIVGHF-NH$_2$	g	1,2
Maculatin 2.1	GFVDFLKKVAGTIANVVT-NH$_2$	t	1,2
Maculatin 3.1	GLLQTIKEKLESLESLAKGIVSGIQA-NH$_2$	t	1,2
Rubellidin 4.1	GLGDILGLLGL-NH$_2$	u	
Rubellidin 4.2	AGLLDILGL-NH$_2$	u	
Riparin 1.1	RLCIPVIFPC-OH	v	6
Riparin 2.1	IIEKLVNTALGLLSGL-NH$_2$	v	1
Riparin 5.1	IVSYPDDAGEHAHKMG-NH$_2$	v	
Rothein 2.1	AGGLDDLLEPVLNSADNLVHGL-NH$_2$	w	
Rothein 3.1	ASAAGAVRAGGLDDLLEPVLNSADNLVHGL-NH$_2$	w	
Signiferin 1	RLCIPYIIPC-OH	x	6
Signiferin 2.1	IIGHLIKTALGMLGL-NH$_2$	x	1
Signiferin 3.1	GIAEFLNYIKSKA-NH$_2$	v,x	5
Splendipherin	GLVSSIGKALGGLLADVVKSKGQPA-OH	b,c	7
Tryptophyllin L 1.1	PWL-NH$_2$	u	
Tryptophyllin L 1.4	FPFPWL-NH$_2$	u	6
Tryptophyllin L 3.1	FPWP-NH$_2$	p,u	
Tryptophyllin L 5.1	pEIPWFHR-NH$_2$	u	
Uperin 1.1	PEADPNAFYGLM-NH$_2$	y	6
Uperin 2.1	GIVDFAKKVVGGIRNALGI-NH$_2$	y	1
Uperin 3.1	GVLDAFRKIATVVKNVV-NH$_2$	y	1
Uperin 4.1	GVGSFIHKVVSAIKNVA-NH$_2$	y	1
Uperolein	pEPDPNAFYGLM-NH$_2$	z	6

[1]**Species: (a)** *Litoria aurea, Litoria raniformis* [59]; **(b)** *Litoria splendida* [60]; **(c)** *Litoria caerulea* [42]; **(d)** *Litoria gilleni* [41]; **(e)** *Litoria xanthomera* [61,62]; **(f)** *Litoria chloris* [63]; **(g)** *Litoria eucnemis* [64]; **(h)** many species of the genus *Litoria* [23]; **(i)** *Litoria citropa* [65]; **(j)** *Litoria subglandulosa* [66]; **(k)** *Litoria dahlii* [67]; **(l)** *Limnodynastes interioris* [68]; **(m)** *Limnodynastes dumerlii* [68]; **(n)** *Limnodynastes terrateginae* [68]; **(o)** *Limnodynastes salmini* [69]; **(p)** *Litoria electrica* [70]; **(q)** *Limnodynastes fletcheri* [69]; **(r)** *Litoria infrafrenata* [71]; **(s)** *Litoria lesueuri* [72]; **(t)** *Litoria genimaculata* [73]; **(u)** *Litoria rubella* [74,75]; **(v)** *Crinia riparia* [76]; **(w)** *Litoria rothii* [77]; **(x)** *Crinia signifera* [78]; **(y)** *Uperoleia inundata* [79]; **(z)** many species of the genus *Uperoleia* [23].

[2]**Activity: (1)** Antibiotic; **(2)** Anticancer; **(3)** Antiviral; **(4)** Fungicide; **(5)** nNOS inhibitor; **(6)** Neuropeptide; **(7)** Pheromone.

The dermal secretions of most Australian frog species contain at least one broad-spectrum antibiotic, and often a series of peptides with differing antibacterial activity to afford greater protection against microbial pathogens [80]. Typically, these are short α-helical molecules that act by disruption of bacterial cell membrane integrity. Biological testing has revealed additional anticancer properties for a number of these peptides, with such coincident activity presumably due to a similar mechanism of action at both bacterial and cancer cells [58]. Good examples of potent antibacterial peptides include caerin 1.1, maculatin 1.1 and aurein 1.2. These are generally more active against Gram-positive bacteria (at concentrations as low as 3 $\mu g.mL^{-1}$) [28], however many are also active against Gram-negative microorganisms. For example, caerin 2.1 is active against *Pasteurella multocida* at 25 $\mu g.mL^{-1}$ [60]. A detailed discussion of the antibacterial activity of amphibian peptides is given in Chapter 8.

The first report of antiviral efficacy was for caerin 1.1, which showed activity against viruses with envelopes, e.g. HIV and *Herpes simplex 1*. A more extensive survey of fourteen antimicrobial peptides against HIV has shown that caerin 1.1, caerin 1.9 and maculatin 1.1, all wide spectrum antibiotics, show minimum inhibitory concentration (MIC) values of 7.8, 1.2 and 11.3 μM respectively [81]. These membrane active peptides are not toxic to target cells, and act by disrupting the virus envelope. Similarly, most of the wide-spectrum antibiotics also display fungicidal activity. For example, these peptides are active against *Candida albicans* and the zoosporic chytrid fungus *Batrachochytrium dendrobatidis* in the low micromolar concentration range [28,82].

Frogs of the *Litoria* genus and toadlets of the *Uperoleia* genus generally possess in their skin secretion at least one neuropeptide of the caerulein and uperolein groups respectively. These are typically the most abundant peptides in the secretion, and are an integral part of the host-defence system, in addition to assisting with regulation of dermal physiological function [16,19,23]. The caerulein peptides contain Tyr sulfate and pyroglutamate residues together with a C-terminal $CONH_2$ group, with the sulfate group essential for full activity [28]. The biological activity of caerulein is very similar to those of the mammalian intestinal peptide hormones gastrin and cholecystokinin (CCK). Caerulein contracts smooth muscle at nanomolar concentrations directly via the

CCK_1 receptor or indirectly via the CCK_2 receptor, and also augments blood circulation, moderates satiety, sedation and thermoregulation, and is a potent analgesic [19,83,84]. Unlike caerulein, uperolein and the uperins do not contain a sulfated Tyr residue. Although these are less well studied, it is known that uperin, a member of the tachykinin family, exhibits potent vasodilator and hypertensive action as well as spasmogenic activity of smooth muscle [23]. In addition, uperin 1.1 contracts guineapig ileum at 0.4 $ng.kg^{-1}$, and effects a reduction in rabbit blood pressure at 5 $ng.kg^{-1}$ [79]. Neuropeptides from the genus *Crinia* are discussed in Chapter 6.

Recently, peptides have been identified that inhibit the enzyme neuronal nitric oxide synthase, which is responsible for the production of the neurotransmitter nitric oxide [72]. Approximately fifty such peptides have been identified thus far, and although no clear sequence similarities have been noted, they have been categorised into three groups based on their higher order structures [58]. This topic is reviewed in detail in Chapter 5.

To date, the only known anuran pheromone has been isolated from the skin secretions of male *Litoria splendida*, and was named splendipherin [60,85]. This 25 residue peptide is a small component of the secretion, and is present only during the reproductive season. Behavioural tests showed the peptide to attract female *L. splendida* at a minimum concentration of 10 pM and in a species-specific manner, demonstrating its effectiveness as a sex pheromone. A number of peptides with sequences similar to splendipherin (e.g. aurein 5.2) have activities which are yet to be determined. It has been hypothesised that these peptides may also have some kind of pheromone role, although to date this has not been verified [59].

Despite much effort dedicated to elucidating the activity of amphibian skin peptides, there are still a large number whose purpose in the secretion remains unknown. Included in this group are the caeridins, dynastins, rubellidins and tryptophyllins [69,75,86]. It is highly unlikely that these molecules would have no purpose, given the significant metabolic cost associated with their production and storage. These peptides may possibly be the inactive remnants of larger precursor proteins, although this remains to be established [87].

1.4 Spider Venoms

Excluding insects, spiders are the most diverse invertebrates on land, with close to 40,000 species described worldwide [88]. They are an ancient group, with the oldest known fossil records dating from the Carboniferous period over 300 million years ago [89]. Spiders rely entirely on predation as a trophic strategy, and consequently have developed complex and potent venoms designed to rapidly subdue or kill their prey. In addition, spider venom may also play a role in self-defence, as it has been suggested that some spiders employ venoms for protection against predators [90]. Whatever the purpose, the use of venom has been vital for the successful evolution of these creatures, possibly more so than their use of silk [91].

There are two main types of spiders, the Orthognatha (primitive or trapdoor spiders) and the Labidognatha (modern spiders), which are distinguished by the physical structure of the chelicera and fangs [4,92]. The largest spiders are the tarantulas (Theraphosidae), and belong to the Orthognaths. However, with the exception of the genus *Atrax*, these are far from the most dangerous. The Labigdognaths comprise the most deadly species for humans, and include black widow spiders (Theridiidae *Lactrodectus*), violin or gaucho spiders (Loxoscelidae *Loxosceles*) and banana spiders (Ctenidae *Phoneutria*), which are responsible for severe envenomation cases and recorded mortalities [93,94]. Despite this, only a few species are truly dangerous to humans, and therefore the study of spider toxins have lagged behind that of other venomous creatures [93].

Spider venoms are heterogenous, not only between species but within species, and contain an impressive assortment of chemical compounds. The interactions between the various chemical classes and their role in the envenomation process are not well understood at present. Nevertheless, spider venom components can be grouped into three categories, namely low molecular mass compounds (<1 kDa), small peptides (typically 3-8 kDa) and a limited number of large proteins (>10 kDa) [4,93-95].

The low molecular weight molecules within the venom include inorganic ions and salts (Na^+, K^+, Mg^{2+} and Cl^-), free acids (citric, lactic, dihydrophenylacetic, amino acids), glucose, biogenic amines (spermine, spermidine, putrescine, cadaverine) and neurotransmitters (glutamate, aspartate, GABA, histamine, dopamine, serotonin, epinephrine, epinin) [4,94]. The role of these constituents is not clear, although they may potentiate the action of the neurotoxins in some cases, or alternatively represent degradation products of other venom components [94]. This group also comprises the acylpolyamines, formed from an aromatic carboxylic acid linked to a lateral chain of one to nine aminopropyl, aminobutyl or aminopentyl units. These interact with both ion channels and nicotinic acetylcholine receptors, and possess essentially insecticidal activity [93,94].

In combination with the polyamines, peptides appear to represent the primary chemical arsenal of spiders. The majority of these are neurotoxins, and are classified according to their mode of action. For example, these peptides may selectively inhibit membrane ion channels [4,93,96]. In addition, they can affect exocytosis of presynaptic vesicles and induce abnormal synaptic neurotransmission, particularly for glutamatergic and cholinergic systems [4,94]. Finally, a number of membrane active antibacterial peptides have also been identified [4,93].

Large venom proteins include a number of enzymes such as proteases, sphingomyelinases, hyaluronidases, phospholipases and isomerases, although in many cases these appear as a result of contamination by saliva or digestive fluids during the course of sample collection [4,94]. Several high mass protein toxins have also been described. For example, the neurotoxicity of black widow venom can be attributed to the 110 kDa latrotoxins, which provoke uncontrolled neurotransmitter release in the victim [97]. Insecticidal toxins have also been isolated from the venom of *Filistata hibernalis* (approximately 20 kDa) [98] and *Phidippus audax* (>100 kDa) [99], however the complete structures of these are yet to be reported.

Spider venoms are of particular interest for several reasons. Insects destroy approximately 25% of the world's annual crop production, and are responsible for the transmission of numerous diseases of both human and veterinary public health importance [100,101]. As a result, insect specific toxins from spiders are attracting significant attention for use in pest management and agriculture [18]. In addition, many toxins isolated from spiders have been invaluable for characterising the function and diversity of neuronal ion channels and the process of exocytosis [4], and offer leads for the development of novel therapeutic agents for ion channel related diseases [93]. Although the use of spider venoms as pharmaceuticals is at present not widespread, delusamine was discovered to be an effective NDMA receptor antagonist during small scale screening of polyamine containing spider toxins, and is currently undergoing phase 1 clinical trials for the treatment of ischemia [102].

Based on reports in journal and patent literature, it appears that less than 1% of the known spider species have been investigated thus far [18]. Spider venoms therefore represent an incredibly diverse and untapped source of novel bioactive compounds that could lead to the broader application of spider toxins in the field of pharmacology.

1.4.1 Venom Collection

Spider venoms are synthesised in relatively small quantities in prosomal glands, located at the anterior of the cephalothorax [92]. All spiders, with the exception of hackled orbweavers and certain primitive mesothelids, have venom glands [89], however, the size and shape can vary greatly between species [103]. These glands are paired structures that are cylindrical in shape with a slight constriction in the middle region. They connect to a thin duct which extends from the front of the gland through the basal segment of the chelicera to its opening at the end of the movable fang (Figure 1.5) [103,104]. Each gland is surrounded by longitudinal bundles of striated muscle fibres that are directly innervated by motor neurons [103,105]. When the spider bites, the fangs penetrate the prey and the muscle bundles contract rapidly, allowing for the express injection of venom into the victim [92]. The spider appears to use its venom economically, with venom expenditure dependent upon prey size and motility [105,106].
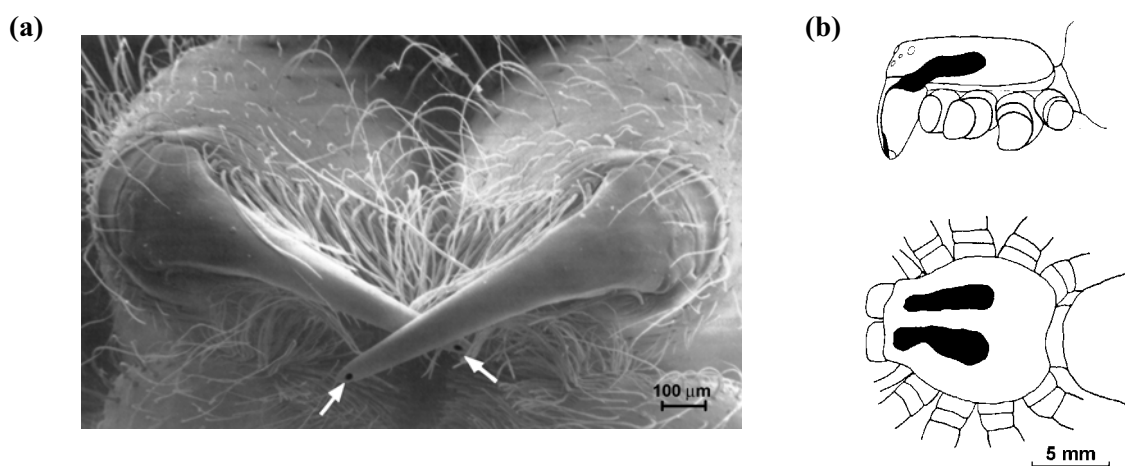
Figure 1.5: Structure and location of a spider venom gland. **(a)** The chelicerae of *Cupiennius salei*. Arrows indicate the openings of venom gland ducts, and **(b)** schematic diagram of the chelicera and venom gland from the lateral (top) and dorsal (bottom) view [104].

For research purposes, spider venoms are typically obtained either by 'milking' or extraction from dissected glands. Milked venoms are generally preferable since they do not contain superfluous glandular material, are assumed to be a better representation of natural venoms, and tend to be more consistent and easier to work with [107,108]. In the milking process, the spiders are anaesthetised with carbon dioxide and the mouth suctioned to remove any regurgitate. Low voltage electrical stimulation is applied across the cephalothorax to induce venom release, and the exudate is collected directly from the fangs into a glass capillary tube for subsequent analysis [108,109].

1.4.2 Peptides from Spider Venoms

Mass spectrometric analysis of some 55 different tarantula venoms led to an estimate of at least 50 peptides per venom, a similar number to that observed for the primitive hunting spider *Plectreurys tristis* [110,111]. Given the vast diversity of spiders, even extremely conservative estimates predict a total of 1.5-1.9 million distinct spider venom peptides, most of which are expected to have biological activity [18]. Consequently, the potential application of this pharmacological repertoire is enormous. To date, only a very small fraction of peptides have been fully characterised from spider venoms [110], and the sequence and activity of selected examples are given in Table 1.2.

Table 1.2: Selected peptides isolated from spider venoms. Table adapted from [4,93,96].

Peptide	Sequence	Species[1]	Activity[2]
δ-ACTX-Ar1	CAKKRNWCGKNEDCCCPMKCIYAWYNQQGSCQTTITGLFKKC-OH	a	1
δ-ACTX-Hv1	CAKKRNWCGKTEDCCCPMKCVYAWYNEQGSCQSTISALWKKC-OH	b	1
ω-ACTX-Hv1a	SPTCIPSGQPCPYNENCCSQSCTFKENENGNTVKRCD-OH	b	2
ω-ACTX-Hv2a	LLACLFGNGRCSSNRDCCELTPVCKRGSCVSSGPGLVGGILG-GIL-OH	b	2
μ-Agatoxin I	ECVPENGHCRDWYDECCEGFYCSCRQPPKCICRNNN-NH$_2$	c	1
μ-Agatoxin II	ECATKNKRCADWAGPWCCDGLYCSCRSYPGCMCRPSS-NH$_2$	c	1
μ-Agatoxin III	ADCVGDGQRCADWAGPYCCSGYYCSCRSMPYCRCRSDS-NH$_2$	c	1
μ-Agatoxin VI	DCVGESQQCADWAGPHCCDGYYCTCRYFPKCICVNNN-NH$_2$	c	1
ω-Agatoxin IA	AKALPPGSVCDGNESDCKCYGKWHKCRCPWKWHFTGEGPCTC-EKGMKHTCITKLHCPNKAEWGLDW-OH	c	2
ω-Agatoxin IIIA	SCIDIGGDCDGEKDDCQCCRRNGYCSCYSLFGYLKSGCKCVV-GTSAEFQGICRRKARQCYNSDPDKCESHNKPKRR-OH	c	2
ω-Agatoxin IVA	KKKCIAKDYGRCKWGGTPCCRGRGCICSIMGTNCECKPRLIM-EGLGLA-OH	c	2
CSTX-1	SCIPKHEECTNDKHNCCRKGLFKLKCQCSTFDDESGQPTERC-ACGRPMGHQAIETGLNIFRGLFKGKKKNKKTK-NH$_2$	d	2
Cupiennin 1a	GFGALFKFLAKKVAKTVAKQAAKQGAKYVVNKQME-NH$_2$	d	3
Cupiennin 1d	GFSALFKFLAKKVAKTVAKQAAKQGAKYVANKHME-NH$_2$	d	3
Curtatoxin 1	SCVGEYGRCRSAYEDCCDGYYCNCSQPPYCLCRNNN-NH$_2$	e	1
Curtatoxin 2	ADCVGDGQRCADWAGPYCCSGYYCSCRSMPYCRCRSDS-NH$_2$	e	1
DW13.3	AECLMIGDTSCVPRLGRRCCYGAWCYCDQQLSCRRVGRKREC-GWVEVNCKCGWSWSQRIDDWRADYSCKCPEDQ-OH	f	2
Grammotoxin	DCVRFWGKCSQTSDCCPHLACKSKWPRNICVWDGSV-OH	g	2
GsMTx4	GCLEFWWKCNPNDDKCCRPKLKCSKLFKLCNFSSA-OH	g	4
Hanatoxin 1	ECRYLFGGCKTTSDCCKHLGCKFRDKYCAWDFTFS-OH	g	2,5
Hanatoxin 2	ECRYLFGGCKTTADCCKHLGCKFRDKYCAWDFTFS-OH	g	2,5
Heteropodatoxin 1	DCGTIWHYCGTDQSECCEGWKCSRQLCKYVIDW-OH	h	5
Heteropodatoxin 2	DDCGKLFSGCDTNADCCEGYVCRLWCKLDW-OH	h	5
Heteropodatoxin 3	ECGTLFSGCSTHADCCEGFICKLWCRYERTW-OH	h	5
Huwentoxin I	ACKGVFDACTPGKNECCPNRVCSDKHKWCKWKL-OH	i	6
Huwentoxin IV	ECLEIFKACNPSNDQCCKSSKLVCSRKTRWCKYQI-OH	i	1
Lycotoxin I	IWLTALKFLGKHAAKHLAKQQLSKL-OH	j	3
Lycotoxin II	KIKWFKTMKSIAKFIAKEQMKKHLGGE-OH	j	3
Oxyopinin 1	FRGLAKLLKIGLKSFARVLKKVLPKAAKAGKALAKSMADENA-IRQQNQ-OH	k	3
Oxyopinin 2a	GKFSVFGKILRSIAKVFKGVGKVRKQFKTASDLDKNQ-OH	k	3
Oxyopinin 2b	GKFSGFAKILKSIAKFFKGVGKVRKQFKEASDLDKNQ-OH	k	3

Table 1.2 (continued):

Peptide	Sequence	Species[1]	Activity[2]
δ-Palutoxin IT1	GCLGEGEKCADWSGPSCCDGFYCSCRSMPYCRCRNNS-OH	l	1
δ-Palutoxin IT2	ACVGDGQRCASWSGPYCCDGYYCSCRSMPYCRCRNNS-OH	l	1
PHTX2-5	ATCAGQDQTCKVTCDCCGERGECVCGGFCICRQGNFLIAAYK-LASCKCK-OH	m	1
PHTX2-6	ATCAGQDQPCKETCDCCGERGECVCGGPCICRQGYFWIAWYK-LANCKK-OH	m	1
PHTX3-1	AECAAVYERCGKGYKRCCEERPCKCNIVMDNCTCKKFISE-OH	m	5
PNTX3-4	SCINVGDFCDGKKDCCQCDRDNAFCSCSVIFGYKTNCRCE-OH	m	7
ω-PLTX II	ADCSATGDTCDHTKKCCDDCYTCRCGTPWGANCRCDYYKARC-DT(Pal)-NH2	n	2
SGTx1	TCRYLFGGCKTTADCCKHLACRSDGKYCAWDGTF-OH	o	5
SNX-325	GSCIESGKSCTHSRSMKNGLCCPKSRCNCRQIQHRHDYLGKR-KYSCRCS-OH	p	2
SNX-482	GVDKAGCRYMFGGCSVNDDCCPRLGCHSLFSYCAWDLTFSD-OH	p	2

[1]**Species: (a)** *Atrax robustus* [112]; **(b)** *Hadronyche versuta* [113]; **(c)** *Agelenopsis aperta* [114,115]; **(d)** *Cupiennius salei* [116,117]; **(e)** *Hololena curta* [118]; **(f)** *Filistata hybernalis* [119]; **(g)** *Grammostola spatulata* [120,121]; **(h)** *Heteropoda venatoria* [122]; **(i)** *Ornithoctonus huwena* [123,124]; **(j)** *Lycosa carolinensis* [125]; **(k)** *Oxyopes kitabensis* [126]; **(l)** *Paracoelotes luctuosus* [127]; **(m)** *Phoneutria nigriventer* [128-130]; **(n)** *Plectreurys tristis* [131]; **(o)** *Stromatopelma calceata* [132]; **(p)** *Segestria florentina* [133].

[2]**Activity: (1)** Na^+ channel effector; **(2)** Ca^{2+} channel effector; **(3)** Pore-forming in membranes; **(4)** Mechano-sensitive ion channel effector; **(5)** K^+ channel effector; **(6)** Nicotinic acetylcholine receptor antagonist; **(7)** Glutamate uptake inhibitor.

By far the most common peptides identified in spider toxins are those with a molecular mass in the order of 3 to 8 kDa, and which are highly reticulated by several disulfide bridges. These peptides are considerably neurotoxic, targeted at either neuronal receptors, neuronal ion channels (in particular selected subtypes of K^+, Na^+ and Ca^{2+} channels), or presynaptic membrane proteins involved in neurotransmitter release, and are often active at concentrations in the low nanomolar range [4]. Recently, nuclear magnetic resonance studies have shown these peptides adopt a common structural motif, composed of a triple-stranded antiparallel β-sheet that is stabilised by internal disulfide bridges, forming a cysteine knot [134]. Despite similarities in secondary structure, the spider toxin peptides have very divergent yet highly specific pharmacology. The biological activity of such peptides is complex, and is the subject of a number of recent reviews [4,18,93,94,96,135].

Membrane active cytolytic peptides have currently only been described from the venom of Labidognath spiders, especially members of the superfamily Lycosidoidae, which are mainly omnivorous hunting spiders that do not build webs [136].   The first description of antimicrobial peptide activity was reported in 1989 for *Lycosa singoriensis* [137], however lycotoxins I and II, isolated from *Lycosa carolinensis*, were the first antibacterial peptides to be fully characterised [125].   Following the lycotoxins, cupiennins [117] and oxyopinins [126] have also been described, and show antimicrobial activity against both Gram-positive and Gram-negative bacteria in the micromolar concentration range.   These are typically amphipathic helices which lack the disulfide bridge motif. The structure and mechanism of action of these membrane active spider venom peptides is discussed further in Chapter 9.

The tremendous range of spider venom peptides results from the semi-combinatorial process by which they are produced. By this approach residues that are functionally relevant are hypermutated, while residues that maintain tertiary structure are highly conserved [18,94].   In addition, the insertion of charged residues is a common diversification mechanism, and alters the interaction sites and electrostatic properties of the peptide in order to increase functional variability [94]. Interspecies comparisons reveal that only the mature peptide is modified, while precursor sequences are nearly identical [18]. A large number of homologous toxins are found in one venom, or in venoms from closely related species. This allows for very fine control of the pharmacological properties of a toxin family against a selected receptor, and provides spiders with an exceptionally valuable chemical arsenal.

~ CHAPTER 2 ~

Methodology I – Mass Spectrometry

2.1 Mass Spectrometry

The foundations of mass spectrometry can be attributed to work done by Sir J. J. Thomson in the early 1900's, with his observations of positive ions and their application to chemical analysis [138]. This technique is based on the production, differentiation and detection of ions in the gas phase, and provides a means for acquiring molecular mass and structural information of molecules in a high-throughput manner.

The earliest mass spectrometers utilised a single magnetic sector for mass analysis, however such instruments were quickly superseded by double sector and tandem double sector spectrometers. These consisted of both a magnetic and electric component, which afforded greater resolution and experimental capabilities [139,140]. Time of flight (TOF) [141,142], quadrupole [143,144] and ion trap mass spectrometers [145,146] evolved in parallel to the preponderant and more expensive magnetic deflection instruments, and are now the most commonly used spectrometers for the study of peptides and proteins. Along with development in mass analysis, methods for ion generation have progressed from the early emission of positive ions to electron impact ionisation [147-149] and chemical ionisation [150,151], amongst others. In particular, major advances in biochemical mass spectrometry can be attributed to the implementation of 'soft ionisation' methods such as matrix assisted laser desorption ionisation (MALDI) [152-154] and electrospray ionisation (ESI - Section 2.3). These techniques allow for the direct analysis of large, polar, thermally labile molecules and are thus well suited for the investigation of complex biological compounds such as proteins and DNA.

Mass spectrometry is today the most sensitive, accurate and rapid method for the structural characterisation of biomolecules [155], and has become an indispensable proteomics tool in many fields of cellular and molecular life sciences.

2.2 The Q-TOF 2 Mass Spectrometer

The mass spectrometric research detailed in this thesis was carried out primarily using a Q-TOF 2 hybrid quadrupole time of flight mass spectrometer. A schematic diagram of the principle components of this instrument is presented in Figure 2.1.
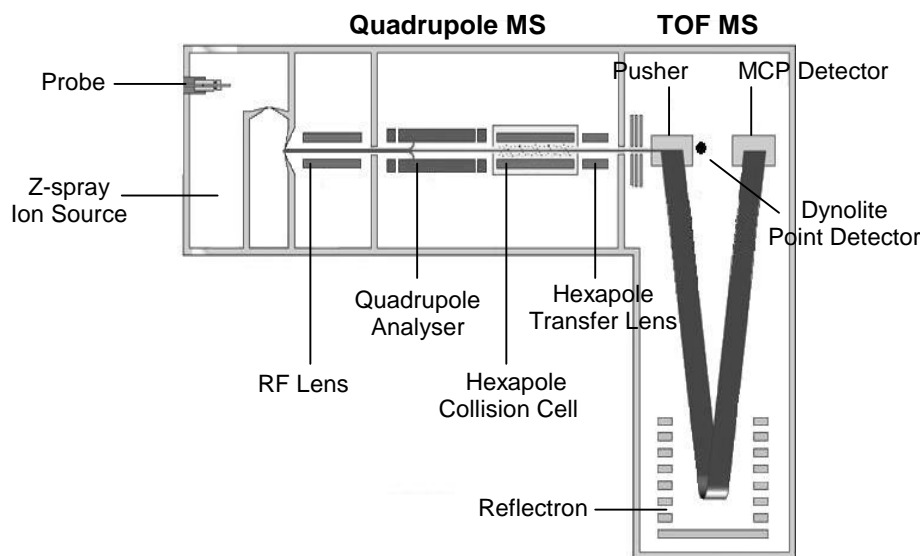
Figure 2.1: Schematic diagram of the Q-TOF 2 mass spectrometer. Figure adapted from [156].

Ionisation is achieved in the Z-spray ion source of the Q-TOF 2 spectrometer by the ESI method (Section 2.3), and the resulting ions are drawn through the sample cone aperture by application of an electric potential. By altering the applied cone voltage it is possible to preferentially select ions of differing mass-to-charge ratio (*m/z*). In general, the higher the voltage employed, the larger *m/z* ions that can be attracted into the analyser [157]. The analysing component of the Q-TOF 2 instrument consists of a quadrupole mass filter and an orthogonal TOF sector, which are separated by a hexapole collision cell.

The quadrupole sector is comprised of four precisely parallel rods, to which a fixed direct current (DC) and alternating radiofrequency (RF) potentials are applied in order to produce an electric field. Ions are then introduced in a continuous beam along the central axis of the rods. The motion of an ion within this sector will depend on the electric field applied, such that only ions of a particular *m/z* will have a stable trajectory and thus pass through to the detector [143,145,158]. All other ions are ejected from the quadrupole (Figure 2.2). The resolution and ion transmission are controlled by variations in the strength and frequency of applied DC and RF potentials between adjacent rod pairs. In this way the electric field is varied to bring ions of different *m/z* into focus on the detector, and thus generate a mass spectrum [143,158,159].
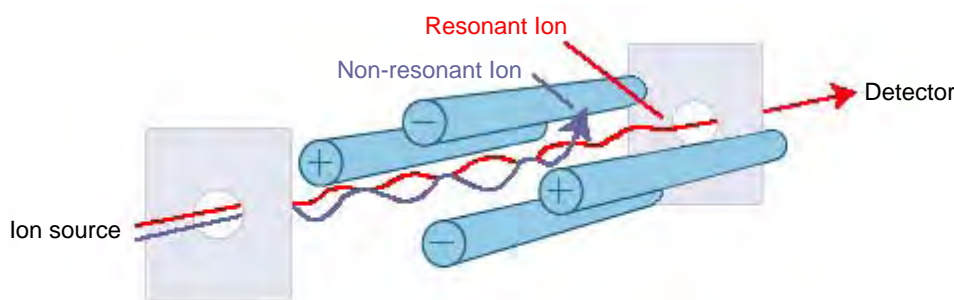
Figure 2.2: Mass selection by a quadrupole analyser. Ions coloured red are transmitted along the quadrupole in a stable trajectory RF field. Ions coloured blue do not have a stable trajectory and are ejected from the quadrupole.

In the MS mode, ions of all *m/z* are allowed to pass through the quadrupole mass analyser to collect at the pusher, which imparts translational energy to these ions for entry into the TOF sector. However, if further structural information is required, tandem mass spectrometry (MS/MS) is utilised [155,160-162]. In this process, the ion of interest is allowed to pass through the quadrupole analyser and into the hexapole collision cell. Here the mass selected ions are energised by collision with a noble gas such as He or Ar, which results in fragmentation of the parent ion into a series of daughter ions that may retain characteristics of the original structure. This process is known as collision-induced dissociation (CID) [162-166]. The resulting fragment ions are then accelerated via the pusher to the TOF analyser for subsequent mass determination.

In the TOF sector an accelerating potential, V, will give an ion of charge z an energy of zV, which can be equated to the kinetic energy as follows;

$$zV = \frac{mv^2}{2}$$

where m and v are the mass and velocity of the ion respectively. Since velocity can be related to distance (d) and time (t), the above equation can be rewritten as;

$$\frac{m}{z} = \frac{2Vt^2}{d^2}$$

Thus, if the ions travel a fixed distance to the detector, those of larger *m/z* will have a longer time of flight. The detector therefore observes a spread in arrival times, and this is interpreted as a mass spectrum [141,142,159]. In the TOF tube, ions are accelerated by an applied potential difference toward the reflectron, where they are electrostatically reflected back towards the detector. The reflectron effectively aids in mass resolution by correcting for the distribution of kinetic energies amongst the ions [167,168].

Detection of ions by the Q-TOF 2 is achieved using a microchannel plate detector, which records a full spectrum at 50 μs intervals. Up to 20,000 scans can be summed per second, and the resulting spectrum displayed for analysis [169]. This instrument has an *m/z* range to 4,000 Th and can acquire spectra at nanomolar concentrations. Hence it is well suited for the investigation of small quantities of peptides obtained from natural sources, as well as fragile non-covalent complexes.

2.3 Electrospray Ionisation Mass Spectrometry

Early ionisation techniques including electron impact and chemical ionisation placed an upper limit on the size of molecules amenable to study by mass spectrometry, as they were restricted to volatile analytes. The introduction of ESI revolutionised the field of biological mass spectrometry, since it allowed for the production of gas phase ions from large, non-volatile molecules directly from solution and at atmospheric pressure. The generation of ions by ESI was first demonstrated by Dole *et al.* in 1968 [170]. However, the development of this method by Fenn and others [171-175] has seen mass spectrometry progress to a state where biomolecules ranging from small peptides in the order of 1 kDa, to whole virus particles as large as 40 MDa [176] can be investigated.

For ESI mass spectrometry (ESI-MS), the analyte is initially dissolved in a solvent where, to some extent, both positive and negative ions are formed [155]. The sample solution is then passed through a heated capillary at a low flow rate, typically in the nL.min^{-1} to µL.min^{-1} range. A potential difference of 1-6 kV is applied between the needle and an adjacent counter electrode, which causes partial charge separation since the field penetrates below the surface of the liquid at the capillary tip [159,177]. Positive or negative ions can be selected for by controlling the polarity bias of this applied field. In either case, charge accumulation at the capillary terminus causes the liquid surface to adopt a conical shape known as a 'Taylor cone', the tip of which is drawn into an elongated filament that becomes unstable as the charge density increases [159,178-180]. The onset of electrospray requires an electric field given by;

$$ E_0 = \left(\frac{2\gamma \cos 49°}{\varepsilon_0 r_c} \right)^{1/2} $$

where γ is the surface tension of the liquid, $\cos 49°$ is the half-angle of the Taylor cone, ε_0 is the permittivity of vacuum and r_c is the radius of the capillary [179,181]. At this point the filament breaks up into a spray of fine droplets (less than 10 µm in diameter) [159], which then travel down a pressure and potential gradient towards the high-vacuum component of the mass spectrometer.

Solvent evaporation is promoted by a combination of heating and dry gas application, and leads to a decrease in the droplet radius at a constant charge. Within approximately 100 μs, the radii are reduced such that the Rayleigh stability limit is approached as follows;

$$q = 8\pi(\varepsilon_0 \gamma R^3)^{1/2}$$

where q and R describe the charge and radius of a supposed spherical droplet respectively [179,182,183]. From this point, Coulombic repulsion overcomes the cohesive surface tension forces and the droplets divide. Repeated solvent evaporation and fission ultimately leads to offspring droplets with radii in the nanometer range, and which only have a few elementary charges (Figure 2.3) [180].
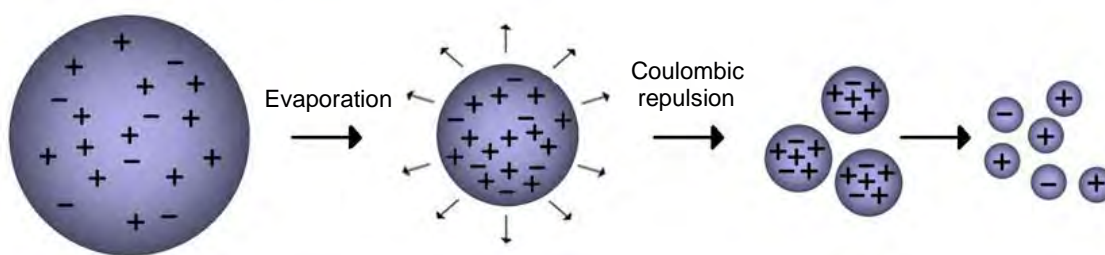
Figure 2.3: Schematic representation of the ESI process.

The mechanisms involved in the production of isolated gaseous ions are to date not entirely understood. Two models have been suggested, namely the charge-residue model [170,177,179,184] and the ion-evaporation model [179,185]. The charge-residue model states that gas phase ions will result when repeated droplet fission continues to the point where no further solvent evaporation can occur. In contrast, the ion-evaporation model proposes that, upon reducing the droplet radius to a range of 10 to 20 nm, direct emission of ions will occur due to electrostatic repulsion. In all probability, both mechanisms are likely to apply in different situations [155,177].

The mildness of the ESI process means ions are formed with low internal energies, which minimises unwanted fragmentation and preserves weak non-covalent interactions [186-189]. In addition, this process often results in the formation of multiply charged species, effectively reducing the *m/z* of the observed ions. An intrinsic property of all mass analysers is that they distinguish ions based on *m/z* rather than just molecular mass. Typical mass analysers may have an *m/z* range of 1 - 4,000 Th [156,157], hence formation of multiply charged analytes is particularly desirable since the masses of very large molecules can be determined over a smaller *m/z* range. The charge state of the ions can be elucidated from the *m/z* values of the isotope peaks, as the mass difference between these peaks is inversely proportional to charge. For example, given an ion with a charge of +2, a mass difference of 0.5 Da will be observed between the signals in the isotope peak envelope [155]. For a protein or large peptide a statistical distribution of multiply charged peaks is observed, from which the molecular mass can be determined by automated deconvolution methods [190-192].

Solvent effects have a major influence on the ESI process, not only in regards to the production of ions but also in the charge state of the resulting ions. Typically, for peptide sequencing a mixture of water and an organic solvent is used. A small percentage of acetic or formic acid may also be added to increase the ionisation of molecules in positive ion mode [189,193]. However, changing the composition of the solvent can significantly alter the charge state distribution. For example, the highest cationic charged state produced may be increased by changing the organic solvent component from isopropanol, to acetonitrile, to methanol [194]. This effect is particularly useful in improving analysis capabilities for large molecules by multiple charging, as described above. Nevertheless, despite improving ionisation efficiency, organic solvents can often act to denature proteins [195-198]. In situations where the higher order structures of peptides and proteins that occur in physiological conditions are to be maintained in the gas phase, the solvent is typically much more mild. Aqueous ammonium acetate is often the solvent of choice for studying proteins in their native state by ESI-MS (Section 2.5.2).

2.4 Peptide Sequencing

Mass spectrometry allows for rapid determination of a peptide sequence, often from minute amounts of sample, and can be applied for the identification of post-translationally modified amino acids which may be impervious to Edman sequencing (Section 2.4.5). In addition, the sample under investigation is not required to be pure, since ions of interest can be selected for and analysed independently using MS/MS capabilities. Mass spectrometry thus remains a principal tool for the primary structure elucidation of peptides and proteins, particularly from natural sources.

2.4.1 High Performance Liquid Chromatography

In the ESI process, analytes compete for charge as they are produced from the spray droplets. Consequently, for a sample containing a large assortment of peptides, only a small number of the most easily ionised species are observed [157,179]. The combination of mass spectrometry with separation techniques such as high performance liquid chromatography (HPLC) has thus become essential for the study of peptides from complex mixtures.

Typically a reverse phase HPLC column is used, in which the peptides equilibrate between the hydrophobic stationary phase and the more polar mobile phase. They are then subjected to a gradient elution profile which increases the concentration of organic solvent in the mobile phase over time, and elution occurs when the percentage of organic solvent is sufficient to shift the equilibrium towards the mobile phase. Partitioning behaviour between the two phases is dependent on subtle differences in hydrophobicity and conformation, and hence the rate at which a given peptide moves through the column is dependent on primary structure [157,199-202]. This forms the basis of separation and purification.

Often an ionic modifier is used to adjust the pH, solubilise the peptides and minimise ionic interactions between the peptides and the stationary phase. Commonly trifluoroacetic acid is chosen since it gives high-resolution separation and is volatile and thus easily removed [200,201]. Peptides are detected in the eluant using an ultraviolet (UV) detector at a wavelength of 214 nm, corresponding to the $\pi \rightarrow \pi^*$ transition of the

CO bond [203]. Finally, acetonitrile is generally employed as the organic solvent due to its low viscosity and high UV transparency.

2.4.2 Sequence Specific Fragmentation of Peptides

The primary sequence of peptides can be determined by analysing the production of daughter ions which occur as a result of CID. Peptides undergo many fragmentation processes during the course of an MS/MS experiment. Several characteristic fragmentations are observed for linear peptides in the positive ion mode, however simple B and Y+2 cleavage patterns are commonly considered for sequence determination [155,157,204,205]. The amide bond is cleaved during both processes between carbon and nitrogen, with the positive charge being retained on the N- and C-terminal portions for the B and Y+2 pathways respectively (Figure 2.4).
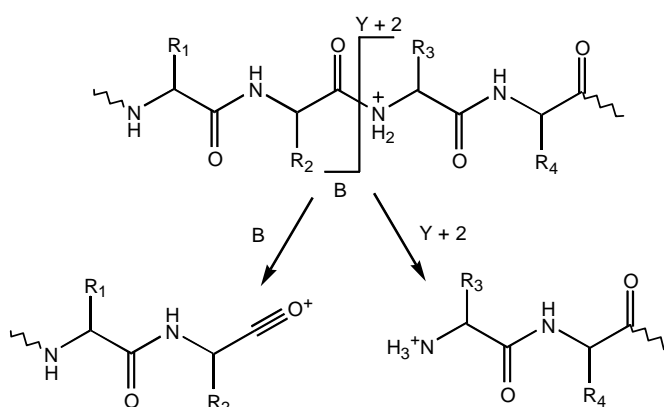
Figure 2.4: Characteristic fragmentation of linear peptides in the positive ion mode.

The additional proton responsible for initiating fragmentation may be localised at any one of the amide bonds. As a result of this heterogenous population of precursor ions, an array of peptide bonds are cleaved to give a complementary series of Y- and B-type ions, with the distinctive mass differences allowing for identification of sequential amino acid residues [155,204]. For the case of B cleavages structural information is obtained from the C-terminus, while Y+2 fragmentation allows for characterisation of the peptide from the N-terminal end.

Fragmentation is not equally likely along the entire length of the peptide backbone [206]. For example, cleavage between the two N-terminal amino acids is energetically unfavourable, and hence the first B ion in the series is often not observed [187]. Fragmentation of the peptide bonds N-terminal to Pro are particularly prevalent since this residue contains a tertiary nitrogen which is comparatively basic, and hence more likely to be protonated [207]. Additionally, dominant cleavage will occur C-terminal to both Asp and Glu, since these residues have acidic side chains that provide a local mobile proton capable of catalysing bond cleavage in this position [206]. Finally, the presence of basic amino acids at or near the C-terminus favours formation of Y+2 fragment ions [204].

2.4.3 Enzymatic Cleavage

Mass spectrometry is sometimes unable to determine the full sequence of a peptide, and more often a protein, due to incomplete fragmentation of the parent ion. In such cases endoproteases can be used to carry out digestion into smaller, more readily sequenced segments, which can then be pieced together to provide missing information [208-210].

In addition, endoproteinase Lys-C, isolated from the bacterial species *Lysobacter enzymogenes* [211], can be used to differentiate between isobaric Lys and Gln. This enzyme cleaves the peptide at the carboxyl side of the Lys residue (Figure 2.5), hence the number and mass of the resulting fragments can be used to determine the number and position of Lys residues in the peptide [212].
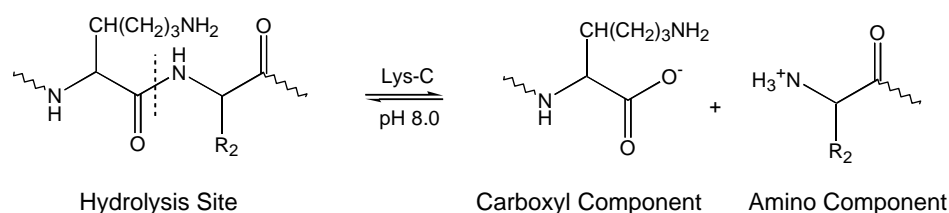
Figure 2.5: Peptide digestion by Lys-C.

2.4.4 Post-Translational Modifications

Post-translational modifications are chemical processing events that alter the properties of a peptide or protein after its translation, either by addition of a modifying functional group or by proteolytic cleavage. These can include conversion of N-terminal Glu to pyroglutamate, phosphorylation, acetylation and glycosylation, formation of disulfide bonds and isomerisation of L-amino acids to the D form [12-14]. In most cases these modifications have been found to be an essential requirement for activity. Because most covalent modifications change the molecular weight of the amino acid involved, mass spectrometry is the most useful method for their detection and identification [213].

C-terminal amidation is a common post-translational modification of bioactive peptides, with physiological activity often diminished by replacement with the analogous acid [214-216]. It is therefore essential when investigating peptide structure to differentiate between C-terminal amides and acids. The first B cleavage ion can be used to identify whether the peptide is a free carboxylic acid (loss of 18 Da from the MH^+ species) or has been post-translationally modified to the amide (loss of 17 Da from the MH^+ species). Another approach involves formation of the corresponding methyl ester and subsequent analysis by mass spectrometry. An increase of 14 Da from the parent peptide is indicative of a carboxylic acid, while an amide group will show an increase of 15 Da on methylation (Figure 2.6).
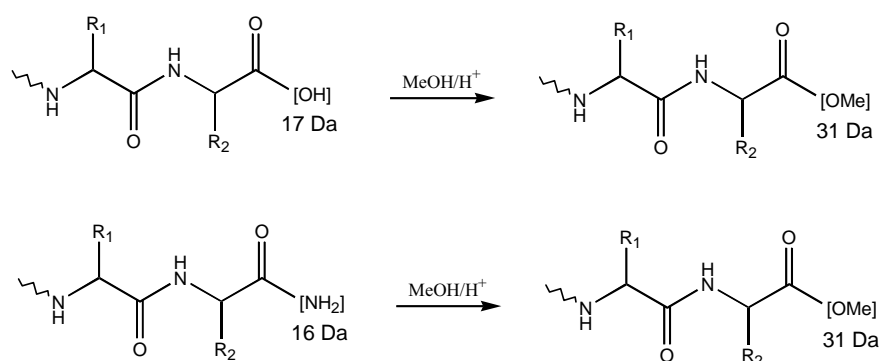
Figure 2.6: Differentiation of acid and amide functionality by formation of a methyl ester.

Consequently, the overall mass difference between the parent peptide and the resultant methylated peptide indicates the number of CO_2H and $CONH_2$ groups present and hence the C-terminal end group can be elucidated. Furthermore, this method is also useful for differentiating between Lys and Gln in a peptide. Gln, an amide, will show an increase of 15 Da on methylation, while Lys will remain unchanged.

Sulfation is the most abundant post-translational modification of Tyr residues and occurs in many biologically active peptides and proteins [217,218]. The SO_3 functionality is generally cleaved from Tyr in the acidic conditions encountered during positive ion spectra acquisition, and the $[MH-(SO_3)]^+$ signal is typically the base peak in the spectrum. Instead, the presence of a sulfated Tyr residue can be established by negative ion mass spectrometry, in which an $[M-H]^-$ peak as well as a pronounced $[(M-H)-(SO_3)]^-$ peak are observed.

2.4.5 Edman Sequencing

A major limitation of positive ion mass spectrometry for protein sequencing is the inability to differentiate between the isomeric residues Leu and Ile (113 Da) and, to a lesser extent, the isobaric residues Lys and Gln (128 Da). For this reason it is often coupled with complementary techniques such as Edman degradation to provide supporting sequence information. Edman sequencing utilises a fixed cycle of standard chemical reactions to allow removal and identification of successive N-terminal amino acid residues [210,219,220]. The peptide is bound to a solid membrane support, and in each cycle of the sequencing process the free N-terminal amine group is reacted with phenylisothiocyanate to yield a phenylthiocarbamoyl derivative. This is subsequently treated with a strong acid to afford a phenylthiohydantoin, with concomitant cleavage of the amide bond (Figure 2.7). The resulting hydantoin is subjected to HPLC and identified based on the known retention times for each common amino acid, while the new N-terminal residue can then be reacted and characterised, and the cycle continued.
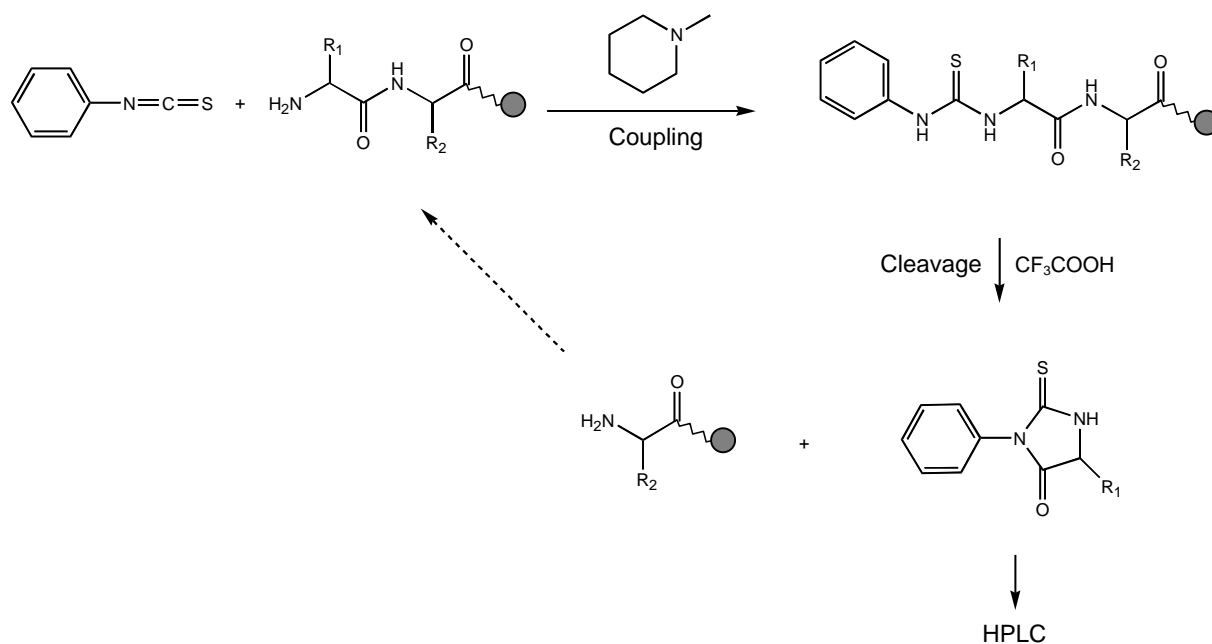
Figure 2.7: Edman sequencing reaction scheme.

This method of stepwise degradation and identification is very sensitive (picomolar range) and can be automated to allow efficient sequencing of the peptide [220]. However, Edman sequencing is not suitable for primary structure determination alone [204,221]. Each cycle is susceptible to contamination as the degradation reactions may not to go to completion, sometimes making conclusive sequencing difficult. Peptides with blocked N-terminal ends such as pyroglutamate residues are unsuitable for sequencing as initial phenylthiocarbamoyl derivatisation is prevented. In addition, amino acid identification is reliant on known HPLC retention times, and hence uncommon or modified amino acids are not suited to this approach. Finally, as the peptide decreases in size there is an increased risk of it being washed from the solid support, thereby missing terminal information. Despite these weaknesses, the complementary nature of Edman sequencing and mass spectrometry are such that, in combination, effective peptide sequencing is achievable.

2.5 ESI-MS of Protein Complexes

The current wealth of information arising from the field of proteomics is principally directed toward identifying protein molecular masses and primary structure. However, cellular processes are often triggered by weak interactions between proteins and binding partners such as DNA, RNA, lipids, polysaccharides, small ligands and other protein or peptide cofactors [9,10,186,222]. Thus, while protein-protein and other protein complexes are recognised to be critical for normal cell activity, relatively little is known about these macromolecular structures and their relation to protein function. It is therefore of great interest and significance that these complexes are investigated.

Non-covalently bound protein complexes are typically maintained by a number of weak, transient interactions, the most significant of which are hydrogen bonding, electrostatic and hydrophobic interactions, and van der Waals forces [186,189]. In order to study such complexes, it is critically important that these interactions are maintained during the course of analysis. A distinctive feature of the ESI method is that the conditions can be controlled in order to produce peptides and proteins in the gas phase that appear to retain aspects of their solution phase structure and non-covalent associations [186,189,223,224]. The stoichiometry, stability of a complex, the types of non-covalent interactions involved, and the conformational changes upon binding are all important when considering the mechanism of action of biomolecular assemblies, and are all amenable to study by ESI-MS.

Evidence for the detection of weakly bound complexes by ESI-MS occurred early in the development of this method somewhat serendipitously, with the identification of salt and solvent adducts [175,225], protein aggregates [226] and functional complexes [225,227]. Since the first two papers describing ESI-MS as a tool for the observation of specific non-covalent interactions [228,229], a vast array of literature has demonstrated its utility for the study of a range of protein complexes in the gas phase. These topics have been reviewed extensively [186,222,230-235].

However, the detection of intact non-covalent complexes by this method is largely dependent on factors including solution pH, the presence of organic solvents and buffer additives, cone and capillary voltages, source temperature and sample flow rate

[186,188,222]. Therefore, the successful study of these species depends on carefully controlled solvent systems, instrumental parameters and data interpretation.

2.5.1 Validity of Gas Phase Measurements

Although ESI-MS can provide important information regarding non-covalent complexes, the validity of the mass spectrometric data must be questioned. For instance, how does the ESI process affect the way in which these molecules interact on a structural level? Following this, do the relative abundances of the various ions in the gas phase reflect the solution phase characteristics?

In general, there is good correlation between ESI-MS data and that which is expected from solution phase studies. For example, native and denatured proteins can be distinguished when sampled from their corresponding equilibrium solutions, even though solvent evaporation might ordinarily be expected to affect higher order structures [198,236,237]. In addition, the CID spectrum of a small cyclic polypeptide was found to show a direct relationship to its solution structure [223]. Other studies have found the dissociation behaviour of non-covalent complexes in the gas phase to be a good representation of solution phase stabilities [224,238]. Finally, the strongest evidence is found in stoichiometric determination and measurement of relative abundances, which show a high degree of consistency between the solution and gas phases [186,239,240].

Despite these correlations, it is now widely accepted that the nature of the interactions responsible for maintaining multimeric assemblies plays a major role in the 'success' of an ESI-MS experiment. Specifically, ionic interactions appear to be strengthened *in vacuo*, giving an overstated measure of binding strength [186,241-243]. Conversely, hydrophobic interactions are typically unaffected or weakened by the ionisation process. In such cases, binding affinities measured by ESI-MS may again not relate well to the solution phase [243,244]. The closest agreement between solution and gas phase data appears to arise for larger complexes, which are stabilised by a greater number of non-covalent interactions [235,245].

Quantitative ESI-MS data interpretation also suffers from a number of imposed assumptions. In particular, the equilibrium between bound and unbound states is assumed to be unaffected by the ESI process, which may not always be valid [246,247]. Additionally, the ionisation efficiencies of the host and complexes are assumed to be identical. In practice this is only expected if the host is much heavier than the guest ligand [247]. For these reasons it is necessary to interpret the data obtained from ESI-MS experiments with caution, and limit its use for the study of non-covalent complexes that have been well characterised in solution.

2.5.2 Solvent Systems

The successful analysis of non-covalent complexes requires preservation of the native state of the protein, and is typically accomplished using buffered aqueous solvents at neutral pH [186,222]. However, the traditional buffers used in protein biochemistry are generally unsuitable for ESI-MS since they lead to the formation of protein adducts in the gas phase [175,225,248]. Instead, ammonium acetate (NH_4OAc), and to a lesser extent ammonium bicarbonate, are the most commonly used solvent systems. When dissolved in water, NH_4OAc gives a pH of approximately 6.8, which is conveniently close to physiological pH. However, the role of NH_4OAc in solution lies not with its ability to act as a buffer, but rather to provide NH_4^+ ions for the protonation of basic side chains in the protein [180,249]. Typically, the concentration of NH_4OAc used is at least 100 times greater than the concentration of protein, giving rise to an excess of NH_4^+ ions at the surface of the electrospray droplets [177].

The mechanism by which proteins are charged by NH_4OAc in positive ion ESI-MS has been summarised by Felitsyn *et al.* [177]. Briefly, a protein in this solution will have both its acidic and basic side chains ionised. In the source of the mass spectrometer, as the charged droplets reduce in size through desolvation, the side chains will become neutralised by interaction with counter ions in the evaporating solvent.

Thus, the following reactions can be observed;

$$Protein....NH_3^+ + {}^-OAc \rightarrow Protein....NH_2 + HOAc$$
$$Protein....CO_2^- + NH_4^+ \rightarrow Protein....CO_2H + NH_3$$
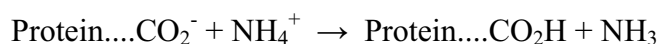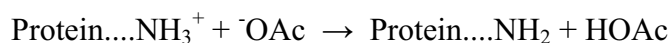
Near gas phase conditions prevail as solvent evaporation continues, and the charging of basic groups then takes place by the NH_4^+ ions at the droplet surface. This is thought to occur via a two-step pathway whereby stable proton-bridged adducts are formed initally, as shown below;

$$Protein....NH_2 + NH_4^+ \rightarrow Protein....NH_2\text{-}H\text{-}NH_3^+$$
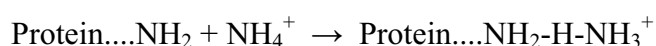
Later in the desolvation process, either in the heated capillary or in the CID stage, side chain protonation is subsequently completed as follows;

$$Protein....NH_2\text{-}H\text{-}NH_3^+ \rightarrow Protein....NH_3^+ + NH_3$$
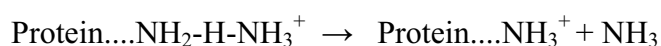
Any given protein will generally have enough basic residues at the surface to ensure its ionisation [180], and a number of studies have investigated the relationship between molecular mass and the maximum observed charge state [250,251]. In addition, HOAc and NH_3 adducts resulting from the neutralisation reactions are expected to be easily removed in the desolvation process, and hence are not observed in the mass spectrum [177].

2.5.3 Investigating Non-Covalent Binding Strength

The levels of free and complexed species can be quantified directly by ESI-MS from their relative abundances within the mass spectrum [252]. As a result, a number of methods exist using ESI-MS to quantitatively investigate the strength of the interactions that maintain non-covalent protein complexes. It should be stated however that these methods are based on a number of assumptions as discussed in Section 2.5.1, and thus are often used more so for the qualitative analysis of non-covalent binding.

The positive correlation between ESI-MS measurements and solution phase behaviour has led to the application of mass spectrometry for the determination of binding constants. One typical approach is to monitor the equilibrium of a host-guest pair by means of a solution phase titration [247,252,253]. Generally, the protein host concentration is kept constant while the guest ligand concentration is varied, and the intensity of the complex signal in an ESI-MS spectrum is quantified. The relative association or dissociation constants (K_D) can then be elucidated by forming a Scatchard plot, according to the equation;

$$\frac{[GH]}{[G_F][H]_0} = \frac{-1[GH]}{K_D[H]_0} + \frac{n}{K_D}$$

where n represents the stoichiometry of the complex and $[H]_0$ is the total host concentration. Plotting the ratio of bound [GH] over unbound guest $[G_F]$ against the concentration of bound guest gives a linear relationship with a slope of $-1/K_D$ [247].

Competition methods can also be employed for the study of binding affinities, whereby the propensity for different host and guest molecules to form complexes is measured simultaneously. For instance, the sample under investigation may contain a number of different hosts competing for one guest, or one host and a number of different guests competing for a binding site [228,239,243,247]. Relative binding affinities can be determined rapidly by noting the proportion of observed complexes in the resulting spectra. In addition, procedures have been devised to allow for the absolute binding constants of different host-guests complexes to be measured by competition studies [254,255].

The gas phase stability and structure of the non-covalent protein assemblies can be probed by inducing decomposition of the complexes. This can be achieved in a number of ways. The simplest approach involves manipulation of variables in the atmosphere-vacuum interface region [256], for example, increasing the temperature of the inlet capillary allows for thermally induced dissociation [257,258]. 'In source' CID can also be applied, in which the cone voltage is increased at the source-analyser interface of the

mass spectrometer. This voltage determines the kinetic energy of the ions, and thus the excitation when it collides with other gaseous molecules [247,256,259]. Finally, conventional CID can be also be used to induce unimolecular decomposition of mass selected ions [256,260]. These dissociation experiments can confirm the non-covalent nature of association, based on the ease with which the complexes decay. In addition, it is possible to obtain direct information about the composition and subunit stoichiometry of a complex by first observing the intact gaseous assembly and subsequently the liberated subunits. Both conventional and in source CID experiments also allow for investigation of the energetics of gas-phase dissociation. For example, the gas phase stability can be related to either threshold dissociation energies/voltages, or the collision energy/cone voltage required to achieve 50% dissociation of the complex [224,238,257,260].

2.5.4 Hydrogen-Deuterium Exchange

In combination with hydrogen-deuterium (H/D) exchange, mass spectrometry is now well developed for the study of secondary structure in both isolated proteins and non-covalent complexes. By this method, not only is it possible to investigate the stoichiometry and stability of a protein complex, but also the binding induced conformational dynamics and subunit interfaces.

Of the many exchangeable hydrogens present in a protein, only those located on peptide amide linkages are used for H/D exchange studies, since those on amino acid side chains or at the C- and N-terminus exchange too rapidly to be observed in a meaningful way [261,262]. In D_2O, the amide exchange reaction rate is minimal in the pH range of 2-3. Below this, exchange occurs via proton addition catalysed by D_3O^+, while above this pH, OD^- predominantly catalyses proton abstraction [263]. In addition, this process is temperature dependent, with exchange rates decreasing by a factor of 10 as the temperature is reduced from 25 to 0 °C [264]. Generally, at pH 2-3 and 0 °C, commonly referred to as 'quench conditions', the half-life for amide hydrogen isotopic exchange in an unstructured peptide is 30-120 minutes [261,265].

The general procedure for studying amide H/D exchange by ESI-MS is initiated by incubating the sample of interest in D_2O. At a series of time points the pH and temperature is decreased, effectively trapping the deuterium label onto the amide group. Importantly, other exchangeable protons exhibit relatively fast back-exchange, and hence the observed deuterium resides selectively on the backbone amide [262]. The level of deuterium incorporated into the intact protein can be determined by the change in molecular mass as a function of time, whereby the molecular mass is calculated from the centroid of the isotope mass envelope [264].

Amide H/D exchange kinetics may vary dramatically within a protein due to features such as hydrogen bonding, solvent accessibility and backbone flexibility. Although side chain effects can alter the amide exchange rates by up to tenfold [265,266], higher order structural features may decrease this exchange by a factor as large as 10^8 [261]. It is a consequence of this significant decrease in exchange rate for a structured peptide or protein that makes H/D exchange a sensitive probe for monitoring conformational changes and dynamic processes. H/D exchange is expected to dominate for amide hydrogens located near the surface or open channels within a protein, however even protons that are buried can exchange at a slower rate through fluctuations in the molecule that allow transient solvent access [263,267]. In addition, amide protons directly involved in hydrogen bonding can take anywhere from hours to weeks to exchange [268], and thus NH exchange rates can indicate regions of defined secondary structure.

For these reasons, H/D exchange mass spectrometry can be used to probe sites for molecular interaction, particularly for non-covalent complexes. In many cases, binding interfaces can be identified by reduction in exchange rates based on the steric exclusion of solvent [269-271]. These methods have also found extensive use for the resolution of structural motifs in native protein states, as well as the dynamics and mechanisms involved in protein folding [272-277].

~ CHAPTER 3 ~

Investigating the Skin Secretion of an Interspecific Hybrid Tree Frog

3.1 Introduction

3.1.1 Hybridisation

The role of hybridisation in evolution has been one of the most controversial topics in the field of evolutionary study. To date natural hybridisation and introgression have been credited with varying levels of importance in regards to the genetic makeup and evolutionary history of species complexes. Traditionally, hybridisation has been viewed as an unimportant evolutionary process, however studies documenting the production of viable hybrid genotypes are becoming increasingly common [278-280]. As a result, the idea that hybridisation is a potentially creative evolutionary pathway has gained support in recent times.

An operational description of hybridisation that does not require subjective determination of a species has been given by Woodruff [281]. Here it is defined as 'the interbreeding of individuals from two populations, or groups of populations, which are distinguishable on the basis of one or more heritable characters such as morphological, ecological, physiological and ethological features'. Similarly, introgression can be defined as 'the transfer of genetic material between hybridising taxa through backcrossing' [282]. Hybridisation is generally thought to be the result of occasional breakdown of reproductive isolating mechanisms, permitting the crossing of individuals that differ from each other genetically and taxonomically [279,283]. Introgressive hybridisation occurs frequently in the plant kingdom, however is comparatively less common amongst higher order animals [283,284].

The view that natural hybridisation is unimportant for evolution is largely based on the observation that crosses between divergent lineages commonly give rise to offspring with decreased levels of viability or potential to reproduce [278,280]. However, despite

the apparent rarity of 'successful' hybrids in nature, a growing body of literature suggests aspects of the evolutionary significance of hybridisation can be quite extensive. Differential fitness between hybrid and parental genotypes plays a critical role in explaining the maintenance of natural hybrid zones, as well as the production of novel genetic variation that may lead to diversification [279,280,283,285].

In the extremes, total introgression may give rise to merging of the hybridising taxa [282,286], while if hybrids are less fit than the parents, the prezygotic reproductive barriers may be reinforced by selection for conspecific mating [287]. In contrast, the creative potential of hybridisation relies on the production of recombinant genotypes that are fitter than one or both parents, at least in some environments. In such cases natural hybridisation can lead to adaptation and speciation in one of two ways. Firstly, the transfer of adaptations from one taxon into another may allow for the expansion of the introgressed form into a new habitat [278,282,288]. Alternatively, if hybrids between two species were able to form a third species coexisting with the parentals, this would be the beginning of speciation by hybridisation [283,284,289,290].

While the evolutionary significance of hybridisation will remain contentious, in any event it provides a setting for the study of genetics and speciation.

3.1.2 Amphibian Hybrids

Many species of amphibians hybridise naturally, with some forming extensive zones of hybridisation. For instance, a number of hybrids have been observed in species of salamanders [291-295] and toads [296-298]. In addition, natural hybridisation occurs among more than two dozen species of North American leopard frogs of the *Rana pipiens* complex [299], and several hybrid zones exist in anurans from southern and especially south-eastern Australia, incorporating the Hylidae and Leptodactylidae families present there [300]. Frogs are one of the few vertebrate groups in which hybridogenetic species are known, i.e. species of hybrid origin from closely related sexually reproducing species that backcross to one of the parent taxa to reconstitute the first generation (F_1) hybrid state. The *Rana esculenta* complex is the best studied

example of this, and has hybrid origins arising from *Rana ridibunda* and *Rana esculenta* [301,302].

The characteristics of amphibian populations separated by hybrid zones may differ to a varying extent. For example, the *R. pipiens* complex contains a large number of species which are morphologically very similar [299]. In contrast, *Bombina maxima* and *Bombina verigata* differ in mating call, colouration and habitat, and have biochemical differences that suggest they have been diverging for 3-4 million years, yet despite this, they exhibit a significant hybrid zone throughout central Europe [298]. Traditionally, anuran hybrids have been discerned on the basis that they show characteristics intermediate between parental types. For instance, in some interspecific hybrids of *Bufo* toads, mating calls and morphology appear partially representative of both parents [297]. However, in some cases amphibian hybrids are not morphologically intermediate [303,304]. In such situations these hybrids may only be distinguished from the parental species by analysis of genetic markers, whose inheritance is presumably independent of the morphological traits [303].

It is these genetic markers that make hybrids or hybrid taxa suitable for studying the heritable nature of a number of physiological characteristics, and the control of gene expression. Bioactive peptides from anuran skin are able to diverge more rapidly than the physical and biological features of the animal [28], however regulation and expression of genes encoding amphibian skin peptides remains largely unexplored. Recent studies of the skin peptide profiles of *Rana esculenta* have either examined only the hybridogen and not the parent taxa [305], or have pooled samples obscuring any possible individual variations [306]. The potential for skin peptides to be under strong local selection pressures because of their roles in host defence [58], and in some cases a sex pheromone role [60], could contribute significantly to steep selection gradients that maintain hybrid zones in nature. If skin peptide profiles are to be useful in investigating the biology of interspecific hybrid amphibians, the pattern of their expression must be understood.

3.1.3 *Litoria caerulea*

The White's tree frog (*Litoria caerulea)* is native to Australia and southern New Guinea, and can be found in a large area across the northern and eastern parts of Australia (Figure 3.1) [307]. These frogs tend to be light blue-green to emerald green dorsally, with scattered white or gold spots on the side and occasionally on the back, and are large in size ranging from 70-110 mm in length (Figure 3.1). *L. caerulea* is usually found within heavy foliaged creepers and similar vegetation, which can often be a considerable distance from water [308].
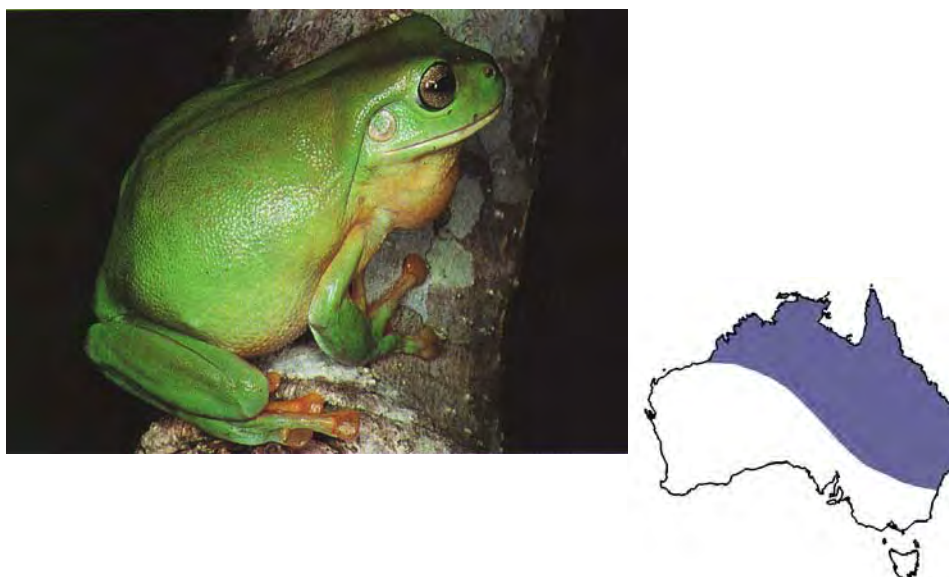
Figure 3.1: Appearance and geographical distribution of *Litoria caerulea* [57].

The skin secretion of *L. caerulea* has been investigated extensively, and to date 26 peptides have been reported from different populations of this species with 19 belonging to the caerin family [42,66,86]. A summary of the peptides isolated from *L. caerulea* is given in Table 3.1.

Table 3.1: Peptide components of the skin secretion from *Litoria caerulea*.

Peptide	Sequence	MH$^+$
Caerin 1.1	GLLSVLGSVAKHVLPHVVPVIAEHL-NH$_2$	2582
Caerin 1.2	GLLGVLGSVAKHVLPHVVPVIAEHL-NH$_2$	2552
Caerin 1.3	GLLSVLGSVAQHVLPHVVPVIAEHL-NH$_2$	2582
Caerin 1.4	GLLSSLSSVAKHVLPHVVPVIAEHL-NH$_2$	2600
Caerin 1.5	GLLSVLGSVVKHVIPHVVPVIAEHL-NH$_2$	2610
Caerin 1.20	GLFGILGSVAKHVLPHVIPVVAEHL-NH$_2$	2600
Caerin 2.2	GLVSSIGRALGGLLADVVKSKEQPA-OH	2464
Caerin 2.3 (Splendipherin)	GLVSSIGKALGGLLADVVKSKGQPA-OH	2364
Caerin 2.4	GLVSSIGKALGGLLADVVKTKEQPA-OH	2450
Caerin 3.2	GLWEKIKEKASELVSGIVEGVK-NH$_2$	2397
Caerin 3.3	GLWEKIKEKANELVSGIVEGVK-NH$_2$	2424
Caerin 3.4	GLWEKIREKANELVSGIVEGVK-NH$_2$	2452
Caerin 3.5	GLWEKVKEKANELVSGIVEGVK-NH$_2$	2410
Caerin 4.1	GLWQKIKSAAGDLASGIVEGIKS-NH$_2$	2326
Caerin 4.2	GLWQKIKSAAGDLASGIVEAIKS-NH$_2$	2340
Caerin 4.3	GLWQKIKQAAGDLASGIVEGIKS-NH$_2$	2353
Caerulein	pEQDY(SO$_3$)TGWMDF-NH$_2$	1352
Caeridin 1	GLLDGLLGTLGL-NH$_2$	1140
Caeridin 2	GLLDVVGNLLGGLGL-NH$_2$	1408
Caeridin 3	GLFDAIGNLLGGLGL-NH$_2$	1428
Caeridin 4	GLLDVVFNVLHSLGL-NH$_2$	1504
Caeridin 5	GLLGMVGSLLGGLGL-NH$_2$	1355
Caeridin 6	GLLGFVGSLLGGLGI-NH$_2$	1371

Caerulein is a major component in the skin secretion of most of the *Litoria* species, as well as certain South American and African frogs [16,38,58]. It is a potent neuropeptide, and can contract smooth muscle at better than nanomolar concentrations, enhance blood circulation, modify satiety, sedation and thermoregulation, and is reported to be several thousand times more effective as an analgesic than morphine [19,83,84].

The caerin 1 peptides are common to a number of species of the genus *Litoria* [58], and possess a broad spectrum of activity. For example, these peptides are wide-spectrum antibiotics, anticancer agents, antiviral agents against viruses with envelopes, antifungal agents active against the chytrid fungus, are lethal towards nematodes and also inhibit the formation of nitric oxide from neuronal nitric oxide synthase (nNOS) [58,72,81].

Conversely, the caerins 2, 3 and 4 are narrow-spectrum antibiotics active against only a few of the microorganisms tested, typically *Escherichia coli* and *Micrococcus luteus* [58]. In addition, the caerin 2 peptides are also effective inhibitors of nNOS [58].

The activity of the caeridin peptides is yet to be elucidated, and hence their role in the amphibian skin remains unknown at this time [80]. The synthesis and storage of host-defence peptides comes at considerable metabolic cost to the animal [309], and therefore it is highly doubtful that the peptides produced would have no purpose. As a result, it is likely the function of the caeridin peptides will be determined with further biological testing.

The peptide profile for *L. caerulea* varies significantly depending on the geographical location of the animals collected [42], possibly as a result of predator or climate driven pressures. There appears to be two major populations of this species, one in the Northern Territory and the second along the eastern coastal region of Queensland. Of particular interest are the differences in peptide profiles noted between individuals at Darwin in the Northern Territory, and those at Melville Island (off the coast from Darwin). The ocean has separated these populations for only 10,000 years and hence this has important implications for the time frame of evolutionary change in these peptide profiles [42].

3.1.4 *Litoria splendida*

The magnificent tree frog (*Litoria splendida*) is a large species (males 88-104 mm, females 96-106 mm), characterised by a distinguishing gland that covers the entire dorsal surface of the head. It is a rich green in colour with small, scattered sulfur-coloured patches, whilst the backs of the thighs are yellow or orange (Figure 3.2) [57]. *L. splendida* is distributed throughout the northwest of Western Australia and the adjacent border of the Northern Territory (Figure 3.2), and is closely related to *L. caerulea*. During the day, the species enters caves or crevices beneath boulders or around buildings in the Kimberley region [57].
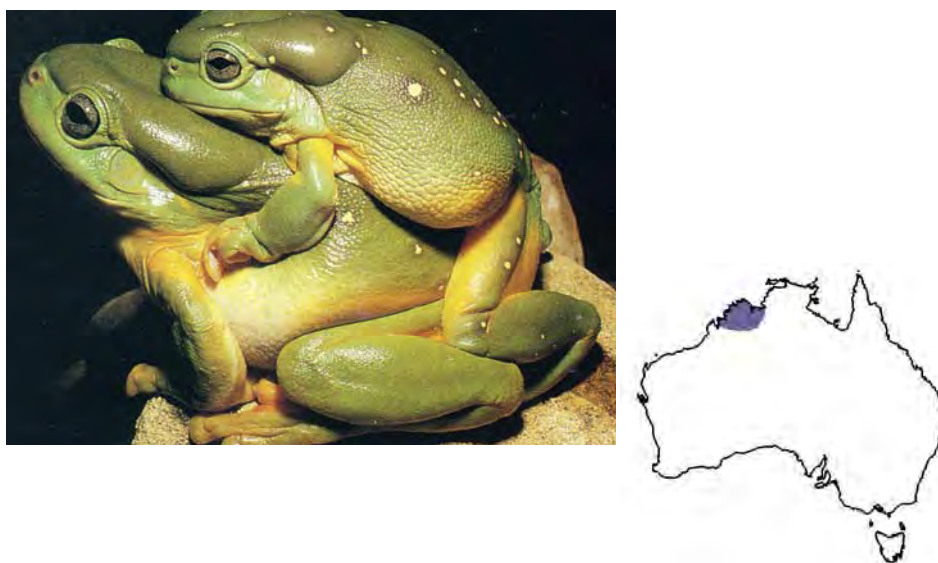
Figure 3.2: Appearance and geographical distribution of *Litoria splendida* [57].

The skin secretion of *L. splendida* has been investigated previously, and is the simplest observed for members of the *Litoria* genus studied to date [60,310,311]. A number of biologically active peptides have been identified, a summary of which is shown in Table 3.2. The peptide spectrum from this frog bears significant resemblance to that of *L. caerulea*, with six peptides conserved between the two species, and the remaining peptides showing considerable sequence similarity. This is not surprising given the close taxonomic relationship of the two species.

Table 3.2: Peptide components of the skin secretion from *Litoria splendida*.

Peptide	Sequence	MH$^+$
Caerin 1.1	GLLSVLGSVAKHVLPHVVPVIAEHL-NH$_2$	2582
Caerin 1.6	GLFSVLGAVAKHVLPHVVPVIAEKL-NH$_2$	2591
Caerin 1.10	GLLSVLGSVAKHVLPHVVPVIAEKL-NH$_2$	2573
Caerin 2.1	GLVSSIGRALGGLLADVVKSKGQPA-OH	2392
Caerin 2.3 (Splendipherin)	GLVSSIGKALGGLLADVVKSKGQPA-OH	2364
Caerin 3.1	GLWQKIKDKASELVSGIVEGVK-NH$_2$	2382
Caerulein	pEQDY(SO$_3$)TGWMDF-NH$_2$	1352
Phe8 Caerulein	pEQDY(SO$_3$)TGWFDF-NH$_2$	1368
Desulfated Caerulein	pEQDYTGFMDF-NH$_2$	1272
Caeridin 1	GLLDGLLGTLGL-NH$_2$	1140

Consistent seasonal variations are observed for the peptide component of the skin secretion from *L. splendida*. During the southern winter period from June through to August, the caerulein concentration decreases whilst formation of desulfated caerulein and Phe8 caerulein are noted. This is thought to play a role in thermoregulation during the inactive months [60]. Similarly, splendipherin is present as a minor peptide component in the skin secretion of male animals during the reproductive season only. Behavioural studies have demonstrated the ability of this peptide to attract female *L. splendida* at an optimum concentration range between 10^{-11} and 10^{-8} M, and in a species specific manner [60]. This peptide has therefore been identified as an aquatic sex pheromone, the first isolated from an anuran.

3.1.5 *Litoria caerulea - Litoria splendida* Hybrids

Despite overlapping natural distribution, there has been no evidence for hybridisation of *L. caerulea* and *L. splendida* in the wild [300]. However, a number of individuals from both species were kept in captivity in a single enclosure during the breeding period of these animals. Inadvertently, a single brood of hybrids was obtained, of which five female specimens reached adult maturity. Since the parental species are closely related, they are often of similar physical appearance. Thus it is not possible to conclusively identify the offspring as hybrids using morphological characteristics alone. Nevertheless, the physical appearance of the *L. caerulea - L. splendida* hybrids appears somewhat intermediate between both parents, with the blue-green colouring typical of *L. caerulea*, and the head-shape more like *L. splendida* (Figure 3.3).

While both parents seem to contribute genetically to the physical features of the hybrids, nothing is known about the way in which the peptide profile of the progeny relates to that of the parents. For example, is one species dominant over the other, imparting all of its peptides to the offspring? Or do the hybrids express a combination of peptides from both parental species?

Figure 3.3: Appearance of the *L. caerulea - L. splendida* hybrids.

In order to gain insight into the heritable nature of the dermal peptides, the primary aim of this project is to investigate the skin secretion of the *L. caerulea - L. splendida* hybrids. The research presented in this chapter details the isolation, sequencing and bioactivity of peptides from the hybrids, and compares the peptides found with those determined previously for the parental species. As these putative hybrids were bred fortuitously in an aquarium containing large numbers of females and males of both potential parent species whose geographic origin was not known, their pedigree is also established.

3.2 Results

3.2.1 Mitochondrial DNA Studies

Mitochondrial DNA (mtDNA) was extracted from tissue samples of two *L. caerulea - L. splendida* hybrid specimens, and 850 base pairs (bp) of the 12S ribosomal RNA (rRNA) gene were amplified and sequenced. Resulting sequences were aligned and compared to a database of 12S rRNA sequences containing representatives of the major Australian clades of *Litoria*. Phylogenetic analysis of the mitochondrial nucleotide sequences is presented in Figure 3.4.
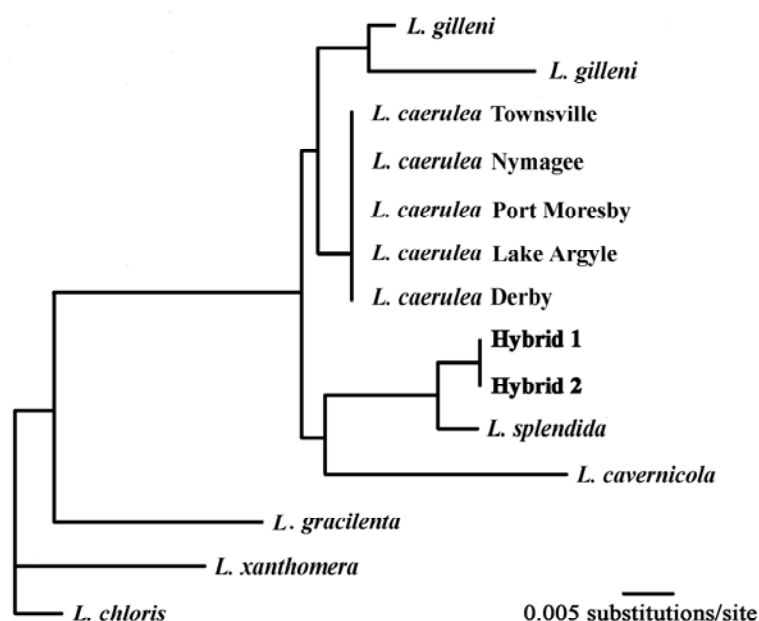
Figure 3.4:   Neighbour-joining tree showing relationships among mitochondrial nucleotide sequences of members of the *Litoria* genus and the *L. caerulea - L. splendida* hybrids.

The two hybrid samples demonstrate identical sequences over the 260 base pairs of aligned sequence available for all taxa, consistent with the animals being of the same brood. *L. caerulea* and *L. splendida* differ by 2.3% uncorrected sequence divergence. The hybrid samples exhibit approximately 2.3% sequence divergence from *L. caerulea* and 0.8% divergence from *L. splendida*. Clearly the maternal parent of the hybrid brood was *L. splendida*.

3.2.2 Peptide Isolation and Sequence Determination

Skin secretions from the five *L. caerulea - L. splendida* hybrids were collected using the SES technique [56], and the peptide components separated by application of HPLC. The secretions were investigated monthly over a nine-month period, from February through to October 2004. The peptide profiles of each hybrid were indistinguishable, and did not change over the period of investigation. A representative partial chromatogram is shown in Figure 3.5, where fractions of interest are labelled A-L. Fractions marked with an asterisk result from enzymatic degradation of the bioactive peptide components, and will not be discussed in detail here.
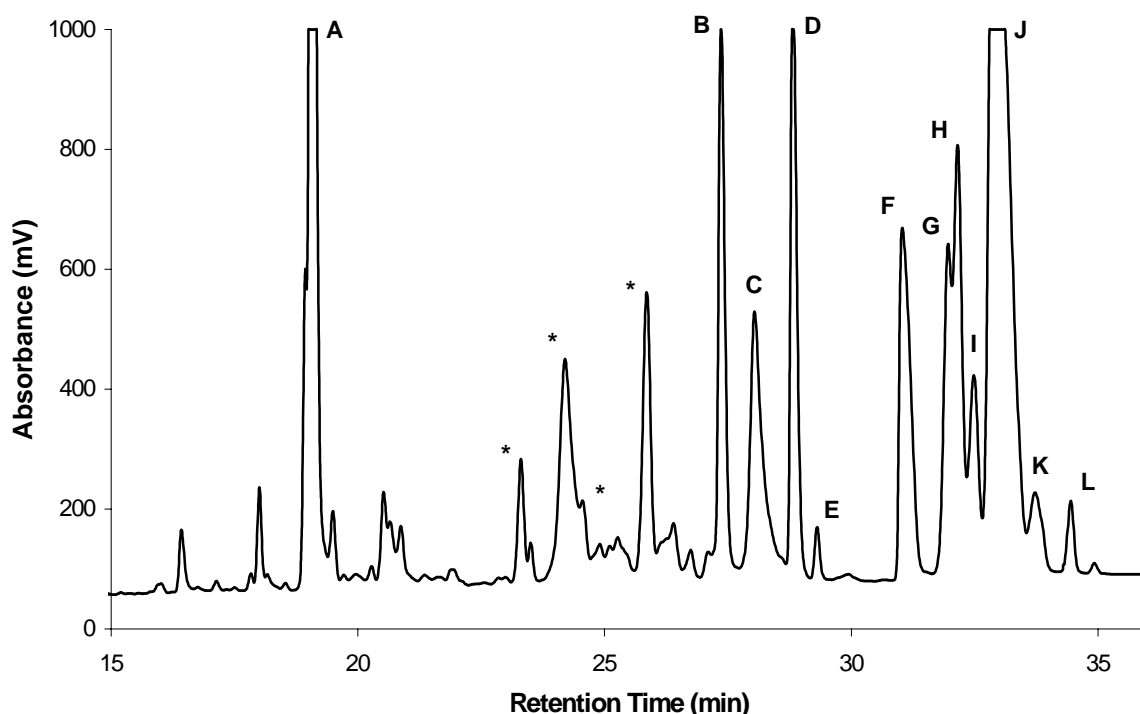
Figure 3.5: Partial HPLC chromatogram of the skin secretion from an *L. caerulea - L. splendida* hybrid (10-70% acetonitrile over 40 minutes). Fractions of interest are labelled A-L, while those marked with * are products of enzymatic degradation.

Fraction F was found to contain three peptide components, caerins 2.2, 2.6 and 2.7, and was thus submitted to further purification by HPLC. A gradient elution profile was employed, in which the acetonitrile content was increased from 33 to 38% over 50 minutes, and 0.5 mL fractions were collected over the period from 28 to 33 minutes (Figure 3.6). This allowed for partial resolution of the peptides, since caerin 2.6 and 2.7 co-eluted in the early fractions (labelled F1), while caerin 2.2 eluted later (labelled F2).

Despite numerous attempts at separation by HPLC, caerins 2.6 and 2.7 could not be resolved. Consequently, these peptides underwent structural analysis collectively.
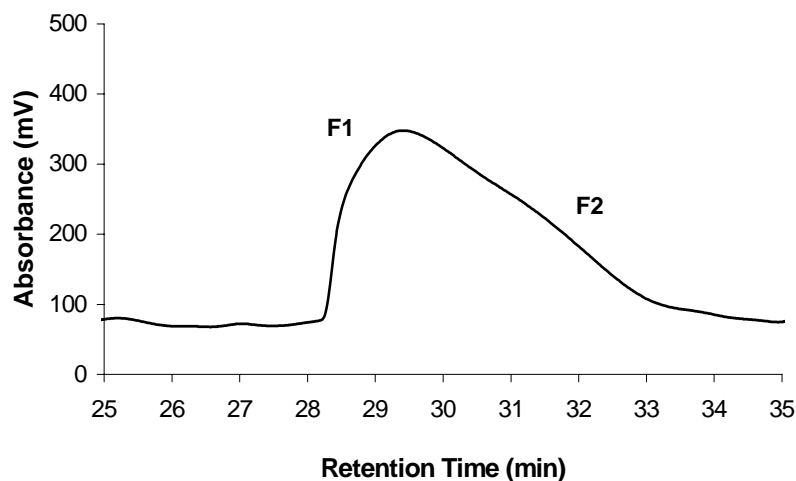
Figure 3.6: Partial HPLC chromatogram of fraction F (33-38% acetonitrile over 50 minutes). Fractions of interest are labelled F1 and F2.

The peptides isolated after HPLC were sequenced by mass spectrometry, using the tandem MS capabilities of a Q-TOF 2 mass spectrometer. MS/MS spectra were acquired in the positive ion mode, with characteristic B and Y+2 fragmentations used to assign the majority of the sequence. Lys and Gln residues were distinguished based on the results of Lys-C digest and methylation experiments. Automated Edman sequencing was employed for all novel peptides to allow for differentiation of isomeric Leu and Ile, and assisted in overall confirmation of the primary sequence. Where Lys/Gln or Leu/Ile are present, the correct residue is always shown in the text. The accuracy of the Q-TOF 2 is such that the C-terminal group could be identified from MS/MS spectra alone, however this was verified using methylation experiments for novel peptides. All masses given are nominal masses, i.e. equal to the sum of the integral masses of the amino acid constituents (Appendix A).

Three peptides have been identified which have not previously been observed in the skin secretion of either parent species, and the structure determination of each of these compounds will be described in detail in subsequent sections. Selected mass spectral sequencing data for the remaining peptides is given in Appendix B. A summary of all fourteen peptides characterised from the *L. caerulea - L. splendida* hybrids is found in Table 3.3.

Table 3.3: Peptides characterised from the skin secretion of the *L. caerulea - L. splendida* hybrids. * indicates the peptide is also present in the secretion of the parent species.

Peptide	HPLC	Sequence	MH^+	*L. caerulea*	*L. splendida*
Caerin 1.1	J	GLLSVLGSVAKHVLPHVVPVIAEHL-NH$_2$	2582	*	*
Caerin 1.6	I	GLFSVLGAVAKHVLPHVVPVIAEKL-NH$_2$	2591		*
Caerin 1.10	K	GLLSVLGSVAKHVLPHVVPVIAEKL-NH$_2$	2573		*
Caerin 1.20	G	GLFGILGSVAKHVLPHVIPVVAEHL-NH$_2$	2600	*	
Caerin 2.2	F2	GLVSSIGRALGGLLADVVKSKGQPA-OH	2464	*	
Caerin 2.6	F1	GLVSSIGKVLGGLLADVVKSKGQPA-OH	2392		
Caerin 2.7	F1	GLVSSIGKALGGLLVDVVKSKGQPA-OH	2392		
Caerin 3.1	D	GLWQKIKDKASELVSGIVEGVK-NH$_2$	2382		*
Caerin 3.5	B	GLWEKVKEKANELVSGIVEGVK-NH$_2$	2410	*	
Caerin 4.2	H	GLWQKIKSAAGDLASGIVEAIKS-NH$_2$	2340	*	
Caerin 5.1	C	AGILFGDVRPPWMPPPIFPEMV-OH	2535		
Caerulein	A	PEQDY(SO$_3$)TGWMDF-NH$_2$	1352	*	*
Caeridin 1	E	GLLDGLLGTLGL-NH$_2$	1140	*	*
Caeridin 5	L	GLLGMVGSLLGGLGL-NH$_2$	1355	*	

3.2.3 Caerin 2.6 and Caerin 2.7

Fraction F1 contains two peptide components, namely the isomers caerin 2.6 and 2.7. When analysed by ESI-MS a weak MH^+ ion is observed at *m/z* 2392, in addition to a pronounced $(M+2H)^{2+}$ species evident at *m/z* 1196.5. The MS/MS spectrum of the $(M+2H)^{2+}$ ion is given in Figure 3.7. Both B and Y+2 cleavages occur predominantly from the C-terminal end, and give partial sequences from this direction for both peptides.
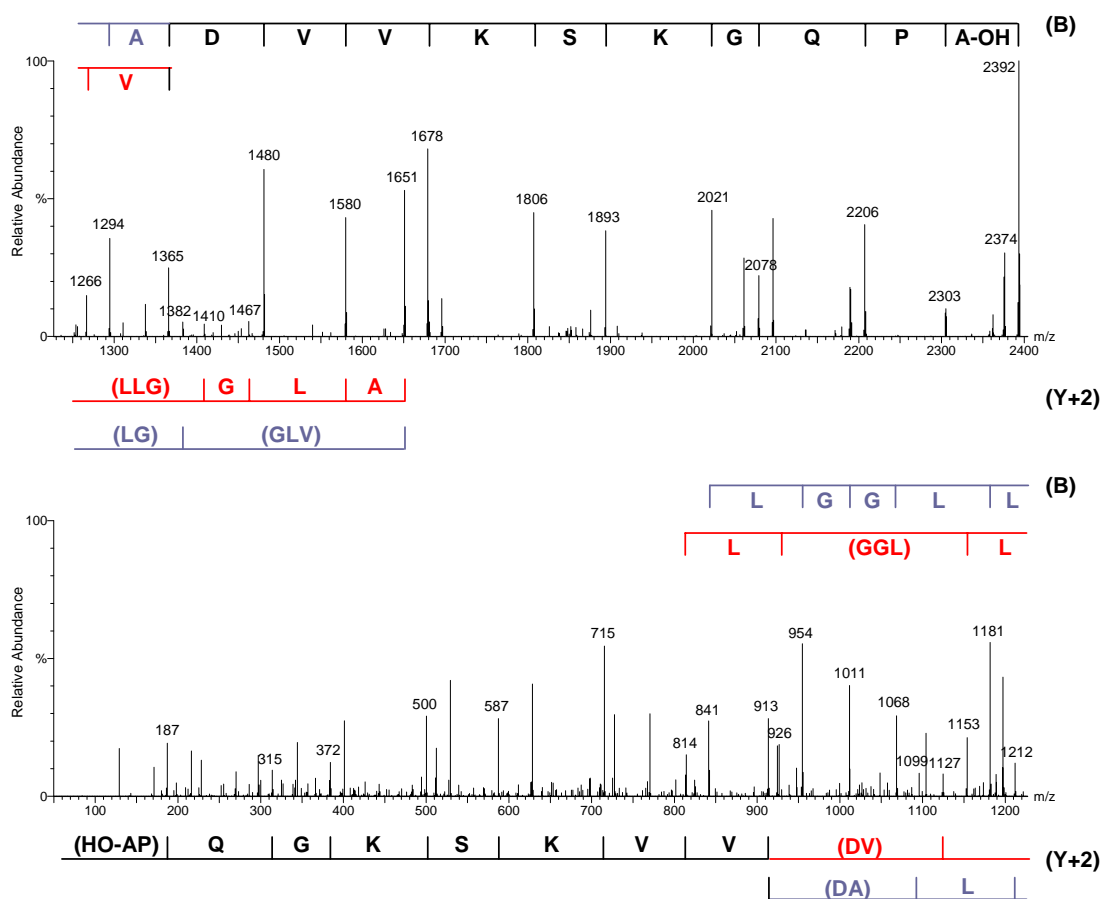
Figure 3.7: Collision induced MS/MS spectrum of the $(M+2H)^{2+}$ ion of caerin 2.6 and caerin 2.7 (m/z 1196.5). The sequence derived from the B cleavages is given above the spectrum, while that from the Y+2 cleavages is indicated below. Fragmentation unique to caerin 2.6 is shown in blue, while fragmentation unique to caerin 2.7 is shown in red. Magnification ranges: m/z 630-1480 (3x), 1500-2200 (3x), 2225-2380 (6x).

Digestion of caerins 2.6 and 2.7 by Lys-C gave rise to two peptide fragments with masses of 586 and 1823 Da, confirming the assignment of residue 19 as Lys. MS/MS data for the $(M+2H)^{2+}$ ion of the 1823 Da fragment is shown in Figure 3.8, and was sufficient to complete the primary structure determination of both caerin 2.6 and 2.7 (with the exception of differentiating between Ile/Leu and Lys/Gln). Additional Lys residues were confirmed by automated Edman sequencing, which established the identity of amino acids at positions 6 (Ile), 2, 10, 13, 14 (Leu), 8, 19, 21 (Lys) and 23 (Gln), and provided overall verification of the primary sequences.
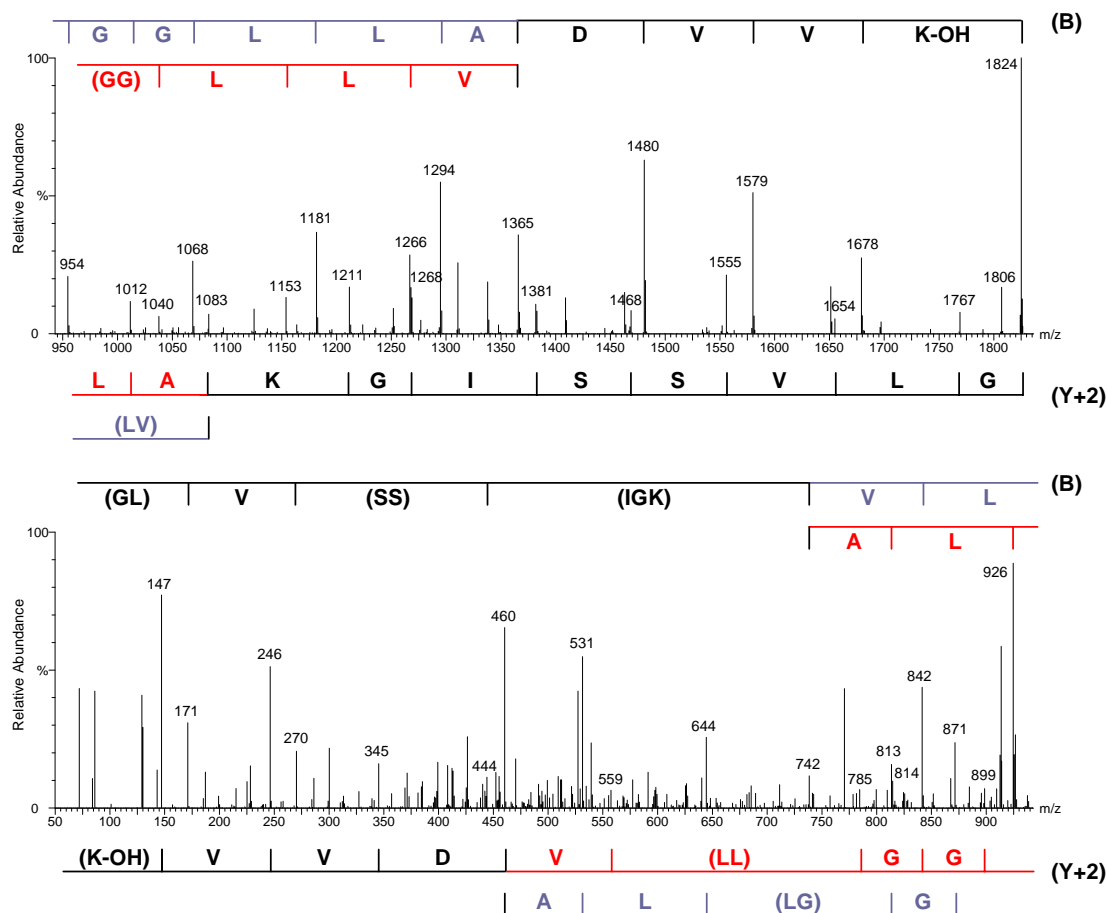
Figure 3.8: Collision induced MS/MS spectrum of the $(M+2H)^{2+}$ ion of caerin 2.6 and 2.7 Lys-C fragment (*m/z* 912.5). The sequence derived from the B cleavages is given above the spectrum, while that from the Y+2 cleavages is indicated below. Fragmentation unique to caerin 2.6 is shown in blue, while fragmentation unique to caerin 2.7 is shown in red. Magnification ranges: *m/z* 50-340 (2x), 350-950 (6x), 1210-1475 (4x), 1500-1810 (4x).

Methylation experiments yielded a methyl ester with a pronounced $(M+2H)^{2+}$ ion at *m/z* 1218, which corresponds to an increase of 43 Da and thus is indicative of one amide group and two acid groups. With Asp and Gln residues evident in the sequences, this implies the C-terminal groups of both caerin 2.6 and caerin 2.7 are carboxylic acids. The peak observed at *m/z* 2374 in the initial MS/MS spectrum occurs due to the loss of H_2O from the parent ion, and therefore is also consistent with C-terminal acid functionality. Mass spectral sequencing data for caerins 2.6 and 2.7 is summarised in Table 3.4.

Table 3.4: Mass spectral sequencing data for caerin 2.6 and caerin 2.7.

Fraction MH$^+$		Sequence Data
Caerin 2.6		
F1	**2392**	B ions	*m/z* 2374, 2303, 2206, 2078, 2021, 1893, 1806, 1678, 1579, 1480, 1365, 1294, 1181, 1068, 1011, 954, 841
			Leu Gly Gly Leu Leu Ala Asp Val Val Lys Ser Lys Gly Gln Pro Ala-OH
		Y+2 ions	*m/z* 1651, 1382, 1212, 1099, 913, 814, 715, 587, 500, 372, 315, 187
			(Val Leu Gly) (Gly Leu) Leu (Ala Asp) Val Val Lys Ser Lys Gly Gln (Pro Ala-OH)
Lys-C	**587**	B ions	*m/z* 569, 498, 401, 273, 216, 88
			Ser Lys Gly Gln Pro Ala-OH
		Y+2 ions	*m/z* 500, 372, 315, 187, 90
			Ser Lys Gly Gln Pro Ala-OH
	1824	B ions	*m/z* 1806, 1678, 1579, 1480, 1365, 1294, 1181, 1068, 1011, 954, 742, 444, 270, 171
			(Gly Leu) Val (Ser Ser) (Ile Gly Lys) Val Leu Gly Gly Leu Leu Ala Asp Val Val Lys-OH
		Y+2 ions	*m/z* 1767, 1654, 1555, 1468, 1381, 1268, 1211, 1083, 871, 814, 644, 531, 460, 345, 246, 147
			Gly Leu Val Ser Ser Ile Gly Lys (Val Leu) Gly (Gly Leu) Leu Ala Asp Val Val Lys-OH

Methylation - MH$^+$ 2435 (1 CONH$_2$ group and 2 CO$_2$H groups)

Fraction MH$^+$		Sequence Data
Caerin 2.7		
F1	**2392**	B ions	*m/z* 2374, 2303, 2206, 2078, 2021, 1893, 1806, 1678, 1579, 1480, 1365, 1266, 1153, 926, 813
			Leu (Gly Gly Leu) Leu Val Asp Val Val Lys Ser Lys Gly Gln Pro Ala-OH
		Y+2 ions	*m/z* 1651, 1580, 1467, 1410, 1127, 913, 814, 715, 587, 500, 372, 315, 187
			Ala Leu Gly (Gly Leu Leu) (Val Asp) Val Val Lys Ser Lys Gly Gln (Pro Ala-OH)
	587	B ions	*m/z* 569, 498, 401, 273, 216, 88
			Ser Lys Gly Gln Pro Ala-OH
		Y+2 ions	*m/z* 500, 372, 315, 187, 90
			Ser Lys Gly Gln Pro Ala-OH
	1824	B ions	*m/z* 1806, 1678, 1579, 1480, 1365, 1266, 1153, 1040, 926, 813, 742, 444, 270, 171
			(Gly Leu) Val (Ser Ser) (Ile Gly Lys) Ala Leu (Gly Gly) Leu Leu Ala Asp Val Val Lys-OH
		Y+2 ions	*m/z* 1767, 1654, 1555, 1468, 1381, 1268, 1211, 1012, 899, 842, 785, 559, 460, 345, 246, 147
			Gly Leu Val Ser Ser Ile Gly Lys Ala Leu Gly Gly (Leu Leu) Val Asp Val Val Lys-OH

Methylation - MH$^+$ 2435 (1 CONH$_2$ group and 2 CO$_2$H groups)

3.2.4 Caerin 5.1

Caerin 5.1 elutes in fraction C of the HPLC chromatogram, and gives rise to a weak MH[+] ion at *m/z* 2537 and an intense $(M+2H)^{2+}$ ion at *m/z* 1269 when analysed by ESI-MS. The collision induced mass spectrum of the $(M+2H)^{2+}$ ion of caerin 5.1 is shown in Figure 3.9.
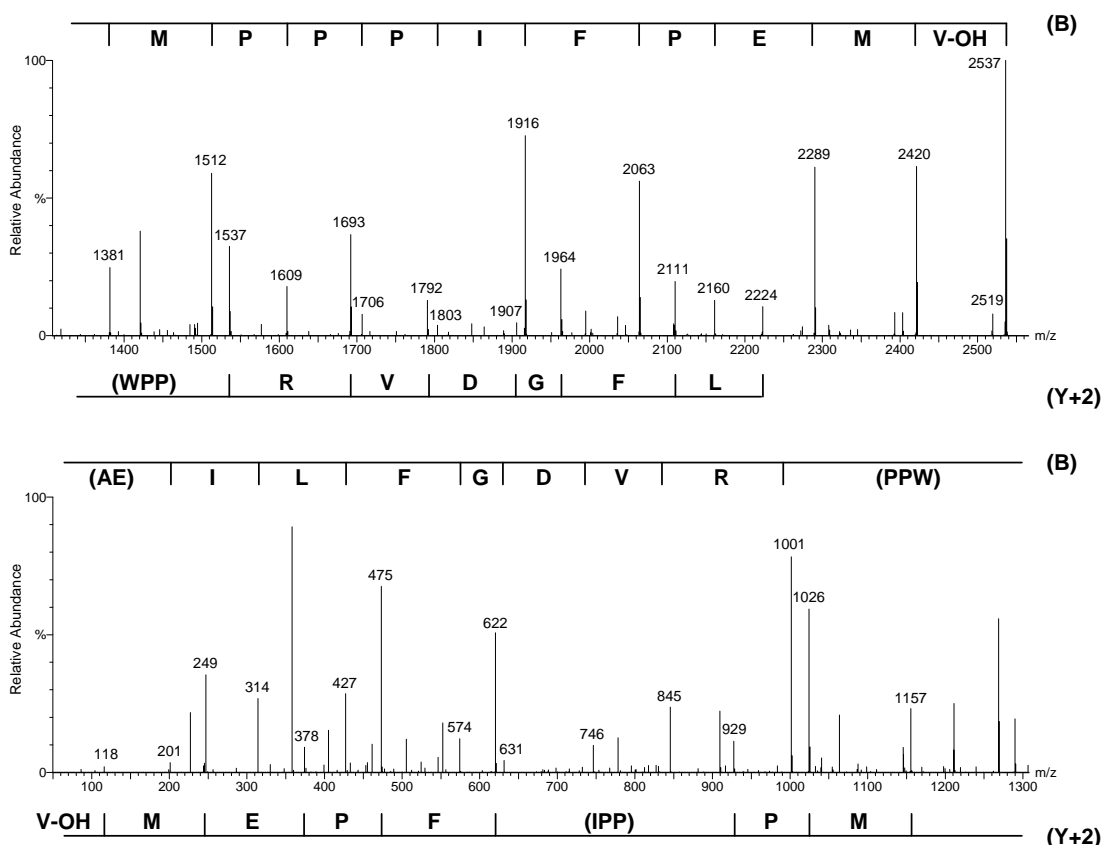
Figure 3.9: Collision induced MS/MS spectrum of the $(M+2H)^{2+}$ ion of caerin 5.1 (*m/z* 1269). The sequence derived from the B cleavages is given above the spectrum, while that from the Y+2 cleavages is indicated below. Magnification ranges: *m/z* 50-450 (4x), 1010-1500 (6x), 1550-2050 (4x), 2100-2400 (4x).

The series of B and Y+2 cleavages are essentially complete in this spectrum, and give the majority of the primary sequence. However, where fragmentation is accounted for by loss of multiple residues, the order of these remains ambiguous (i.e. residues 1-2 and 11-13). Methylation of caerin 5.1 gave rise to an ester with a pronounced $(M+2H)^{2+}$ ion at *m/z* 1297, representing a mass difference of 56 Da from the parent peptide, and is therefore indicative of four CO_2H groups. According to the MS/MS data, Glu2, Asp7

and Glu20 account for three of these acid groups and thus the C-terminal group is also a carboxylic acid. This is consistent with the initial MS/MS spectrum, which shows a peak at *m/z* 2519 corresponding to the $[M+H-H_2O]^+$ ion.

No digestion was observed after treatment with Lys-C, indicating the absence of Lys residues in the peptide, as was expected from initial MS/MS data. Finally, automated Edman sequencing allowed for the identification of Ile at positions 3 and 17 and Leu at position 4, provided unambiguous order of amino acids where required, and gave overall confirmation of the primary structure. Mass spectral sequencing data for caerin 5.1 is given in Table 3.5.

Table 3.5: Mass spectral sequencing data for caerin 5.1.

Fraction	MH$^+$	Sequence Data	
G	2537	B ions	*m/z* 2519, 2420, 2289, 2160, 2063, 1916, 1803, 1706, 1609, 1512, 1381, 1001, 845, 746, 631, 574, 427, 314, 201
			(Ala Glu) Ile Leu Phe Gly Asp Val Arg (Pro Pro Trp) Met Pro Pro Pro Ile Phe Pro Glu Met Val-OH
		Y+2 ions	*m/z* 2224, 2111, 1964, 1907, 1792, 1693, 1537, 1157, 1026, 929, 622, 475, 378, 249, 118
			Leu Phe Gly Asp Val Arg (Pro Pro Trp) Met Pro (Pro Pro Ile) Phe Pro Glu Met Val-OH

Lys-C - No digestion by Lys-C

Methylation - MH$^+$ 2593 (4 CO$_2$H groups)

3.2.5 Biological Activity

All novel peptides were synthesised commercially in order to test for biological activity, and were shown to be identical to the natural version by mass spectrometry. The antibacterial properties of the caerin peptides isolated from the *L. caerulea - L. splendida* hybrids are indicated in Table 3.6. Caerins 2.6 and 2.7 show moderate narrow-spectrum activity against certain Gram-positive bacteria, consistent with other peptides in the caerin 2 family [58].

Table 3.6: Antibiotic activities of the caerin peptides isolated from the *L. caerulea - L. splendida* hybrids. MIC is the minimum concentration required for pathogen growth inhibition. Where no figure is indicated, MIC is > 100 μg.mL^{-1}. The first and second groups of bacteria are Gram-positive and Gram-negative respectively.

Organism	MIC (μg.mL^{-1})										
	1.1	1.6	1.10	1.20	2.2	2.6	2.7	3.1	3.5	4.2	5.1
Bacillus cereus	50			100							
Enterococcus faecalis	25										
Leuconostoc lactis	1.5	3	3	25		25	50		100		
Listeria innocua	25	50	50	25		50					
Micrococcus luteus	12	25	25	20	50			< 0.4		60	
Staphylococcus aureus[a]	3	6		50							
Staphylococcus aureus[b]	12	12		25							
Staphylococcus epidermidis	12	12.5	100	25							
Streptococcus uberis	12	25	50	50							
Enterbacter clocae			100								
Eschericha coli			100							50	
Pasteurella multocida	12	25									

[a] Strain ATCC 25923
[b] Strain ATCC 29213

A number of peptides isolated from the skin secretion of the *L. caerulea - L. splendida* hybrids have previously been shown to inhibit the formation of NO by nNOS [72]. Additionally, caerin 1.20 and caerin 2.6 were tested in the current study for activity towards this enzyme. The nNOS inhibition activities of the caerin peptides isolated from the hybrids are given in Table 3.7. Caerin 1.20 shows only moderate inhibitory effects, while caerin 2.6 is considerably more active.

Table 3.7: nNOS inhibition activities of selected caerin peptides isolated from the *L. caerulea - L. splendida* hybrids. IC$_{50}$ is the concentration required for 50% inhibition of enzyme activity.

Name	IC$_{50}$ (μM)
Caerin 1.1	36.6
Caerin 1.6	8.5
Caerin 1.10	41.0
Caerin 1.20	70.9
Caerin 2.6	15.8

Caerin 5.1 is inactive against the organisms tested in the antibacterial assay, and shows little sequence identity with any of the peptides isolated from Australian frogs to date. As such, its role in the amphibian skin remains unknown. Similarly, the biological activity of the caeridin peptides is yet to be elucidated. The remaining peptide expressed by the hybrid is the ubiquitous neuropeptide caerulein, which demonstrates potent smooth muscle activity and analgesic properties as discussed previously.

3.2.6 Behavioural Testing

Using a procedure consistent with that of the initial pheromone tests conducted by Wabnitz *et al.* [60], and quantities of splendipherin ranging from 40 to 300 ng, no significant effect was observed on the female *L. caerulea - L. splendida* hybrid test specimen when the peptide was added to the tank. For example, no change in posture or alertness was noted, and only random movements throughout the aquarium were witnessed. In all cases, the animal did not successfully make contact with the pad containing the test substance. Therefore, it appears that the pheromone splendipherin induces no behavioural response in the hybrids.

3.3 Discussion

3.3.1 Peptide Profile, Structure and Biological Activity

The skin secretions of five female interspecific hybrids from the crossing of *L. caerulea* and *L. splendida* have been investigated, allowing for the characterisation of fourteen peptides which are listed in Table 3.3. The presence of caerulein was revealed, along with caeridin 1 and caeridin 5. The majority of the peptides however belong to the caerin family, three of which are not common to the secretions of either parent and are in fact novel compounds previously unidentified in the amphibian integument. The hybrid skin secretions were investigated over a nine-month period, encompassing both the reproductive (summer) and inactive (winter) seasons. The peptide profiles of each hybrid were identical, and consistent over the period of study.

With the exception of *L. rubella* and *L. electrica*, all frogs of the *Litoria* genus studied thus far secrete caerulein [32,70]. It is therefore unsurprising that this peptide was identified as one of the major components in the skin secretion of the hybrid frogs. Caerulein is a potent neuropeptide, with multifaceted activity which has been described in detail previously [19,83,84]. Similarly, the caeridin peptides have been isolated from a number of frogs of the *Litoria* genus, however to date their biological function remains unknown [80].

The caerin 1 peptides identified in the hybrid frogs have all previously been characterised from the skin secretions of either *L. caerulea* or *L. splendida* [42,60,66,86]. All are wide-spectrum antibiotics with MIC values typically in the low micromolar concentration range, and are active mainly against Gram-positive bacteria (Table 3.6). In addition, the major peptide component of the *L. caerulea - L. splendida* hybrid skin secretion, caerin 1.1, is a potent anticancer agent with IC_{50} values in the 10^{-5} to 10^{-6} M range against all classes of human cancer cell lines tested in the standard assay of the National Cancer Institute (Washington, USA) [58]. This peptide demonstrates antiviral activity against viruses with envelopes (e.g. HIV and *Herpes simplex 1* with MIC values of 7.8 and 11.3 µM respectively) [81], and effectively kills the chytrid fungus at micromolar concentrations [82].

The caerin 1 peptides adopt an amphipathic α-helical structure with a flexible hinge region around Pro15, as shown by 2D NMR experiments in membrane mimicking media for caerin 1.1 and caerin 1.4 [312,313]. This amphipathic helix-hinge-helix motif is common to a number of antimicrobial peptides, and is essential for the biological activity of these molecules [314].

Caerin 2 peptides are the only caerin molecules to possess C-terminal CO_2H groups, generally regarded as an indication of poor antibiotic activity. Typically these peptides demonstrate limited activity against a range of bacteria, and essentially no anticancer properties [58]. Caerins 2.6 and 2.7 are novel caerin 2 peptides isolated from the *L. caerulea - L. splendida* hybrids, and show antibacterial activity consistent with other members of this family. These peptides are simply isomers of one another, with Val9 and Ala15 of caerin 2.6 swapping positions to give caerin 2.7.

The 'Schiffer-Edmundson' helical wheel diagram is a graphical method for displaying an α-helical peptide, and provides a simple means for analysing the degree of amphipathicity of a peptide sequence [315]. The wheel presents an end-on view of the helix looking down the long axis, with each residue placed at intervals of 100° corresponding to the 3.6 residues per turn in an ideal α-helix. While the solution structures of members of the caerin 2 family have not yet been determined, Schiffer-Edmundson projections suggest amphipathicity does not result from an α-helical structure (Figure 3.10). Since formation of an amphipathic helix is generally considered fundamental to the antibacterial activity of such peptides (Chapter 8), this could possibly explain the limited antibacterial efficacy of caerins 2.6 and 2.7. The helical wheels for caerin 2.6 and 2.7 can be compared with those of more potent antibacterial peptides, such as citropin 1.1 and maculatin 1.1 (Section 8.3).

Figure 3.10: Schiffer-Edmundson helical wheel projections of **(a)** caerin 2.6 and **(b)** caerin 2.7. Hydrophilic residues are coloured blue, while hydrophobic residues are coloured red.

Although the caerin 2 peptides are narrow-spectrum antibacterial compounds, caerin 2.6 is active against both *Leuconostoc lactis* and *Listeria innocua* with MIC values of 25-50 μg.mL^{-1}, while caerin 2.7 is only active against *Listeria innocua*. Similarly, these peptides have only two residues different to caerin 2.2, which is active against *Micrococcus luteus* with an MIC value of 50 μg.mL^{-1}. Considering the close structural relationship of caerins 2.2, 2.6 and 2.7, it is somewhat surprising that they have a different range of activity, however the factors governing this specificity are currently not entirely understood.

A number of the peptides isolated from the skin secretions of the *L. caerulea - L. splendida* hybrids have previously been reported as inhibitors of the enzyme nNOS [72]. Furthermore, caerins 1.20 and caerin 2.6 were selected for biological testing in the current study. Caerin 1.20 shows relatively poor activity with an IC$_{50}$ concentration of 70.9 μM, while caerin 2.6 is considerably more efficacious (IC$_{50}$ = 15.8 μM). nNOS inhibition occurs since the peptides complex with the regulatory protein calmodulin (CaM), altering its shape and thus hindering the interaction of CaM with its binding site on nNOS (Chapter 5).

CaM is capable of recognising positively charged α-helical peptides, independent of their precise amino acid sequences, and although amphipathicity does correlate with CaM binding, it need not be ideal for binding to occur [316]. The nNOS active peptides isolated from the *L. caerulea - L. splendida* hybrids are not perfectly amphipathic, however they do contain a number of basic residues which probably contribute to CaM binding. CaM is also the regulatory protein for a number of other enzymes including a variety of kinases [317], thus any peptide which complexes with calmodulin will effectively interfere with a number of cellular functions in any predator, and could possibly act to regulate some aspects of the animal's own physiology.

Caerin 5.1 is extremely hydrophobic, and by inspection of the Schiffer-Edmundson projection is not expected to form a linear amphipathic helix (Figure 3.11). Consequently, it is not surprising that this peptide was found to be inactive in the antibacterial assay, and would not be expected to be an effective inhibitor of nNOS. Caerin 5.1 demonstrates little sequence homology with any other peptide previously isolated from the amphibian integument, and in particular contains an unusually large number of Pro residues. Pro is known to disrupt regular secondary structure since it does not have an amide proton available for hydrogen bonding. As such it is difficult to predict the three-dimensional structure of caerin 5.1, and to date its role in the amphibian skin remains unclear.

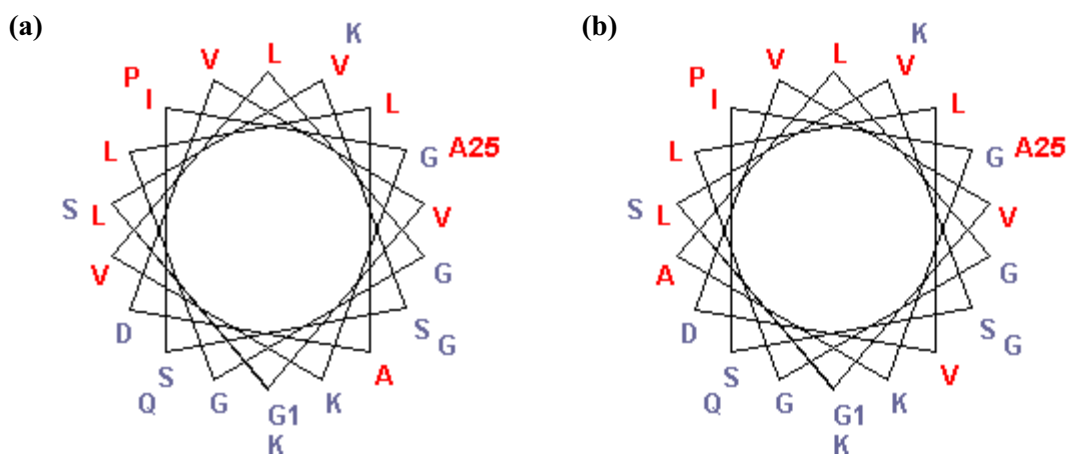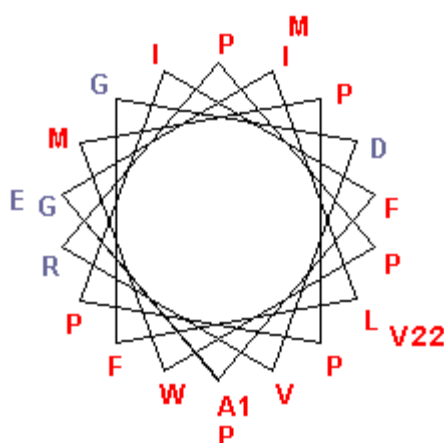**Figure 3.11:** Schiffer-Edmundson helical wheel projection of caerin 5.1. Hydrophilic residues are coloured blue, while hydrophobic residues are coloured red.

It is not unusual for the dermal peptides to be cytotoxic to the frog, and consequently they are typically deactivated by an endoprotease after some period of time on the skin [58]. This often involves removal of several amino acid residues from the N-terminal end of the peptide. A number of peptides were observed in the *L. caerulea - L. splendida* hybrid skin secretions which eluted between 22 and 26 minutes during HPLC separation (Figure 3.5). These were identified using mass spectrometry as degradation products resulting from the enzymatic cleavage of the first two N-terminal residues of the respective parent peptide. Since cleavage of N-terminal residues typically results in a loss of biological function [41,58], these peptides were presumed to be inactive.

Splendipherin is present in the skin secretion of male *L. splendida*, and has been shown to be an effective aggregation pheromone [60]. This peptide acts in a species and sex specific manner, attracting female *L. splendida* with an optimal concentration of approximately 10^{-11} to 10^{-8} M. Splendipherin is a major peptide component of the glandular secretion of *L. caerulea*, however it does not induce any behavioural response in similar pheromone tests with either the female or male of this species [60]. Although this peptide was not identified in the skin secretion of the *L. caerulea - L. splendida* hybrids, it was of interest to determine the responsiveness of these animals to the pheromone activity of splendipherin. The presence of splendipherin causes a distinct and observable change in posture and alertness of *L. splendida* within 20 seconds, after which the animal approaches the peptide source in an average of 7 minutes and remains there until removed [60].

Under similar conditions, splendipherin was found to cause no observable behavioural effects on the *L. caerulea - L. splendida* hybrids. No change in the physical activity of the animal was noted, and at no time was the test specimen attracted to the peptide source. Thus it appears splendipherin elicits no pheromone based response in the hybrid frogs. The hybrid specimen was three years old at the time of behavioural testing, an age when females of both *L. caerulea* and *L. splendida* are reproductively mature. It is possible that the hybrid genetic background may have disrupted the sex limited expression of sensitivity towards splendipherin in these animals. Alternatively, since *L. caerulea* are insensitive to the pheromone effect, the heterozygous constitution

at the genetic loci which confer sensitivity to splendipherin may have reduced the capacity of the hybrid to detect the pheromone. Nevertheless, this experiment demonstrates the effectiveness of splendipherin in exhibiting specificity towards female *L. splendida*.

3.3.2 The *L. caerulea - L. splendida* Hybrid Pedigree

Since the putative *L. caerulea - L. splendida* hybrids were bred fortuitously in the presence of large numbers of females and males of both potential parent species, identification and analysis of the individual parent specimens was precluded. Thus it was necessary to not only confirm the animals were in fact hybrids, but also to establish their parentage. This was achieved both by peptide profile analysis and mtDNA studies.

mtDNA is found exclusively in the mitochondria, and contains genetic information essential for the function of this organelle [9,10,318,319]. In contrast to chromosomal genes which are inherited biparentally, mtDNA is derived solely from the maternal parent [320-322] and thus provides a means to trace a direct maternal genetic line. The mutation rate of mtDNA is high in comparison with nuclear DNA [323], making it easier to resolve differences between closely related individuals, and because mitochondrial genes do not recombine, interspecific hybridisation does not affect the genealogical reconstruction of mitochondrial sequences [297,323].

Sequence alignment was carried out for an 850 bp region of the mitochondrial 12S rRNA gene of two *L. caerulea - L. splendida* hybrid specimens. Upon comparison with a database containing representatives of the major Australian clades of *Litoria*, a significant difference was observed between the DNA sequence of the hybrid samples and that of *L. caerulea*. In contrast, the hybrid samples exhibit only 0.8% sequence divergence from *L. splendida*. Thus the maternal parent of the hybrid brood was conclusively found to be *L. splendida*. Given the difficulty in breeding interspecific hybrids between these two species, it is likely that the offspring are the product of only one mating. This is also supported by mtDNA analysis since the two hybrid samples demonstrate identical sequences over the entire aligned region.

The skin secretion of *L. splendida* is relatively simple, with only ten peptide components. However, the skin secretion of the putative hybrids is significantly different, both in the number and identity of observed peptides. *L. splendida* has a relatively small geographic range in the Kimberley region of northwestern Australia [57], and to date no variation has been detected in the peptide profile of this species, irrespective of the sample origin [60]. It is therefore implausible that the unique peptide spectrum of the hybrid could be attributed to two parental *L. splendida* specimens originating from a location yet to be surveyed. Accordingly, the father of the brood must be *L. caerulea*, and hence the offspring are indeed interspecific hybrids.

Since the peptide profile of any given specimen of *L. caerulea* is highly dependent upon geographic distribution, this can provide insight into the possible location from which the parental *L. caerulea* originated. In Table 3.3 it can be seen that one of the peptides isolated from the hybrids, caerin 4.2, is not expressed by *L. splendida*. However, it has been identified in populations of *L. caerulea*, but only in the area from Groote Eylandt southeast into Queensland, and also Derby (Figure 3.12) [42,66]. The hybrid peptide profile also has some similarities with that of the *L. caerulea* population from Longreach. For example, both contain caerins 1.20 and 3.5 [66]. The likelihood is that the male *L. caerulea* which sired the hybrids originated from this region of northern Australia. However, it is not reasonable to exclude the possibility that the male parent originates from a locality not included in the previous survey.
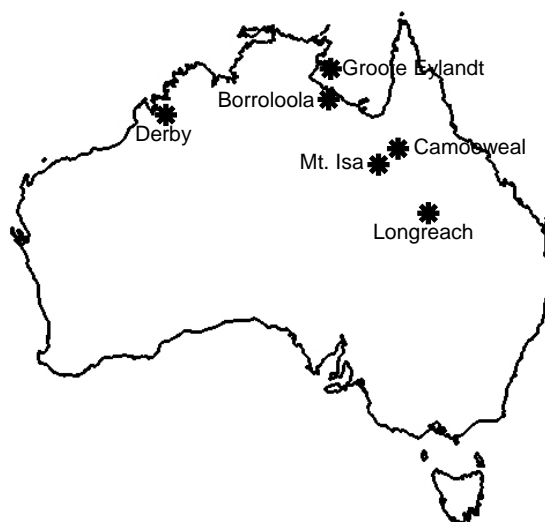
Figure 3.12: Geographical location of *Litoria caerulea* populations which express caerin 4.2 [42,66].

3.3.3 Peptide Inheritance

Of the fourteen peptides characterised from the skin secretion of the *L. caerulea - L. splendida* hybrids, five were found to be inherited from *L. caerulea* only, while three were from *L. splendida* only. The hybrid peptides not expressed by either parental species are caerins 2.6, 2.7 and 5.1. In addition, caerin 1.10 is expressed by male *L. splendida* but not the female, however this peptide was observed in the female hybrids.

cDNA cloning experiments have revealed the precursor peptides for the major antimicrobial component in the skin secretions, caerin 1.1, for both *L. caerulea* and *L. splendida* as well as the hybrids [17,66]. The pre-pro-caerin 1.1 sequences are similar in all cases, however it is of interest that only one clone for pre-pro-caerin 1.1 was reported for both *L. caerulea* and *L. splendida*, whereas two clones were identified for the hybrid. This is consistent with (but by itself does not prove) interspecies breeding, since a different DNA sequence may be inherited from each parent species. The sequences of the four caerin 1.1 precursors are similar in any case, and are compared in Table 3.8.

Table 3.8: Sequences of caerin 1.1 precursor peptides from *L. caerulea*, *L. splendida* and the hybrid.

	Signal (pre) peptide	Spacer (pro) peptide
L. caerulea	MA**S**LKKSLFL**VL**LLGFVSVSIC	EEEKRQEDEDEH**EEE**GE**S**QEEGSEEKR
L. splendida	MA**F**LKKSLFL**VL**F**LGFVSVSIC	EEEKRQEDEDEH**EEE**GE**N**QEEGSEEKR
Hybrid	MA**F**LKKSLFL**VL**F**LGFVSVSIC	EEEKRQEDEDEH**V**EEGE**N**QEEGSEEKR
Hybrid	MA**F**LKKSLFL**GL**F**LGFVSVSIC	EEEKRQEDEDEH**D**EEGE**N**QEEGSEEKR

The appearance of novel peptides in the *L. caerulea - L. splendida* hybrids that have not been observed in either parental species raises the question of whether their presence is due to the inheritance of peptides from parents of populations that to date have not had their skin peptide profiles characterised, or to some form of altered regulation of expression in the hybrid genetic background. No evidence has been presented to suggest the skin secretion of *L. splendida* changes with geographical location [60],

however different populations of *L. caerulea* show substantial variation in peptide profile even over small geographic distances [42]. Although the skin secretions of *L. caerulea* have been extensively investigated, it is not feasible to ignore the possibility that the male parent of the hybrids originated from a location not previously studied.

Alternatively, the explanation that the peptides expressed only in the hybrid resulted from some form of modified regulation of expression in the hybrid genetic background is also not presently excluded by this analysis. Comparisons of gene expression between interspecific hybrids and their parental taxa demonstrate that quantitative differences in expression [324], misexpression [324,325] and novel gene expression patterns [325] can occur in F_1 hybrids. Indeed, the apparent alteration of the limited expression of caerin 1.10 in *L. splendida* (i.e. produced by males but not females) compared with the hybrids may be an example of this phenomenon.

Determining whether the mature mRNA transcripts for the peptides found only in the hybrid are present in the parental taxa, and if so where they are expressed, would show if gene expression differences account for the novel peptides. However, in order to unequivocally demonstrate such altered regulation of expression, direct comparison is necessary of DNA data for the hybrid offspring and their parents. Although the gender and species of the parents were known, the identity of individual parents was not, and hence direct analysis is not possible in this study. Nevertheless, if in fact the novel peptides can be generated by interspecific hybridisation, this genetic variation provides the potential for diversification and, in turn, would offer support for hybridisation as a creative evolutionary process.

3.4 Experimental Procedures

3.4.1 Mitochondrial DNA Analysis

DNA testing was carried out with the assistance of Dr. Terry Bertozzi of the South Australian Museum and the University of Adelaide. Briefly, tissue samples were taken from two hybrid specimens in the form of toe clippings, and total cellular DNA extracted using a Puregene DNA isolation kit (Gentra Systems). Polymerase chain reactions (PCR) were used to amplify 850 bp of the mitochondrial 12S rRNA gene using primers H1478 [326] and L669 [327]. Amplifications were carried out using Amplitaq Gold DNA Polymerase (Applied Biosystems) according to the manufacturer's specifications, with an annealing temperature of 65 ˚C.

PCR products were purified using an UltraClean PCR Clean-up kit (Mo-Bio Laboratories) before sequencing, using the BigDye Terminator V3.1 Cycle Sequencing kit (Applied Biosystems). Samples were analysed on an Applied Biosystems 3700 DNA sequencer, and compared to a database of *Litoria* 12S rRNA sequences which contained the putative parents of the hybrids in addition to representatives of the major Australian clades of *Litoria*.   Reference sequences were obtained from EMBL via the European Bioinformatics Institute Server at the www address: ftp://ftp.embl-heidelberg.de/pub/databases/embl/align/(alignment:ds38405) or from the South Australian Museum (unpublished data). All sequences were aligned by eye and phylogenetically analysed with the Neighbour-Joining algorithm from Kimura 2-parameter [328], estimating genetic distances between sequences with the software package PAUP* version 4b10 [329].

3.4.2 Collection of Secretory Products

Dermal secretions were acquired with the assistance of Prof. Michael Tyler from the School of Earth and Environmental Sciences, University of Adelaide. Samples were obtained from five *L. caerulea - L. splendida* hybrid specimens by the SES method [56], which could be repeated on a monthly basis. The animal was held by the back legs, and its skin moistened with deionised water to remove debris and improve conductivity. A bipolar electrode of 21G platinum with a 3 mm gap was rubbed gently over the dorsal glandular surface of the animal, while the attached C.F. Palmer student model electrical stimulator applied 10 V pulses of 3 ms duration, at a pulse repetition rate of 50 per second. Resulting secretory products were rinsed off with a stream of deionised water, to which an equal volume of methanol was immediately added. The mixture was then filtered through a Millex HV filter unit (0.45 μm), centrifuged and the supernatant concentrated *in vacuo* to approximately 5 mL. All procedures comply with the University of Adelaide Animal Ethics Committee code of practice [330].

3.4.3 HPLC Separation

A VYDAC C_{18} column (5 micron, 300 Å, 4.6 x 250 mm) was equilibrated initially with 10% acetonitrile/aqueous 0.1% trifluoroacetic acid. 100 μL of prepared sample was injected on to the column for each run and exposed to a linear solvent gradient, controlled by a Waters Automated Gradient Controller and ICI DP-700 Data Station. Acetonitrile content was increased to 70% over 40 minutes, while flow rate was maintained by Waters Millipore 510 and 501 HPLC pumps at 1 mL.min^{-1}, and the eluant monitored by ultra-violet absorbance at 214 nm using an ICI LC-1200 UV/VIS spectrophotometer. Major fractions were collected and subsequently analysed by mass spectrometry.

Where fractions were found to still contain multiple components, they were lyophilised and reconstituted in deionised water (50 μL). Using the HPLC system described above, this sample was then injected onto the column and exposed to a linear solvent gradient, increasing acetonitrile content from 33 to 38% over 50 minutes. 0.5 mL fractions were collected and analysed by mass spectrometry.

3.4.4 Mass Spectrometry

Samples were investigated by ESI-MS, using a Micromass Q-TOF 2 mass spectrometer with a mass range to 10,000 Da. Fractions taken directly from HPLC were diluted with an equal amount of acetonitrile/water/formic acid (50:48:2 v/v/v) and infused into the source at a flow rate of 5 μL.min^{-1}. Conditions were typically as follows; capillary voltage 3.1 kV, source temperature 80 ˚C, desolvation temperature 150 ˚C and cone voltage 40-60 V. An argon collision gas energy of approximately 50 eV was applied to give optimal fragmentation for MS/MS data. Peptides were sequenced from MS/MS spectra by inspection of the B and Y+2 fragmentations observed in the positive ion mode.

For negative ion mass spectra, fractions taken from HPLC were lyophilised before being dissolved in acetonitrile/water (100 μL, 1:1 v/v) and infused into the source at a flow rate of 5 μL.min^{-1}. Conditions were typically as follows; capillary voltage 2.8 kV, source temperature 80 ˚C, desolvation temperature 150 ˚C and cone voltage 40-60 V.

In both positive and negative ion mode, MS/MS spectra of multiply charged ions were processed using a commercially available maximum entropy algorithm (MaxEnt 3, Micromass) to give a true molecular mass spectrum.

3.4.5 Lys-C Digestion

Endoprotease Lys-C was prepared by dissolving 3 units in water (200 μL). 1 μL was then added to a sample of lyophilised peptide (~10 μg) dissolved in aqueous ammonium hydrogen carbonate solution (0.1 M, 5 μL, pH 8). The resulting mixture was heated at 45 °C for 45 minutes, then diluted with water/acetonitrile/formic acid (50:48:2 v/v/v) and analysed by mass spectrometry.

3.4.6 C-Terminal Group Determination

'Acidified methanol' was used to afford the methylated peptide for C-terminal group determination. Methanol (858 µL) was cooled using dry ice for 5 minutes, after which acetyl chloride (142 µL) was added under a nitrogen atmosphere and the mixture cooled for a further 5 minutes. The solution was then allowed to warm to ambient temperature over 1 hour, flushing with nitrogen every 15 minutes.

A sample of lyophilised peptide (~10 µg) was dissolved in acidified methanol (100 µL) and the solution heated at 45 °C for 1 hour. The resulting product was then diluted with an equal volume of acetonitrile/water (50:50 v/v) and analysed by mass spectrometry.

3.4.7 Automated Edman Sequencing

Automated Edman sequencing was performed by the Department of Molecular Biosciences, University of Adelaide. A standard procedure was followed [220], using an applied Biosystem 492 Procise Sequencer equipped with a 900A data analysis module. The peptide was absorbed from aqueous acetonitrile (90%) onto a disc of immobilon film treated with biobrene in ethanol, which was subsequently pierced several times with a razor blade to assist with solvent flow.

3.4.8 Bioactivity Testing

Peptides were synthesised by Mimotopes (Clayton, Victoria) using L-amino acids and the standard N-α-Fmoc method [331], and were shown to be identical to the natural peptides by mass spectrometry.

Antibacterial testing was conducted by the Microbiology Department of the Institute of Medical and Veterinary Science (Adelaide, South Australia) and involved measurement of inhibition zones resulting from peptide application to microorganism coated agarose plates [332]. Activities are recorded as MIC values, which are the minimum concentrations ($\mu g.mL^{-1}$) required to completely inhibit bacterial growth.

nNOS inhibition assays were conducted by the Australian Institute of Marine Science (Townsville, Queensland). Inhibition was measured by monitoring the conversion of ^{3}H-arginine to ^{3}H-citrulline, using methods reported previously [72].

3.4.9 Behavioural Studies

Splendipherin was synthesised by Mimotopes (Clayton, Victoria) as described above. Two *L. caerulea - L. splendida* hybrids were used for all behavioural tests, and the experiments were repeated at least twice on four separate occasions. A glass aquarium, with dimensions 65 cm x 200 cm x 75 cm, was filled with water to a depth of 2 cm. Two sterilised cotton gauze pads (dimensions 10 cm x 10 cm) were secured at opposite ends of the tank. The animal was then placed in the middle of the aquarium and allowed to stabilise over a period of 5 minutes. After this time, solutions of splendipherin (containing from 40 to 300 ng of the pheromone in 100 μL deionised water) were absorbed onto one of the gauze pads. At this point all movements of the animal were recorded using time-lapse photography, and the experiment concluded ten minutes after the introduction of peptide. After each test the aquarium was washed thoroughly, and filled with fresh water and new gauze pads in readiness for the next experiment.

3.4.10 cDNA Studies

cDNA analysis was performed by Dr. Katharina Surinya-Johnson, Dr. Yanquin Liu and Rebecca Jackway at the Department of Molecular Biosciences, University of Adelaide, using the procedure of Chen *et al.* [333]. 3' RACE analysis of mRNA, producing the cDNA clones of pre-pro-caerin 1.1, was carried out for skin secretions of a female *L. splendida* and a female hybrid. The sense primer was designed from the published sequence of the 5'-untranslated region of pre-pro-caerin 1.1 of *L. caerulea* [17] (EMBL accession no. AY218778-AY218782), and is given below.

5'-GVCTTGTAAAGACCAAVCATG-3'

~ CHAPTER 4 ~

Methodology II – Nuclear Magnetic Resonance Spectroscopy

4.1 NMR Spectroscopy for the Study of Peptides

Nuclear magnetic resonance (NMR) spectroscopy was first described independently by Felix Bloch and Edward Mills Purcell in 1946, both of whom shared the Nobel Prize in physics for their discovery. The earliest reported application to a biological system came in 1954 [334], and three years later Saunders, Wishnia and Kirkwood obtained the first ^{1}H NMR spectrum of a protein, ribonuclease [335]. Rapid development of biological NMR was spurred on by key advances in the field including the introduction of Fourier transform NMR, high field spectrometers, multidimensional experiments and improved computational facilities [336,337]. As a result, NMR spectroscopy has grown in power and versatility over the past few decades, and is now routinely used for studying the structure and dynamics of complex organic molecules such as proteins and DNA.

The three-dimensional (3D) structure of peptides and proteins has significant implications for their biological function, and thus forms an important and continually growing branch of study in the field of proteomics. Numerous techniques have been developed to investigate these structures, ranging from circular dichroism to probe the presence of secondary structure [338,339], to electron microscopy for the study of large protein complexes [340,341]. However, NMR spectroscopy and X-ray crystallography are currently the only practical techniques that can provide the structure of macromolecules with atomic resolution. The X-ray method is extremely powerful [342,343], although it requires the protein to be crystallised, which in many cases is difficult or not possible. In addition, there is no guarantee the protein in a crystalline form will be representative of that in physiological conditions, due to additional crystal packing considerations present in the solid state. NMR spectroscopy has superseded these techniques in recent times, and is now well established and consistently used to determine the 3D structures of proteins up to approximately 30 kDa in mass [344].

NMR spectroscopy can also supply a wealth of information on dynamics, conformational equilibria, molecular folding and intra- as well as intermolecular interactions [344]. In addition, solid state NMR spectroscopy allows for investigation of peptide structure, orientation and function in more complex systems such as lipid bilayers (Chapter 7). Consequently, NMR is frequently used to provide insight into the mechanism of action of biologically active peptides. The following chapter describes the basic principles of NMR spectroscopy, as well as its use for the 3D structure determination of peptides in solution and the study of peptide bioactivity.

4.2 Fundamental Principles of NMR Spectroscopy

A number of reference texts are available which detail the fundamental principles of NMR spectroscopy and the acquisition of one-dimensional (1D) spectra [203,268,344-347]. A brief overview will be given here. The NMR phenomenon is based on the principle that subatomic particles (electrons, protons and neutrons) have an intrinsic angular momentum, and as such, possess a quantum mechanical property known as 'spin'. In many atoms (such as ^{12}C and ^{16}O) the total spin of the nucleus is zero due to pairwise cancellation, however in some atoms the nucleus does retain an overall spin, I. Where $I \neq 0$, the nuclei are said to be NMR active, and for those relevant to biological studies (^1H, ^{13}C and ^{15}N), $I = ^1/_2$. In the absence of an external magnetic field these nuclei possess the same energy. However, in the presence of an external field, quantum mechanics dictates that nuclei can align themselves in one of (2I + 1) orientations. Consequently, for atoms with $I = ^1/_2$, two spin states exist corresponding to a low energy orientation (N_α - alignment with the applied field) and a high energy orientation (N_β - opposing the applied field). The energy difference between these two states is small, and is given by the equation;

$$\Delta E = \frac{h\gamma B_0}{2\pi}$$

where h is Planck's constant, γ is the gyromagnetic ratio (a proportionality constant differing for each nucleus) and B_0 is the strength of the applied magnetic field.

The initial populations of the energy levels are determined by thermodynamics, and are described by the Boltzmann distribution as follows;

$$\frac{N_\beta}{N_\alpha} = e^{-\Delta E/kT}$$

where k is the Boltzmann constant and T (K) is the temperature. For a million ^{1}H nuclei at room temperature only around 60 additional nuclei are in the low energy state, even at some of the strongest magnetic field strengths currently available for NMR. Since the signal intensity of any spectroscopic method depends largely on the population difference of the energy levels involved, NMR spectroscopy is thus an inherently insensitive technique. Even so, the difference in populations of the two energy states yields a net magnetic moment which can be manipulated in a range of useful ways depending on the information required.

Application of electromagnetic radiation to the system under study can promote a number of nuclei from the N_α state to the higher energy N_β state, thereby altering the overall magnetic moment. In order for this to occur, the applied radiation must correspond to the energy difference between the two states, and hence match the frequency at which the nuclei naturally precess in the magnetic field. This is known as the Larmor frequency, defined by the equation;

$$\nu = \frac{\gamma B_0}{2\pi}$$

For a magnetic field of 14.1 Tesla, the Larmor frequency is 600 MHz for ^{1}H nuclei, and falls within the radio frequency (RF) range.

The effect of RF pulses in a basic 1D experiment can be described using vector representations. As previously discussed, the rotational axis of each spinning nucleus will precess about the applied field **B$_0$** (z-axis), with a higher population having a magnetic moment parallel to the field rather than anti-parallel. This creates a bulk magnetization vector **M$_0$** in the direction of the applied field. To generate a spectrum, the RF signal is applied as a short powerful pulse which lasts for a time t_p in the order of

a few microseconds, and can cover the entire frequency range of interest. An oscillating magnetic field $\mathbf{B_1}$ is produced along the x-axis which effectively rotates the net magnetisation through some angle given by;

$$\theta = \gamma B_1 t_p$$

Generally t_p is chosen such that θ is 90°, which will equalise the populations of the two energy states and tip $\mathbf{M_0}$ into the xy-plane. Once in this plane, $\mathbf{M_0}$ continues to precess about the direction of applied magnetisation. A receiver coil placed along the y-axis is used to detect the induced electric current produced by the oscillating field during an acquisition period (typically a few seconds), and this constitutes the NMR signal. Consequently, as $\mathbf{M_0}$ relaxes to its equilibrium state the induced current along the y-axis reduces with time, producing an exponentially decaying cosine signal. This process is called a free induction decay (FID), which is recorded for all irradiated nuclei, and can be summed over a number of pulse/acquisition cycles to improve the signal-to-noise ratio. The FID is then converted using a Fourier transform function from the time domain to the frequency domain, yielding a 1D NMR spectrum from which the Larmor frequency of each nucleus can be determined.

If every atom in the sample was identical, the amount of energy required to manipulate the spins would be the same for all nuclei, and hence only one peak would be observed in the NMR spectrum. However, moving electrons generate a small local magnetic field which effectively alters the magnitude of the applied field experienced by each nucleus, and in turn changes the energy difference between the states. This also means the Larmor frequency of a spin is sensitive to chemical structure and geometry and hence, during the NMR experiment, each nucleus contributing to $\mathbf{M_0}$ will precess at a slightly different frequency in the xy-plane based on the local magnetic environment. Consequently, the FID of a molecule will have multiple frequency components, and the Fourier transformation will produce an NMR spectrum with signals from each of the structurally distinct nuclei in the molecule.

For ease of analysis the frequency signals are normalised using the chemical shift scale, generated by comparing the frequencies with a standard reference compound such as tetramethylsilane (TMS) as follows;

$$\delta = \frac{\nu - \nu_{TMS}}{\text{operating frequency}} \times 10^6$$

For water-soluble peptides the reference is likely to be trimethylsilylpropionic acid (TSP) or dimethyl-2-silapentane-5-sulphonate (DSS). The overall process for performing a 1D NMR experiment is summarised graphically in Figure 4.1.
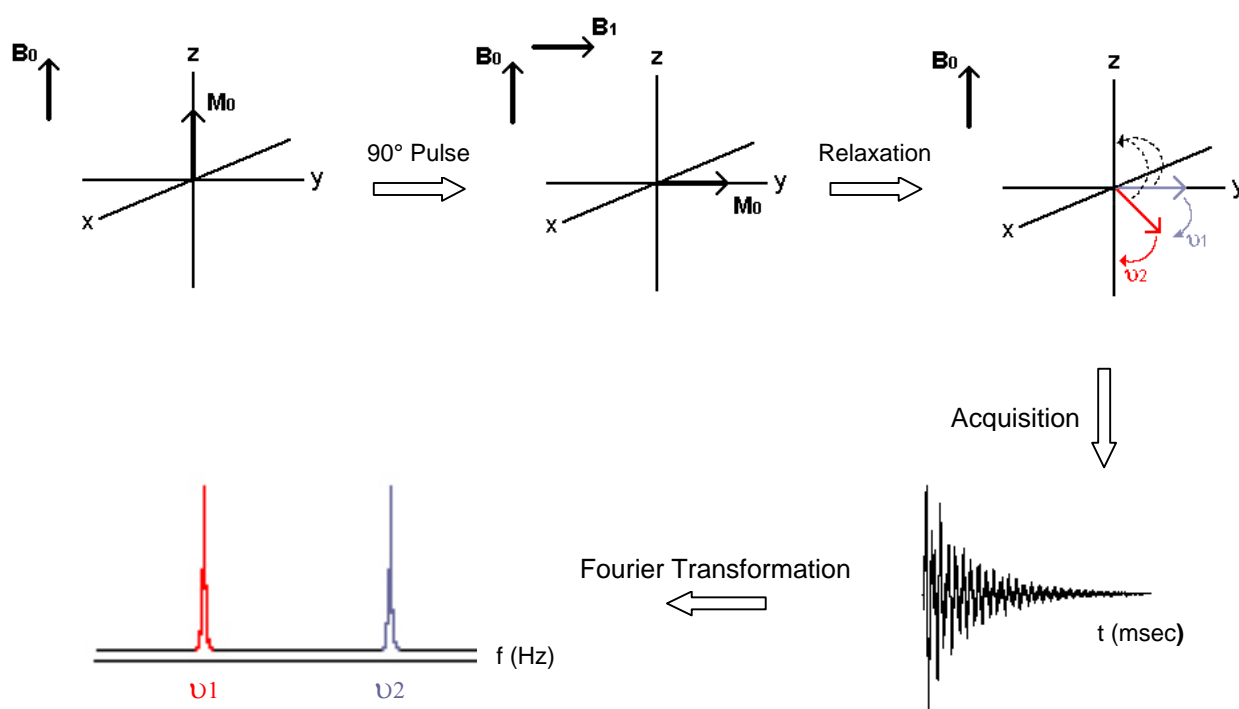
Figure 4.1: Acquisition of a typical 1D NMR spectrum. Initially oriented with the applied magnetic field, M_0 is rotated into the xy-plane after the application of a 90° RF pulse. Precession of spins in the xy-plane as M_0 relaxes back to its equilibrium position is recorded as a free induction decay, and the resultant 1D NMR spectrum is obtained after Fourier transformation.

4.3 Two-Dimensional NMR Spectroscopy

Large molecules such as peptides and proteins possess a number of magnetically non-equivalent nuclei, and it therefore becomes more difficult to assign the signals in a conventional 1D NMR spectrum. This puts a practical limit on the molecular size that can be studied using NMR methods. In order to address this problem, resolution can be increased by extending the basic 1D experiment into multiple dimensions.

All two-dimensional (2D) experiments involve the same basic scheme, which consists of a preparation period, an evolution period (t_1), a mixing period (τm) and finally a detection period (t_2) [268,336,348]. During the preparation period, the spins are established such that the chemical shifts can be identified during t_1 as in a standard 1D experiment. Additional pulses are applied in the mixing period which allow the spins to correlate with one another, and this interaction is detected during t_2 as a typical FID. To obtain a 2D data set, a number of experiments are recorded with incremented values of t_1, and Fourier transformation in both dimensions then yields the desired 2D frequency spectrum. If two spins suitably interact (determined by the type of experiment carried out), a peak will be observed in the spectrum at a position characterised by the resonance frequencies of the nuclei involved, providing important structural information [268]. This process is summarised graphically in Figure 4.2.

Using a combination of the 2D experiments described in the following sections, assignment of all the resonances in a peptide is possible. This in turn provides the basis for secondary structure determination.
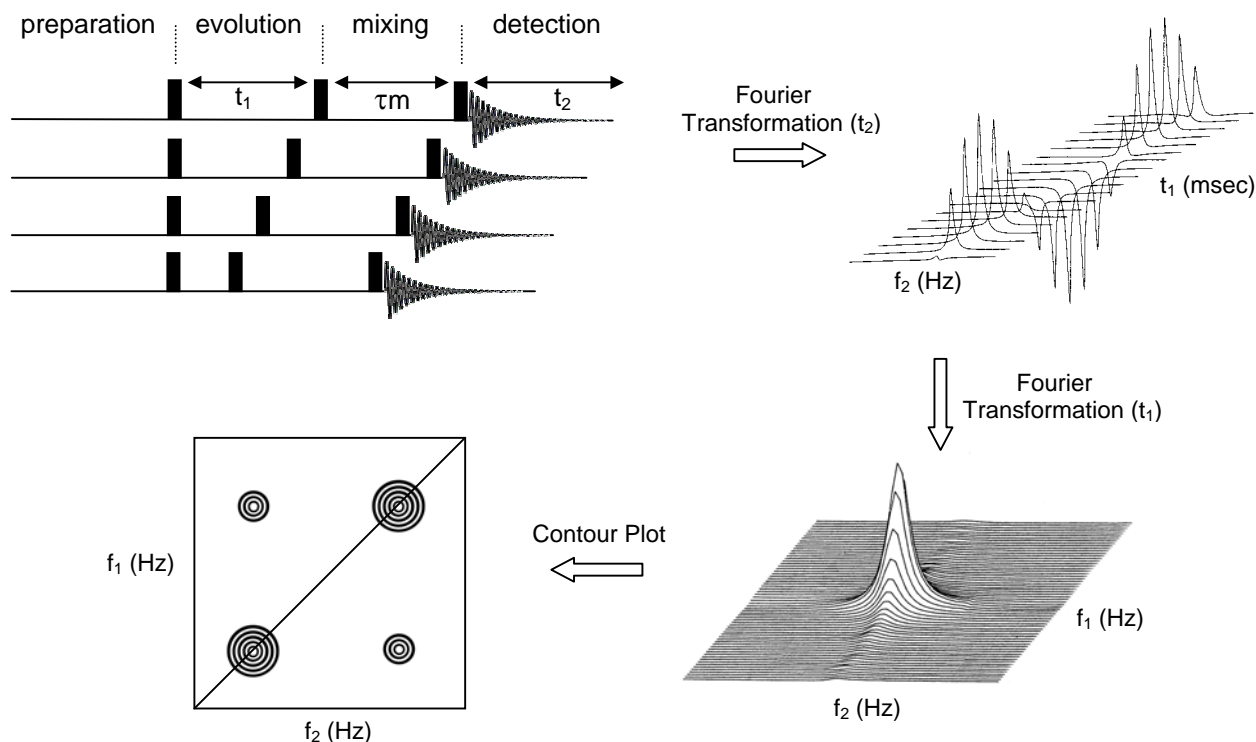
Figure 4.2: Generalised representation of a 2D NMR experiment. Figure adapted from [348].

4.3.1 Correlated Spectroscopy

Correlated Spectroscopy (COSY) gives rise to NMR signals based on the through bond interactions of homonuclei. For the purpose of peptide structure determination, it allows for the investigation of the connectivity of a molecule by determining which protons are coupled to each other by either two or three bonds. The pulse sequence of a typical COSY experiment is shown in Figure 4.3, and involves application of two 90° RF pulses separated by a variable delay, t_1 [349].
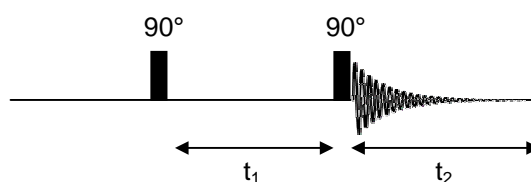
Figure 4.3: The pulse sequence of a simple COSY experiment.

81

In this experiment, the first pulse creates magnetisation in the transverse plane which evolves over the t_1 time interval. The y-axis component of the evolved magnetisation is then rotated through 90° by the second RF pulse. This leads to a situation in which the magnetisation can be potentially redistributed among scalar coupled nuclei in a process known as coherence transfer [268,350,351]. As a result, coupled spins communicate the information about their precession frequencies, which is recorded during t_2. After Fourier transformation in both time domains, a cross-peak between two spins, i and j, will occur at positions (δi, δj) and (δj, δi) in the spectrum if spins i and j are directly coupled to one another [348]. The scalar coupling between the two protons responsible for the signal causes the cross-peak to appear as an anti-phase multiplet, which can itself give further structural information (Section 4.5.3).

The major limitation of the standard COSY experiment arises from the presence of diagonal peaks, which occur with the same chemical shift in both dimensions as a result of magnetisation that is unaffected by the second 90° pulse [268]. Since the diagonal multiplets are in-phase, the intensity of these peaks increases binomially and at a greater rate than the anti-phase multiplets. In addition, anti-phase cross-peak components tend to cancel each other out, and hence the diagonal peaks are enhanced relative to the information rich signals [352]. Furthermore, diagonal peaks have dispersive line shapes compared with the absorptive line shapes of the cross-peaks, and often their long dispersion tails obscure any cross-peaks in close proximity [353]. The basic COSY experiment has now been superseded by more complex pulse sequences such as the double quantum filtered COSY (DQF-COSY) [268,352]. This has the advantage of absorptive diagonal peaks while retaining anti-phase cross-peaks to improve the effectiveness of the experiment.

4.3.2 Total Correlation Spectroscopy

In a protein spectrum, signal overlap tends to increase when moving from the NH and αH protons down the side chain. Consequently, experiments that demonstrate only direct through bond correlations are of restricted use alone, and are instead combined with experiments that also reveal longer-range interactions [348,354]. The Total Correlation Spectroscopy (TOCSY) experiment is similar to that of the COSY, with the exception that it relies on cross-polarisation rather than coherence transfer to provide relayed through bond connectivities [355,356].

Cross-polarisation is obtained by applying a single coherent RF field, known as a spin locking pulse, during the mixing time τm (Figure 4.4). When the effective RF field experienced by two scalar coupled protons is identical, the spins become temporarily equivalent and oscillatory exchange of magnetisation occurs [357,358]. Therefore, during the mixing sequence, relayed connectivity results in which the magnetisation of the scalar coupled protons is extensively transferred across all coupled spins. Consequently, cross-peaks are observed for all resonances in the same spin system [355,359]. For a simple two-spin system, complete exchange occurs with a τm corresponding to ½ J, where J is the two spin scalar coupling constant, while in more elaborate cases the time dependence is further complicated [355]. Often a series of spectra are obtained with different values of τm to achieve complete magnetisation transfer across the spin system.
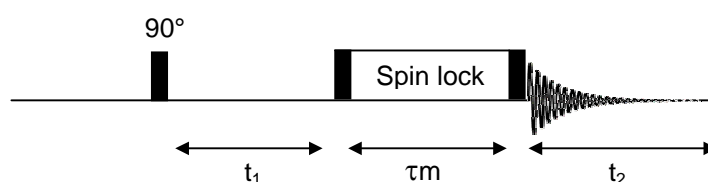
Figure 4.4: The pulse sequence of a typical TOCSY experiment.

Due to the absence of scalar coupling across an amide bond, each amino acid residue in a peptide or protein effectively corresponds to a single spin system. Thus, by observing the cross-section through a particular resonance, it can be possible to correlate peaks for all protons in the same spin system [203,360]. For example, under favourable

conditions signals from the amide proton will correlate with all side chain protons from the same residue. The unique connectivity patterns for each amino acid have been published [268], and this allows for their identification. In combination with the COSY experiment, investigation of the TOCSY spectrum can lead to assignment of most proton resonances in a peptide (Section 4.4).

The peak components in a TOCSY spectrum are all in-phase and absorptive in nature, including the diagonal peaks, and as a result, this experiment is generally more sensitive and affords better resolution than a COSY experiment [348,355,361]. Problems with the TOCSY experiment can occur however due to nuclear Overhauser effects (Section 4.3.4) which results in the emergence of negative peaks in the spectrum [268,356]. This is generally not an issue with short mixing times, and nevertheless can be addressed with 'clean' TOCSY pulse sequences which prevent the cross-relaxation peaks from occurring [361].

4.3.3 Heteronuclear Correlation Spectroscopy

Heteronuclear correlation spectroscopy provides useful information regarding the interaction of a proton and a heteronucleus such as ^{13}C and ^{15}N. In particular, the Heteronuclear Single-Quantum Coherence (HSQC) experiment is used to indicate which protons are attached to which heteroatom via one-bond coupling information [268]. This is particularly useful for assignment of αC resonances in a peptide or protein. The HSQC experiment utilises a coherence transfer process in an analogous fashion to the COSY experiment, however the magnetisation is now allowed to transfer to a heteronucleus [268,362,363]. The pulse sequence for the simplest HSQC experiment is shown in Figure 4.5. Here a single 90° RF pulse is applied to the most abundant spin I (e.g. ^{1}H), which precesses at its Larmor frequency during the variable interval t_1. A second 90° pulse is then applied to both I and the rare spin S (e.g. ^{13}C) simultaneously, after which it is possible for the magnetisation from I to be transferred to the S spin to which it is scalar coupled. This gives rise to a cross-peak between atoms which are directly bonded, and a 2D spectrum results in which I spin frequencies appear in one dimension and S spin frequencies appear in the other. No diagonal peaks appear in the spectrum since there is no 90° pulse applied to the S spins before t_1 [268].
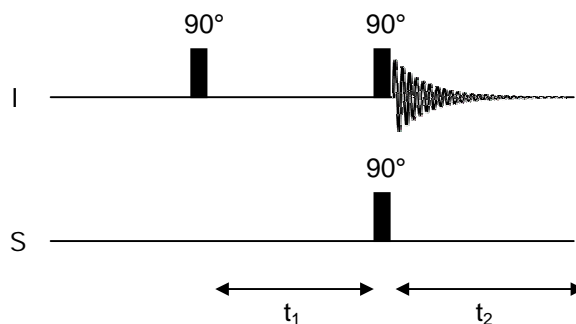
Figure 4.5: The pulse sequence of a simple polarisation transfer experiment.

Heteronuclear correlation experiments are inherently insensitive for biological NMR since it is the rare spin magnetisation being detected. However, beginning with proton polarisation and finishing with proton detection allows for optimum sensitivity [268]. In addition, HSQC spectra offer pure absorptive line shapes which are often narrow and hence generally well resolved [268]. A delay time is often inserted before and after the mixing pulse in order to prevent signals appearing as multiplets as a result of proton coupling [364]. This delay is typically set to $^1/_2$ J_{IS} where, for a one-bond ^{13}C-^{1}H correlation, J_{IS} is the heteronuclear coupling constant in the order of 100-200 Hz [203].

4.3.4 Nuclear Overhauser Effect Spectroscopy

The nuclear Overhauser effect (NOE) is the fractional change in intensity by cross-relaxation of one NMR signal when the transitions of other nearby nuclei are perturbed by irradiation [203,347,365]. Unlike the examples of correlated spectroscopy which rely on through bond interactions, the NOE effect results from mutual dipolar relaxation (through space interactions) between nuclei, and can be related to the internuclear distance of the atoms contributing to the signal [345,366]. The NOE spectroscopy (NOESY) experiment can identify all of the NOEs present in a molecule during a single experiment, and hence identify protons that are close together in space [365]. This is essential for sequential assignment of resonances in a peptide (Section 4.4), and also forms the basis of three-dimensional structure investigations (Sections 4.5 and 4.6).

The pulse sequence for a generalised NOESY experiment is illustrated in Figure 4.6 [365,367]. Again, a 90° pulse is applied to the system which tips the magnetisation into the xy-plane where it evolves over the variable time t_1. A second pulse is then applied orthogonal to the first which conveys some of the magnetisation to the z-axis. During the following mixing period τm, the non-equilibria z components will exchange among spins in close proximity via intra- or intermolecular dipolar relaxation [268,345,365]. After some time the transverse magnetisation is restored to observable magnetisation by application of a third 90° pulse, which is detected during t_2 [367].
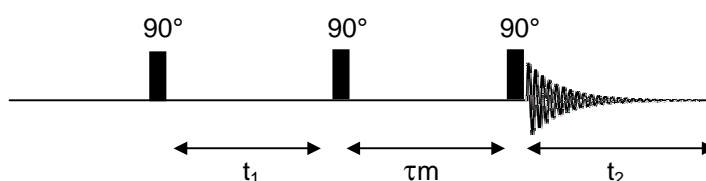
Figure 4.6: The pulse sequence of a typical NOESY experiment.

The NOESY spectrum therefore gives cross-peaks which are generated from the magnetisation transfer, and hence are due to proton pairs which are close together in space [268]. The relative intensity of a NOESY cross-peak can be correlated to the inverse sixth power of the distance between two protons responsible for the peak (i.e. $I \propto r^{-6}$). As a result, the maximum distance separation that can be detected is approximately 5 Å [203,368].

Distance measurement is not entirely accurate in a NOESY experiment since a number of factors can contribute to the intensity of a NOE signal. In addition, the NOE intensities represent an average of the inter-proton distances and hence are susceptible to conformational flexibility and chemical exchange [268]. Coherence transfer gives rise to COSY type peaks in the NOESY spectrum, however these can be suppressed with phase cycling or pulsed field gradients [369]. Finally, spin diffusion arising from the propagation of cross-relaxation among nuclei can affect peak intensities, but is typically only an issue for molecules with molecular weights > 10 kDa, and can be minimised with appropriate selection of experimental parameters [366,370]. As a

86

result, inter-peak distances are generally defined with upper and lower bounds to account for the uncertainty in measurement (Section 4.6.1).

4.4 Resonance Assignment in Peptides

NMR spectroscopy does not supply an image of a molecule directly, rather it provides an abundance of structural data which can be pieced together with extensive analysis and computer calculations to yield the protein structure in solution. In order for this to occur however, complete assignment of the proton resonances in the molecule is required [344]. This is done using a combination of 2D experiments, and a sequential assignment procedure [360]. Briefly, this assignment process can be divided into two stages. Firstly, the signals in individual spin systems are correlated and hence the resonances for each amino acid can be obtained. Finally, each spin system is assigned to a particular position in the protein sequence.

Initial assignment of each spin system is typically achieved using TOCSY and COSY spectra. TOCSY experiments can correlate all resonances in the same spin system and hence cross-sections of these spectra show cross-peaks from the NH to the α, β, γ, δ and ε protons (where present). By comparison with published chemical shift patterns [268] and random coil shifts [371], each spin system can be identified as a particular type of amino acid. Where signal overlap is an issue, the COSY experiment is employed to provide complementary information. This shows cross-peaks for each pair of nuclei coupled through two or three bonds, and hence allows protons within an amino acid to be correlated. In this way, amide protons are correlated to α protons, which in turn are correlated to β protons, and this process continues until the entire spin system has been identified. In very crowded spectra, this experiment allows easier determination of which spins are coupled to which, while the lack of a cross-peak is often indicative of an incorrect assignment in another spectrum.

Once assignment of the spin systems is essentially complete it becomes necessary to identify each amino acid according to its position in the sequence. This is most commonly achieved using information from the NOESY experiment, which shows correlations for protons close together in space. Distances between protons in adjacent

residues are termed 'sequential' distances, and will depend strongly on the molecular conformation. However, for all types of sterically allowed secondary structure, at least one sequential distance is always less than 3Å and is therefore observable in the NOESY spectrum [360]. As a result, such cross-peaks between adjacent residues are used to correlate sequential spin systems. Particularly useful are the NH_i-NH_{i+1}, αH_i-NH_{i+1} and βH_i-NH_{i+1} signals [348]. Breaks in the sequential NH_i to NH_{i+1} cross-peaks occur for Pro residues since these do not have an amide proton. In such cases, NH_i to δH_{i+1} and δH_i to NH_{i+1} cross-peaks can be observed.

Assignment of the αC ^{13}C resonances is sometimes also necessary for the analysis of secondary structure by NMR spectroscopy. This is typically achieved using a HSQC spectrum in which protons are correlated to the carbon atoms via the α^1H assignments. Cross-peaks from αHs in the proton dimension will directly give the associated αC ^{13}C chemical shifts in the carbon dimension [268].

4.5 Secondary Structure Analysis Using NMR Spectroscopy

There is extensive statistical data dealing with the qualitative relationship between various NMR parameters and regular secondary structure. As a result, once the sequence specific resonance assignments have been determined, NMR spectroscopy can be used to qualitatively investigate the 3D structure of a peptide.

4.5.1 Secondary Shifts

The magnetic environment of a nucleus is not only dependent on the nearby chemical surroundings, but also on the shielding effects which result from long-range interactions. Factors including polar and charged neighbouring groups, local fields around aromatic rings, bond hybridisation states and magnetic anisotropies contribute to the chemical shift of a nucleus [203,268,372], and are in turn affected by conformation and molecular geometry. Consequently, chemical shift is highly sensitive to 3D structure, and therefore this property can be used to predict regions of regular secondary structure in peptides.

Random coil shifts have been determined empirically for the twenty common amino acids in unstructured peptides [371]. The difference between an observed shift and the corresponding random coil resonance is termed the secondary shift ($\Delta\delta$), with a positive $\Delta\delta$ indicative of a shift downfield from random coil values and a negative $\Delta\delta$ denoting a shift upfield. Plotting $\Delta\delta$ against amino acid sequence allows for the identification of regions with consistent secondary shift, and hence specific secondary structure. The difference in chemical shift is often smoothed over a window of $\pm$ 2 residues to reduce the effect of local chemical shift influences, such as nearby aromatic rings and polar or charged groups, so that regions of secondary structure are more easily identified [373].

Statistical analysis and theoretical calculations have shown that αH resonances demonstrate a distinct upfield shift in the order of 0.39 ppm when part of an α-helix, and are shifted downfield by approximately 0.37 ppm when part of a β-strand or extended conformation [372,374]. Studies of αC resonances demonstrate the converse, with α-helices and β-strands exhibiting positive and negative $\Delta\delta$ values respectively [372]. Amide proton resonances are generally more sensitive to temperature and pH [373], however correlation between secondary structure and NH secondary shifts has also been observed with NH resonances generally upfield in helices and downfield in strands [372]. In addition, N-terminal amide resonances are usually downfield relative to those at the C-terminus for a helix, possibly due to the deshielding effect of the helix-dipole at the N-terminus and shielding of the C-terminus [372,375]. Finally, secondary shifts allow identification of regions with greater conformational flexibility. Here the peptide is more random-like and hence $\Delta\delta$ approaches zero [372,373].

Amphipathic α-helices show a distinct secondary shift pattern for NH resonances, with periodic variation over 3-4 residues [376,377]. Resonances from the hydrophobic face show positive $\Delta\delta$ values, while the hydrophilic residues demonstrate negative secondary shifts [376]. This is thought to be a consequence of hydrogen bond lengths on either face. In particular, the intramolecular hydrogen bonds between hydrophilic residues are weakened as the carbonyl groups tilt away from the helix to form additional hydrogen bonds with the solvent, while on the hydrophobic face the intermolecular hydrogen

bonds are strengthened as solvent access is reduced. Greater shielding of the NH nucleus occurs with shortened hydrogen bonds, giving rise to downfield shifts. The contrary is true where hydrogen bonds are lengthened [376,378].

4.5.2 NOE Connectivities

In addition to intra-residue and sequential signals, a number of medium- or long-range ^{1}H-^{1}H distances are sufficiently short in regular peptide secondary structures to be observable in the NOESY experiment [360,365,379]. These distances are described using standard notation, where $d_{AB(i,j)}$, is the distance between two protons A and B on residues i and j. Distances are defined from the N- to the C-terminus of the peptide sequence and the residue indices are often omitted for sequential distances (i.e. $d_{AB} \equiv d_{AB(i, i+1)}$). For methylene or methyl βHs and the αHs of Gly the notation refers to the shortest distance, and for Pro residues in which no amide protons exist the corresponding distances are instead described from the δ protons [360].

The pattern of observed NOE signals can be used to give an indication of regular secondary structures in peptides and proteins [348,354,360,365]. The spiral feature of an α-helix means that inter-residue NOEs are usually observed between protons which are three and four residues apart. Consequently, this secondary structure is characterised by strong sequential d_{NN}, medium $d_{\alpha N}$, $d_{\alpha Ni+3}$ and $d_{\alpha\beta i+3}$, and weak $d_{\alpha Ni+4}$ NOEs. β-sheets however show much less pronounced long-range NOEs, with only strong $d_{\alpha N}$ and weaker d_{NN} signals present, along with diagnostic short interstrand d_{NN}, $d_{\alpha N}$ and $d_{\alpha\alpha}$ distances. In a similar manner, NOE connectivity data may also indicate the presence of tight turns in a peptide or protein. The standard pattern of NOE connectivities for idealised α-helices and β-strands are given in Figure 4.7.
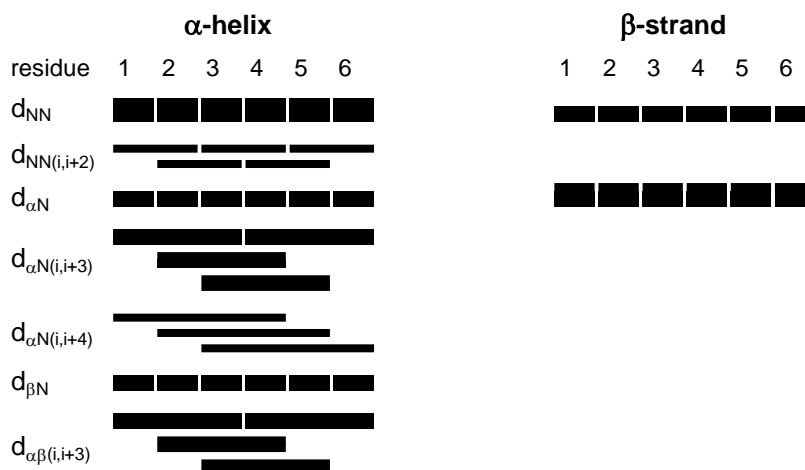
Figure 4.7: Characteristic short-range NOEs observed for ideal α-helices and β-strands. Bar thickness indicates the relative intensity of the NOE signal.

NOE connectivities can also give an indication of the extent of *cis-trans* isomerisation about the imide bond between Pro and its preceding residue [379]. In the *cis* form the $d_{\alpha\alpha}$ and $d_{N\alpha}$ distances are quite short, while in the more common *trans* form short $d_{\alpha\delta}$ and $d_{N\delta}$ distances are observed (Figure 4.8).
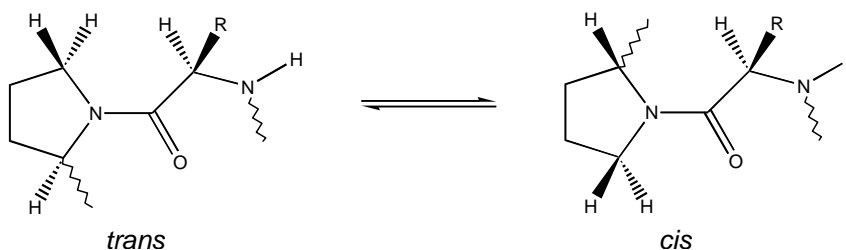
Figure 4.8: *Cis-trans* isomerisation of the X-Pro bond.

NOE connectivity patterns are typically not complete in a NOESY spectrum for a number of reasons [268]. For example, resonances which have similar chemical shifts may not be distinguishable from the diagonal, and presaturation of the water resonance can cause saturation of resonances in this region, particularly for αH signals. Finally, signal overlap will contribute some uncertainty into the NOE pattern.

4.5.3 Coupling Constants

Spin-spin coupling constants characterise interactions between nuclei linked by a small number of covalent bonds. The scalar coupling effect is a result of the spin pairing of each nucleus to the electrons in the bonds between them, causing each nucleus to be sensitive to the possible orientations of the neighbouring spins [268]. Thus, a coupled nucleus will have its signal split into multiplets, with the number of lines equal to $2I + 1$ where I is the spin of the neighbour, and the spacing between the lines equal to the coupling constant J [203,345,346].

Vicinal spin-spin coupling constants (^{3}J) can provide useful structural information to supplement inter-proton distance restraints, by giving an estimated range of torsion angles in the peptide backbone. The magnitude of a ^{3}J coupling constant can be approximated by the Karplus equation, which has the form;

$$^3J = A + B\cos\theta + C\cos\theta$$

where A, B and C are constants dependant upon substituent electronegativity, and θ is the dihedral angle [380].

By examination of known peptide structures, values of the Karplus coefficients have been empirically determined for different classes of protein dihedrals. The backbone dihedral angle defined by the atoms C'_i, N_{i+1}, αC_{i+1} and C'_{i+1} is called the phi angle (ϕ) (Figure 4.9) and can be related to the NH-αH coupling constant ($^3J_{NH\alpha H}$) by the following specific form of the Karplus equation [381];

$$^3J_{NH\alpha H} = 6.4\cos^2(\phi - 60^o) - 1.4\cos(\phi - 60^o) + 1.9$$
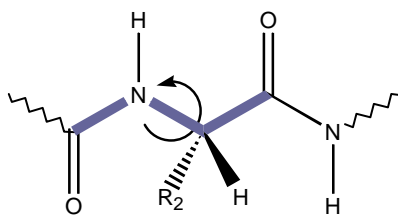
Figure 4.9: The phi (ϕ) dihedral angle shown in blue. In this representation ϕ is equal to 180°.

This equation is summarised graphically in Figure 4.10, where it can be seen that a given $^3J_{NH\alpha H}$ can correlate to as many as four different ϕ values. However, in known proteins the ϕ angles for all amino acids, excluding Gly, typically fall in the bounds of -30° to -180°. Furthermore, this range can be additionally refined for $^3J_{NH\alpha H}$ values of less than 6 Hz, where the ϕ values are clustered between -50° and -90° [382].
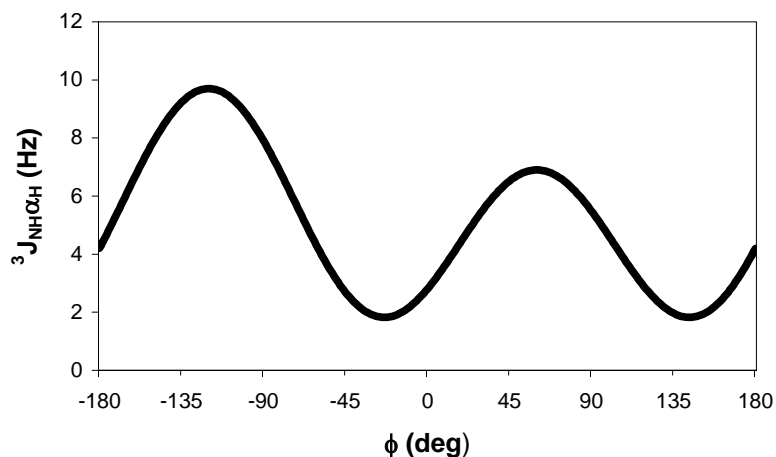
Figure 4.10: Karplus curve showing the relationship between the $^3J_{NH\alpha H}$ coupling constant and the ϕ dihedral angle.

Given that ϕ is equal to -57° ($^3J_{NH\alpha H}$ = 3.9 Hz) for an ideal α-helix, -139° ($^3J_{NH\alpha H}$ = 8.9 Hz) for an antiparallel β-sheet and -119° ($^3J_{NH\alpha H}$ = 9.7 Hz) for a parallel β-sheet [381], the magnitude of the vicinal coupling constants can be related to protein secondary structure. However, since the secondary structural features of real proteins are often somewhat distorted, the ϕ values and in turn the ^3J values may show sizable deviations from the standard values [381]. In addition, local motion about the N-αC bonds may also cause variations in the dihedral angles, hence the observed vicinal coupling constants represent a time-average of all conformations [268]. In general, observation of three to six sequential $^3J_{NH\alpha H}$ values of less than 6 Hz is a reliable qualitative measure of helical structure in that part of the molecule, while consecutive values greater than 8 Hz indicate β-sheet arrangement [360].

Vicinal coupling constants can be measured directly from the amide region of a high-resolution 1D ^{1}H spectrum, however this is limited to small peptides in which there is little overlap of signals in this region [268]. Alternatively, $^3J_{NH\alpha H}$ values can be extracted from phase sensitive COSY experiments. The active coupling between the two protons responsible for the peak results in anti-phase multiplets in the COSY spectrum. The coupling constant can therefore be measured by observing the separation between the peak and trough of the anti-phase signals [383]. Care must be exercised whilst using this method however, as the coupling constants can be significantly overestimated if the value of $^3J_{NH\alpha H}$ is less than the signal line width [268,360].

4.6 Structure Calculations

Although the chemical shifts, NOE connectivities and coupling constants can give a qualitative view of the structure of a peptide or protein, more complex analysis is required to obtain an accurate representation of the molecule in solution. This is achieved using NMR data as input for structural calculations. The basic steps involved in this process can be summarised as follows: Initially, the sequence specific resonance assignments must be completed, as detailed in Section 4.4. Next, structural restraints are generated. These are primarily inter-proton distance restraints from NOESY spectra, and may be complemented by dihedral angle restraints obtained by inspection of $^3J_{NH\alpha H}$ coupling constants. These restraints form the basis of the restrained molecular dynamics and simulated annealing protocols which are used to determine the 3D structure. Finally, the quality of the calculated structures must be assessed to ensure a reasonable representation of the peptide in solution has been produced.

Structure calculations detailed in this thesis were carried out using the program ARIA (Ambiguous Restraints for Iterative Assignment, version 1.2) [384,385]. This program consists of a series of routines that perform partial assignment and calibration of structural restraints, together with organisation of an iterative calculation procedure that is interfaced with CNS (Crystallography and NMR System, version 1.1) [386]. Each stage of the structure calculation process will be discussed in detail in the following sections.

4.6.1 Distance Restraints

The intensity of a NOE signal initially increases with mixing time before reaching a maximum and thereafter decaying to zero (Figure 4.11) [268]. In addition, the rate of molecular tumbling as described by the correlation time of a molecule $(\tau_c)^{\dagger}$ is also an influential factor on peak intensity, with the initial rate of NOE build-up proportional to τ_c (Figure 4.11) [337,387]. This implies longer distances will only be observed in a NOESY spectrum if a sufficiently long mixing time is used. However, while the initial rate of cross-peak build-up increases with increasing correlation time, the onset of decay occurs sooner. The importance of the time development of cross-peak intensities is that initial build up rates are proportional to r^{-6}, and thus when the initial rate approximation is satisfied, peak intensities can be used to estimate proton-proton distances [348,388].
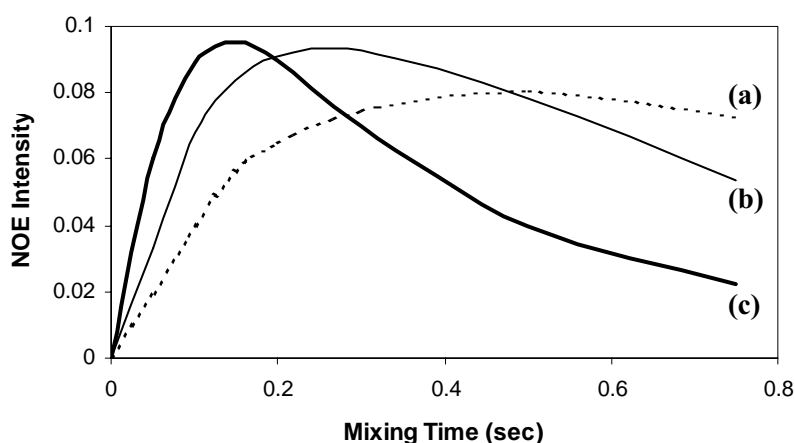
Figure 4.11: Time dependence of the intensity of the δH-εH cross-peak of Tyr68 in dihydrofolate reductase, calculated for the correlation times **(a)** 2 ns, **(b)** 4 ns and **(c)** 8 ns. Figure adapted from [389].

Numerous methods have been developed to convert the series of peak volumes into distance restraints. For example, distances between protons i and j (r_{ij}) can be estimated by comparison with a reference distance between protons k and l (r_{kl}), for which there is a well resolved and uniquely assigned cross-peak with intensity I_{kl}.

---

† Assuming molecular weight, M_r, is proportional to the molecular radius, r, then the correlation time can be approximated as $\tau_c \approx M_r \times C$, where C is typically 1.3×10^{-12} [268].

Thus, the distance estimate is given according to the following relationship [348,389];

$$r_{ij} = r_{kl} \left(\frac{I_{kj}}{I_{ij}} \right)^{1/6}$$

This is only true however for the initial rate approximation [268], and applies only for the same effective τ_c. The reference distance must be accurately known, and hence is typically chosen between protons with fixed relative positions such as non-degenerate methylene protons [389], δ and ε aromatic protons [268], δ and γ protons of Pro [312], or α and NH protons in regions identified as α-helical [360]. However, systematic errors associated with measuring the distance of each of these internal references often result in inaccuracies in the calculated distances [268].

In order to avoid the use of reference distances, an alternative approach may be taken in which distances are estimated from NOE intensities according to the following equation;

$$I_{ij} = \alpha r_{ij}^{-6}$$

where α is a calibration factor dependent on the properties of the system under investigation as well as the experimental setup, and is determined during the course of the calculations [390]. Using ARIA, α is obtained by a comparison of theoretical (I_{ij}^{th}) and experimental (I_{ij}^{exp} – measured from a preliminary ensemble of structures) NOE intensities as follows;

$$\alpha = \frac{\sum_{ij} I_{ij}^{exp}}{\sum_{ij} I_{ij}^{th}}$$

In this way, the target distances for the next iteration of structure calculations can be estimated [390,391]. For the first iteration where no structure ensemble is specified, the initial estimate of the calibration factor, α_0, is calculated by assuming the average distance, r_{av}, of spin pairs causing NOEs is known.

This is summarised in the following equation [390];

$$\alpha_0 = n^{-1} \sum_{ij=1}^{n} \frac{r_{ij}^{exp}}{r_{av}^{-6}}$$

Spin diffusion results as cross-relaxation is propagated across the molecule from one nucleus to another [268]. This indirect transfer of magnetisation causes a decrease in intensity of strong peaks while increasing the intensity of weak peaks [385,388]. Thus, if the initial rate condition is not upheld and the mixing time is too long for the molecule under consideration, spin diffusion will affect NOE peak intensities, causing errors in the estimated distances [268]. In addition, the intensity-distance relationship assumes that the correlation time is the same for each proton in the molecule, which is clearly an oversimplification [366,388]. In particular, the long amino acid side chains are subject to rapid local motions which act to reduce the NOE buildup rate [354]. As a result of these and other factors which can affect NOE intensities [348], exact calibration is not possible in practice, and hence distances are restrained with upper and lower bounds.

One common method for determining distance ranges is to classify the NOEs into three categories, namely strong (1.8-2.8 Å), medium (1.8-3.3 Å) and weak (1.8-5.0 Å), whereby the lower limit of 1.8 Å corresponds to the sum of the van der Waals radii of two protons [348,388,392]. An alternative approach to calculating error bounds is employed in the ARIA methodology, and involves adding an estimate of the distance error to the calibrated distance to define lower (L) and upper (U) distance constraints [385,390];

$$L = r_{ij} - \delta \qquad \text{and}$$
$$U = r_{ij} + \delta$$

The value of δ is often calculated as a percentage of the distance, to allow for the errors while retaining the continuum of restraints. However, as the error is expected to increase at a greater than linear rate, a better approach is often to vary the error estimate with the square of the calibrated distance [385].

By default, ARIA uses a second order polynomial to calculate the error margin as follows [390];

$$\delta = 0.12 \text{ x } r_{ij}^2$$

However, other functional forms are supported [384,390]. In general, varying the tightness of the distance bounds does not have a pronounced effect on the resultant structures, with even very loose restraints significantly limiting the conformational space available to the peptide [385,393].

4.6.2 Ambiguous NOEs

As the size of a peptide increases, the likelihood of multiple atoms having the same chemical shift also increases. Ambiguity also occurs when methylene or isopropyl methyl resonances are degenerate. A NOE cross-peak involving these protons cannot be directly converted into a distance restraint between two atoms since the contribution of all interacting atoms must be considered. Thus, even after the proton chemical shifts have been completely assigned, the task of assigning the ambiguous NOE cross-peaks remains [394].

One approach for overcoming this problem involves performing structure calculations in an iterative manner, beginning with only uniquely assigned signals. Resulting structures give an indication of distances for each proton pair in the ambiguous region, and those that are excessively distant can be excluded. Continual refinement in this way can result in clarification of initially ambiguous signals and improve calculated structures [394,395]. This procedure may fail however if several assignments of the NOESY spectrum may be possible, resulting in different 3D structures [396]. In addition, the distance between two protons in a preliminary structure may be larger than 5 Å even though these give rise to a NOE cross-peak since, for example, a side chain rotation can increase the distance by several Å without affecting the overall fold [394].

Ambiguous assignments may also be managed using the sum averaging method [394,397]. On the basis of the isolated spin pair approximation [365], the cross-peak volumes depend simply on the distances for each spin pair as follows;

$$I_{xy} \propto \sum_{a=1}^{N_\delta} r_a^{-6}$$

where I is the intensity of the signal, a runs through all N_δ contributions to a cross-peak at frequencies x,y and r_a is the distance between two protons corresponding to the ath contribution [387]. As a result, the ambiguous NOE is related to an effective distance defined by;

$$D \propto \left(\sum_{a=1}^{N_\delta} r_a^{-6} \right)^{-1/6}$$

Here the volume of the ambiguous peak is treated as a sum of the volumes of each possible contributing peak, and distance restraints account for multiple contributions to a single NOE signal by constraining r_a values such that this equation is satisfied [387]. Although this approach is generally less accurate, it allows the information contained in ambiguous resonances to be retained, which improves the quality of the derived structures overall [394].

4.6.3 Stereospecific Assignments

Individual methylene protons or methyl groups of an amino acid can often be resolved in a 2D spectrum, and consequently necessitate stereospecific assignment to improve both the accuracy and precision of calculated structures [393,398,399]. This can sometimes be achieved for β-methylene protons by inspection of the relative intensities of NOE signals involving NH, αH and βHs, as well as from $^3J_{\alpha H\beta H}$ coupling constants [348]. Similar methods exist for stereospecifically assigning the methyl groups of Val and Leu residues [400]. Although these procedures are effective, they are tedious and not always possible. Futhermore, internal motions often produce degenerate resonances that cannot be stereospecifically assigned from spectral data alone.

An alternative approach to stereospecific assignment involves the floating chirality method [401,402]. Here NOEs are measured for individual resonances and are assigned arbitrarily. They are then allowed to either 'float' between pro-S and pro-R configurations by starting with a small force constant for the improper dihedrals and gradually increasing this over the course of the calculations [348,402], or explicitly swap configurations at different points in the calculation provided a decrease in energy is observed [401,403]. In this way the most energetically favourable orientation is reached, and protons are retained in correct stereo-assignment [402]. Hence valuable structural information is retained by this method without direct assignment of these resonances.

4.6.4 Dihedral Angle Restraints

As outlined in Section 4.5.3, the relationship between ϕ dihedral angles and the $^3J_{NH\alpha H}$ coupling constant can be described by the following version of the Karplus equation [381];

$$^3J_{NH\alpha H} = 6.4\cos^2(\phi \text{ - } 60^o) - 1.4\cos(\phi \text{ - } 60^o) + 1.9$$

Thus, $^3J_{NH\alpha H}$ values give specific ϕ angles that can be used as dihedral angle restraints to supplement the inter-proton distance information provided by NOESY spectra. However, coupling constants can only be obtained with limited accuracy as local motion around the N-αC bonds results in time-averaged $^3J_{NH\alpha H}$ values [268]. As a result, dihedral angles are typically restrained to a range of possibilities for structure calculations, commonly as follows; $-60 \pm 40°$ for $5Hz < ^3J_{NH\alpha H} < 6Hz$, and $-60 \pm 30°$ for $^3J_{NH\alpha H} < 5Hz$. For $^3J_{NH\alpha H} > 8Hz$, ϕ values are restrained to $-120 \pm 40°$ [404,405].

4.6.5 Restrained Molecular Dynamics

Many different methods exist for calculating protein structures from NMR-derived restraints. One general approach however is to minimise an objective potential energy function that incorporates experimental data in the form of conformational restraints, as well as physical knowledge using a molecular dynamics force field [393,394,406-409]. This forms the basis of restrained molecular dynamics (RMD) calculations.

RMD attempts to simulate the motions of a system of atoms according to classical laws of motion, while introducing a set of experimentally derived restraints [336,388,410]. The particles are allowed to evolve across a series of positions and velocities, and at each step the force on every atom is evaluated according to Newton's equation of motion;

$$F_i = m_i a_i$$

where $\mathbf{F_i}$ is the force on atom i, m_i is the mass and $\mathbf{a_i}$ is the acceleration, and the force and acceleration are vector quantities. The force on atom i can also be calculated from the derivative of the potential energy (V) with respect to the position r_i of the atom, and the acceleration can be expressed as the second derivative of position with respect to time. Consequently, the previous equation can be expressed in the following form [268];

$$\frac{dV}{dr_i} = m_i \frac{d^2 r_i}{dt_i^2}$$

Since the atomic masses are known, given an appropriate potential energy function and a set of starting coordinates, this equation can be integrated over small, successive time-steps to determine the velocity and displacement of the atoms [410,411]. The initial starting conformation can be arbitrary, although in practice a starting structure may be obtained by means of distance geometry algorithms or model building [348,354,388,406,409]. Random velocities are then assigned to each atom in the system from a Maxwellian distribution at a specified temperature [410] to account for the thermal motions of the atoms.

The temperature (T) of the system is measured by the mean kinetic energy, according to the following equation;

$$\sum_{i=1}^{N} \frac{m_i(v_i)^2}{2} = \frac{3N}{2} k T$$

where k is Boltzmann's constant, v_i is the velocity of the atom and N is the total number of atoms in the system [410]. Excess potential energy within the system is converted to kinetic energy during calculations, and removed by coupling to a theoretical heat bath [388]. In this way, the energy minima of the system are elucidated, giving the most favourable conformations. Many structures may be consistent with the experimental restraints, and hence the calculation procedure must be repeated multiple times to give an ensemble of structures [344]. This is achieved by randomly varying the initial structure or the assigned velocities for each repetition [268].

The success of the RMD protocol depends on the quality of the potential energy function used to locate the global minimum, which is given by the following equation [348,354,388];

$$V_{total} = V_{covalent} + V_{repel} + V_{NOE}$$

The covalent term acts to maintain the correct bond lengths, angles, chirality and planes during the calculation. The potential energy of these properties is frequently given by harmonic potentials, as can be seen for V_{bond} below;

$$V_{bond} = \sum_{bond} K_b (b - b_0)^2$$

where K_b is the bond force constant, determined empirically, b is the bond length and b_0 is the ideal bond length. [348,410]. Deviations from the ideal values are thus penalised by higher energies.

The second term in the potential energy function is the sum of the non-bonded potential energies. This consists of the Lennard-Jones potential and the Coulomb potential which describe van der Waal's interactions and electrostatic interactions respectively, and are given by the following equations;

$$V_{vdW} = \sum_{pairs\,(ij)} \left[\frac{A}{r_{ij}^{12}} - \frac{B}{r_{ij}^{6}} \right] \qquad \text{Lennard-Jones potential}$$

$$V_{electrostatic} = \sum_{pairs\,(ij)} \frac{q_i q_j}{D r_{ij}} \qquad \text{Coulomb potential}$$

where A and B are experimentally determined parameters dependent upon the particular atoms involved, and r_{ij} refers to the distance between atoms i and j. The charges on atoms i and j are indicated by q_i and q_j and D is the effective dielectric function for the medium [410]. Use of partial charges in the electrostatics term avoids the need for a separate description of hydrogen bonding interactions [410].

The final term in the potential energy function distinguishes RMD from more conventional molecular dynamics simulations, and provides a means for introducing the experimentally derived restraints. The NOE distance restraints are often described as square-well potentials in the form;

$$V_{NOE} = \begin{cases} K_{NOE}(r_{ij} - r_{ij}^{u})^2 & \text{if } r_{ij} > r_{ij}^{u} \\ 0 & \text{if } r_{ij}^{l} \leq r_{ij} \leq r_{ij}^{u} \\ K_{NOE}(r_{ij} - r_{ij}^{l})^2 & \text{if } r_{ij} < r_{ij}^{l} \end{cases}$$

where r_{ij}^{u} and r_{ij}^{l} are the values of the upper and lower limits of the target distances respectively, and K_{NOE} is the NOE force constant or weighting factor [348,406]. A similar potential is applied for dihedral angle restraints. Unlike the other potential energy terms, the NMR restraint potentials do not correspond to any real physical forces [268]. Therefore, although the force constants are set somewhat arbitrarily, the values must be sufficiently high to ensure that the experimental restraints are the governing factor in the structure determination [348].

Numerous local minima exist on the potential energy surface which correspond to alternative conformations, and must be overcome to reach the global minimum. While basic energy minimisation techniques are good at finding such local minima, they do not allow the system to overcome the energy barriers required for the continued descent toward the global minimum [268,388]. Consequently, RMD calculations are often combined with simulated annealing (SA) in which high initial temperature (in the order of 1000 K) is imparted to the system to introduce greater kinetic energy. Slow cooling then follows, allowing a molecule initially trapped in a local minimum to overcome energy barriers and reach the global minimum, giving a more accurate representation of peptide structure [348,388]. This can also be achieved more conveniently by varying the applied force constants rather than the temperature. While these methods are not entirely equivalent, scaling of a force constant by a factor of x corresponds to scaling the temperature by $^1/_x$ [406].

4.6.6 Structure Quality

As NMR derived restraints are described as ranges rather than discrete values, multiple structures may satisfy the experimental data. Accordingly, the consistency, precision and accuracy of the calculated structures must be investigated to ensure they are a reasonable representation of the peptide in solution.

One of the most straightforward indicators of the quality of an experimental data set is the number of restraints, since the accuracy of calculated structures improves with increasing data content [412,413]. Where the NMR restraints are satisfied but widely varying structures result, the information contained in the restraints is inadequate for defining an accurate protein structure [348]. Fewer than average NOEs are typically observed for regions with conformational disorder, however mobility cannot be inferred from this alone [348,412].

Restraint violations are an indication of how well the structures satisfy the NMR-derived data, and provide another means for checking the quality of structures. These occur when calculated distances disagree with the restraints derived from NOE

intensities. The number of violations should be minimal and as a general consensus structures with violations less than 0.5 Å are acceptable, however in recent times cut-off values of 0.3 Å have been reported [412]. Recurring restraint violations are a strong suggestion that there are inconsistencies in the experimental data. This could occur because of mistakes in the assignment process, and implies that the restraints should be reanalysed [268,412].

The root-mean-square deviation (RMSD) from a calculated average indicates how well an ensemble of structures has converged, and gives a measure of the precision of the structure ensemble. Generally the RMSD is acceptable if lower than 2 Å [414]. Regions with high RMSD values are those that are less well-defined by the data. If the restraints are satisfied and RMSD values suggest a significant proportion of the structures have converged, then the ensemble of structures is likely to closely resemble the actual protein structure [268].

In addition, the angular order parameters can be calculated for a structure ensemble according to the equation;

$$S(\alpha_i) = \frac{1}{N} \left\| \left(\sum_{x=1}^{N} \alpha_i^{x} \right) \right\|$$

where $S(\alpha_i)$ is the order parameter of the dihedral angle α_i of residue i, and x refers to the individual structures, from 1 to N [415]. These provide a measure of the distribution of dihedral angles for each residue over the range of calculated structures. For an angle that shows no deviation over the ensemble of structures S is equal to one, while for a randomly distributed dihedral angle S is equal to zero. Angular order parameters are most often used to assess the order of the backbone angles phi (ϕ) and psi (ψ), where ϕ is defined by C'_i, N_{i+1}, αC_{i+1} and C'_{i+1} and ψ is defined by N_i, αC_i, C'_i and N_{i+1} (Figure 4.12). Consistent structures will show well-defined backbone dihedral angles in which $S > 0.9$, corresponding to a standard deviation of 18º [415,416].
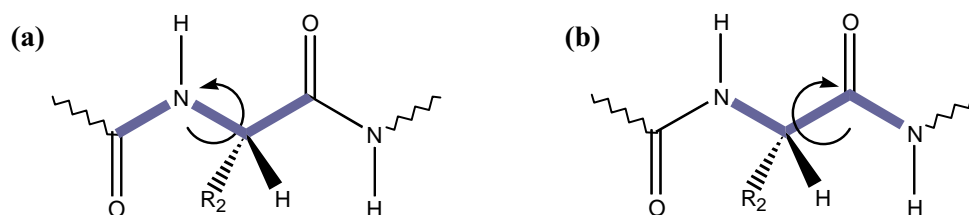
Figure 4.12: **(a)** Phi (ϕ) and **(b)** psi (ψ) dihedral angles. In these representations ϕ and ψ are both equal to 180°.

The most powerful check for stereochemical quality of a protein structure is the Ramachandran plot. Ramachandran *et al.* showed that only certain combinations of ϕ and ψ angles are permitted in peptides and proteins due to steric interactions [417]. When the ϕ and ψ angles from known protein structures (with the exception of Pro and Gly residues which are excluded due to their atypical ϕ/ψ distributions) are plotted against each other, they tend to fall in certain regions based on the secondary structure in which the residue is contained [414]. Over 80% of the residues will fall within the highest density regions, collectively called favourable regions. Other areas can be defined with progressively lower residue densities and these are known as the allowed, generous and disallowed regions. This constitutes the Ramachandran plot (Figure 4.13).
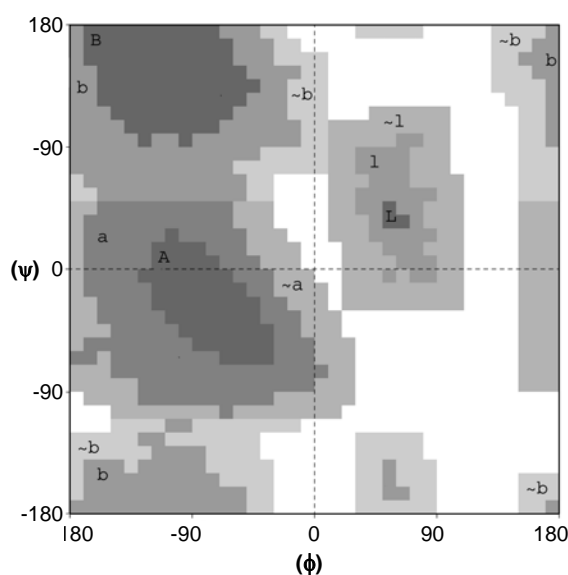
Figure 4.13: Ramachandran plot. Favourable regions for α-helices are labelled A, allowable and generous regions are labelled a and ~a respectively. Regions are labelled in a similar manner for β-sheets (B) and left handed α-helices (L).

High quality structures would therefore see well-defined residues appearing in the favourable and allowed regions of a Ramachandran plot [414]. As residues from different classes of secondary structure fall into specific regions, these plots can also give an indication of the secondary structure present in the molecule.

Finally, the calculated structures should demonstrate covalent properties such as bond lengths, angles and impropers which correlate closely to idealised covalent geometry [268].

4.7 Model Solvent Systems

A wide variety of biologically active peptides are thought to exert their effects by interaction with the cell at its outer surface, either with the membrane directly [418-420], or with membrane bound receptors [421,422]. The NMR spectra of peptides bound to native bilayers or even vesicles are usually so broadened due to the slow tumbling of these structures in solution, that the methods of high-resolution NMR are not applicable [423,424]. Consequently, in order to probe the conformation and activity of such peptides using NMR spectroscopy, it is necessary to have an alternative solvent system which most closely emulates this environment.

Water on its own forms hydrogen bonds with both the carbonyl and amide groups of the peptide, interrupting the regular intramolecular bonding responsible for maintaining secondary structure. However, alcohols are much larger than water and are significantly less polar and less basic. As such, water is displaced from the solution shell of the peptide and the potential for intermolecular hydrogen bonding is reduced, favouring formation of regular secondary structure [425,426]. Mixed organic solvents are the simplest and least expensive of the membrane mimicking systems, and have been used extensively for the study of membrane active peptides and proteins [427-430]. Importantly, alcohol/water mixtures have been shown to induce secondary structure in peptides that are similar to those observed in lipid environments [425,427].

2,2,2-Trifluoroethanol (TFE) is probably the most common alcohol used in such mixed solvent systems, and has a greater stabilising effect than methanol or ethanol [431]. The stabilising properties of such fluorinated alcohols may be accounted for by the high tendency of these molecules to form micelle-like clusters in aqueous solution [432]. Clustering gives rise to microscopic regions of low polarity, in which the intramolecular hydrogen bonds responsible for maintaining secondary structure are further strengthened [431,432]. Nevertheless, this low polarity weakens the hydrophobic interactions that stabilise the tertiary structure of proteins, and as such there is a poor correlation between native protein conformations and those determined in aqueous TFE [431,433]. This is not an issue for small peptides such as those studied in this research, since they do not have tertiary structural features.

Although TFE is widely thought of as a helix-inducing solvent, Sönnichsen *et al.* found that helical structure was only observed where there was helical propensity in the sequence [434]. In addition, many examples of β-turn and β-sheet structures have been observed in aqueous TFE mixtures [425,429,435], demonstrating that TFE does not enforce helical structure but merely enhances it if the propensity exists. However, a number of cases are also evident whereby addition of TFE can promote switching between different secondary structures, generally from a β-sheet to an α-helix [436-438]. Thus, despite its wide application, some care must still be applied when interpreting structural data using TFE as a membrane mimicking solvent system.

The proton peak for water in the solvent is by far more intense than the protons in the peptide sample. In order to overcome this a number of solvent suppression methods have been developed to reduce the intensity of the solvent signal and reveal the peaks of interest. Presaturation is the easiest way of suppressing the water signal, and involves application of continuous low power RF radiation at the same frequency of the solvent peak during the relaxation delay [268,439,440]. Alternatively, methods such as the WET or WATERGATE sequences can be employed, and are based on a selective dephasing of the solvent signals using gradient pulses [441-444].

~ CHAPTER 5 ~

Calmodulin-Peptide Complexes and the Inhibition of Nitric Oxide Synthase

5.1 Introduction

5.1.1 Nitric Oxide as a Biological Signalling Agent

Despite being virtually unknown in biology until the late 1980's, the seemingly ubiquitous involvement of nitric oxide (NO) in a vast array of physiological processes, and the novel oxidative chemistry involved in its synthesis, has resulted in an explosion of interest in the field during the past two decades. NO is an important molecule in the nervous, immune and cardiovascular systems, where it performs a number of regulatory roles. The best characterised examples of NO controlled activity include vasodilation and regulation of smooth muscle tone, inhibition of platelet aggregation, neuronal transmission and sensory perception [445,446]. In addition, it appears that high levels of NO play a part in the immune response, and function in macrophage-mediated killing of tumour cells and microbial pathogens [447,448].

NO is a relatively stable radical which does not dimerise, yet is reactive in physiological conditions and has a biological half life in the order of 5-15 seconds [449]. Unlike virtually every other messenger molecule, the activity of NO results from covalent reactions as opposed to non-covalent ligand-receptor interactions. From a biological standpoint, the most important reactions of NO are those with transition metal ions, oxygen in its various redox forms, thiol containing molecules and other radical reactions, all of which provide an extraordinary number of potential biological targets [450-452]. NO is also small, uncharged and hydrophobic, making it readily diffusible across cell membranes without the need for specific transport mechanisms. Consequently, in contrast to most other neurotransmitters and hormones, the key to regulating NO function is not through storage, release, reactivity or degradation, but rather to control NO synthesis at the site of action [445,449].

Since NO acts as a biological signal in low concentrations and a toxin in high concentrations, its production is carefully managed in healthy organisms. This dual role also makes it a complicated pharmaceutical target. Dysfunctions of the synthetic pathway which result in excessive NO production have been characterised in multiple disease states including diabetes, neurotoxicity, inflammatory bowel disease, rheumatoid arthritis, cancer, septic shock and multiple sclerosis [445,446]. Thus, the challenge remains to develop selective inhibition of NO synthesis in order to address the treatment of NO related pathologies.

5.1.2 Nitric Oxide Synthesis

NO is synthesised in the body by highly regulated enzymes called nitric oxide synthases (NOS). Currently, three distinct isoforms of NOS have been identified, namely neuronal NOS (nNOS, also called NOS1), inducible NOS (iNOS or NOS2) and endothelial NOS (eNOS or NOS3). These names reflect the activity or the tissue type in which the enzymes were first described, however nearly every cell type studied thus far has demonstrated the ability to synthesise NO by one of the three enzyme subtypes [447,453].

All functional NOS proteins are homodimers with subunits of 130-160 kDa and are products of different genes, with an average of 50% homology between isoforms and 90% homology between the same isoform in different species [445,454]. Although differing in tissue distribution, functional regulation, catalytic properties and inhibitor sensitivity, the fundamental structure of the three isoenzymes is the same. Each contains an N-terminal catalytic oxygenase domain that binds haem (iron protoporphyrin IX), tetrahydrobiopterin (BH_4) and the substrate L-arginine, a C-terminal reductase domain that binds flavin mononucleotide (FMN), flavin adenine dinucleotide (FAD) and nicotinamide adenine nucleotide phosphate (NADPH) and finally, an intervening regulatory calmodulin (CaM) binding region (Figure 5.1) [445,453,455,456].
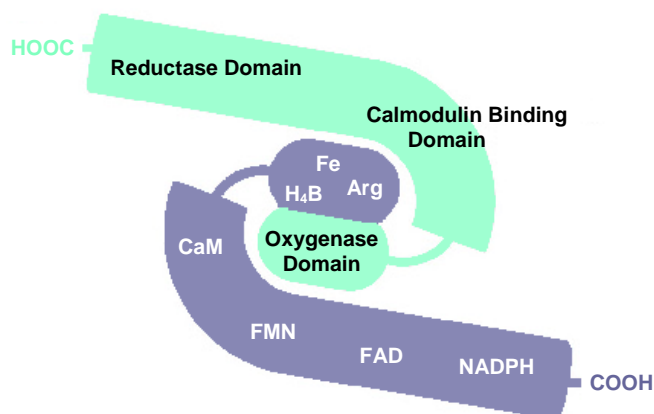
Figure 5.1: Schematic representation of the NOS enzyme. Structural domains are labelled in black, while co-factor binding sites are labelled in white.

Formation of NO occurs by a two-step, five electron oxidation of L-arginine to L-citrulline, via the stable intermediate N-hydroxyl-L-arginine (Figure 5.2) [451,454,455]. NADPH acts as the source of electrons for oxygen activation and substrate oxidation. These electrons flow from the reductase domain of one monomer via FAD then FMN to the haem iron in the opposing monomer, since the redox potentials are poised thermodynamically for this to occur [455]. The haem moiety of NOS resembles that of cytochrome P450s, and it is thought that many aspects of the NOS biochemistry relate to the action of these enzymes [455]. Maximal activity of NOS depends on binding of BH_4 which is suspected to play a role in dimer formation and stabilisation, however the exact role of this molecule remains unclear [454,456]. Finally, CaM is required for activation of NOS, and regulates electronic communication between the oxygenase and reductase domains by increasing the efficiency of electron flow through the enzyme to the catalytic site [453]. The cofactor requirements of NOS are not only important for catalytic activity, but they also appear obligatory in permitting dimerisation to give the active protein [453].
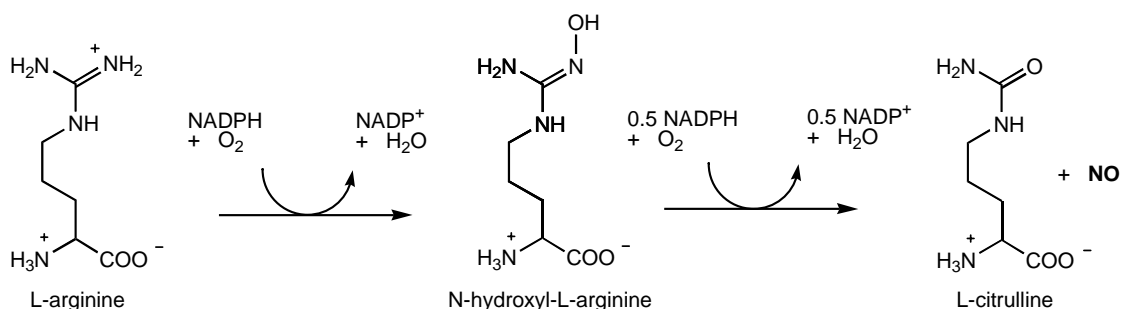
Figure 5.2: The production of nitric oxide by NOS.

The amount of NO produced by NOS is regulated in a cell and isozyme specific fashion. Both nNOS and eNOS are expressed constitutively, and the level of calcium in the cell primarily controls their activity. At normal resting levels of Ca^{2+} these isoforms are inactive, however when Ca^{2+} levels increase, binding of CaM to NOS is facilitated and catalytic activity is stimulated [445,457,458]. By this mechanism, NO synthesis can be efficiently coupled with physiological stimuli such as shear stress, neural depolarisation and second messenger systems such as cGMP which lead to rises in cellular Ca^{2+} concentrations [317,445]. In contrast, CaM is tightly bound to iNOS irrespective of Ca^{2+} concentration, hence its regulation occurs generally at the level of transcription. In most cell types iNOS protein levels are either very low or undetectable. Stimulation of these cells usually occurs with mediators such as cytokines, interleukins or growth factors, which leads to increased transcription of the iNOS gene and subsequent production of high concentrations of NO for longer periods [445,452,456].

5.1.3 Calmodulin

CaM is a highly conserved Ca^{2+} binding protein present in all eukaryotic cells, which acts to regulate a large number of proteins involved in a wide variety of Ca^{2+} mediated cell signalling pathways [317,459]. This 148-residue protein forms a dumb-bell-shaped molecule in which two globular domains are connected by a long central helix. NMR studies have shown this helix to be disrupted near its midpoint, and thus serve as a flexible linker between the two domains [460]. Each lobe contains three α-helices and two Ca^{2+} binding EF hand loops, allowing for the occupation of four Ca^{2+} ions

(Figure 5.3) [461-463]. Binding of calcium occurs in a stepwise manner, and gives CaM its functional conformation [461].
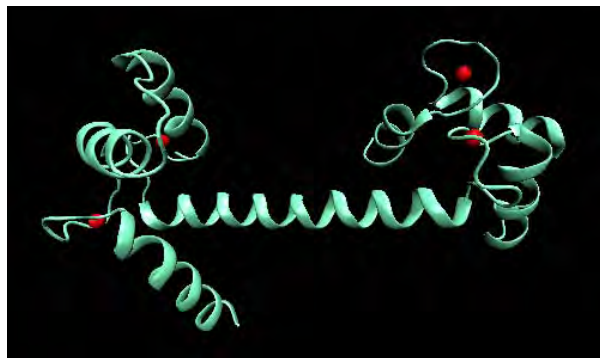
Figure 5.3: The three-dimensional structure of CaM [461]. Ca^{2+} ions are represented as red spheres.

CaM was the first protein shown to interact with NOS, and as previously mentioned, regulates catalytic activity by triggering electron flux from FMN to the haem moiety, thereby coupling the oxygenase and reductase domains [455]. It does this by binding to an amphipathic α-helical region at the centre of NOS [454,464,465], which in turn increases both the rate of electron transfer to the flavins from NADPH, and the rate at which electrons are accepted by the haem in the reductase domain [466-468]. Since CaM is critical to the function of NOS, it provides a possible mechanism to modulate NOS activity and control NO synthesis.

Most physiologically relevant CaM targets are proteins, however numerous studies have suggested that CaM with its full complement of calcium, Ca_4-CaM, can also form complexes with short, positively charged peptides whose binding domains demonstrate a propensity for amphipathic α-helix formation [316,469,470]. Despite little sequence homology between binding targets, many peptides bind very tightly, with association binding constants $K_{ass} \geq 10^7$ M^{-1} [471]. The structural basis in which Ca_4-CaM recognises its binding partners remains the subject of debate, although a number of models have been proposed, typically based on strong hydrophobic interactions [472-474]. Commonly, CaM binding peptides display large hydrophobic residues in conserved positions at either 1-5-10 or 1-8-14, which point to one face in a presumed α-

helical conformation [470]. Met residues, unusually abundant in CaM, also play a particularly important role in the binding of target peptides [470].

It is known that upon binding to a peptide, Ca_4-CaM undergoes a significant structural change involving the dissolution of the long central helix. Several binding modes have been identified, although the 'collapsed conformation' appears to be the most common. A number of such examples exist in the literature whereby CaM adopts a compact, globular shape, while the peptide is engulfed in a hydrophobic channel formed by the two terminal domains [470,471,475,476]. A good illustration of this type of structure was determined for the binding of a 26-residue peptide fragment of skeletal muscle myosin light chain kinase with Ca_4-CaM (Figure 5.4a) [471].

However, it has always been clear the binding mode in which CaM encapsulates the target peptide in a collapsed conformation could not generally apply to all CaM complexes [470]. For example, the binding domain of the plasma membrane Ca^{2+} pump (peptide C20) was shown to interact only with the C-terminal lobe of CaM, which remains in an extended conformation (Figure 5.4b) [477]. Many variations exist for this 'extended' binding mode, and in the case of larger binding partners, multimers can form between the ligand and two CaM molecules [470].
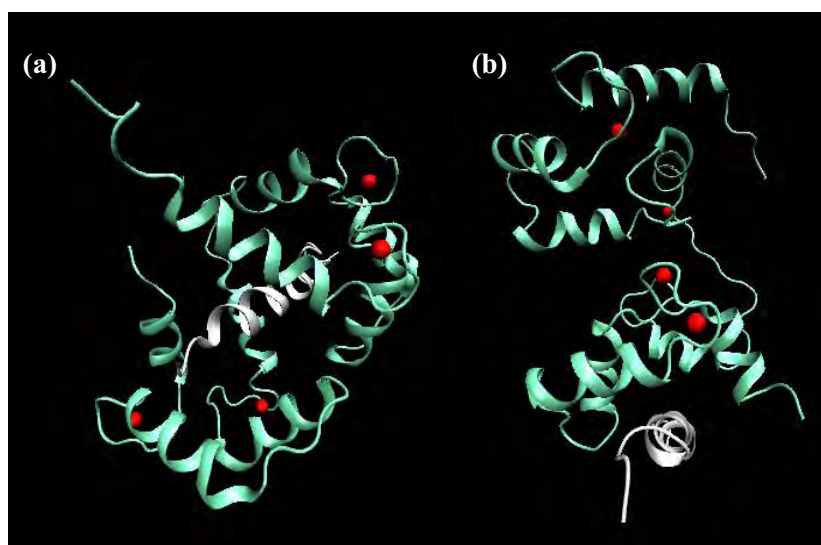
Figure 5.4: The three-dimensional structure of CaM (green) bound to a peptide (white) in **(a)** a collapsed conformation [471], and **(b)** an extended conformation [477]. Ca^{2+} ions are represented as red spheres.

Upon complexation with small peptides, CaM can no longer interact with its biological targets. Consequently, peptides that bind with high affinity to CaM should prevent the activity of the constitutive NOS isoforms, and thus act as effective inhibitors of NO synthesis.

5.1.4 Amphibian Peptides and the Inhibition of nNOS

The majority of frogs studied to date from the genus *Litoria* possess at least one major peptide in the glandular secretion that can inhibit the formation of NO by nNOS [58]. These may play a regulatory role in the animal, since NO is known to be involved in sight, reproduction and gastric modulation in anurans [478-480]. Alternatively, these nNOS inhibitors may form part of the animal's primary defence, by interfering with the NO messenger capabilities of an invading predator or pathogen.

A summary of selected nNOS inhibiting amphibian peptides and their synthetic derivatives is presented in Table 5.1. Here it can be seen that these active peptides fall into 3 well-defined groups, namely; (a) the aurein/citropin group, which are short, linear amphipathic α-helices [59,65], (b) the caerin 1 peptides, particularly those with a Phe residue in position 3, which adopt two helical regions separated by a central flexible hinge [32,312], and (c) the frenatin 3 type peptides, characterised by a C-terminal CO_2H group and a Lys-X-Lys motif near this terminus [405].

Detailed studies of these amphibian peptides during *in vitro* testing indicated a non-competitive mode of nNOS inhibition, evidenced by the observed Hill slopes (which give a measure of the slope in a dose-response curve) being greater than 1 (Table 5.1). In addition, the possibility that these peptides exert their inhibitory effects by complexation with CaM is supported experimentally since; (a) the inhibition of nNOS by the peptides is partially reversed by addition of excess CaM [72], (b) these peptides inhibit the activity of calcineurin, which is also regulated by Ca_4-CaM [72,481], and (c) NMR titration studies show large chemical shift changes at significant residues of CaM upon addition of peptide [482].

Table 5.1: nNOS inhibition activities of selected amphibian peptides and synthetic derivatives [72,405,483,484].

Name	Species	Sequence	IC_{50} (μM)	Hill Slope
Inhibitor Group 1				
Lesueurin	*L. lesueuri*	GLLDILKKVGKVA-NH$_2$	16.2	1.5
Aurein 1.1	*L. aurea*	GLFDIIKKIAESI-NH$_2$	33.9	2.0
Citropin 1.1	*L. citropa*	GLFDVIKKVASVIGGL-NH$_2$	8.2	1.6
Citropin 1.1 all D isomer		Glfdvikkvasvi GGl-NH$_2$	30.7	1.0
Citropin 1.1 (mod. 13)		GLFDVIKKVASVI**KK**L-NH$_2$	2.0	2.5
Citropin 1.1 (mod. 18)		GLF**A**VIKKVA**K**VI**KK**L-NH$_2$	1.2	2.2
Aurein 2.2	*L. aurea*	GLFDIVKKVVGALGSL-NH$_2$	4.3	2.5
Aurein 2.3	*L. aurea*	GLFDIVKKVVGIAGSL-NH$_2$	1.8	1.7
Aurein 2.4	*L. aurea*	GLFDIVKKVVGTLAGL-NH$_2$	2.1	3.1
Inhibitor Group 2				
Dahlein 5.1	*L. dahlia*	GLLGSIGNAIGAFIANKLKP-OH	3.2	2.2
Dahlein 5.2	*L. dahlia*	GLLGSIGNAIGAFIANKLKPK-OH	1.3	a
Dahlein 5.3	*L. dahlia*	GLLASLGKVLGGYLAEKLKP-OH	1.4	a
Frenatin 3	*L. infrafrenata*	GLMSVLGHAVGNVLGGLFKPKS-OH	6.8	1.4
Frenatin 3 (mod. 3)		GLM**R**VLGHAVGNVLGGLFKPKS-OH	2.4	2.3
Spendipherin	*L. splendida*	GLVSSIGKALGGLLADVVKSKGQPA-OH	8.5	1.3
Inhibitor Group 3				
Caerin 1.1	*L. splendida*	GLLGVLGSIAKHVLPHVVPVIAEHL-NH$_2$	36.6	1.4
Caerin 1.6	*L. chloris*	GLFSVLGAVAKHVLPHVVPVIAEKL-NH$_2$	8.5	1.7
Caerin 1.8	*L. chloris*	GLFKVLGSVAKHLLPHVVPVIAEKL-NH$_2$	1.7	3.7
Caerin 1.9	*L. chloris*	GLFGVLGSIAKHVLPHVVPVIAEKL-NH$_2$	6.2	2.2
Caerin 1.10	*L. chloris*	GLLSVLGSVAKHVLPHVVPVIAEKL-NH$_2$	41.0	0.6
Caerin 1.19	*L. gracilenta*	GLFKVLGSVAKHLLPHVAPIIAEKL-NH$_2$	4.1	a

a Data not reported.

By investigating the CaM-peptide complexes, it may be possible to gain further understanding of both binding properties and the way in which these peptides inhibit nNOS, in turn providing information for the potential design of improved NOS inhibitors. This is possible using ESI-MS (Chapter 2) and NMR spectroscopy (Chapter 4). The aims of this study were therefore to firstly confirm that the amphibian peptides do in fact interact with CaM in the inhibition of nNOS. Once identified, the stability, binding affinity and conformation of the complexes can be probed to gain insight into the non-covalent interactions between the binding partners.

5.2 Results

5.2.1 Mass Spectrometry of Calmodulin

As a reference, the calculated masses of ions expected in the negative ion ESI-MS spectra of CaM and the peptide complexes described in detail in subsequent sections are given in Table 5.2.

Table 5.2: Ions expected in the negative ion mode for the mass spectrometric investigation of CaM and peptide-CaM complexes.

Charge	*m/z*				
	CaM	**CaM + 4Ca^{2+}**	**CaM + 4Ca^{2+} + caerin 1.8**	**CaM + 4Ca^{2+} + splendipherin**	**CaM + 4Ca^{2+} + citropin 1.1 (mod. 18)**
0	16790	16943	19605	19307	18699
-1	16789	16942	19604	19306	18698
-2	8394	8470	9802	9653	9348
-3	5596	5647	6534	6435	6232
-4	4197	4235	4900	4826	4674
-5	3357	3388	3920	3860	3739
-6	2797	2823	3267	3217	3115
-7	2398	2419	2800	2757	2670
-8	2098	2117	2450	2412	2336
-9	1865	1882	2177	2144	2077
-10	1678	1693	1960	1930	1869
-11	1525	1539	1781	1754	1699
-12	1398	1411	1633	1608	1557
-13	1291	1302	1507	1484	1437
-14	1198	1209	1399	1378	1335
-15	1118	1129	1306	1286	1246
-16	1048	1058	1224	1206	1168
-17	987	996	1152	1135	1099
-18	932	940	1088	1072	1038
-19	883	891	1031	1015	983
-20	839	846	979	964	934

Figure 5.5 shows the negative ion ESI mass spectrum obtained for CaM in 10 mM ammonium acetate buffer (pH 6.8). Despite extensive dialysis before analysis, evidence of up to four bound Ca^{2+} ions is apparent upon transformation of the spectrum (Figure 5.5, inset). Nevertheless, under these conditions the predominant species is in fact CaM free of Ca^{2+}. Two charge distribution patterns can be observed in this spectrum, centred upon $(M-15H)^{15-}$ and $(M-7H)^{7-}$. This suggests at least two different protein conformations exist in these electrospray conditions [485,486]. The experimentally determined mass of CaM was 16,790 Da, which agrees with the theoretical mass based on the primary sequence, and confirms both the acetylation at the N-terminus and the presence of a trimethyl-Lys residue (at position Lys115) [463].
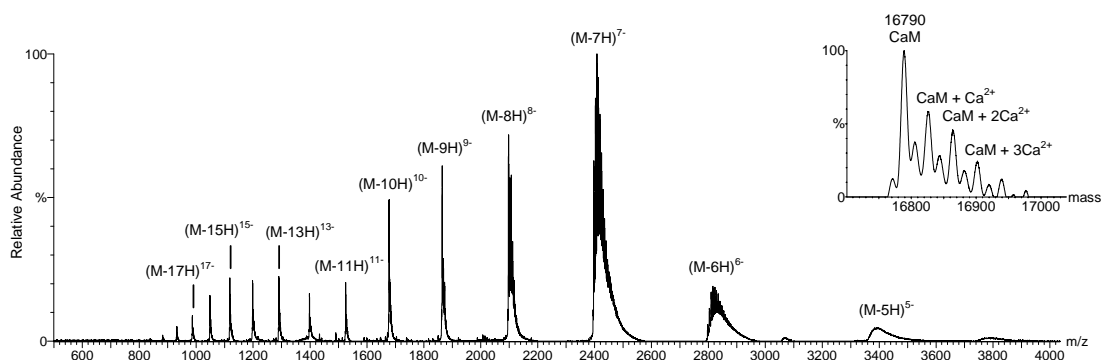
Figure 5.5: ESI-MS spectrum of CaM in the negative ion mode. Inset shows the transformed spectrum.

Addition of a 2.5 times excess of Ca^{2+} in the form of 5 mM calcium acetate was sufficient to cause fully loaded Ca_4-CaM to become the most abundant species (Figure 5.6). Note that a four times excess was not necessary due to the residual Ca^{2+} present after dialysis. Transformation of the data reveals that some non-specific Ca^{2+} attachment has occurred, with up to eight Ca^{2+} ions bound (Figure 5.6, inset). When a divalent Ca^{2+} ion is incorporated into the protein molecule, two protons are displaced to maintain charge balance, giving an overall increase of 38 Da [487]. Again, the experimentally determined mass of Ca_4-CaM (16,942 Da) is therefore consistent with the theoretical mass.
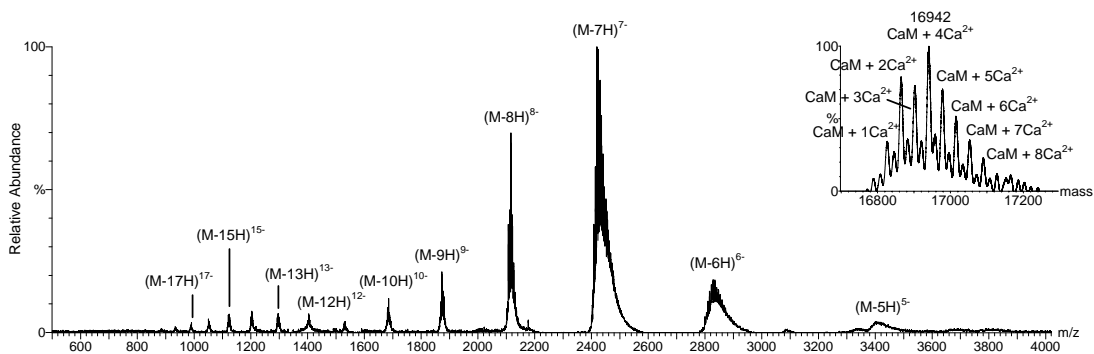
Figure 5.6: ESI-MS spectrum of Ca_4-CaM in the negative ion mode. Inset shows the transformed spectrum.

5.2.2 Peptide-Calmodulin Complexes

The primary aim of this study was to develop conditions for the observation of intact peptide-CaM complexes in the Q-TOF 2 mass spectrometer, and as such, initial attempts were made using different solvent systems. Organic solvents are known to improve ionisation efficiency in the presence of a base [198,488], and therefore solvents using acetonitrile, methanol and isopropanol in NH_4OAc were employed at various pH values. In all cases negligible levels of the peptide-CaM complexes were observed, and the negative ion spectra obtained were similar to that shown in Figure 5.7 where both free peptide (in this case caerin 1.8) and free CaM are evident. In these conditions, the charge distribution of the protein is shifted towards higher charge states, consistent with a degree of unfolding [485,486].
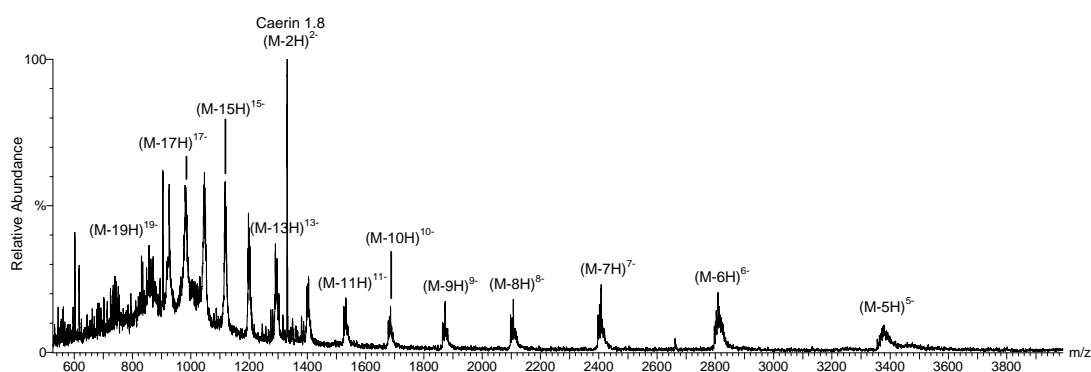
Figure 5.7: Negative ion ESI-MS spectrum of Ca_4-CaM in the presence of caerin 1.8 and isopropanol.

Subsequent investigations were carried out in the absence of such denaturing solvents, and the first evidence of complex formation in the gas phase was observed for caerin 1.8, with ions detected for the caerin 1.8-CaM complex at low abundance using 10 mM NH_4OAc at pH 6.8. A significant increase in abundance of the complex ions was noted upon reduction of the cone voltage from 50 to 35 V, and desolvation temperature from 120 to 40 °C. These conditions were used in ensuing experiments to detect the peptide-CaM complexes. An example of the resultant spectra is given in Figure 5.8 for members of all three nNOS inhibitor groups, namely caerin 1.8, citropin 1.1 (mod. 18) and splendipherin.
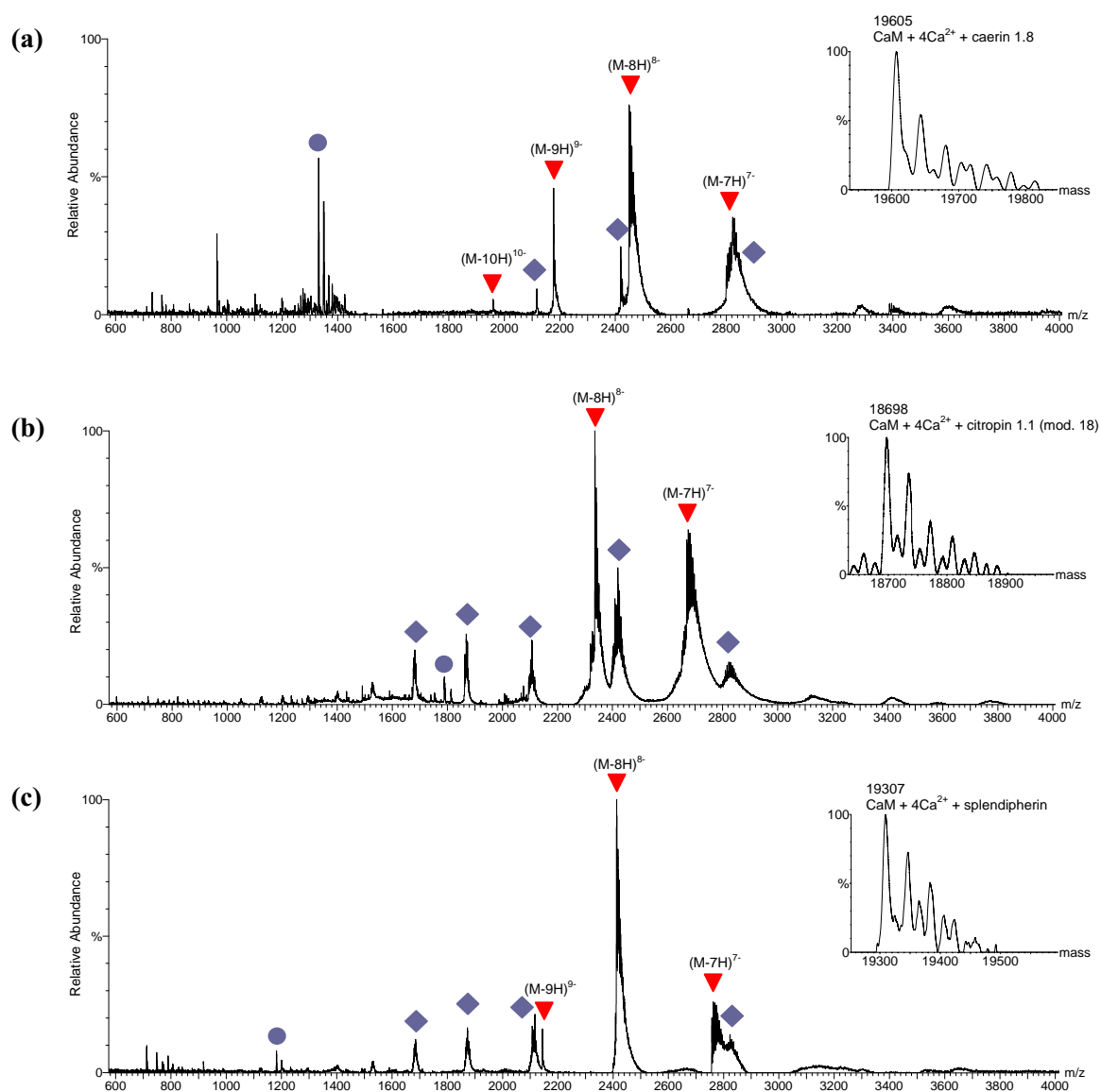
Figure 5.8: ESI-MS spectra of Ca_4-CaM with **(a)** caerin 1.8, **(b)** citropin 1.1 (mod. 18), and **(c)** splendipherin in the negative ion mode. Insets show the transformed spectra. Free peptide (●); Free CaM (◆); Peptide-CaM complexes (▼).

Peptide-CaM complexes were also observed in the gas phase for frenatin 3, dahlein 5.1, citropin 1.1, citropin 1.1 (all D isomer), citropin 1.1 (mod. 13) and aurein 2.3 (data not shown). In all cases 1:1 peptide/protein complexes were observed, and increasing the peptide/protein ratio to as much as 5:1 did not change the appearance of the spectra, nor provide any evidence for the binding of multiple peptide molecules.

Comparison of the spectra from CaM alone with that of the peptide-CaM complexes indicates that the charge state distribution patterns and relative intensities of the signals are altered upon addition of peptide, suggesting a global conformational change of the protein takes place upon binding. As can be seen from the transformed spectra in Figure 5.8, in all cases at least four Ca^{2+} ions are necessary for formation of the complexes, however additional non-specific binding of a further one or two Ca^{2+} ions is also apparent.

5.2.3 Binding Competition Studies

Relative binding affinities of the amphibian peptides were studied using competitive binding methods, in which two peptides were simultaneously introduced into solution with Ca_4-CaM, and allowed to compete for binding sites on the protein. The comparative abundance of each potential complex was then analysed by ESI-MS. Caerin 1.8, citropin 1.1 (mod. 18) and splendipherin were chosen primarily because the relative binding affinity of these peptides in solution has been determined previously using NMR spectroscopy [482], and therefore direct comparison between solution and gas phases is possible.

A good example of the competition binding method is given in Figure 5.9, in which both citropin 1.1 (mod. 18) and splendipherin are present with Ca_4-CaM. Here, evidence of the citropin-CaM complex is provided by observation of the (M-8H)[8-] and (M-7H)[7-] ions for this species, while only free splendipherin is detected. In a similar manner only the caerin 1.8-CaM complex was observed from a mixture of caerin 1.8 and citropin 1.1 (mod. 18) (data not shown). This suggests the CaM binding affinities of the three peptides are as follows; caerin 1.8 > citropin 1.1 (mod. 18) > splendipherin.
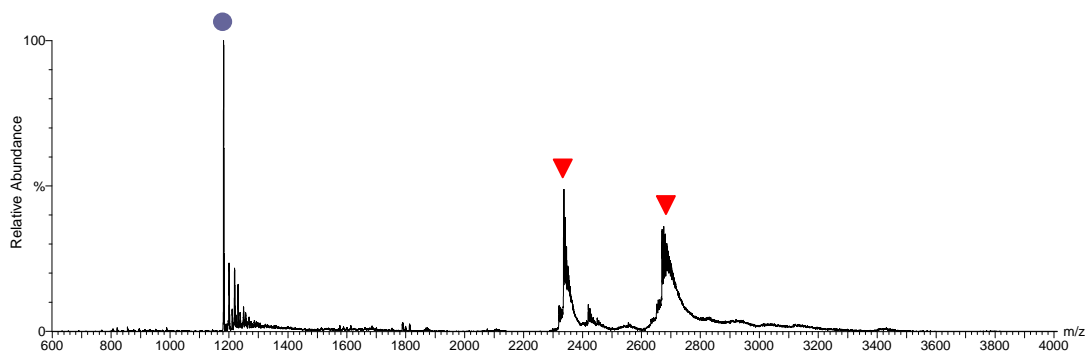
Figure 5.9: Negative ion ESI-MS spectra of Ca^{2+} loaded CaM with both citropin 1.1 (mod. 18) and splendipherin. Free splendipherin (●); Citropin 1.1 (mod.18)-CaM complex (▼).

Interestingly, these results do not appear to parallel the IC_{50} values for the inhibition of nNOS as given in Table 5.1, since citropin 1.1 (mod. 18) has the lowest inhibitory concentration and might therefore be expected to bind with highest affinity to CaM. However, the relative binding strengths do in fact agree with that observed in solution, since caerin 1.8, citropin 1.1 (mod. 18) and splendipherin were found to be in slow, intermediate and fast exchange binding modes with CaM respectively [482]. Consequently, at least in the case of these peptides, mass spectrometry appears to provide good correlation with the more physiologically relevant solution state.

5.2.4 Complex Dissociation Studies

The gas phase stability of the peptide-CaM complexes was further studied by in source CID experiments in which the cone voltage, and hence the acceleration of ions through the intermediate pressure region of the source, is gradually increased. An example of this is given for caerin 1.8 in Figure 5.10. As seen in this figure, the caerin 1.8-CaM complex began to dissociate at a cone voltage near 40 V, and at voltages higher than this, the predominant ions were from free peptide and free CaM. Similar results were obtained by maintaining a constant cone voltage of 35 V, while increasing the collision energy from 4 to 20 eV. At 15 eV, no ions from the complex of caerin 1.8 with Ca_4-CaM were present in the negative ion spectra.
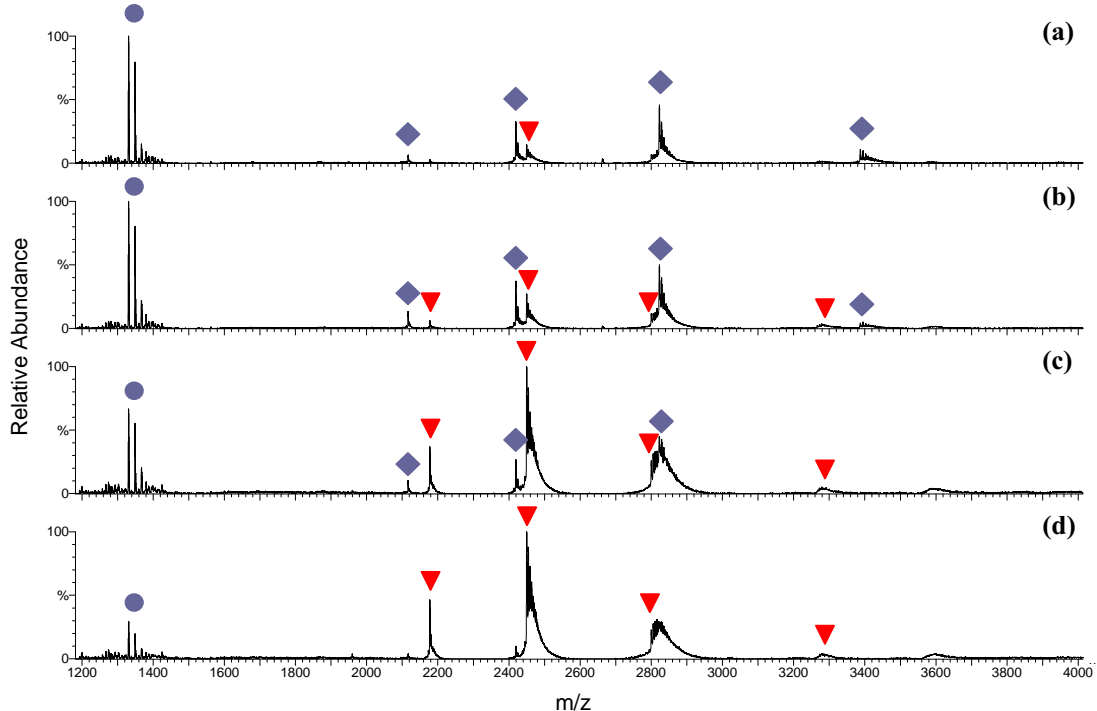
Figure 5.10: Effect of increasing cone voltage on the ESI mass spectra of the caerin 1.8-CaM complex. Cone voltages are as follows; **(a)** 35 V; **(b)** 42 V; **(c)** 50 V; **(d)** 60 V.

In source CID experiments were also conducted for citropin 1.1 (mod. 18) and splendipherin, and in order to compare these, the voltage at which the intensity of the signal from the $(M-8H)^{8-}$ ion of the complex (typically near m/z 2400) is equal to that of the $(M-7H)^{7-}$ ion of free Ca_4-CaM (m/z 2419) was noted. While this is not an entirely accurate measure of the voltage required to achieve 50% dissociation of the complex, it still provides a method for the observation of general trends in the gas phase stabilities of the non-covalent assemblies.

The voltages measured for dissociation of the peptide-CaM complexes were 45, 41 and 40 V for caerin 1.8, citropin 1.1 (mod. 18) and splendipherin respectively. The relative ease with which these complexes dissociate confirms that non-covalent interactions are indeed responsible for maintaining the assemblies. Again, there does not appear to be a direct correlation between gas phase stabilities and the IC_{50} values given in Table 5.1, however these results are consistent with the relative binding strengths observed using the competitive binding methods described above, as well as those determined by solution NMR spectroscopy [482].

123

5.2.5 D$_2$O Exchange

Conformational changes can be readily monitored by mass spectrometry using H/D exchange experiments, since the rate of exchange of a given proton is dependent upon structurally related features such as solvent exposure and hydrogen bonding. In order to demonstrate the application of this method for the complexes between the nNOS inhibiting peptides and CaM, and to provide further evidence for a significant conformational change of CaM upon peptide binding, the extent of H/D exchange for CaM was monitored over a time course of 90 minutes both in the presence and absence of equimolar caerin 1.8.

As discussed previously, other amphibian peptides such as citropin 1.1 (mod. 18) and splendipherin have been shown by NMR spectroscopy to exist in either fast or intermediate exchange, while caerin 1.8 is the only example thus far identified as being in a slow exchange complex with CaM [482]. Consequently, only this peptide was chosen for analysis by H/D exchange methods to reduce the complications arising from the equilibrium between bound and unbound forms of CaM. Figure 5.11 displays the results of the mass spectrometric analysis, demonstrating the time dependent incorporation of deuterium into the protein.
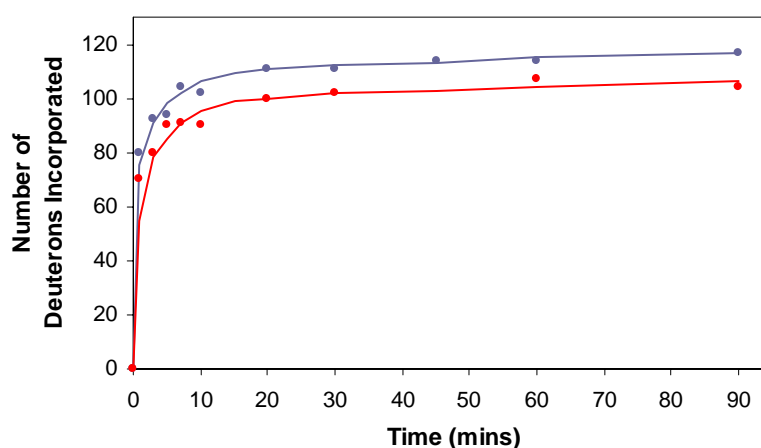
Figure 5.11: Extent of H/D exchange with time for Ca$_4$-CaM (blue) and caerin 1.8-CaM (red). Data is the average of two runs, repeated under identical experimental conditions.

After 30 minutes the protein mass (and presumably the exchange) had become relatively constant. During the 90 minute time course, Ca_4-CaM exchanged a maximum of 117 amide protons for deuterons as determined by the increase in molecular mass. The extent of deuterium incorporation is therefore 80% of the total available amide hydrogens. In contrast, in the presence of caerin 1.8, only 107 (or 73%) of available amide protons are exchanged. The decrease in extent of H/D exchange upon peptide binding indicates that some amide proton sites are now less solvent accessible. This is possibly a result of the protein folding to a more compact structure, or simply because the peptide itself blocks some CaM sites from H/D exchange.

5.2.6 NMR Spectroscopy of Unbound Caerin 1.8

Despite providing conclusive evidence for the non-covalent bonding of the amphibian peptides and CaM, mass spectrometry is unable to give any detailed information regarding the structure of the binding partners. In order to further probe the interaction between these species, it was decided to undertake NMR studies on the non-covalent assemblies. The complex between caerin 1.8 and CaM was chosen for analysis since this peptide appears to bind most strongly to CaM, and therefore is most amenable to study by these methods.

Caerin 1.8 was synthesised commercially and selectively labelled with ^{15}N at the amide position of residues Val5, Leu6, Ile21 and Ala22[†]. In this manner the two ends of the peptide could be investigated independently. The use of NMR spectroscopy for the study of protein structure first requires the assignment of each resonance to its corresponding proton in the molecule. To this end, 2D NMR spectra were acquired for ^{15}N labelled caerin 1.8 in aqueous solution, and proton chemical shifts were assigned using standard sequential assignment methods [489], and a combination of NOESY, TOCSY and COSY experiments as outlined in Section 4.4. A partial TOCSY spectrum is shown in Figure 5.12, where labelled cross-sections for each amino acid are indicated.

[†] Uniformly ^{15}N labelled caerin 1.8 was not used, since previous attempts at the biochemical expression of this peptide were unsuccessful [482].

The NH and αH regions of this spectrum are sufficiently dispersed to permit relatively easy identification of individual cross-peaks, and allow for classification of spin systems corresponding to the different amino acid types in the peptide sequence. Where signal overlap remained a problem, the 3-bond correlations in the COSY spectrum were used to make conclusive assignments.

No d_{NN} NOE cross-peaks were observed in the HN region of the NOESY spectrum, and thus sequential assignment was based primarily on the αH_i - NH_{i+1} signals which gave an almost continuous pattern of sequential connectivities (Figure 5.12). Exceptions to this arose from Pro15 and Pro19, which of course lack an amide proton. In such cases, analogous assignments were made using αH_i - δH_{i+1} NOE peaks. Other characteristic signals including $d_{\beta N}$ peaks were used in cases where $d_{\alpha N}$ signals were not observed, and also to confirm the position of residues within the sequence.
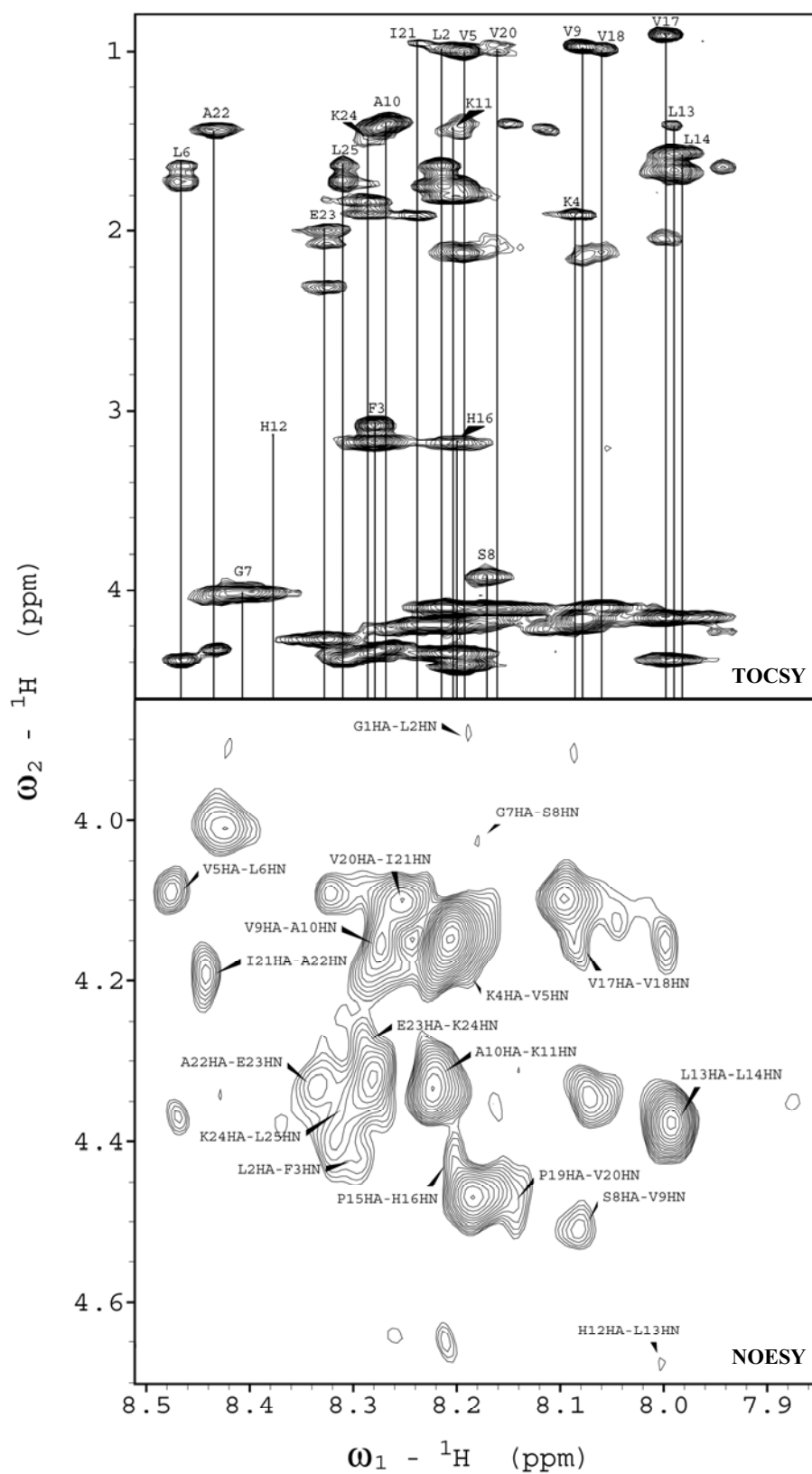
Figure 5.12: Partial TOCSY and NOESY spectra of caerin 1.8 in H_2O. Vertical lines connect resonances of the same spin system in the TOCSY spectrum, and αH_i - NH_{i+1} signals used for sequential assignment are indicated in the NOESY spectrum.

αC resonances were identified by direct investigation of the αH/αC region of a HSQC spectrum, as shown in Figure 5.13. The αCs of His12 and His16 could not be reliably assigned as these have chemical shifts close to the value of the water resonance, and as such are obscured by water breakthrough.

A summary of all assigned proton and αC resonances can be found in Table 5.3. Amide nitrogen chemical shifts are also included in this table for the four ^{15}N labelled residues, which were assigned based on the results of the titration experiments described in Section 5.2.8.
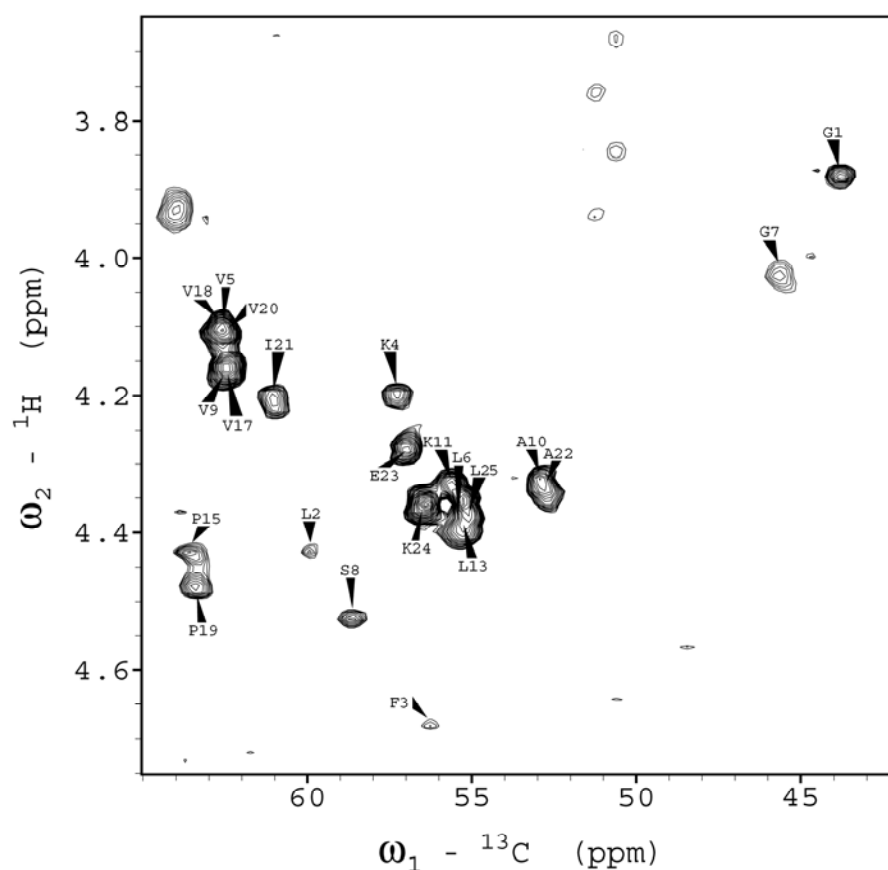
Figure 5.13: αH/αC region of the HSQC spectrum of caerin 1.8 in H_2O.

Table 5.3: ^{1}H and ^{13}C chemical shifts for caerin 1.8 in H_2O. n.o. indicates resonance was not observed. Amide ^{15}N chemical shifts are also included where applicable.

Residue						
	NH	**αH**	**βH**	**Other H**	**αC**	**Amide N**
Gly1	n.o.	3.88			43.8	
Leu2	8.21	4.42	1.75, 1.65	γ-CH 1.70	58.2	
				δ-CH$_3$ 1.01, 0.99		
Phe3	8.28	4.68	3.17, 3.08	H2, H6 7.30	56.3	
				H3, H5 7.40		
				H4 7.35		
Lys4	8.09	4.20	1.91	γ-CH$_2$ 1.44	57.3	
				δ-CH$_2$ 1.81, 1.72		
				ε-CH$_2$ 3.03		
				ε-NH$_3^+$ n.o.		
Val5	8.20	4.10	2.13	γ-CH$_3$ 1.02, 0.99	62.6	122.3
Leu6	8.46	4.39	1.73	γ-CH 1.64	55.4	126.6
				δ-CH$_3$ 0.97, 0.91		
Gly7	8.41	4.02			45.7	
Ser8	8.17	4.52	3.92		58.6	
Val9	8.08	4.15	2.14	δ-CH$_3$ 0.98, 0.95	62.6	
Ala10	8.27	4.32	1.40		52.9	
Lys11	8.20	4.35	1.93	γ-CH$_2$ 1.41	55.6	
				δ-CH$_2$ 1.81		
				ε-CH$_2$ 3.04		
				ε-NH$_3^+$ 7.78		
His12	8.38	4.67	3.20, 3.13	H2 7.11	n.o.	
				H4 8.05		
Leu13	7.99	4.39	1.66	γ-CH 1.57	55.3	
				δ-CH$_3$ 0.92, 0.88		
Leu14	7.98	4.59	1.70, 1.57	γ-CH 1.55	55.4	
				δ-CH$_3$ 0.98, 0.94		
Pro15	–	4.42	2.30, 1.85	γ-CH$_2$ 2.05	63.5	
				δ-CH$_3$ 3.84, 3.67		
His16	8.20	4.69	3.18	H2 7.14	n.o.	
				H4 8.14		
Val17	8.00	4.16	2.04	γ-CH$_3$ 0.92, 0.90	62.4	
Val18	8.06	4.10	2.11	γ-CH$_3$ 1.00	62.7	
Pro19	–	4.47	2.32, 1.90	γ-CH$_2$ 2.09, 2.03	63.4	
				δ-CH$_3$ 3.93, 3.76		
Val20	8.17	4.10	2.07	γ-CH$_3$ 1.00, 0.96	62.4	
Ile21	8.24	4.20	1.92	γ-CH$_3$ 0.95	61.0	125.3
				γ-CH$_2$ 1.52, 1.23		
				δ-CH$_3$ 0.93		
Ala22	8.43	4.33	1.43		52.7	128.8

Table 5.3 (continued):

Residue	Chemical shift (ppm)					
	NH	**α-CH**	**β-CH**	**Other H**	**α-C**	**Amide N**
Glu23	8.33	4.27	2.07, 2.00	γ-CH$_2$ 2.31	57.0	
Lys24	8.28	4.35	1.90	γ-CH$_2$ 1.50, 1.44	56.5	
				δ-CH$_2$ 1.84, 1.74		
				ε-CH$_2$ 3.05		
				ε-NH$_3^+$ 7.83		
Leu25	8.31	4.39	1.72	γ-CH 1.63	55.1	
				δ-CH$_3$ 0.97, 0.91		
				CONH$_2$ 7.55, 7.09		

5.2.7 Secondary Structure of Caerin 1.8

Secondary shift data and NOE connectivity patterns are generally the most common NMR parameters used to identify and characterise elements of short secondary structure in linear peptides, without the need for extensive calculation based methods. This approach has therefore been employed to analyse the conformation of caerin 1.8 in aqueous solution.

The difference between observed shifts and random coil values determined in water [371] (i.e. the secondary shift, $\Delta\delta$) was plotted against the amino acid sequence for αH, αC and NH resonances, as illustrated in Figure 5.14. αH and αC secondary shifts are smoothed over a window of n $\pm$ 2 residues, while those for amide protons are plotted unsmoothed.

The secondary shift plots show no clear trend, either upfield or downfield, along the sequence of the peptide. Furthermore, the magnitude of $\Delta\delta$ is considerably less than typically observed for a peptide which is maintained in either a helical or β-sheet type structure. For example, the characteristic helix-type shift of αH resonances is on average around 0.4 ppm upfield [372,374,490], while for caerin 1.8 the smoothed secondary shifts are all well below 0.1 ppm. This implies that the observed shifts are not significantly different from the random coil values, and that the peptide is unlikely to adopt a unique spatial conformation in an aqueous environment.
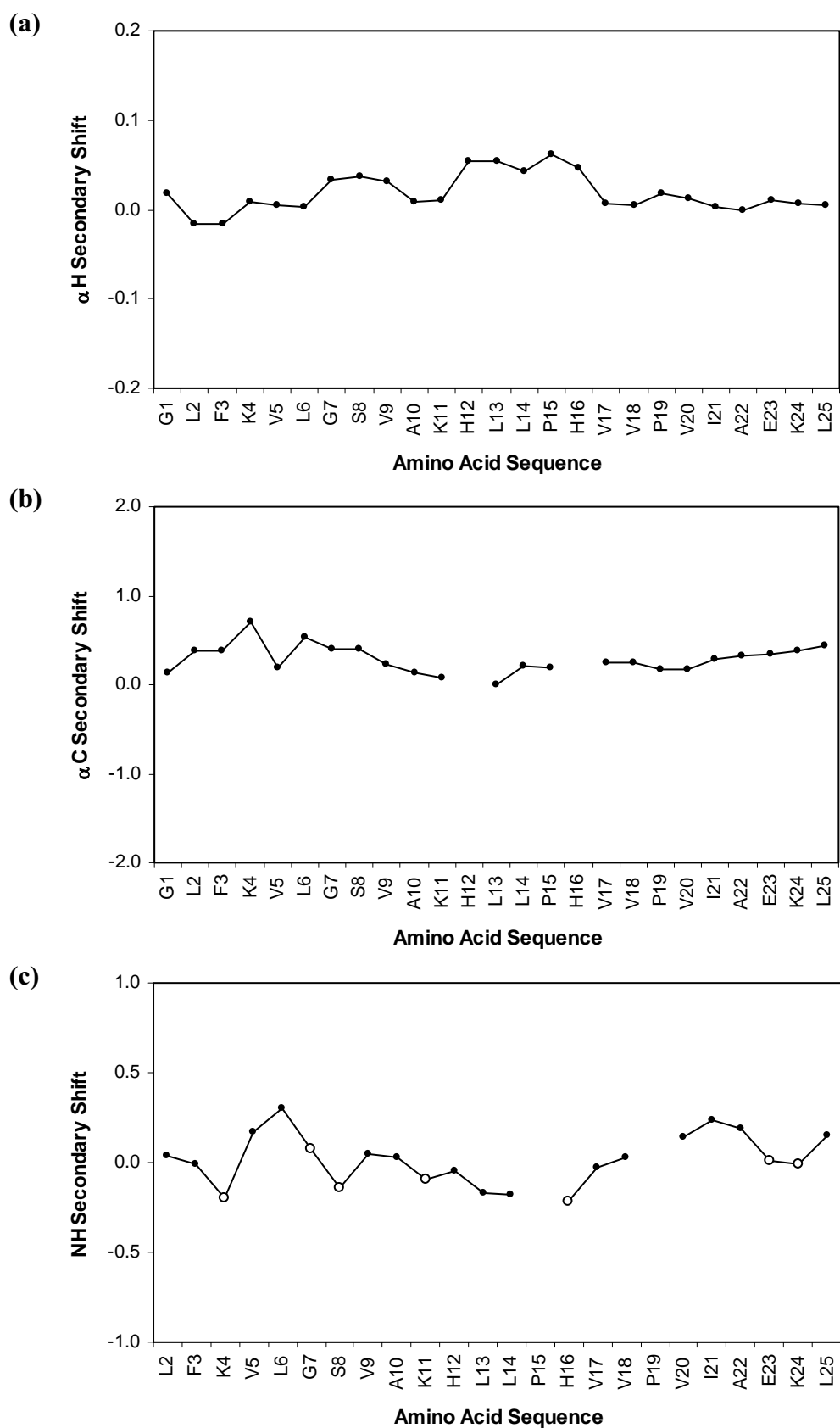
Figure 5.14: **(a)** αH ^{1}H, **(b)** αC ^{13}C and **(c)** NH ^{1}H secondary shifts of caerin 1.8 in H$_2$O. αH and αC shifts are smoothed over n ± 2 residues, whereas NH shifts are plotted unsmoothed. Hydrophilic residues are represented by open symbols. Negative values indicate an upfield shift from random coil resonances, while positive values indicate a shift downfield.

A summary of the diagnostic NOE connectivities observed in the NOESY spectrum of caerin 1.8 in H_2O is given in Figure 5.15. As already mentioned, the strong series of d_{NN} signals expected if the peptide were to adopt a helical conformation is conspicuously absent. Instead, the predominant intra-residue signals are those of sequential $d_{\alpha N}$ and $d_{\beta N}$ NOEs, which occur along the majority of the sequence. Furthermore, relatively few medium-range NOEs are present from three and four residues apart, and of these, most are ambiguous. This data suggests caerin 1.8 adopts a more extended or random conformation in H_2O.
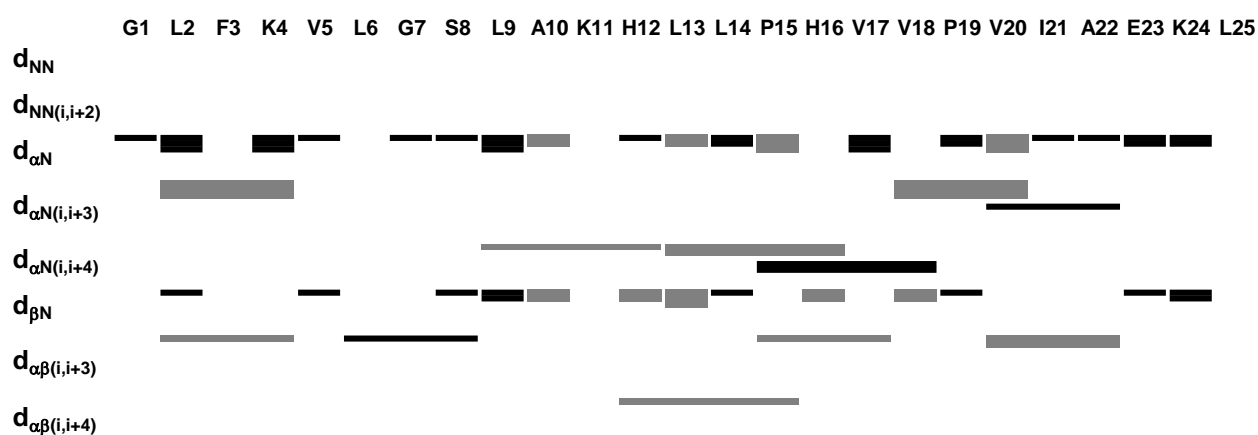
Figure 5.15: A summary of NOEs found in the NOESY spectrum of caerin 1.8 in H_2O. The thickness of the bars is proportional to the cross-peak intensity, as evaluated by volume integration. Grey shaded boxes represent ambiguous NOEs. For Pro residues in which no amide protons exist, the corresponding NOEs are instead described from the δ protons.

Taken together, the pattern of observed NOEs and their intensities, along with the secondary shift data, is generally consistent with the peptide having no defined secondary structure along the majority of the sequence in these conditions. This is in fact quite typical of a linear peptide in aqueous solution [491].

5.2.8 ^{15}N HSQC Titration

The interaction between caerin 1.8 and CaM was monitored by performing a ^{15}N HSQC titration. Increasing quantities of unlabelled protein were added to ^{15}N labelled caerin 1.8 until a 1:1 peptide/protein concentration was reached, and a high-resolution ^{15}N HSQC spectrum was recorded after each addition. The chemical shift changes were then tracked by overlaying each of the spectra (Figure 5.16). As expected for the peptide which has four residues labelled with ^{15}N at the amide position, four proton-nitrogen correlations are observed in the HSQC spectrum. The signals are well resolved in both dimensions, and are easily assigned for unbound caerin 1.8 before the addition of CaM, based on the amide proton chemical shifts determined for the free peptide.
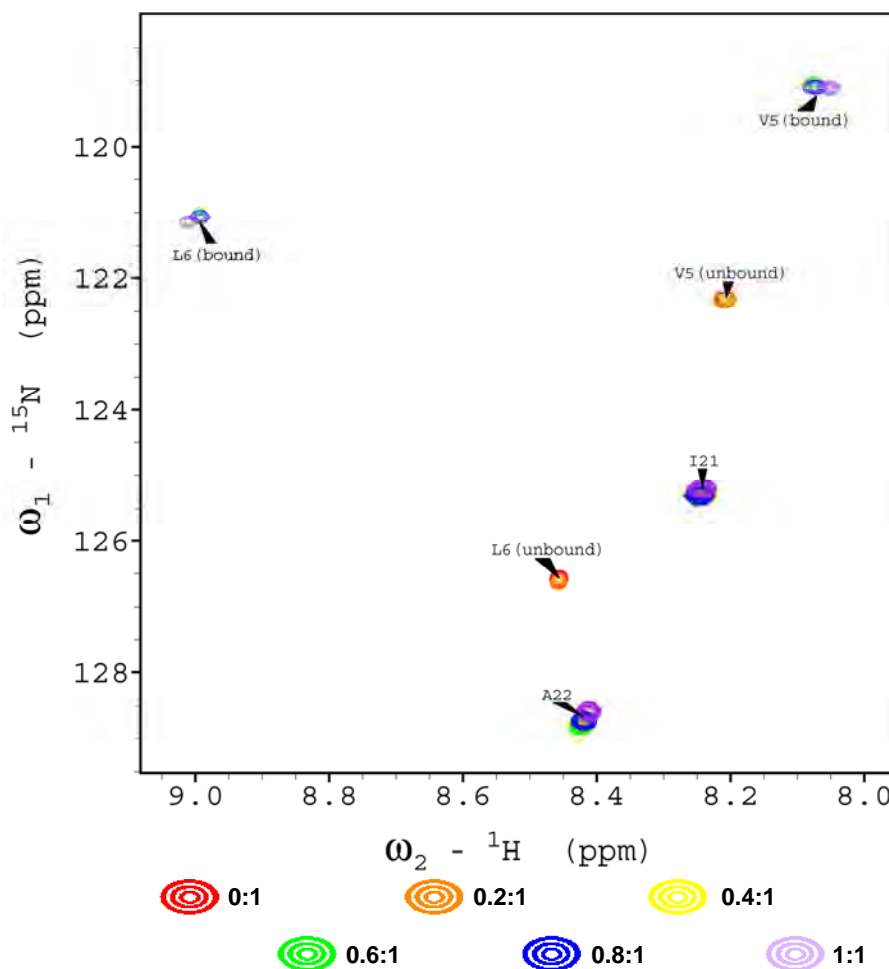
Figure 5.16: Partial overlaid ^{15}N HSQC spectra for the titration of ^{15}N labelled caerin 1.8 with Ca$_4$-CaM. The legend is shown below the spectrum, indicating the protein/peptide ratio.

After addition of only 0.4 equivalents of CaM, a significant difference in the NMR spectrum of caerin 1.8 can be observed, with distinct chemical shift changes noted for two of the four signals. At this protein concentration, signals arising from both bound and unbound conformers are observable, suggesting a 1:1 stoichiometry and providing evidence of slow exchange on the NMR time scale. At equimolar levels of CaM, observation of a single set of resonances for the bound peptide is indicative of a unique strong binding site, and a single conformation for the caerin 1.8-CaM complex.

Marked differences in chemical shift are noted for Val5 and Leu6, while that of Ile21 and Ala22 remain unaffected. Such chemical shift variations are indicative of environmental and/or conformational changes upon complexation, and suggest the N-terminal portion of caerin 1.8 is interacting directly with CaM, while the C-terminal end is not. This is further evident by analysis of the peak shapes observed in the HSQC experiment. Resonances in the bound state have variable line widths, with those assigned to Val5 and Leu6 showing a discernable decrease in intensity, and a broadening of the signal. This can be attributed to the fact that the N-terminal residues which are involved in binding have a longer effective correlation time as a result of the large increase in mass associated with complex formation. In contrast, the residues not directly involved in the complex continue to behave with approximately the same molecular flexibility as in the free state, and as such have signals comparable with unbound caerin 1.8.

5.2.9 NMR Spectroscopy of Bound Caerin 1.8

Assignment of the proton and nitrogen resonances for the labelled residues of caerin 1.8 in the Ca_4-CaM bound form was again achieved using heteronuclear NMR spectroscopy. These experiments were based on standard 3D gnoesyNhsqc and gNhsqctocsy pulse sequences, but were acquired such that the evolution time was arrayed in one dimension only, effectively giving 2D TOCSY and NOESY spectra edited by ^{15}N. Assignment of resonances arising from the non-interacting residues Ile21 and Ala22 was readily accomplished starting from the known nitrogen frequencies (the same as in the free state), and using the HSQC-TOCSY spectrum (Figure 5.17).
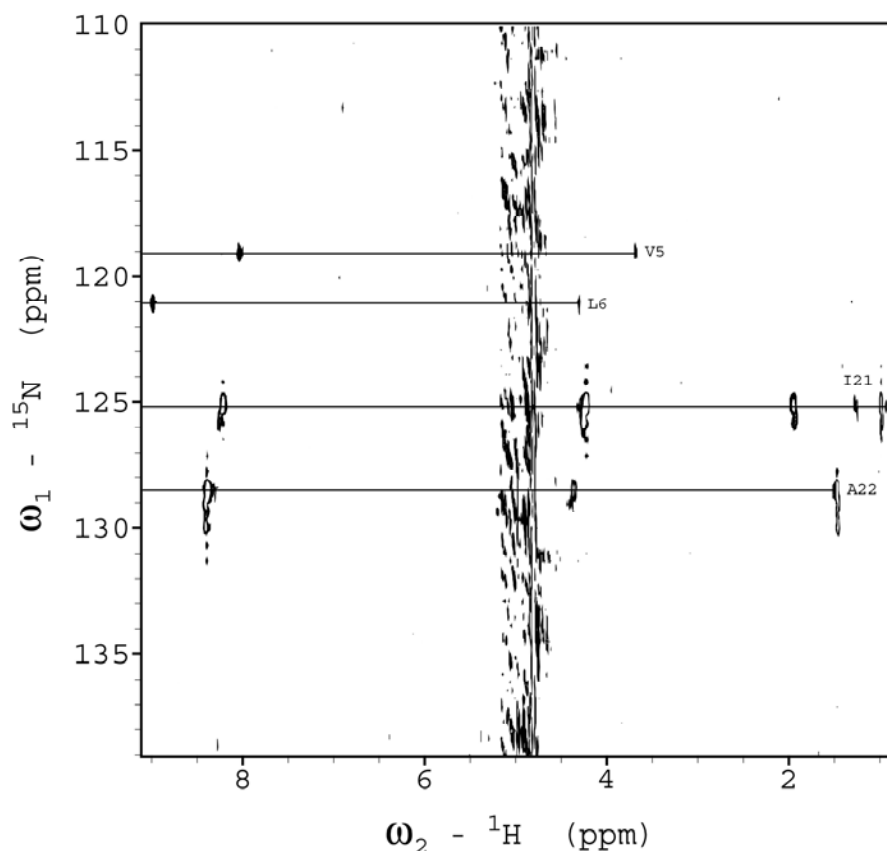
Figure 5.17: Partial 2D HSQC-TOCSY spectrum of ^{15}N labelled caerin 1.8 bound to Ca$_4$-CaM in H$_2$O. TOCSY mixing time is 70 ms. Horizontal lines connect resonances of the same spin system.

The sensitivity of this experiment was not sufficient to allow observation of correlations beyond HN-Hα for the bound residues, Val5 and Leu6, despite employing a range of mixing times. In this case the NOE based information was used. Given the known amino acid type of the ^{15}N labelled residues, analysis of the NOESY-HSQC spectra enabled assignment of the remaining resonances originating from the CaM bound peptide, as can be seen in Figure 5.18 where labelled cross-sections are indicated.

A summary of the assigned proton and nitrogen resonances for the ^{15}N labelled resides of Ca$_4$-CaM bound caerin 1.8 is given in Table 5.4.
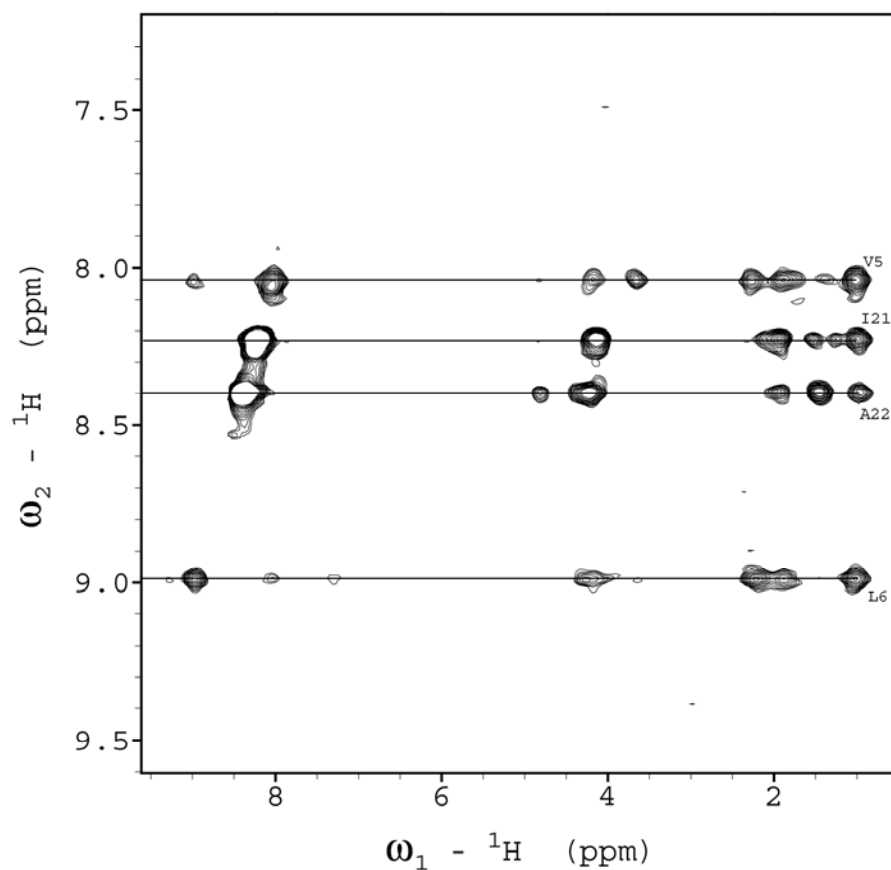
Figure 5.18: Partial 2D NOESY-HSQC spectrum of ^{15}N labelled caerin 1.8 bound to Ca$_4$-CaM in H$_2$O. NOESY mixing time is 150 ms. Horizontal lines connect correlations for the same residue.

Table 5.4: ^{1}H and ^{15}N chemical shifts for the ^{15}N labelled residues of caerin 1.8, bound to Ca$_4$-CaM in H$_2$O.

Residue	Chemical shift (ppm)				
	NH	**αH**	**βH**	**Other H**	**Amide N**
Val5	8.06	3.71	2.30	γ-CH$_3$ 1.05	119.2
Leu6	9.01	4.32	1.90	γ-CH 1.49	121.3
				δ-CH$_3$ 1.06	
Ile21	8.24	4.23	1.96	γ-CH$_3$ 1.00	125.3
				γ-CH$_2$ 1.55, 1.28	
				δ-CH$_3$ 0.97	
Ala22	8.43	4.36	1.49		128.8

Significant chemical shift changes were taken to be greater than 0.5 ppm in the nitrogen dimension and greater than 0.05 ppm in the hydrogen dimension [492]. Although some small chemical shift changes were noted for residues Ile21 and Ala22, which were generally slightly downfield, none of these were above the threshold to be considered significant. In contrast, differences in chemical shift between the free and bound peptide are more obvious for Val5 and Leu6, especially for the amide N, NH and αH protons, which are particularly sensitive to conformational changes.

As is shown in Figure 5.19, the assigned resonances for the peptide backbone of residues 5 and 6 change to various extents and in both directions. The αH protons are high-field shifted, as expected for a stabilised helical structure (Section 4.5.1). Furthermore, the large upfield shifts noted for ^{15}N amide nitrogen resonances in the bound peptide may also be associated with a conformational transition towards helical structure [372,493]. Changes of amide proton chemical shift are thought to indicate differences in hydrogen bonding strength [494]. The large downfield shift of the Leu6 NH resonance may be accounted for by the formation of an intramolecular hydrogen bond as a result of helix formation. However, the Val5 NH resonance shows an opposing shift, which may possibly be explained by ring current effects induced by nearby aromatic residues in the bound protein [495,496].
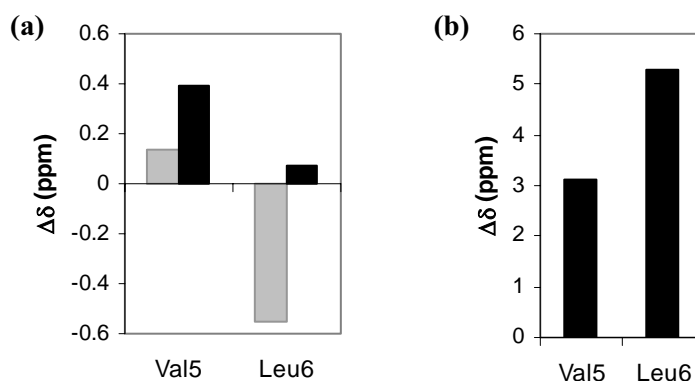
Figure 5.19: The difference between chemical shifts of free and Ca$_4$-CaM bound caerin 1.8 for the **(a)** NH (grey) and αH (black) proton, and **(b)** amide nitrogen resonances assigned for residues Val5 and Leu6. Positive values indicate an upfield shift relative to the unbound peptide.

Finally, the NOE cross-peak patterns of the ^{15}N bound protons are altered upon complexation with CaM, with a number of additional signals observed. Of particular note are the d_{NN} NOEs identified between residues Val5 and Leu6, which were absent in the spectrum of free caerin 1.8, and remain absent for residues Ile21 and Ala22. This is a strong suggestion that the Φ dihedral angles in the N-terminal fragment lie in the α-type region, and further supports the notion that the bound portion of caerin 1.8 is now in a helical conformation.

5.3 Discussion

5.3.1 Insights from Mass Spectrometry

Calcium binding proteins such as CaM are acidic, with pI values ranging from 4 to 4.5 [487]. Thus, within the pH range used in this study where Ca^{2+} binds with maximum affinity, the protein molecules will have a net negative charge. In addition, non-specific metal ion binding gives rise to cations that are readily detectable in the positive ion mode. Therefore, the analysis of acidic CaM in the negative mode should reduce the likelihood of observing non-specific metal attatchment, since it is not necessary for charging the protein [487]. For these reasons, negative ion ESI-MS was primarily selected for analysis of the CaM-peptide interactions.

Under ideal experimental conditions, the ESI-MS technique can measure molecular masses with a precision as good as 0.01% [497]. However, preserving the solution associations before transfer into the gas phase in this study required the use of an aqueous buffer, low instrument temperatures and relatively low cone voltage, all factors which typically reduce the quality of the obtained spectrum. As a result, under such conditions an increase in background noise and a broadening of signals is noted. Nevertheless, this technique was readily applicable for the study of non-covalent interactions between the small amphibian peptides and CaM.

In agreement with previous studies, at least two charge distribution patterns were observed in the ESI mass spectra of both CaM and Ca_4-CaM in NH_4OAc, indicating at least two different protein conformations exist in the electrospray conditions used [485,486]. The higher charge state distribution centred around $(M-15H)^{15-}$ is similar to that observed for CaM when sprayed from aqueous organic solvents (for example, compare Figure 5.6 and Figure 5.7), and is likely to correspond to denatured CaM conformations [486]. The lower charge envelope, containing the base peak in the spectrum at $(M-7H)^{7-}$, is attributed to folded CaM conformations, and is present due to the more physiologically relevant buffer systems applied in these experiments [485]. If the relative abundances in the gas phase parallel those in solution, it is possible to

conclude that the tightly folded native conformer is the most populated structure in these solvent conditions.

The Ca^{2+} binding properties of CaM observed here are also consistent with what is already known for this protein. For example, saturation of CaM with Ca^{2+} gives rise to a distribution of species with anywhere from 1 to 8 bound calcium ions, with 4 Ca^{2+} being the most likely. The observation of such non-specific binding, and even the relative abundance of each of the Ca^{2+}-bound species, is directly comparable to those obtained in similar conditions by Nemirovskiy *et al.* during their studies on the binding of CaM and melittin [498].

The detection of peptide-CaM complexes in the gas phase constitutes direct evidence for the binding of amphibian peptides with CaM, and provides further support for their suspected mode of nNOS inhibition. CaM was found to bind in a similar manner to a range of amphibian peptides, which are significantly different at both the primary and secondary structure level, demonstrating the inherent flexibility in CaM binding specificity. Taking into account both the instrumental parameters and sample conditions required to observe the intact complexes, and the ease with which they dissociate, it is highly probable they are maintained by a number of weak, non-covalent interactions.

A small number of specific examples exist in the literature whereby CaM complexes have stoichiometries that differ from the typical 1:1:4 calmodulin/peptide/Ca^{2+} ratio. For instance, incorporation of two Ca^{2+} ions is sufficient to cause binding of melittin to CaM [498], while non-covalent interaction between the synthetic peptide RS20 and CaM can occur without associated Ca^{2+} and allows for the occupation of up to four peptide molecules [485]. In addition, two K^+ channel domains are clamped together by two molecules of CaM in the complex between CaM and a 96 residue fragment corresponding to the C-terminal cytosolic portion of the K^+ ion channel [499]. However, in all cases the amphibian peptides examined here bound in a 1:1 stoichiometry with CaM, with no evidence for dimerisation of the protein or further addition of peptide, even at a range of peptide/protein ratios.

Although some non-specific binding of Ca^{2+} was evident, a minimum of four Ca^{2+} ions was required for complex formation. The absence of peptide-Ca_2-CaM complexes in which two Ca^{2+} ions are bound, and the dominance of peptide-Ca_4-CaM complexes are consistent with the idea that the two globular domains are mutually dependent. Binding of Ca^{2+} occurs in a stepwise manner, and as each calcium binds, it effects changes in conformation of the protein to allow the subsequent ligands to bind [461]. It is therefore likely that the functional conformation of CaM that is able to bind the amphibian peptides is only formed upon addition of a full complement of Ca^{2+}.

Wintrode and Privoalov have described a view of the peptide binding process in which the first step is either occupation of all four Ca^{2+} binding sites, or the occupation of two Ca^{2+} binding sites in the C-terminal domain of CaM [500]. Subsequently, the peptide bridges the N- and C-terminal domains of the protein if four Ca^{2+} ions are present. Conversely, if only the two C-terminal sites are occupied, the peptide binds to the C-terminal domain alone. If this depiction is indeed correct, it is likely the amphibian peptides interact with both termini of the protein, since four Ca^{2+} ions are involved.

For all of the peptides examined, the base peak in the spectrum was that of the $(M-8H)^{8-}$ ion of the complex, and a relatively small charge distribution envelope was observed. The amount of charge that a biomolecule exhibits in an ESI-MS spectrum has been correlated to a global structure, and therefore this narrow charge distribution centred about a low charge state (at high *m/z*) represents retention of the higher order structure of the native complex [186,251]. In all cases, the envelope of the lower charge states of the peptide-bound CaM are shifted relative to that of unbound CaM, and are centred upon $(M-8H)^{8-}$ compared with $(M-7H)^{7-}$ for the free protein. This suggests that the complex is more compact than unbound CaM, and some acidic residues in the bound state are buried and not accessible for deprotonation. Furthermore, peptide binding was only observed at the lower charge states of CaM, and implies folded protein conformations are necessary for complex formation.

This is further supported by D_2O experiments, in which the extent of H/D exchange for Ca_4-CaM is decreased in the presence of caerin 1.8. The reduction in deuterium incorporation must result from new protection of exchangeable amide hydrogens, presumably because the peptide-bound CaM assumes a more compact conformation. Additional experiments in which the protein is digested and the peptide fragments investigated by MSMS may be useful in accurately identifying the location of exchangeable sites, and in turn provide a more detailed picture of the overall structure and binding interface for the peptide-CaM complexes.

Increasing either the cone voltage or collision energy causes dissociation of the complexes, and at a sufficient level the only ions present are those of free Ca_4-CaM and free peptide. By these methods the most abundant ion produced for Ca_4CaM remained the -8 charge state, while in contrast, the most prevalent species in the negative ion spectra of Ca_4CaM which had not been treated with peptide was $(M-7H)^{7-}$. The most likely explanation for this difference is that desolvation is complete when the peptide dissociates, and there is no opportunity for the protein to pick up protons even if there are accessible sites of suitable gas-phase basicity, irrespective of a probable conformational change [501].

An indication that solution phase binding events are in fact being monitored in the gas phase arises from the relative binding affinities determined for three model peptides chosen for analysis, namely caerin 1.8, citropin 1.1 (mod. 18) and splendipherin. Using both competition binding studies and gas phase dissociation methods, the relative strength with which these peptides bind to CaM was found to mirror that observed in the solution state. Surprisingly, these results do not directly correlate with the IC_{50} values derived experimentally for the inhibition of nNOS, and hence other factors may also contribute to efficacy. For example, the affinity of the peptides for CaM may be associated with their abilities to form positively charged amphipathic helices [316]. Further experiments with other peptides may be useful to analyse in more detail the relationship between experimentally derived IC_{50} values and CaM binding affinity, and to verify the general applicability of these methods for the determination of solution phase binding strengths.

The mass spectrometric results presented throughout this chapter not only provide significant insight into the way in which the amphibian peptides interact with CaM, and in turn exert their biological activity, but also demonstrate the complementary nature of mass spectrometry with more established techniques such as NMR spectroscopy for the study of complex biomolecular systems.

5.3.2 Insights from NMR Spectroscopy

A better understanding of the way in which the amphibian peptides bind to CaM to inhibit the formation of NO by nNOS, requires investigation of the structural motifs of the binding partners. The NMR experiments presented here are mainly directed towards the characterisation of caerin 1.8, both in free and complexed states, and therefore the results are complementary to those concerning the CaM features described previously for the caerin 1.8-CaM complex [482].

It is commonly accepted that small linear peptides do not have a unique secondary structure in aqueous solution, but rather sample a range of different conformational states [491]. Although a number of exceptions to this rule have been described, including specific examples which have been shown to bind to CaM [405,495,496], the NMR structural study of unbound caerin 1.8 indicates that this peptide indeed exists in a random, extended conformation in H_2O. However, while caerin 1.8 itself has not been investigated, previous analysis of caerin 1 peptides including caerin 1.1 (Figure 5.20) and caerin 1.4 using NMR methods suggests that in structure enhancing solvents such as TFE, these peptides adopt an amphipathic α-helical structure with a flexible bend initiated by Pro15 [312,313]. It is therefore extremely likely that caerin 1.8, which shows a high degree of sequence homology with these peptides, has a similar propensity to form such a structure.
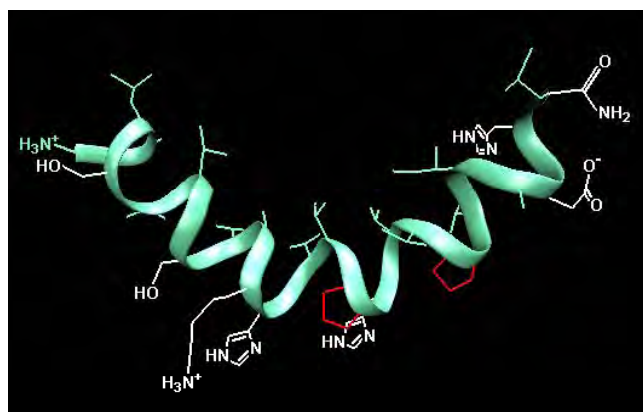
Figure 5.20: The three-dimensional structure of caerin 1.1 [313]. Hydrophobic groups are shown in green, hydrophilic groups in white, and Pro residues are coloured red.

Differences in overall conformation and physicochemical environment of caerin 1.8 upon binding CaM are reflected in a number of NMR parameters. Chemical shift changes and intramolecular NOE connectivities for the bound peptide are compatible with formation of a stable helix over the N-terminal portion of the peptide. It is not apparent from this data where the borders of this helix both begin and end. However, it is clear that the labelled residues Val5 and Leu6 are involved, while those residues in the C-terminal direction of at least Ile21 are not included in this structural motif.

The specificity of biomolecular interactions is often explained by either the 'lock and key' model, whereby a ligand binds only if it fits the exact shape required by a rigid binding site, or by the 'induced fit' model in which a dynamic structural adjustment occurs during the interaction which enables the flexible ligand and receptor site to effectively combine [8,9]. In the case of the caerin 1.8-CaM complex, the intermolecular interactions appear to selectively induce the formation and stabilisation of a predisposed helical structure in the peptide. Simultaneously, CaM also undergoes detectable conformational changes, consistent with the induced fit mode of binding.

Data presented here indicates that the binding of caerin 1.8 to CaM perturbs only a limited region of the peptide, and appears to have insignificant consequences on the C-terminal end. Based on the helix-bend-helix conformation of caerin 1.1 shown in Figure 5.20, Schiffer-Edmundson helical wheel projections can be constructed for caerin 1.8 which take into account the presence of the Pro-induced hinge. As can be

seen in Figure 5.21, the N-terminal portion of the peptide is less hydrophobic and instead more amphipathic in a helical form. In addition, this region is also more basic, with an overall charge of +2 compared with 0 for the C-terminus. Since the affinity of peptides for CaM appears to correlate somewhat with the ability to form positively charged amphipathic α-helices [316,469], it is not surprising that CaM binds preferentially to the N-terminal helix of caerin 1.8. As the C-terminal portion of the peptide is not influenced upon binding it is likely to remain in a flexible, random state, consistent with the observed NMR data.
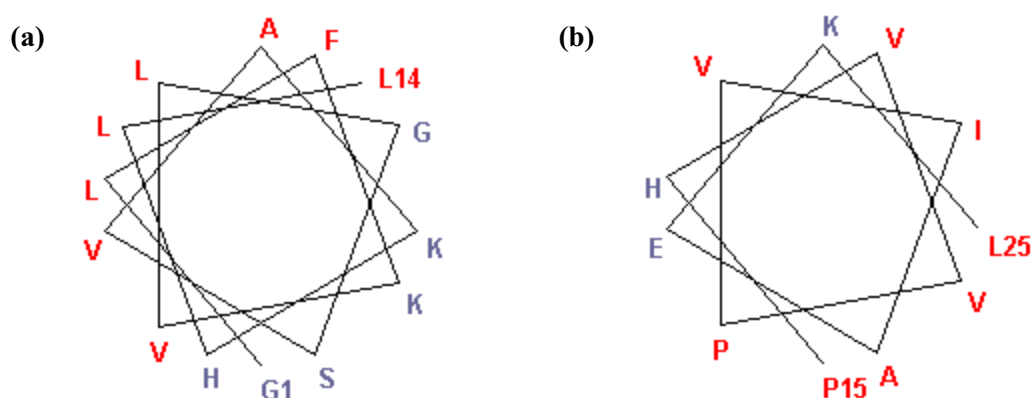
Figure 5.21: Schiffer-Edmundson helical wheel projections of **(a)** residues 1-14, and **(b)** residues 15-25 of caerin 1.8. Hydrophilic residues are coloured blue, while hydrophobic residues are coloured red.

Furthermore, caerin 1.19.3, identified in the skin secretion of the dainty green tree frog, *Litoria gracilenta*, is a natural degradation product of caerin 1.19 resulting from enzymatic cleavage between Leu6 and Gly7. This peptide demonstrates no inhibitory effect on nNOS, and therefore further reinforces the requirement of the N-terminal residues for biological activity, and hence the likely interaction between this region of the peptide and CaM [484].

Caerin 1.19.3   GSVAKHLLPHVAPIIAEKL-NH$_2$

The specific interaction between CaM and the N-terminal region of caerin 1.8 makes it possible to rule out a number of potential binding modes. For example, O'Neil and DeGrado suggested that the two ends of a synthetic peptide with idealised amphipathic helicity, Baa17, interact simultaneously with both globular domains of CaM [502]. According to this model, the N- and C-terminal regions of the peptide would be more immobile than the central fragment, which is inconsistent with a number of features observed for caerin 1.8.

Complementary experiments undertaken previously, which monitored the chemical shift changes of CaM upon binding to caerin 1.8, suggest both the N- and C-terminal globular domains of the protein interact with the peptide, and that the protein undergoes a structural change towards a collapsed conformation upon binding. The most significant changes appear to occur in the inter-helical regions, especially in the central hinge (residues 77-82) and in calcium binding loops numbers I and IV (between residues 19-29 and 127-138 respectively) [482]. Combined with the data from the present study, and what is already known about the peptide binding properties of CaM, a broad picture of the caerin 1.8-CaM complex emerges. It is likely that the dissolution of the central helix of Ca_4CaM allows the two globular domains to move as semi-rigid bodies to form a more compact structure. The N-terminal portion of the peptide, which is now in a helical conformation, is engulfed in a hydrophobic binding pocket. This is most consistent with the 'collapsed' conformation binding modes described in Section 5.1.3.

The experiments described throughout this chapter do not allow for a more detailed characterisation of the intermolecular interactions between caerin 1.8 and CaM. Extensive ^{15}N and ^{13}C labelling of both the peptide and protein, in combination with multidimensional heteronuclear NMR methods, would be necessary for higher resolution structure determination. Nevertheless, the approach presented here provides a good experimental basis for further understanding the interactions between Ca_4-CaM and the amphibian nNOS inhibiting peptides.

5.4 Experimental Procedures

5.4.1 Sample Preparation - Mass Spectrometry

Bovine brain CaM was purchased from Sigma (St. Louis, USA). Preparation of CaM for mass spectrometry was achieved by dissolving in water, followed by dialysis at 4 °C against; 4 x 2 L 10 mM NH_4OAc, 2mM in EDTA, pH 5.6; 4 x 2 L 10 mM NH_4OAc, pH 5.2; 1 x 2 L 10 mM NH_4OAc pH 6.8. CaM concentrations were elucidated by measurement of the absorbance at 277 nm using an absorbance coefficient of 3300 $M^{-1}.cm^{-1}$ [503], and were typically 100 μM. Ca_4-CaM was prepared by adding 2.5 molar equivalents of Ca^{2+} ions in the form of calcium acetate (5 mM in 10 mM NH_4OAc, pH 6.8), which was sufficient to observe CaM with its full complement of Ca^{2+}.

Peptides were synthesised commercially by Mimotopes (Clayton, Victoria) using L-amino acids and standard solid phase methods [331], and were typically greater than 90% pure as verified by HPLC and mass spectrometry. Stock solutions were prepared by dissolving appropriate amounts of peptide in ammonium acetate (10 mM, pH 6.8) to give a concentration in the range of 1-3 mM. Small aliquots were then added to CaM solutions to achieve the desired peptide/CaM molar ratios.

To investigate the effect of different solvents, CaM solutions were also diluted 1:1 by volume in the following organic solvent systems; methanol/H_2O (1:1 v/v); isopropanol/H_2O (1:1 v/v); acetonitrile/H_2O (1:1 v/v); acetonitrile/H_2O/triethylamine (50:49:1 v/v/v).

5.4.2 Mass Spectrometry

Peptide-CaM complexes were investigated by ESI-MS, using a Micromass Q-TOF 2 mass spectrometer, with a Z-spray ionisation source and a mass range to 10,000 Da. Samples were directly injected using a Harvard model 22 syringe pump (Natick, USA) at a flow rate of 10 $mL.min^{-1}$. Spectra were acquired in the negative ion mode, over the mass range *m/z* 500-5000.

Typical operating parameters included a capillary voltage of 2.6 kV, a cone voltage of 35 V, argon collision gas energy at approximately 4 eV and source block and desolvation temperatures of 40 ˚C. In general, 20-30 acquisitions of 5 seconds were summed to obtain representative spectra. Data processing was performed using the program MassLynx (Micromass Ltd., version 4.0). Dissociation experiments were recorded under the same conditions used for ESI-MS, with the cone voltage varied in the range of 35-60 V.

5.4.3 D_2O Exchange

The method for H/D exchange was based on that of Nemirovskiy *et al*. [504], using 100 μM Ca_4-CaM in 5 mM NH_4OAc, pH 6.8, and a peptide/protein ratio of 1:1. An NH_4OAc solution was also prepared in D_2O at a concentration of 5 mM and pH 6.8 for initiation of exchange. 10 μl aliquots were taken to determine the extent of H/D exchange for each given time point, in which the reaction was initiated at room temperature by mixing the 10 mL aliquot with 90 ml D_2O solution. After the required exchange period, which varied from 1 to 90 minutes, the reaction was quenched by addition of 300 mL of ice-cold water/methanol/formic acid solution (90:9:1 v/v/v). This sample was then analysed by mass spectrometry in the positive ion mode, using the following conditions; capillary voltage 3.1 kV, source temperature 80 ˚C, desolvation temperature 150 ˚C and cone voltage 40 V.

5.4.4 Sample Preparation - NMR Spectroscopy

Caerin 1.8 was synthesised commercially by Mimotopes (Clayton, Victoria) using L-amino acids and standard N-α-Fmoc methods reported peviously [331], and was shown to be greater than 95% pure by HPLC and ESI mass spectrometry. ^{15}N-L-amino acids were specifically incorporated at positions Val5, Leu6, Ile21 and Ala22. Bovine brain CaM was purchased from Sigma (St. Louis, USA) at greater than 95% purity, and was used as received.

[15]N-caerin 1.8 (4.0 mg, 1.5 μmoles) was dissolved in potassium chloride (100 mM), calcium chloride (40 mM) and 10% D_2O in aqueous solution at pH 6.3 with a total volume of 500 mL, giving a peptide concentration of 3 mM. Sodium azide (0.02%) was added as a preservative [505]. CaM (25 mg, 1.5 μmoles) was dissolved in water, adjusted to pH 6.3 using sodium hydroxide, then divided into five portions such that successive additions would give the desired peptide/CaM ratio as given in Table 5.5. The aliquots were then lyophilised, and added to the ^{15}N labelled caerin 1.8 sample in sequence. pH was re-adjusted back to 6.3 with the addition of small quantities of hydrochloric acid or sodium hydroxide solutions as required.

Table 5.5: Quantities of CaM used for titration with caerin 1.8.

Step	CaM (mg)	Concentration (mM)	CaM:Caerin 1.8
1	0	0	0:1
2	5.0	0.595	0.2:1
3	10.0	1.191	0.4:1
4	15.0	1.787	0.6:1
5	20.0	2.382	0.8:1
6	25.0	2.977	1:1

5.4.5 NMR Spectroscopy

All spectra were recorded using a Varian Inova-600 NMR spectrometer, with a ^{1}H frequency of 600 MHz and a ^{13}C frequency of 150 MHz. Experiments were conducted at 25 ˚C, and referenced to DSS at 0 ppm in ^{1}H and ^{13}C, while the ^{15}N dimension was centred at 120 ppm.

For the titration series, the standard gNhsqc pulse sequence from the VNMR library was used, with 256 increments, each comprising 16 transients, acquired over 2048 data points. A spectral width of 6000.2 Hz was used in the ^{1}H dimension and 2500 Hz in the ^{15}N dimension. Resultant spectra were processed using NMRPipe [506], and viewed with Sparky software (version 3.111).

At step 1 of the titration series described previously, a series of 2D NMR spectra were acquired to investigate unbound caerin 1.8. TOCSY, DQF-COSY and NOESY experiments were collected in the phase sensitive mode, with solvent suppression typically achieved by centring the transmitter frequency on this resonance, and applying low power presaturation from the proton transmitter during a 1 second relaxation delay. Gradient methods for suppression were used in the DQF-COSY experiment [507]. 200 increments, each comprising 16 transients, were acquired over 2048 data points, with a spectral width of 6000.2 Hz. NOESY spectra were acquired with mixing times of 100 and 250 ms, while the TOCSY pulse sequence employed a 60 ms MLEV-17 spin-lock [361]. A HSQC spectrum was also recorded with an interpulse delay of $1/2J_{CH}$ = 3.6 ms, corresponding to J_{CH} = 140 Hz. This experiment consisted of 128 increments, with 64 transients per increments, acquired over 2048 data points in the directly detected (^1H, F_2) dimension. A spectral width of 25632.0 Hz was used in the ^{13}C, F_1 dimension. All 2D spectra were processed using VNMR software (VNMRJ, version 1.1D). Data matrices were multiplied by a Gaussian function in both dimensions before zero-filling to 4096 data points prior to Fourier transformation.

For bound caerin 1.8, TOCSY experiments were based on the 3D gNhsqctocsy pulse sequence from the VNMR library, with only the first F_2F_3 plane recorded. In this plane, 64 increments, each comprising 256 transients, were acquired over 2048 data points. Spectral widths of 6000.2 and 2500 Hz were used in the ^1H and ^{15}N dimensions respectively, and mixing times of 30, 55 and 70 ms were incorporated. For the NOESY experiments, the 3D gnoesyNhsqc pulse sequence from the VNMR library was used, with only one increment acquired in the ^{15}N dimension, effectively giving a ^{15}N-edited NOESY spectrum. In the proton plane, 64 increments, each comprising 64 transients, were acquired over 2048 data points, with a spectral width of 6000.2 Hz and mixing times of 80, 150 and 250 ms. Resulting spectra were processed using VNMR software (VNMRJ, version 1.1D), in which the data matrices were again multiplied by a Gaussian function in both dimensions before Fourier transformation.

~ CHAPTER 6 ~

Three-Dimensional Structure Determination of Neuropeptides from the Genus Crinia

6.1 Introduction

6.1.1 Peptides from the Genus *Crinia*

The *Crinia* genus is part of the family Myobatrachidae, and currently comprises fifteen species which are distributed throughout most of Australia, excluding the central arid regions [57]. Species of this genus are typically small, with polymorphic appearance, and are often difficult to distinguish on physical characteristics alone. Examples of the *Crinia* genus include the common froglet, *C. signifera* and the streambank froglet, *C. riparia*.

Crinia signifera is small in size measuring 16-28 mm in length, and is highly variable in appearance even in local breeding aggregations. In general, the animal is predominantly grey-brown with dark bands, irregular patches or vertical stripes on the dorsal surface (Figure 6.1). Adults have a white, granular ventral surface which is heavily mottled with black or dark brown, whilst the skin also varies in texture from smooth to ridged or warty [308]. *C. signifera* is most common in forests, woodlands, floodplains and alpine grasslands of southeastern Australia (Figure 6.1). Within these habitats it shelters amongst logs and other debris, usually in moist depressions or near water bodies [57].

Crinia riparia is South Australia's only endemic frog species, with a geographical distribution confined wholly to the Flinders Ranges (Figure 6.2). These animals are found in the moist shallow spaces beneath boulders and stones on the edges of rock-strewn creeks, often in close aggregations of up to forty individuals [508]. *C. riparia* is closely related to *C. signifera* and reaches a similar adult size (16-25 mm), while also exhibiting the same characteristic variable colour pattern and skin texture (Figure 6.2) [57]. This frog can be readily identified however by the lack of a tympanum which is unique within the genus, and its distinctive male mating call [508].
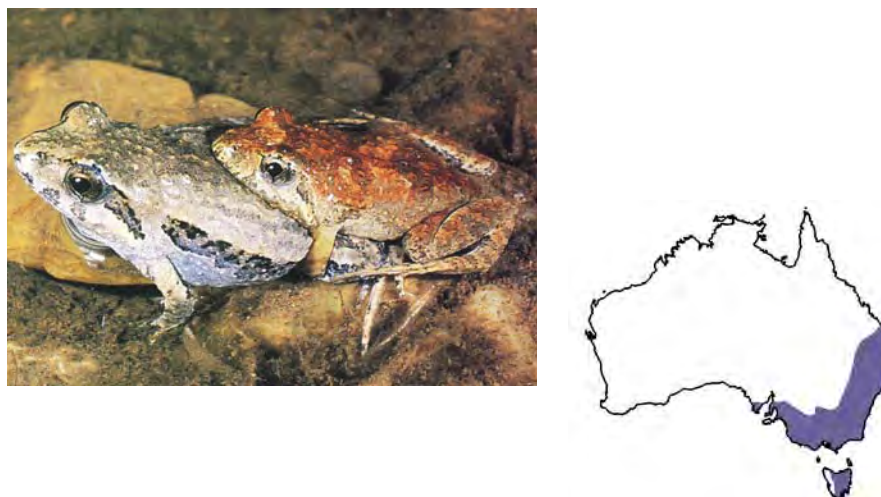
Figure 6.1: Appearance and geographical distribution of *Crinia signifera* [57].

Figure 6.2: Appearance and geographical distribution of *Crinia riparia* [57].

Recently, the skin secretions of both *C. signifera* and *C. riparia* have been investigated, and a number of novel peptides characterised [76,78]. These constitute the signiferin and riparin peptide groups, and are summarised in Table 6.1. Both the signiferin and riparin families include peptides which demonstrate neurological and antibacterial activity, as well as those which inhibit the formation of NO by nNOS.

Table 6.1: Peptides identified from the skin secretions of *Crinia signifera* and *Crinia riparia*.

Peptide	Sequence	Activity[1]
Signiferin 1	RLC<u>IYIIFP</u>C-OH	a
Signiferin 2.1	IIGHLIKTALGMLGL-NH$_2$	b
Signiferin 2.2	IIGHLIKTALGFLGL-NH$_2$	b
Signiferin 3.1	GIAEFLNYIKSKA-NH$_2$	c
Signiferin 4.1	GFADIFGKVANLIKS-NH$_2$	c
Signiferin 4.2	GFADLFGKAVDFIKS-NH$_2$	c
Signiferin 4.3	GFADLFGKAVDFIKSRV-NH$_2$	c
Riparin 1.1	RLC<u>IPVIF</u>PC-OH	a
Riparin 1.2	FLPP<u>CAYKGT</u>C-OH	a
Riparin 1.3	FPLP<u>CAYKGT</u>YC-OH	a
Riparin 1.4	FFLPP<u>CAYKGT</u>C-OH	a
Riparin 1.5	FFLPP<u>CAHKGT</u>C-OH	a
Riparin 2.1	IIEKLVNTALGLLSGL-NH$_2$	d
Riparin 5.1	IVSYPDDAGEHAHKMG-NH$_2$	e

[1]**Activity: (a)** Neuropeptide; **(b)** Wide-spectrum antibiotic; **(c)** nNOS inhibitor; **(d)** Narrow-spectrum antibiotic; **(e)** Activity unknown.

The riparin and signiferin peptides show little structural similarity to those isolated from the skin secretions of other Australian amphibians thus far. For example, the signiferin 2 and riparin 2 families are the first to be identified with two initial Ile residues. These have subsequently been tested for antibacterial efficacy, and show moderate activity against Gram-positive organisms in the micromolar range [76]. Interestingly, both *C. signifera* and *C. riparia* possess no neuropeptides in their glandular secretions analogous to the caeruleins or uperoleins [58]. Instead, the major neuropeptide components in each case are those which have a disulfide bridge linking two Cys residues spaced six or seven amino acids apart.

Although some disulfide bridge containing peptides have been previously identified in the skin secretions of other amphibians, these are the first cyclic peptides to be isolated from an Australian anuran, and hence their structures and biological activities are of particular interest.

6.1.2 Biological Activity of Signiferin 1 and Riparin 1.1

Recent pharmacological testing reveals that signiferin 1 and riparin 1.1 have quite different functions in the amphibian integument. However, despite their distinct spectra of activity, both peptides bring about their biological effects by activation of cholecystokinin (CCK) receptors [28,509].

Natural ligands for CCK receptors include CCK and gastrin peptides, which have roles as both hormones and neuropeptides in the gastrointestinal and nervous systems [510-512]. They are mostly involved in digestive processes such as gastric secretion and gut motility. In the brain, CCK also regulates nociception, anxiety, memory and satiety. The CCK receptors are divided into two subtypes based on their affinities for selected agonists, and are named CCK_1 and CCK_2. CCK_1 receptors are located predominantly in peripheral tissues such as the gastrointestinal tract, while CCK_2 receptors are distributed principally throughout the central nervous system [510,513].

The guineapig ileum longitudinal muscle and myenteric plexus contain both CCK receptors, and provide a useful model for observing peptide-induced smooth muscle activity [514,515]. CCK_1 receptors exist on the muscle itself and cause contraction directly, while CCK_2 receptors act indirectly by effecting the release of acetylcholine from cholinergic nerves in the myenteric plexus, which in turn activates muscarinic receptors on the smooth muscle [514]. Using the guineapig ileum functional assay, signiferin 1 demonstrates dose-dependent contraction of smooth muscle indirectly via CCK_2 receptors, at concentrations as low as 10^{-9} M. In contrast, riparin 1.1 displays no smooth muscle activity in this assay, even at concentrations as high as 10^{-5} M [509].

Neuropeptides can also influence proliferation, differentiation and function of immune cells. For example, lymphocytes possess CCK_2 receptors on their surface. Upon stimulation these contribute to cell proliferation, and may therefore indicate a possible role for CCK in the antigen processing and sensitisation phases of the immune response [516]. Due to this, the *Crinia* neuropeptides were also tested for immunomodulatory activity. Riparin 1.1 produces a concentration-dependent increase in lymphocyte proliferation at a minimum concentration of 10^{-7} M, while signiferin 1 has no observable effect in this system [509].

The wide spectrum of biological activity mediated by CCK receptors makes them candidates for a therapeutic approach to a number of diseases [517]. In fact, during the last few years, increasing effort has been devoted to the development of selective CCK analogues endowed with either agonist or antagonist activity [518,519]. This makes peptides such as signiferin 1 and riparin 1.1, which are able to elicit different biological responses through the same receptor, particularly interesting. However, to fully appreciate the potential of such compounds, it is important to understand their function at a molecular level.

CCK receptors belong to the superfamily of G-protein coupled receptors, in which the membrane associated G-proteins provide a versatile relay between a variety of hormone receptors on the cell exterior, and the intracellular effector enzymes and secondary messenger systems directly responsible for the observed biological outcome [5,513,520-522]. The high-resolution 3D structure of rhodopsin is given in Figure 6.3, which is the only comprehensive structure of a member of the G-protein coupled receptor superfamily reported to date [523]. By analogy, the structure of rhodopsin can provide general information regarding the structure of other G-protein coupled receptors such as CCK_1 and CCK_2, which are also thought to consist of seven transmembrane α-helical domains linked by alternating intracellular and extracellular loops, with the N-terminus located on the extracellular side and the C-terminus on the cytoplasmic side [510,513,522].

Figure 6.3: The three-dimensional crystal structure of rhodopsin [523].

The sequences of the CCK receptors are known, and representations of their 3D structures have been reported [510,513]. Interactions between CCK receptors and their ligands are best understood for small molecules which are known to bind within the transmembrane helices [524]. However, the extracellular domains appear to be of critical importance for recognition and binding of peptide ligands. The structure of one of the natural peptide ligands, CCK-9 is given below.

CCK-9   `RDY(SO`$_3$`H)MGWMDF-NH`$_2$
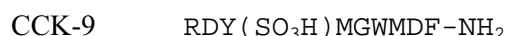
Although the CCK$_2$ receptor binding site has not been fully defined, indirect structural insight into the localisation and nature of the peptide agonist binding site in the CCK$_2$ receptor has been provided primarily by site directed mutagenesis and photoaffinity labelling studies [525-529]. Based on this data, a 3D model of the CCK$_2$ receptor bound to CCK-9 has been proposed (Figure 6.4) [528].
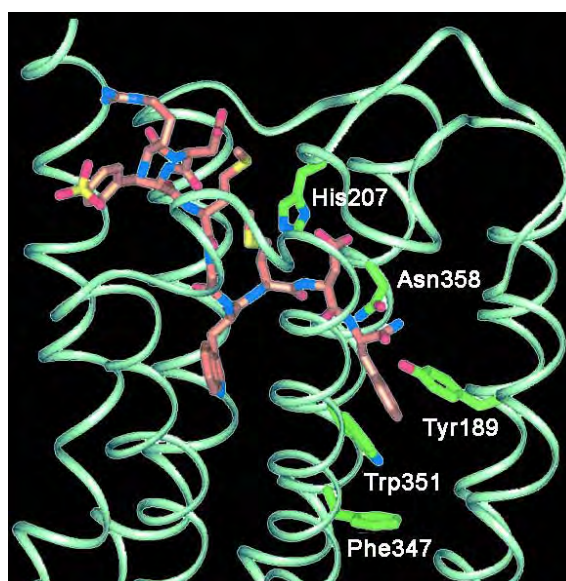
Figure 6.4: Three-dimensional model of the CCK-9/CCK$_2$ receptor complex. Side chains of important residues in close proximity to the C-terminus of CCK-9 are highlighted and labelled. Figure adapted from [528].

A number of important residues in the CCK_2 receptor binding site have been identified, and include hydrophilic residues such as His207 and Asn358, as well as the aromatic residues Tyr189, Trp351 and Phe347 [528,530,531]. It has recently been shown that structurally related peptide agonists, partial agonists and antagonists all occupy a similar binding pocket within the CCK receptor [532], and therefore it is possible that peptides such as signiferin 1 and riparin 1.1 also bind in a comparable location. This provides some basis for structure-activity investigations of these peptides.

6.1.3 Structure of Cysteine Bridged Amphibian Peptides

More than ten distinct families of cyclic peptides have been identified from amphibians of the *Rana* genus, and are grouped based on structural similarity [533]. The majority of these peptides demonstrate broad-spectrum antibacterial properties. They are typically basic, containing a heptapeptide loop linked by a disulfide bridge at the C-terminus and a highly variable N-terminal tail. It is also known that a number of these *Rana* disulfide-containing peptides have other roles in addition to antimicrobial activity. For example, the pipinins 1-3 are histamine release agents, while brevinin 1 and palustrin 1c are insulin release agents [534,535]. Other *Rana* disulfide containing peptides show some sequence similarity to the signiferins and riparins, and it may be that a number of these shorter examples could demonstrate some type of neuropeptide activity in addition to their documented antimicrobial properties.

Often the 3D structure of a peptide has significant implications for the way in which it can exert biological activity. It is therefore likely that the interesting cyclic structure imparted to both signiferin 1 and riparin 1.1 by the Cys disulfide bond will be important for understanding the activity of these molecules. The signiferin 1 and riparin 1 peptides closely resemble the tigerinin peptides, isolated from *Rana tigerina*, the sequences of which are given below [536].

Tigerinin 1	FCTMIPIPRCY-NH$_2$
Tigerinin 2	RVCFAIPLPICH-NH$_2$
Tigerinin 3	RVCYAIPLPICY-NH$_2$
Tigerinin 4	RVCYAIPLPIC-NH$_2$

Conformational analysis by circular dichroism spectroscopy and molecular dynamics calculations suggest the tigerinins adopt unordered and β-turn structures as shown in Figure 6.5 [536], and therefore it is expected that the structures of signiferin 1 and riparin 1.1 might be similar.
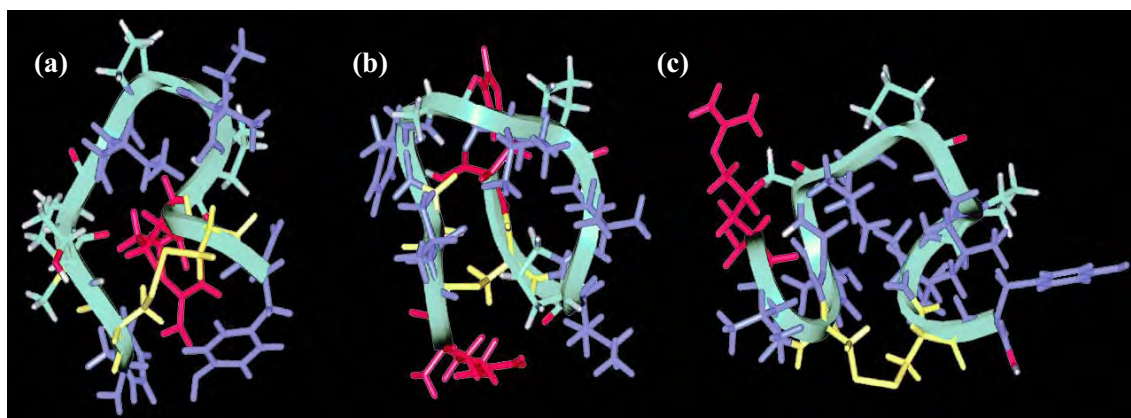
Figure 6.5: Structure of **(a)** tigerinin 1, **(b)** tigerinin 2, and **(c)** tigerinin 3 following molecular dynamics simulations. Side chains of cationic residues are indicated in red and hydrophobic residues in blue. Backbone structure is depicted as green ribbons, while cysteine side chains are in yellow. Figure adapted from [536].

Understanding the molecular basis of ligand binding and selective agonist-induced receptor activation would greatly facilitate the design of new therapeutic agents to target the CCK receptors. A step towards achieving this entails the structure determination of the ligands involved. This project therefore aimed to identify the 3D structures of both signiferin 1 and riparin 1.1 using NMR spectroscopy and RMD calculations. The results presented in the following chapter shed light on the unusual Cys bridged cyclic structure of the peptides, and provide possible insight into the way in which these peptides modulate pharmacological activity via CCK_2 receptors.

6.2 Results

6.2.1 NMR Spectroscopy

NMR spectra were acquired for signiferin 1 and riparin 1.1 in TFE/H$_2$O (1:1 v/v), and the proton resonances assigned as described in Section 4.4 using a sequential assignment method [489] and a combination of NOESY, TOCSY and COSY experiments.

A significant degree of overlap was observed in the amide region of the spectra for signiferin 1, with residues Cys3, Ile4, Ile7 and Ile8 being almost coincident. For these residues, unambiguous assignments were conclusively made by examination of the appropriate regions of the COSY spectrum. However, this degree of overlap, in addition to the multiple Pro residues in the peptide, meant there were limited NH$_i$ - NH$_{i+1}$ cross-peaks expected in the NOESY spectrum, and thus these could not be used for sequential assignment. Instead, the strong αH$_i$ - NH$_{i+1}$ peaks observed were used primarily for this purpose. Partial TOCSY and NOESY spectra are shown in Figure 6.6 to illustrate this point.

For riparin 1.1, amide resonances for each amino acid are well resolved, with the only exceptions being that of Ile4 and Ile7 which are almost coincident, and Val6 and Phe8 which are coincident. Again, unambiguous resonance assignments were made for these residues based on inspection of the COSY spectrum. A strong series of αH$_i$ - NH$_{i+1}$ peaks was once more observed for all residues of riparin 1.1, and was used primarily for sequential resonance assignment. Partial TOCSY and NOESY spectra for riparin 1.1 are given in Figure 6.7.
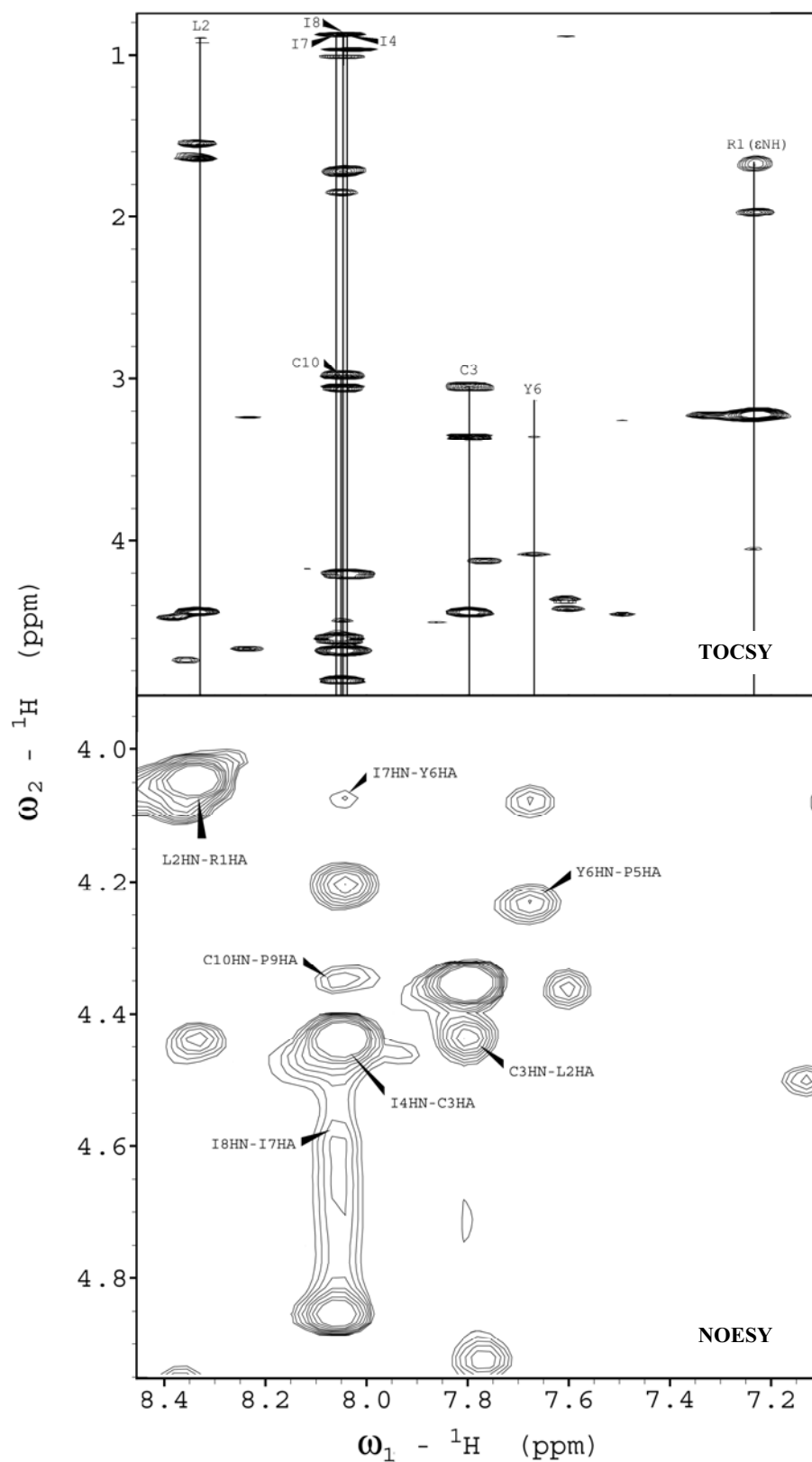
Figure 6.6: Partial TOCSY and NOESY spectra of signiferin 1 in TFE/H$_2$O (1:1 v/v). Vertical lines connect resonances of the same spin system in the TOCSY spectrum, and αH$_i$ - NH$_{i+1}$ signals used for sequential assignment are indicated in the NOESY spectrum.
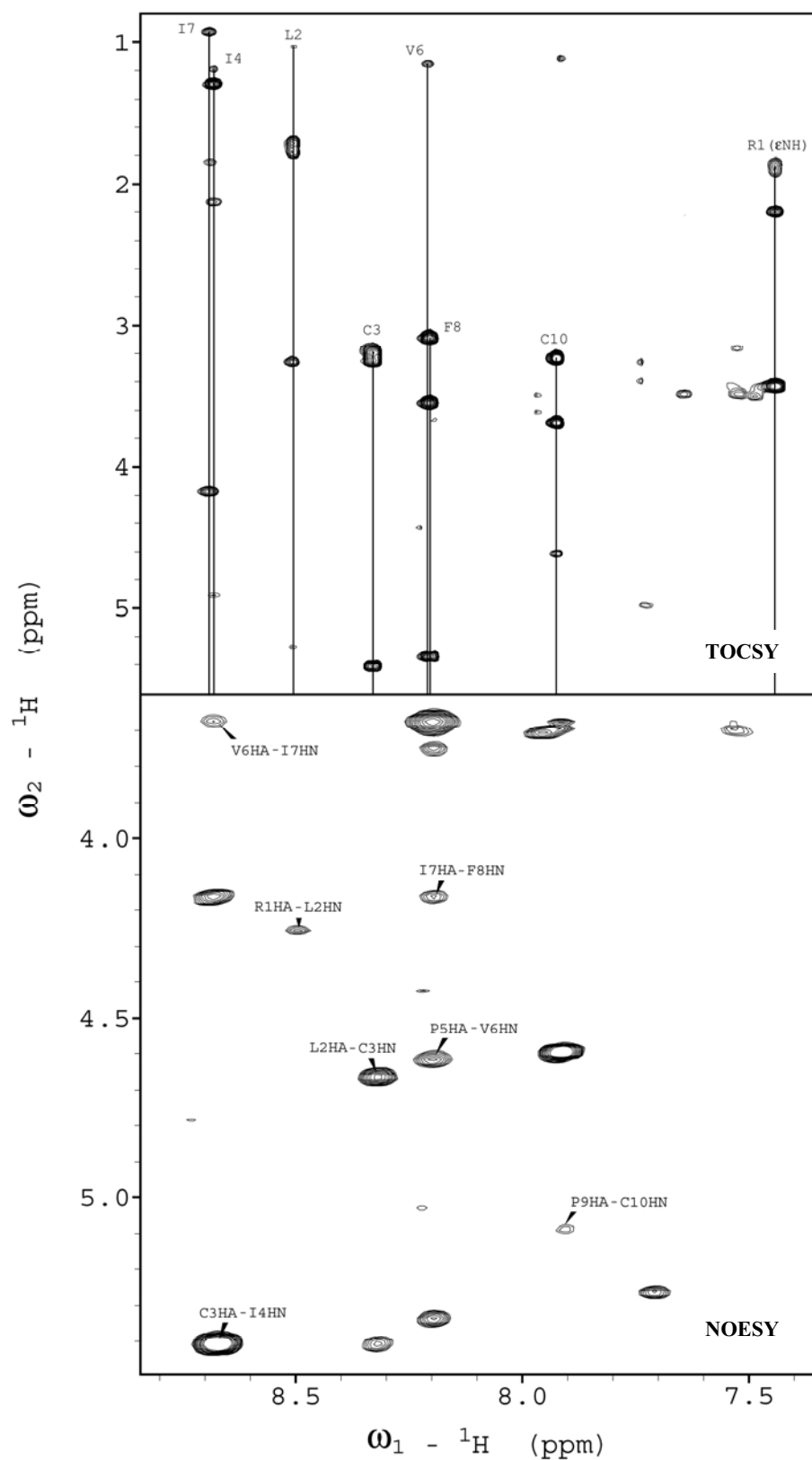
Figure 6.7: Partial TOCSY and NOESY spectra of riparin 1.1 in TFE/H$_2$O (1:1 v/v). Vertical lines connect resonances of the same spin system in the TOCSY spectrum, and αH$_i$ - NH$_{i+1}$ signals used for sequential assignment are indicated in the NOESY spectrum.

An additional series of peaks with much lower intensity was observed in the NOESY spectra of both signiferin 1 and riparin 1.1. This is likely to be a result of *cis-trans* isomerisation about the Pro imide bonds in each peptide [537,538], giving rise to a small population of molecules with an alternative conformation. However, these peaks were not assigned, and hence will not be discussed further.

Table 6.2 and Table 6.3 present a summary of all the assigned ^{1}H resonances for signiferin 1 and riparin 1.1 respectively.

Table 6.2: [1]H chemical shifts for signiferin 1 in TFE/H$_2$O (1:1 v/v). n.o. indicates resonance was not observed.

Residue	Chemical shift (ppm)			
	NH	**αH**	**βH**	**Other H**
Arg1	n.o.	4.05	1.97	γ-CH$_2$ 1.67
				δ-CH$_2$ 3.22
				ε-NH 7.22
Leu2	8.33	4.44	1.54	γ-CH 1.63
				δ-CH$_3$ 0.90
Cys3	8.06	4.86	3.05, 2.98	
Ile4	8.04	4.20	1.71	γ-CH$_3$ 0.96
				γ-CH$_2$ 1.51, 1.15
				δ-CH$_3$ 0.87
Pro5	–	4.23	2.08, 1.89	γ-CH$_2$ 2.02, 1.94
				δ-CH$_2$ 3.82
Tyr6	7.68	4.08	3.36, 3.13	δ-CH 7.05
				ε-CH 6.82
Ile7	8.06	4.58	1.72	γ-CH$_3$ 1.09
				γ-CH$_2$ 1.47
				δ-CH$_3$ 0.87
Ile8	8.05	4.68	1.85	γ-CH$_3$ 1.00
				γ-CH$_2$ 1.54, 1.17
				δ-CH$_3$ 0.88
Pro9	–	4.35	2.20	γ-CH$_2$ 1.98, 1.90
				δ-CH$_2$ 3.62
Cys10	7.80	4.44	3.35, 3.05	
				COOH n.o.

Table 6.3: ^{1}H chemical shifts for riparin 1.1 in TFE/H$_2$O (1:1 v/v). n.o. indicates resonance was not observed.

Residue	Chemical shift (ppm)			
	NH	**αH**	**βH**	**Other H**
Arg1	n.o.	4.26	2.19	γ-CH$_2$ 1.92, 1.86
				δ-CH$_2$ 3.43
				ε-NH 7.43
Leu2	8.49	4.66	1.78	γ-CH 1.71
				δ-CH$_3$ 1.10, 1.03
Cys3	8.32	5.41	3.25, 3.19	
Ile4	8.67	4.90	2.12	γ-CH$_3$ 1.29
				γ-CH$_2$ 1.85, 1.45
				δ-CH$_3$ 1.19
Pro5	–	4.62	2.52	γ-CH$_2$ 2.32, 2.26
				δ-CH$_2$ 4.11, 3.95
Val6	8.20	3.67	2.81	δ-CH$_3$ 1.15
Ile7	8.68	4.17	1.84	γ-CH$_3$ 1.09
				γ-CH$_2$ 1.69, 1.30
				δ-CH$_3$ 0.92
Phe8	8.20	5.34	3.55, 3.08	δ-CH 7.54
				ε-CH 7.47
				ζ-CH 7.49
Pro9	–	5.09	2.48, 2.24	γ-CH$_2$ 2.24, 2.15
				δ-CH$_2$ 3.75, 3.70
Cys10	7.92	4.60	3.69, 3.23	
				COOH n.o.

6.2.2 Secondary Shifts

Random coil chemical shifts determined in water were obtained from the literature [371]. αH secondary shifts, smoothed over a window of n ± 2 residues, were plotted against the sequence for both signiferin 1 and riparin 1.1, and are shown in Figure 6.8. Both NH and αC secondary shifts provided little structural information in this case, and hence are not included in this discussion.
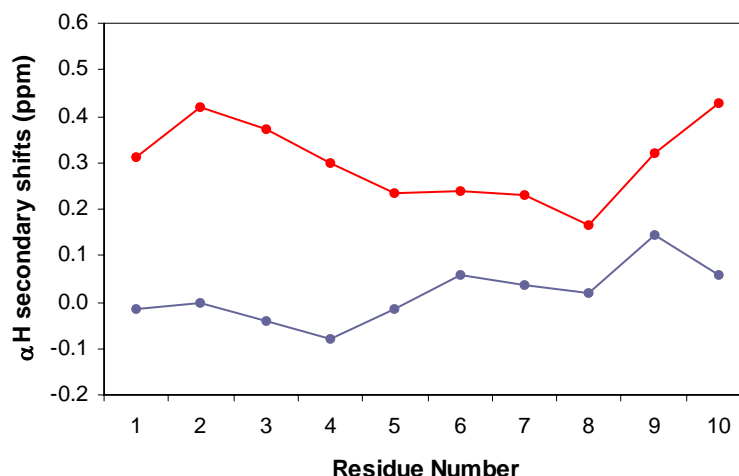
Figure 6.8: αH ^{1}H secondary shifts of signiferin 1 (blue) and riparin 1.1 (red) in TFE/H$_2$O (1:1 v/v), smoothed over n ± 2 reisdues. Negative values indicate an upfield shift from random coil resonances, while positive values indicate a shift downfield.

No distinct trend is observed for the αH resonances of signiferin 1, with the magnitude of the secondary shifts close to zero, indicating that the conformation of the peptide approximates random coil. In contrast, the chemical shifts for riparin 1.1 are clearly downfield compared with random coil values, consistent with a more extended structure along the length of this peptide.

6.2.3 NOE Connectivities

Figure 6.9 displays a summary of the diagnostic NOEs present in the NOESY spectra for both signiferin 1 and riparin 1.1, based on ARIA resonance assignments after eight iterations of structure calculations. For riparin 1.1, a strong series of sequential d$_{\alpha N}$ and d$_{\beta N}$ NOEs are evident, along with selected d$_{NN}$ peaks observed principally within the disulfide bond. No diagnostic medium-range NOEs were present. This pattern of observed NOEs and their intensities is generally consistent with the peptide having extended structure along the majority of the sequence.   In contrast, the NOE connectivity pattern for signiferin 1 is less informative. Some sequential d$_{\alpha N}$, d$_{\beta N}$ and d$_{NN}$ NOEs can be observed, however a small number of medium-range signals are also apparent. It may be that signiferin 1 adopts a more extended structure which is not

typical of either an α-helix or β-sheet. Nevertheless, the NOE connectivity data appears in agreement with that of the secondary shifts.
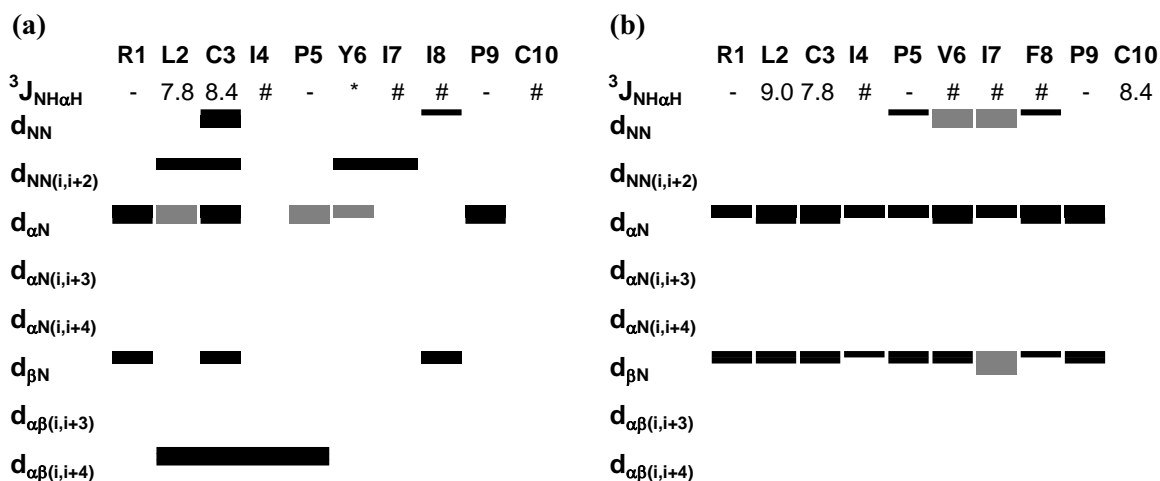
Figure 6.9: A summary of NOEs used in structure calculations for **(a)** signiferin 1, and **(b)** riparin 1.1 in TFE/H$_2$O (1:1 v/v). The thickness of the bars indicate the relative strength of the signal (strong < 3.1 Å, medium 3.1-3.7 Å, weak > 3.7 Å). Grey shaded boxes represent ambiguous NOEs, while peaks overlapped on the diagonal have been omitted. For Pro residues in which no amide protons exist, the corresponding NOEs are instead described from the δ protons. $^3J_{NH\alpha H}$ values are indicated where possible. * indicates that no coupling constant was detected, while # indicates the coupling constant could not be reliably assigned due to overlap.

Strong sequential αH$_i$ to δH$_{i+1}$ cross-peaks were observed from Ile4 to Pro5 as well as Phe8 to Pro 9 in the NOESY spectrum of riparin 1.1, consistent with both Pro residues primarily adopting a *trans* conformation in this peptide. Similar analysis of the signiferin 1 NOESY spectrum was less definitive due to greater spectral overlap, however NH$_i$ to δH$_{i+1}$ cross-peaks could be observed for both Pro residues, again indicating a preference for the *trans* conformation.

A number of long-range NOEs (> 4 residues apart) were also noted for both peptides, which can often imply intermolecular association. However, it is more likely that the long-range NOEs simply result as the Cys bridge causes the terminal ends of the peptide to be in closer proximity.

6.2.4 Coupling Constants

Also shown in Figure 6.9 are the $^3J_{NH\alpha H}$ values for signiferin 1 and riparin 1.1, determined directly from the NH region of the high-resolution 1D ^1H spectra. A large proportion of the $^3J_{NH\alpha H}$ coupling constants could not be reliably determined due to overlap in both cases. Nonetheless, the $^3J_{NH\alpha H}$ values which could be measured were found to be relatively large (in the order of 8 Hz), suggesting the peptides are likely to adopt a more extended or β-strand type structure, again consistent with other NMR data.

6.2.5 Structure Calculations

The NOESY spectra of signiferin 1 and riparin 1.1 in TFE/H_2O (1:1 v/v) were fully assigned and the volumes of the cross-peaks converted to distance restraints using the method of Nilges *et al.* [384]. For signiferin 1, a total of 130 non-redundant distance restraints were produced, of which thirteen were ambiguous. Slightly more restraints were generated for riparin 1.1, with a total of 161 employed for structure calculations. A comparison of the distance restraints for signiferin 1 and riparin 1.1 resulting after eight iterations of ARIA structure calculations is given in Table 6.4. In addition, three dihedral angle restraints were incorporated into the structure calculations.

Table 6.4: Experimental distance restraints derived from the NOESY spectra of signiferin 1 and riparin 1.1.

	Number of Restraints	
	Signiferin 1	Riparin 1.1
Sequential NOEs	22	52
Medium-range NOEs	6	8
Long-range NOEs	6	3
Intra-residue NOEs	83	84
Ambiguous NOEs	13	14
Total	130	161

Sixty final structures were generated for each peptide by the ARIA RMD and SA protocol, of which the twenty with lowest potential energy were chosen for analysis. Figure 6.10 shows the twenty lowest energy structures of both signiferin 1 and riparin 1.1 superimposed over the well-defined backbone residues (residues 3-8 and 4-9 respectively)[†]. The structures overlay well throughout the regions enclosed by the disulfide bonds, with RMSD values for the backbone atoms of the well-defined residues being just $0.17 \pm 4.98 \times 10^{-2}$ and $0.10 \pm 4.18 \times 10^{-2}$ for signiferin 1 and riparin 1.1 respectively. However, the greater deviation of the backbone atoms at the N-termini indicates increased conformational flexibility in these areas. The majority of NOEs for both signiferin 1 and riparin 1.1 originate from well-defined residues, however, a number of medium- and long-range NOEs observed to the N-terminal residues suggest the differences seen in the resultant structures of each peptide are likely to be significant.
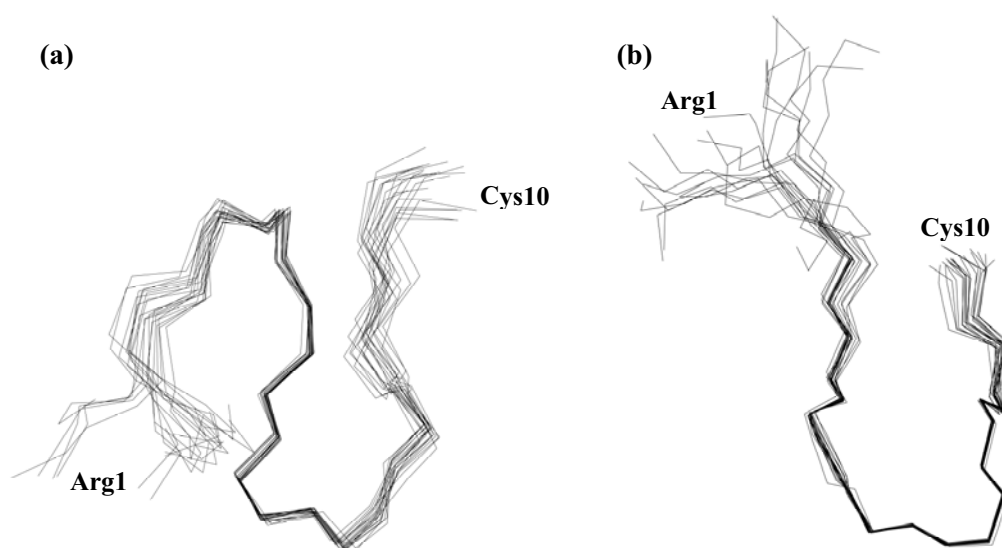
Figure 6.10: 20 most stable calculated structures of **(a)** signiferin 1, and **(b)** riparin 1.1 in TFE/H_2O (1:1 v/v), superimposed over the backbone atoms of well-defined residues.

[†] Despite both peptides having a free C-terminal carboxyl group, the pH difference between signiferin 1.1 (3.60) and riparin 1.1 (4.80) is not likely to contribute to the apparent structural differences, given the rigid conformational restraints imparted by the disulphide bridge at the C-termini.

The energy and structural statistics for both the signiferin 1 and riparin 1.1 ensembles are given in Table 6.5. Final structures demonstrate only minor deviation from idealised covalent geometry (≤ 0.05 Å for bonds, $\leq 5°$ for angles and impropers). For signiferin 1, three restraint violations in the order of 0.45 Å were observed, while just a single restraint violation of 0.38 Å was apparent for riparin 1.1. This suggests the resultant structures adequately satisfy the NMR derived data.

Table 6.5: Structural statistics of signiferin 1 and riparin 1.1 following RMD/SA calculations.

	Signiferin 1	Riparin 1.1
Energies (kcal.mol^{-1})		
E_{total}	18.74 ± 1.27	10.23 ± 0.44
E_{bond}	0.94 ± 0.15	0.29 ± 0.03
E_{angle}	6.43 ± 0.48	3.63 ± 0.18
$E_{improper}$	0.35 ± 0.18	0.15 ± 0.04
E_{VDW}	10.11 ± 0.90	6.13 ± 0.32
E_{NOE}	0.91 ± 0.85	0.02 ± 0.03
E_{cdih}	0.00 ± 0.01	0.00
Well-defined residues	3-8	4-9
RMSD from mean geometry (Å)		
Backbone atoms of well-defined residues	$0.17 \pm 4.98 \times 10^{-2}$	$0.10 \pm 4.18 \times 10^{-2}$
Heavy atoms of well-defined residues	0.55 ± 0.16	$0.43 \pm 4.80 \times 10^{-2}$
All backbone atoms	0.78 ± 0.32	0.86 ± 0.19
All heavy atoms	1.62 ± 0.64	2.02 ± 0.37

By analysis of the angular order parameters (S, ϕ and ψ) of the final twenty structures, it is evident that only the residues contained within the disulfide bond are well-defined (residues 3-8 for signiferin 1, and 4-9 for riparin 1.1). A Ramachandran plot of the average ϕ and ψ angles shows that all residues are distributed within the allowed regions for regular peptide structure (Figure 6.11), providing evidence for the quality of calculated structures. For signiferin 1, the dihedral angles tend to fall within the areas typical of α-helical structure, while for riparin 1.1 the dihedral angles are more consistent with those of a β-sheet.
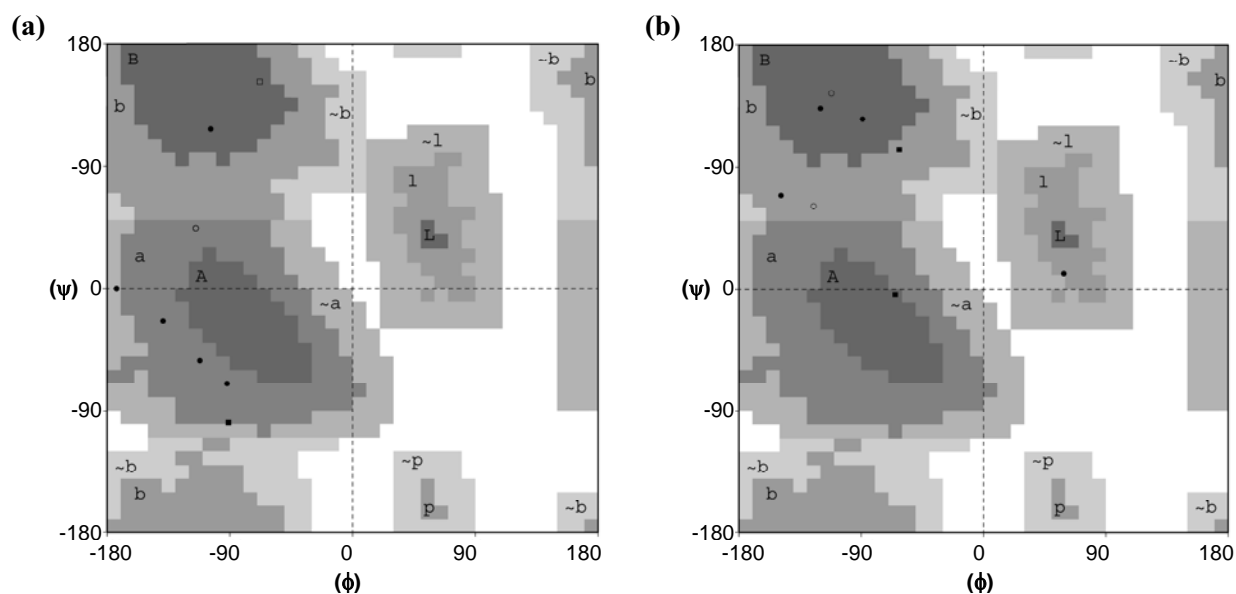
Figure 6.11: Ramachandran plot for **(a)** signiferin 1, and **(b)** riparin 1.1 in TFE/H$_2$O (1:1 v/v). Pro residues are indicated by □, remaining residues are indicated by ○, and well-defined residues are indicated by filled symbols.

The most energetically stable structures of signiferin 1 and riparin 1.1 are shown in Figure 6.12. In this representation it is evident that both peptides adopt a similar turn type structure involving residues 5-8, as a result of the structural constraints imparted by the disulfide bond. However, the N-terminal regions of each peptide adopt very distinct conformations. Signiferin 1 appears more globular in shape, with the N-terminal Arg directed back towards the turn. On the contrary, Arg1 of riparin 1.1 projects in an opposite direction from the turn structure, giving this peptide a more elongated form.
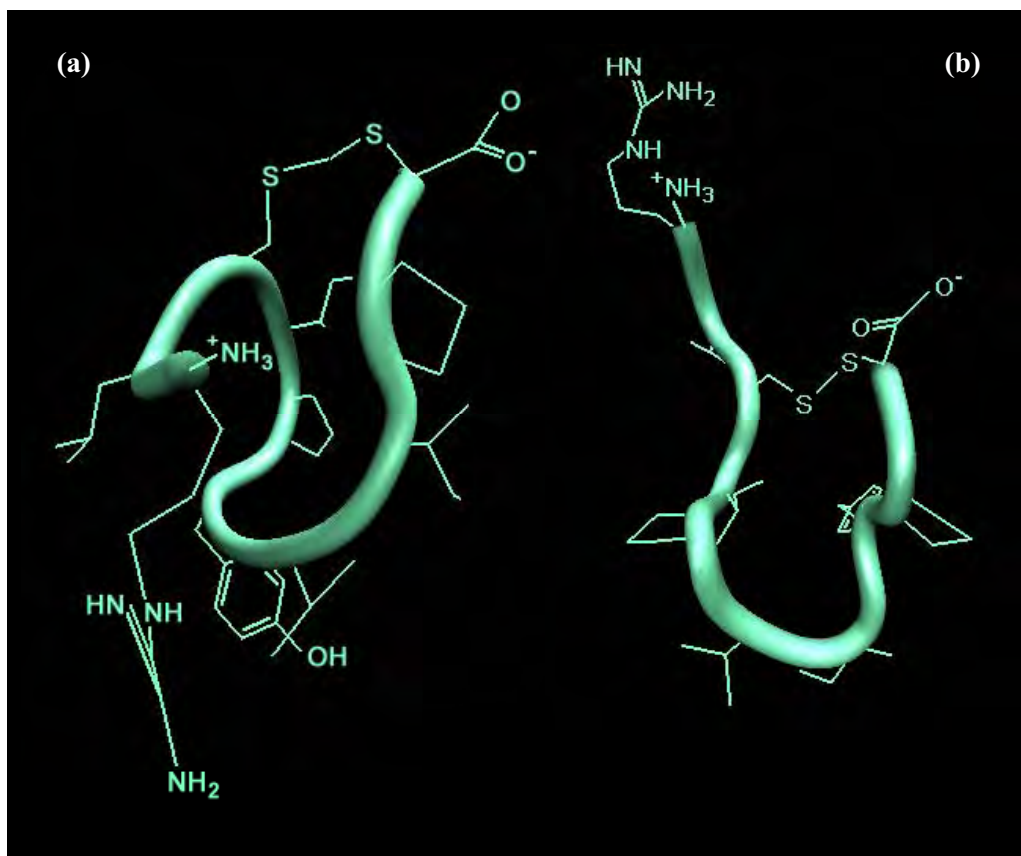
Figure 6.12: The lowest calculated potential energy structure of **(a)** signiferin 1, and **(b)** riparin 1.1 in TFE/H₂O (1:1 v/v).

6.3 Discussion

6.3.1 Structure Analysis

The NMR data and structure calculations presented here show that both signiferin 1 and riparin 1.1 adopt a turn-like, cyclic conformation in aqueous TFE as a result of the disulfide bridge. The generated structure ensembles are consistent and well-defined, suggesting they are likely to be high quality representations of the peptides in this medium.

Turn structures are particularly important in peptides and proteins since they allow for a polypeptide chain to fold into a compact globular structure, and furthermore usually occur on the exposed surface of proteins [539]. As a result such turns are often involved in molecular recognition processes, and provide useful information for defining template structures for the rational design of novel active compounds [540]. Tight turns are classified on the basis of how many residues are involved, and a β-turn involves four amino acids. Although the distance between the αC atoms bounding the turn is a key criterion common to all β-turns, the backbone dihedral angles in the inner residues will define the turn subtypes. The β-turns originally recognised by Venkatachalam [541] are stabilised by a hydrogen bond between the backbone atoms CO_i and NH_{i+3}. However, approximately 25% of β-turns are 'open' and in fact have no such intra-turn hydrogen bond at all [542]. Open turns do not lend themselves to classification by dihedral angles, therefore the definition widely accepted for β-turns is 'that which comprises four consecutive residues where the distance between $αC_i$ and $αC_{i+3}$ is less than 7 Å, and the tetrapeptide chain is not in a helical conformation' [382,539].

For both signiferin 1 and riparin 1.1, residues 5 to 8 constitute a β-turn, with the distances from $αC_i$ and $αC_{i+3}$ being less than 7 Å in both cases (Figure 6.13). The dihedral angles for residues 6 and 7 in these peptides were compared with the representative values reported in the literature for standard β-turn types [540]. On this basis both signiferin 1 and riparin 1.1 could not be further categorised as one of the nine standard β-turn subtypes, and hence belong to the class of open β-turns.
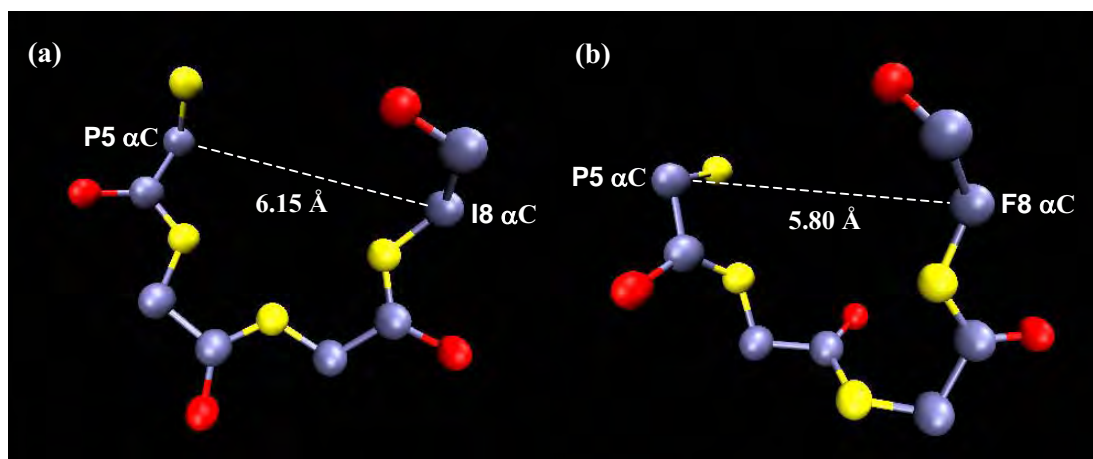
Figure 6.13: Partial backbone of **(a)** signiferin 1, and **(b)** riparin 1.1 illustrating the β-turn region. Oxygen atoms are shown in red, carbon atoms in blue, and nitrogen atoms are coloured yellow.

The most obvious difference between the secondary structures of signiferin 1 and riparin 1.1 is the relative conformation of the N-terminus. For signiferin 1, Arg1 is oriented directly towards the turn region, while for riparin 1.1 it is directed away. This difference is likely to have a significant impact on the activity of the two peptides.

6.3.2 Structure Activity Relationship

In spite of its intrinsic flexibility, CCK-8 was found by NMR to exist preferentially in a folded form in aqueous solution, with Asp1 and Gly4 in close proximity [543]. This led to the synthesis of cyclic peptides through amide bond formation between Asp1 or α-, β-Glu1 and Lys4 side chains, to give compounds with highly potent and selective CCK_2 agonist activity [544,545]. Thus the finding that the cyclic peptides signiferin 1 and riparin 1.1 are selective agonists of CCK_2 receptors is not without some precedent. Furthermore, CCK receptor ligands can act as full agonists, dual agonist/antagonists, or partial agonists depending upon the species, cell type or biological response under consideration [546]. Consequently, it is not entirely unexpected that signiferin 1 and riparin 1.1 are able to educe different biological responses despite both interacting with CCK_2 receptors.

The way in which an agonist activates a G-protein coupled receptor is difficult to elucidate, and at present is not entirely understood. The general simplified belief is that the resting state of the receptor is the most stable, and that binding of the agonist induces or stabilises an alternative state which is coupled to a G-protein [517]. Several authors have described CCK_2 receptor agonists apparently capable of discriminating two, or even three, different affinity states [510,547]. Each of these has a distinct affinity for the ligands, or depending on the molecular interaction of a ligand with its binding site, preferential or differential coupling with a specific G-protein [510]. This in turn accounts for the observed biological signal transduction and target cell function [513].

On the basis of site-directed mutagenesis studies, a number of important residues in the CCK_2 receptor binding site have been elucidated. Selected examples of these are depicted in the model shown in Figure 6.14. Arg57 was identified as important for CCK binding and selectivity [530], while a number of residues including His207, Asn358, Tyr189, Trp351 and Phe347 have been reported to directly interact with the critical C-terminal tetrapeptide of natural agonists such as CCK-8 and CCK-9 [528,531]. Fluorescence resonance energy transfer experiments have suggested that CCK analogues designed as either full or partial agonists most likely interact with the CCK receptor in a similar binding pocket [532], and therefore this model may also be appropriate for understanding the way in which agonists such as signiferin 1 and riparin 1.1 interact with the CCK_2 receptor.
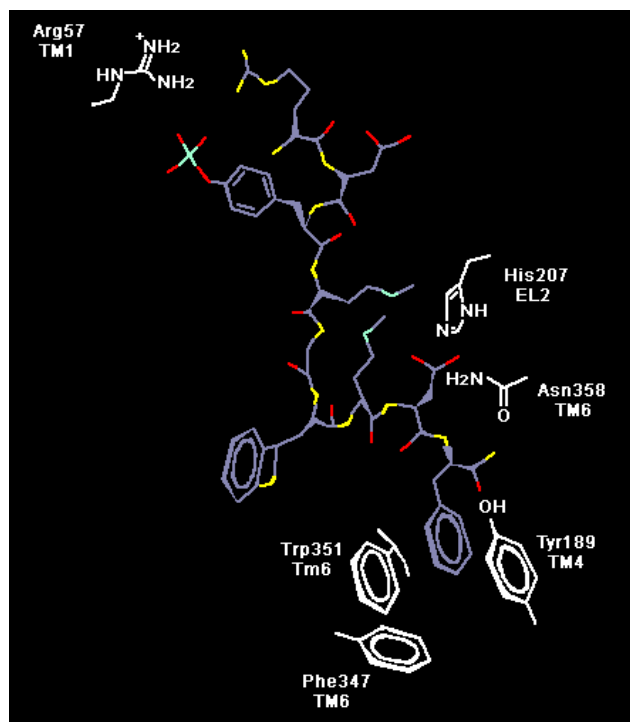
Figure 6.14: Two-dimensional representation of the CCK-9 binding site in the CCK2 receptor. Residues in the receptor (in white) reported to be in interaction with CCK-9 are indicated. Figure adapted from [528].

As can be seen from the model in Figure 6.14, Arg57 of the CCK$_2$ receptor interacts with hydrophilic groups at the N-terminus of the natural ligands, including Arg1 of CCK-9. However, the secondary structure determination of signiferin 1 and riparin 1.1 presented here demonstrates that Arg1 of each of these peptides is in a clearly distinct orientation. Thus, the N-terminal region of the peptides may differentially interact with Arg57 of the CCK$_2$ receptor, and potentially contribute to their varied biological activity. The importance of Arg1 is further supported by the fact that replacement of this residue with Gly in signiferin 1 gives a peptide which is no longer effectual in the smooth muscle contraction assay [509], indicating the N-terminal end of the peptide may be critical for receptor activation in this system.

In addition, a number of aromatic residues in the CCK_2 receptor, including Tyr189 Trp351 and Phe347, are known to be critical for binding and signal transduction. Signiferin 1 and riparin 1.1 differ only at two of their 10 residues, involving a change in position and type of aromatic residue. As can be seen in Figure 6.12, the aromatic residue of signiferin 1 (Tyr6) and of riparin 1.1 (Phe8) are located in different regions of the β-turn, and therefore project in an entirely different direction from the molecule. Thus the ability to establish π-π interactions with aromatic residues in the receptor may be altered, and could also possibly contribute to the differences in biological response observed for these peptides.

Clearly these explanations are only speculative, and more detailed analysis of the binding site and binding interactions specific for signiferin 1 and riparin 1.1 are necessary to fully probe the structure-activity relationship of such Cys-bridged peptides. Nevertheless, the dissimilarity in both primary and secondary structure may influence the way in which signiferin 1 and riparin 1.1 bind to and activate the CCK_2 receptor, providing a possible basis for the differences in observed bioactivity, and a template for the design of selective CCK_2 agonists.

6.4 Experimental Procedures

6.4.1 Sample Preparation

Peptide synthesis was carried out by Mimotopes (Clayton, Victoria) using L-amino acids and the standard N-α-Fmoc method [331]. Samples used for NMR studies were greater than 90% pure as determined by HPLC and ESI-MS. For signiferin 1, the peptide (22.4 mg, 18.9 μmol) was dissolved in a mixture of d_3-TFE and water (1:1 v/v, 0.7 mL), giving a final concentration of 26.8 mM. Similarly, riparin 1.1 (10.1 mg, 8.7 μmol) was dissolved in aqueous d_3-TFE (1:1 v/v, 0.7 mL) to give a final concentration of 12.4 mM. pH was recorded using a Eutech Cyberscan pH 500 Meter with an AEP 331 glass-body pH probe (183 x 4 mm, thin stem) and found to be 3.60 and 4.80 for signiferin 1 and riparin 1.1 respectively. pH was not corrected.

6.4.2 NMR Spectroscopy

A Varian Inova-600 NMR spectrometer was used for acquisition of all NMR spectra, with a ^{1}H frequency of 600 MHz and a ^{13}C frequency of 150 MHz. Experiments were carried out at 25 °C, and referenced to the methylene protons (3.918 ppm) or the ^{13}CH$_2$ signal (60.975 ppm) of residual unlabelled TFE. Presaturation allowed for suppression of the water signal in the TOCSY and NOESY experiments, and was achieved by centring the transmitter frequency on this resonance and applying low power presaturation from the proton transmitter during a 1 second relaxation delay between scans. Gradient methods for suppression were used in the COSY experiment [507].

TOCSY, DQF-COSY and NOESY experiments were collected in the phase sensitive mode. Typically, 16 time-averaged scans were acquired per increment with a total of 256 increments for each experiment. The FID consisted of either 2048 or 4096 data points in t$_2$, over a spectral width of 6123.2 Hz and 6499.8 Hz for signiferin 1 and riparin 1.1 respectively. NOESY spectra were acquired with a mixing time of either 150 or 250 ms, while the TOCSY pulse sequence included a 70 ms spin-lock.

1D ^{1}H NMR spectra were also acquired for both signiferin 1 and riparin 1.1, with 0.038 and 0.125 Hz per point digital resolution respectively, and allowed for direct investigation of ^{3}J$_{NH\alpha H}$ coupling constants.

Resultant spectra were processed using VNMR software (VNMRJ, version 1.1D). Data matrices were multiplied by a Gaussian function in both dimensions before zero-filling to 4096 data points prior to Fourier transformation.

6.4.3 Structure Calculations

Sparky software (version 3.111) was used to assign ^{1}H resonances in the NOESY spectra via a standard sequential assignment procedure [360]. For each symmetric pair of cross-peaks, the volume of the larger peak was converted to a distance restraint by the method of Nilges *et al.* [384]. ^{3}J$_{NH\alpha H}$ values were measured from the high-resolution 1D ^{1}H NMR spectrum for both signiferin 1 and riparin 1.1, and dihedral angles were restrained as follows: ^{3}J$_{NH\alpha H}$ < 5 Hz, ϕ = -60° ± 30°, 5 < ^{3}J$_{NH\alpha H}$ < 6 Hz, ϕ = -60° ± 40°, ^{3}J$_{NH\alpha H}$ > 8 Hz, ϕ = -120° ± 40°.

Structures were generated from random starting conformations using the standard RMD and SA protocol of ARIA (version 1.2) [391] implemented with CNS (version 1.1) [548], as described in Chapter 4. A single ARIA run consisted of eight iterations, and for riparin 1.1, default ARIA parameters were used. However, better convergence was achieved for signiferin 1 using optimised parameters based on those described by Pari *et al.* [549]. Assignment of distance restraints involving methylene and isopropyl group resonances was achieved using the floating chirality approach [401].

In the final iteration, 60 structures were calculated, from which the 20 with lowest potential energy were selected for analysis. 3D structures were viewed using VMD software (version 1.8.2) [550] and the program MOLMOL (version 2k.2) [551].

~ CHAPTER 7 ~

Methodology III – Solid State
Nuclear Magnetic Resonance Spectroscopy

7.1 Solid State NMR Spectroscopy

The difference between solution and solid state NMR spectroscopy lies not with the physical phase of the sample, but instead with the dynamic properties of the observed nuclei. Solution NMR deals with molecules that are rapidly moving in three dimensions such that there is no overall preferred orientation with respect to the applied magnetic field. Molecules which do not satisfy the requirements of such fast isotropic motion fall into the realms of the 'solid state'. The orientation, motion and degree of ordering in the sample affect solid phase interactions in a predictable fashion. Consequently, the resultant characteristic NMR behaviour provides a powerful probe for investigating the chemical and physical properties of molecules in the solid state [552].

In solution, the rapid tumbling of a molecule causes the overall orientation of its spins to become averaged, and therefore the angular dependent NMR parameters appear representative of an isotropic value. In the solid state however, molecular motions are significantly reduced and the nuclear interactions with the magnetic field are inherently anisotropic [268,346,552]. In particular, the chemical shift anisotropy (CSA), quadrupolar and dipolar interactions typically represent the most pronounced features of a solid state NMR spectrum, and are each reliant upon the position of the nucleus with respect to the applied field. The CSA and quadrupolar interactions can provide insight into electronic structure and bonding, while the dipolar coupling offers information regarding internuclear distances. In addition, all three anisotropic interactions are useful measures of molecular dynamics [553]. A detailed description of these anisotropic interactions important for solid state NMR spectroscopy is given in subsequent sections.

7.1.1 Chemical Shift Anisotropy

The concept of CSA is fundamental to solid state NMR and its applications, in particular for spins where $I = {}^1/_2$. This effect originates as the electron cloud around a nucleus generates a local magnetic field that acts to alter the apparent strength of the external field experienced by the nucleus. This in turn modifies the Larmor frequency of the spin, and hence a change in chemical shift is observed [203,268]. Since the electron density is not uniform about a nucleus, but is instead reliant on the bonding network of a molecule, the shielding effect is active to a different extent at various positions in space. Consequently, the CSA interaction depends on the orientation of the molecular segment with respect to the applied field [552,554].

The 3D nature of shielding can be characterised by a tensor consisting of three principal elements, σ_{11}, σ_{22} and σ_{33}. This in turn can be represented graphically by an ellipsoid in which the principle tensor elements correspond to the main axes (Figure 7.1). The observed chemical shift for a particular molecular orientation relates to the length of a vector parallel to $\mathbf{B_0}$, which starts at the centre of the ellipsoid and finishes at the outer edge [268,554]. Thus it is possible to determine the orientation of a molecule with respect to the field, provided the values of the three principal elements and the orientation of the chemical shift tensor with respect to the molecular frame are known.
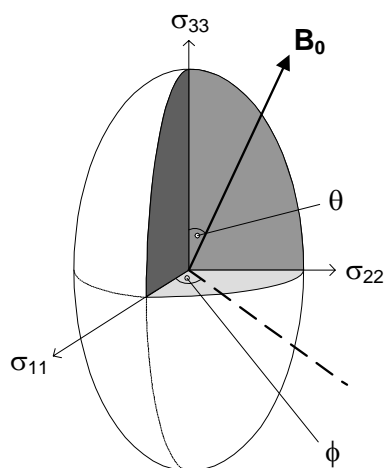
Figure 7.1: The chemical shift tensor represented by an ellipsoid is defined by the principal tensor elements σ_{11}, σ_{22} and σ_{33}. Different orientations of the tensor with respect to the applied field B_0, as defined by angles θ and ϕ, result in different chemical shift values for the nucleus. Figure adapted from [268].

For a single crystal, a sharp signal will be observed for every unique orientation of the nucleus within the applied magnetic field. However, for a powdered sample in which there is a wide dispersion of molecular orientations, peaks will be observed corresponding to all the possible resonance frequencies originating from different nuclei in each crystallite. This gives rise to a broad line with a distinctive shape, which is related to the principal elements of the shielding tensor as well as the orientational distribution of the micro-crystallites (Figure 7.2) [346,553].
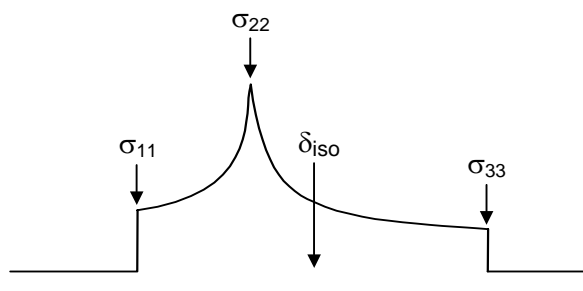
Figure 7.2: Theoretical powder pattern for a nucleus with asymmetric chemical shift anisotropy ($\sigma_{11} \neq \sigma_{22} \neq \sigma_{33}$).

Any nuclear motion that is faster than the frequency range under consideration will cause some degree of averaging of the CSA. In the isotropic case, the CSA is averaged to the isotropic value which is given by;

$$\delta_{iso} = {}^1/_3 \, (\sigma_{11} + \sigma_{22} + \sigma_{33})$$

This averaging effect allows the CSA to be a valuable source of information regarding the dynamics of the system under study [268,555].

7.1.2 Quadrupolar Interactions

Nuclei which have spin where $I > {}^1/_2$ have an asymmetric arrangement of nucleons, and hence a non-spherical positive charge distribution. This gives rise to a quadrupolar moment, which is an intrinsic property of the nucleus and provides a measure of the extent from which the nuclear charge distribution deviates from spherical symmetry

[346,556]. Each nucleus in a molecule will experience the effect of electrostatic field gradients, which exist throughout the molecular space as a result of the arrangement of surrounding charges. Although the net force on the nucleus is zero and there is no tendency for it to be displaced, for a nucleus with non-spherical charge distribution the electrostatic forces resulting from the field gradients will be experienced to a differing extent depending upon orientation. For example, in some orientations the extended reaches of the nuclear charge could be marginally closer to high potential fields, while in other orientations may be closer to regions of negative potential (Figure 7.3a). This forms the basis of the quadrupolar effect [556-558].

In the absence of quadrupolar interactions, application of an external magnetic field causes the nuclear spins to orient themselves in one of $(2I + 1)$ orientations, with a fixed energy difference between the orientational states. However, for a nucleus with non-spherical charge distribution, these energy levels are affected by the interaction of the quadrupolar moment of the nucleus and the electric field gradient. As a result, the transitions between adjacent energy levels are shifted by amounts proportional to the nuclear spin quantum number, and hence the different resonance frequencies cause the signal to appear as a multiplet with $2I$ components. This is demonstrated in Figure 7.3b for a nucleus with $I = 1$ [346,556].
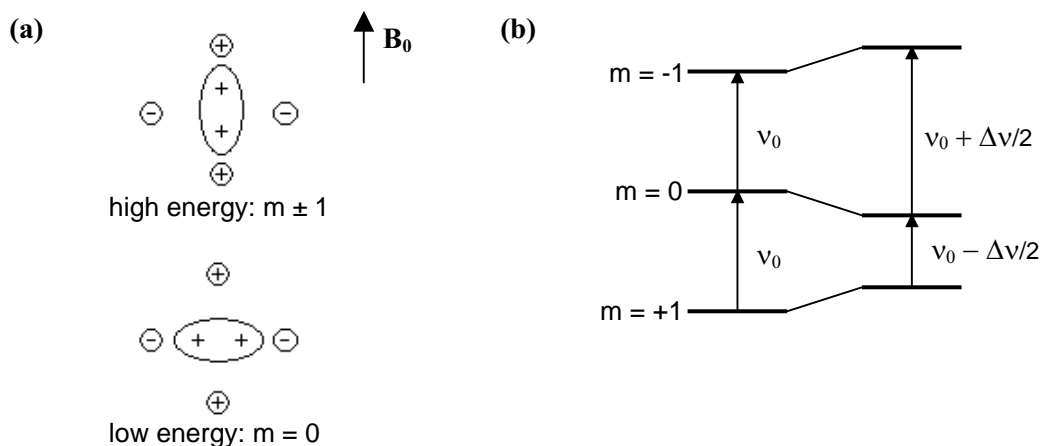
Figure 7.3: (a) Orientational interaction of a nucleus ($I = 1$) with the electric field gradient, and **(b)** the energy level diagram as a result of quadrupolar interactions. Figure adapted from [346].

In the case where the electric field gradients are axially symmetric, such as that for ^{2}H in a typical C-D bond, the magnitude of the quadrupolar splitting or the frequency difference between adjacent peaks is given by;

$$\Delta\nu = {}^3\!/_4\,(e^2qQ/h)(3\,\cos^2\theta - 1)$$

where (e^2qQ/h) is the quadrupolar coupling constant, and θ describes the angle between the principal axis of the nucleus and the applied magnetic field [268]. Since the quadrupolar splitting is dependent on orientation, motion of the nuclei leads to a partial averaging of the splitting and hence a reduction in $\Delta\nu$. For a single crystal with fixed orientation the signal consists of well resolved peaks, however for a powdered sample the range in orientations causes the signal to appear as the superimposition of powder patterns. For an I = 1 nucleus in an axially symmetric field gradient, this gives rise to a characteristic spectrum known as the Pake doublet (Figure 7.4), in which a pair of asymmetric powder line shapes are overlaid back-to-back [268,559].
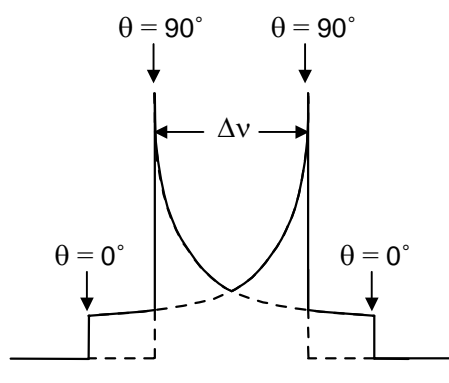
Figure 7.4: Theoretical powder pattern for a quadrupolar nucleus with spin I = 1. The solid line shows the overall pattern, while the dashed lines indicate the two contributing powder patterns. Resonance positions are indicated for the $\theta = 0°$ and 90° orientation of the principal axis with respect to **B$_0$**.

Quadrupolar interactions are field independent, and are of such magnitude that for most nuclei they are the dominant interactions in the spectrum [552]. Although often acting to complicate the interpretation of NMR spectra, quadrupolar interactions are a potentially valuable source of structural information, as they reflect the local symmetry of the studied nucleus and are again sensitive to molecular motions [556].

7.1.3 Dipolar Interactions

Nuclear spins exhibit a dipole moment, which results in a local magnetic field that can influence the effective magnetic environment of other nearby nuclei. The energy levels of each spin are slightly altered depending on the orientation of the coupled spin, and for a pair of unlike nuclei where $I = {}^1/_2$, dipolar coupling perturbs the energy levels as depicted in Figure 7.5 [558,560]. This gives rise to a splitting of the resonance lines according to the dipolar coupling constant D in a similar manner to that described previously for quadrupolar nuclei, whereby the signal for a single crystal will appear as a multiplet, and a characteristic Pake powder pattern is observed for unoriented powder samples [559].
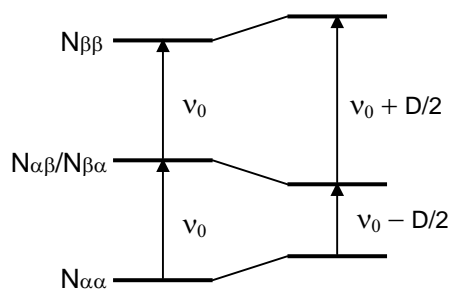
Figure 7.5: Energy levels for a pair of unlike spin $I = {}^1/_2$ nuclei perturbed by dipolar coupling. Figure adapted from [558].

The dipolar coupling is a direct, through space interaction that is dependent upon the gyromagnetic ratios (γ) of each nucleus, as well as the internuclear distance (r) and the orientation of the vector connecting the two spins with respect to the applied field. The maximum dipolar coupling is given by the dipolar coupling constant as follows;

$$D = \frac{h\mu_0 \gamma_i \, \gamma_j}{2\pi^2 r^3}$$

where h is Planck's constant and μ_0 is the permeability of a vacuum [268,558]. In most organic molecules the dipolar couplings are typically the strongest interactions of spin $I = {}^1/_2$ nuclei, and can occur as homonuclear coupling among the abundant ^{1}H spins, heteronuclear coupling between the dilute and nearby ^{1}H spins, and finally between

nuclei of different molecules [560,561]. Since the splitting depends very strongly upon the distance between the nuclei, in principle it is possible to measure the internuclear distances with relatively high accuracy [268,562].

In high-resolution NMR spectroscopy, dipolar coupling can cause severe unwanted broadening of signals. In order to overcome this, the dipolar interactions can be removed by a process known as decoupling. This involves application of a powerful, gated RF field composed of all the frequencies in the ^{1}H region, and causes the transitions between orientational states to be rapid compared with the frequency of the dipole interaction. As a result, the average orientation of the ^{1}H magnetic moments tends to zero, and hence spin coupling does not occur [563,564].

Dipolar coupling does however provide a means for connecting abundant and dilute spins. Cross-polarisation techniques rely upon this mechanism in order to transfer the large and rapidly acquired magnetisation of the protons to nuclei of low gyromagnetic ratio (typically ^{13}C or ^{15}N) by matching the applied $\mathbf{B_1}$ RF fields such that $\gamma_i\mathbf{B}_{1i} = \gamma_j\mathbf{B}_{1j}$ [357,358,563]. This not only affords a dramatic increase in sensitivity, but also allows faster recycle times determined by the generally short spin-lattice relaxation time of protons rather than the long relaxation of the dilute spin [560,561].

7.2 Magic Angle Spinning

The dipolar, chemical shielding and first order quadrupolar interactions all have essentially the same angular dependence, which can be expressed in the form;

$$\nu \propto {}^1\!/_2\,(3\cos^2\theta - 1)$$

where ν is the orientationally dependent frequency component and θ denotes the angle between the axis of rotation and applied magnetic field, $\mathbf{B_0}$ [553,558]. In solution, the isotropic molecular motion modulates θ on a time scale that is short in comparison with the NMR measurement. As a result, these θ-dependent terms are integrated over all possible orientations, accounting for the observation of narrow peaks with a chemical shift corresponding to δ_{iso}. In the solid state however, when the condition is met such

that $(3 \cos^2 \theta - 1) = 0$, i.e. $\theta = 54.7°$ or the so-called 'magic angle', these directionally dependent terms are again averaged. In the practical case this means spinning the sample at an angle of 54.7° with respect to $\mathbf{B_0}$, effectively introducing artificial motion to a solid state system. This forms the basis of the magic angle spinning (MAS) technique [565,566].

The rate of MAS must be greater than or equal to the frequency range spanned by the relevant tensor in order to accomplish effective averaging. The necessary spinning rates are often achievable, particularly for CSA and dipolar interactions, and in practice are in the order of 10,000 to 25,000 revolutions per second [346,567]. If the sample is spun at a rate less than the magnitude of the anisotropic interaction, a series of spinning sidebands becomes visible, which are separated by the rate of spinning (in Hz). The sideband envelopes mimic the shape of the powder patterns, and hence retain some information regarding the chemical shift anisotropy [568].

The quadrupolar interaction, unlike all other anisotropic NMR effects, can be written as the sum of first and second order interactions. The second order term is no longer a second-rank tensor and hence is not averaged to zero by MAS [556]. This complicates the spectra of quadrupolar nuclei under MAS conditions.

7.3 Biological Membranes

Biological membranes play a vital role in almost all cellular phenomena and are fundamental to the organization of the cell. In eukaryotic organisms, membranes act as a boundary for the cell and enclose most organelles [569,570], while prokaryotic cells possess complex multiple outer membrane systems as well as numerous intracellular invaginations [9,571]. In addition to maintaining cell structure and compartmentalisation, membranes act to modulate communication and molecular exchange within the cell and between the cytoplasm and cell exterior [572-574], and provide an environment suitable for non-aqueous processes to occur [575]. The study of biological membrane structure and function therefore contributes significantly to understanding basic cellular processes.

Biological membranes consist primarily of lipids and proteins, in addition to a small carbohydrate component [9,10,569]. The lipids are amphipathic molecules, constructed from a polar head group connected to two hydrophobic acyl chains which can vary in length, saturation and stereochemistry. Glycerophospholipids are a common constituent of cellular membranes and possess a glycerol backbone in which the C1 and C2 hydroxyl groups are esterified to fatty acids, and the C3 hydroxyl is bonded to a phosphate moiety [569]. The molecular axis which runs along the lipid length is known as the director axis. Early x-ray diffraction studies demonstrated that the lipids in cellular membranes are arranged predominantly in bilayer systems, in which the acyl chains are directed toward the middle and the head groups face the aqueous surroundings [576,577]. Combined with further spectroscopic and thermodynamic investigations, the fluid mosaic model was proposed [578], which encompasses both the transmembrane arrangement of proteins embedded throughout the lipid bilayer as well as the movement of lipids and proteins alike.

In aqueous environments, lipids will spontaneously assemble according to the distribution of hydrophobic and hydrophilic regions into large supramolecular aggregates, with the lamellar phase similar to that of biological membrane bilayers being the most dominant [575,579]. The interactions between the bilayers gives rise to a thermodynamically stable superstructure, with many of the physical properties of natural membranes [580]. Although the protein component of biomembranes can

compose up to 75% of the dry membrane weight [581], it is essentially the lipids which are responsible for maintaining structure. Hence it is justified to use artificial bilayers as adequate models for the biological membrane, particularly for pure lipid-protein interactions. A schematic diagram of a lipid bilayer is given in Figure 7.6, along with the chemical structure of 1,2-dimyristoylphosphatidylcholine (DMPC), which readily forms aqueous bilayer dispersions [575].

(a)

(b)
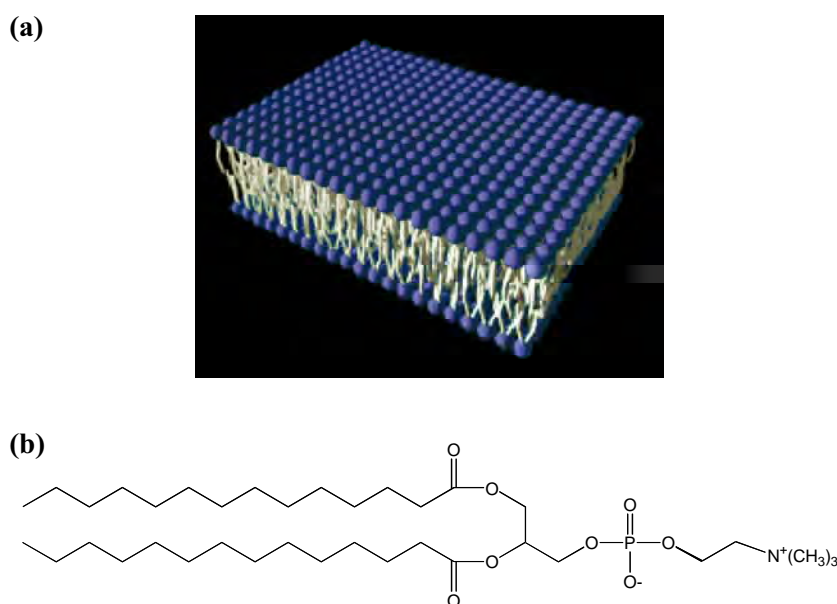
Figure 7.6: (a) Schematic diagram of a lipid bilayer. Hydrophilic head groups are shown in blue and hydrophobic tails are shown in white. **(b)** The structure of the bilayer-forming lipid DMPC.

The difficulties associated with preparing suitable membrane samples for diffraction studies has led to much interest in the application of solid state NMR spectroscopy to the investigation of lipid systems [582]. Solid state NMR can give a dynamic picture of the membrane lipids [552], in contrast to the static view from X-ray crystallography or electron microscopy. In addition, it does not require the use of additional probes which can perturb the natural lipid state [583], such as is required for fluorescence and electron spin resonance studies. Aqueous dispersions have been extensively used as membrane models for NMR studies, and a range of nuclei can be employed with NMR spectroscopy to yield information about the structure and function of membranes and their interaction with proteins and peptides.

7.4 Phosphorus NMR Spectroscopy

Due to the large abundance of phosphorus in biological lipid membranes, and the 100% natural abundance of ^{31}P [203], solid state NMR is a useful tool for the investigation of the conformation and dynamics of lipid head groups in membrane systems.

The ^{31}P NMR spectrum of a dry phospholipid powder gives a spectrum with a CSA in the order of -190 ppm and a characteristic line shape (Figure 7.7a) [555,584]. Upon hydration, the phospholipids can form bilayer dispersions in which the molecules rotate more rapidly about their director axis. This causes an averaging of the principle tensor elements σ_{22} and σ_{33} which are approximately perpendicular to the director axis, to give the new element $\sigma_{\perp}$ which denotes the chemical shift when the unique axis is perpendicular to the applied field. Similarly, there is also limited but rapid movement of the director axis (σ_{11}) over a conical path. σ_{11} is now designated as $\sigma_{\parallel}$ which specifies the chemical shift when the applied field is parallel to the unique axis, and the partial averaging of the $\sigma_{\parallel}$ element further contributes to a reduction in CSA to approximately -50 ppm (Figure 7.7b) [584-586]. The phosphorus CSA in a lipid bilayer, $\Delta\sigma$, is now defined as the difference between the effective tensor elements $\sigma_{\parallel}$ and $\sigma_{\perp}$, and can be estimated by direct measurement of the principal values of the chemical shift tensor from the spectrum [555].
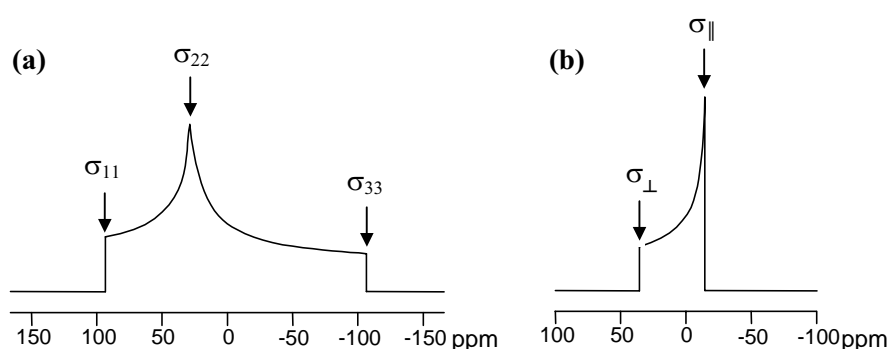
Figure 7.7: Characteristic ^{31}P spectra for (a) dry phospholipid powder, and (b) hydrated phospholipid bilayers [555].

The amount by which the CSA is reduced is related to the amplitude of the motion about the director axis, and hence $\Delta\sigma$ can be considered an approximate measure of the degree of order of the phosphate group, or the amplitude of angular excursion during motional averaging [555]. Changes in the amplitude of this motion, for example due to a peptide interacting with the surface of the lipid bilayer, will result in further alterations of the CSA. Both the line width and line shape of a ^{31}P spectrum have been shown to be qualitatively sensitive to changes in fluidity and the presence of perturbants in the phospholipid environment [587].

Although the lamellar phase is by far the most dominant form for phospholipids and is fundamental to biological membranes, depending on external conditions such as hydration, temperature and the presence of proteins or metal ions, lipids can form aggregates with quite different long-range structure [579,588]. ^{31}P NMR spectroscopy is susceptible to such lipid polymorphism, however is not definitive since the same line shape can arise from more than one type of phase or head group conformation. Nevertheless, three different spectra can be distinguished. For example, altered motion and orientation of lipids in the hexagonal phase results in distinctive ^{31}P spectra, while micelles, vesicles and the cubic phase all give rise to a single isotropic peak (Figure 7.8) [555,579,587].
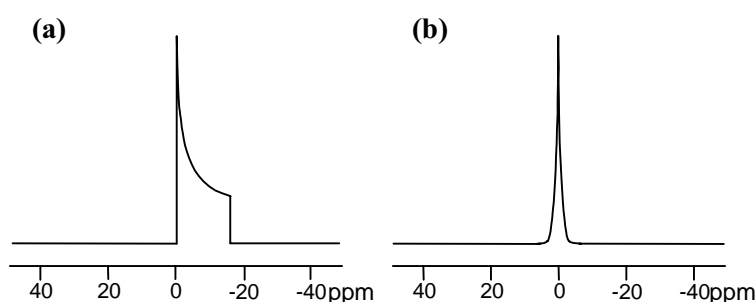
Figure 7.8: Characteristic ^{31}P NMR spectra of (a) inverted hexagonal (H$_{II}$) phase, and (b) isotropic phases.

Proton-phosphorus dipole-dipole interactions can affect the appearance of a ^{31}P spectrum. Because dipolar couplings are generally larger than the CSA, it is necessary to remove the broadening caused by the dipolar interactions in order to observe the

underlying line shape due to the chemical shift interaction [589]. This is generally achieved by applying a proton decoupling field during the acquisition period as described in Section 7.1.3.

7.5 Deuterium NMR Spectroscopy

Deuterium can be incorporated by chemical or biochemical synthetic techniques into specific sites of phospholipid molecules, including the phosphate head group, glycerol backbone and acyl side chains [590,591]. Replacement of a proton with deuterium is not likely to perturb the arrangement of the molecule in a membrane [592], and since the natural isotopic abundance of ^{2}H is just 0.015% [203] the NMR signal can be directly assigned to the labelled site. In this way, all regions of the lipid molecule are accessible to study by ^{2}H solid state NMR spectroscopy.

Deuterium nuclei have spin I = 1 and hence possess a quadrupolar moment. Although the ^{2}H quadrupolar coupling constant is relatively small compared with other quadrupolar nuclei (approximately 167 kHz) [557], it is still by far the dominant anisotropic interaction observed in the NMR spectrum. As a result, a doublet signal is present for each type of deuterium nucleus in the sample and for every orientation of the ^{2}H nuclei, giving rise to a Pake powder pattern. For an unoriented bilayer dispersion in which the lipid acyl chains are perdeuterated, the resulting ^{2}H spectrum is the superimposition of the powder patterns for each type of deuteron present (Figure 7.9) [557,593].
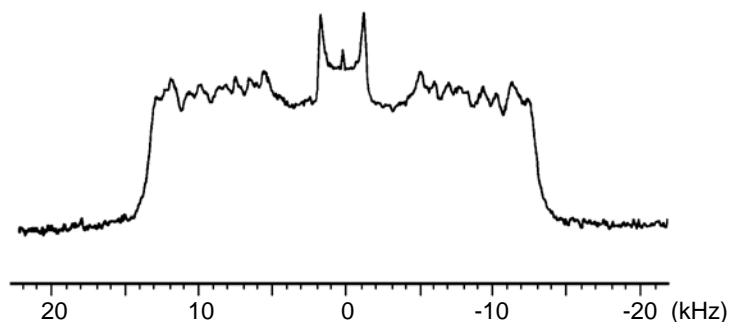
Figure 7.9: Typical ^{2}H spectrum of an unoriented lipid bilayer dispersion (d_{54}-DMPC). Figure from [594].

Interpretation of the ^{2}H NMR spectrum of perdeuterated lipids often constitutes a challenge due to the complex line shapes observed. Numerical deconvolution provides a non-invasive method to enhance spectral resolution while retaining details of the orientational dependence. A particularly useful approach is the 'dePakeing' technique which calculates an aligned spectrum from a powder pattern [595,596]. The resulting improvement in resolution therefore facilitates spectral analysis.

The mobility of a carbon-deuterium bond can be related to an order parameter S_{CD}, given by the equations;

$$S_{CD} = \frac{1}{2} < 3 \cos^2 \theta - 1 > \qquad \text{and}$$

$$\Delta v = \frac{3}{4} (e^2qQ/h) \, S_{CD}$$

where θ is the angle between the direction of the chain segment and the bilayer normal, and the angled brackets indicate a time-average of the function [552,557,583]. It is therefore evident that increased motional freedom, or decreased order of the acyl chains, gives rise to a partial averaging of the quadrupolar splitting, while reduced motion (increased order) will increase splittings. It is possible to calculate S_{CD} since the quadrupolar coupling constant is known to be approximately 170 kHz in a paraffin chain [597], and the quadrupolar splitting can be measured directly from the ^{2}H NMR spectrum.

Upon hydration of lipid bilayers the acyl side chain motion is increased, and as a result the Pake doublets show reduced quadrupolar splitting compared with a dry sample [598]. In addition, the ends of the hydrated lipid chains are extremely mobile and disordered. Consequently, the orientational order varies in a characteristic manner along the acyl chains. The methylene groups closest to the lipid water interface have the largest quadrupolar splitting, which then decreases rapidly towards the terminal methyl groups, which show the smallest value of Δv in the spectrum [590,592,599]. Although it is difficult to accurately assign the ^{2}H spectrum of a perdeuterated lipid dispersion due to signal overlap, the situation can be simplified by assuming the order parameters increase monotonically along the chain from the free end to the position nearest the head groups [592,593].

Order parameters can also be used to give an indication of the effect of peptide addition on lipid side chains. Typically, peptides which insert into membranes parallel to the bilayer surface cause a decrease in acyl chain ordering [600,601], while peptides which insert perpendicular to the membrane normal increase the order of the acyl chains [602,603]. The S_{CD} order parameters are often plotted against acyl-chain carbon position to give a visual representation of these changes, and a quantitative measure can be obtained by calculating the percentage change in comparison with control bilayers.

Finally, ^{2}H spectra can also give an indication of the phase-state of the lipids. For example, the acyl chains are packed less regularly in the hexagonal phase compared with bilayers, and hence have greater conformational freedom. As a result, the quadrupolar splitting of deuterated lipids in this phase is reduced by approximately half [579,588]. In addition, the constant order in the methylene groups near the interface which is characteristic of a bilayer phase is lost upon conversion to a hexagonal phase, where more regular variation of order parameters are seen along the chain length [599].

Practical problems arise from ^{2}H NMR experiments due to the large spectral width of the signals, since hardware limitations prevent the application of a uniform pulse over such a range of frequencies [555]. In addition, the probes used in high-resolution NMR spectrometers can take a relatively long time to ring-down (approximately several μs). Since the transverse relaxation time of deuterium nuclei is quite short, remains of the RF pulse may be detected during acquisition, causing signal distortion [555,557]. This is generally overcome using a quadrupole echo pulse sequence [604,605]. This is analogous to the spin echo pulse sequence described in Section 7.7.2, however it is difficult to describe what is occurring in this case with a vector representation since all three spin states of the I = 1 nucleus must be considered.

7.6 Nitrogen NMR Spectroscopy

Model membrane systems have been used on numerous occasions to study the interaction of small peptides with lipid surfaces [606-610]. Typically these peptides are α-helical, and it is of interest to know the orientation of the helical axis with respect to the bilayer in order to understand the mechanism by which the peptides exert their effects. The orientation of a peptide within a magnetic field can be determined, provided the alignment of the chemical shift tensor of the nucleus is known relative to the molecular frame [554]. Hence both the position of the nuclei within the molecule and the conformation of the peptide must be stable on the NMR time scale. Peptide backbone atoms satisfy these requirements and are labelled with ^{15}N in order to be susceptible to NMR spectroscopy.

The principal elements of the amide ^{15}N chemical shift tensor have been investigated for a number of model peptides, and σ_{33} appears to make an angle in the order of 20° with the N-H bond [611,612]. Consequently, the orientation of the σ_{33} tensor element can be considered to be approximately equivalent to the orientation of the amide bond, and in turn the long axis of an α-helical peptide. The values of the principal elements in this tensor are approximately $\sigma_{11} = 64$ ppm, $\sigma_{22} = 77$ ppm and $\sigma_{33} = 217$ ppm [610,612], and vary by less than 20 ppm [613]. As a result, for a peptide aligned parallel to $\mathbf{B_0}$ the observed ^{15}N chemical shift will be around 200 ppm, while a chemical shift of around 80 ppm indicates σ_{33} and the peptide are oriented perpendicular to the field [586]. If the orientation of a lipid membrane is known with respect to the applied field, the direction in which the peptide sits within the lipid bilayer can be determined.

The major limitation of ^{15}N NMR spectroscopy arises due to the inherent insensitivity of ^{15}N nuclei [203,346]. Often a 1D ^{15}N NMR spectrum can require days in order to acquire the very large number of transients necessary for a suitable spectrum. This issue is typically addressed using cross-polarisation techniques (Section 7.1.3).

7.7 Relaxation Rates

Another important feature of the NMR phenomenon is nuclear spin relaxation, the details of which have been documented in a number of texts [203,268,345-347]. During an NMR experiment, the thermal equilibrium of a spin is perturbed by the application of RF radiation. When this perturbation ceases, the system will relax until equilibrium is re-established. Two fundamental processes contribute to this; relaxation in the direction of the applied field is characterised by the spin-lattice or longitudinal relaxation, while relaxation perpendicular to $\mathbf{B_0}$ is characterised by the spin-spin or transverse relaxation. These are quantitatively described by the relaxation time constants T_1 and T_2 respectively.

In contrast to electronic, vibrational and rotation excited states, nuclear relaxation is relatively slow, with relaxation times ranging from a few microseconds up to several hours depending on the system under study [347]. Relaxation times depend on the strength of the relaxation mechanisms, which are in turn intricately related to molecular motions. T_1 and T_2 can be described by the following relationships;

$$T_1 \propto \left[\frac{\tau c}{(1+\nu^2\tau c^2)} + \frac{4\tau c}{(1+4\nu^2\tau c^2)} \right] \quad \text{and}$$

$$T_2 \propto \left[3\tau c + \frac{5\tau c}{(1+\nu^2\tau c^2)} + \frac{2\tau c}{(1+4\nu^2\tau c^2)} \right]$$

where ν is the Larmor frequency and τ_c is the correlation time, which gives a measure of the rate of reorientation or positional changes of the molecule [345,346]. As a result, relaxation studies are a sensitive tool for investigating molecular dynamics.

7.7.1 Longitudinal Relaxation

A saturated spin system has greater energy than one at thermal equilibrium, and therefore T_1 relaxation is associated with a change in energy of the system. While there are only limited energy levels for each nucleus, the surroundings are capable of exchanging any amounts of energy with the spin system. Therefore, initial spin

populations are restored as the absorbed energy from the applied pulse is transferred from the spins to the molecular lattice, and is lost as vibrational or translational energy. Nuclear spins couple weakly with lattice energy levels since they do not interact directly with the mechanical or electrical forces present in the lattice. Instead, weak fluctuating magnetic fields are present as a result of phenomena such as dipolar and spin coupling, CSA, spin rotation and chemical exchange. Components that oscillate at the Larmor frequency are the most effective relaxation agents since they can induce spin state transitions.

The principles of T_1 measurements can be described by an inversion-recovery type experiment [268,345,346]. In this method, a 180° pulse is initially used to move the system away from the Boltzmann equilibrium without transferring magnetisation to the xy-plane, in order to avoid the effects of T_2 relaxation (Section 7.7.2). The system is then allowed to relax by means of a spin-lattice process, during the delay period τ. Throughout the relaxation process, the magnetisation in the longitudinal axis $\mathbf{M_z}$ will go from a value of $-M_0$ immediately after the pulse, through zero, and return to its equilibrium position. Finally, a 90° pulse converts the remaining magnetisation from the z-axis to the observable xy-plane for detection, and the intensity of the signal is proportional to $\mathbf{M_z}$ at the time τ (Figure 7.10).
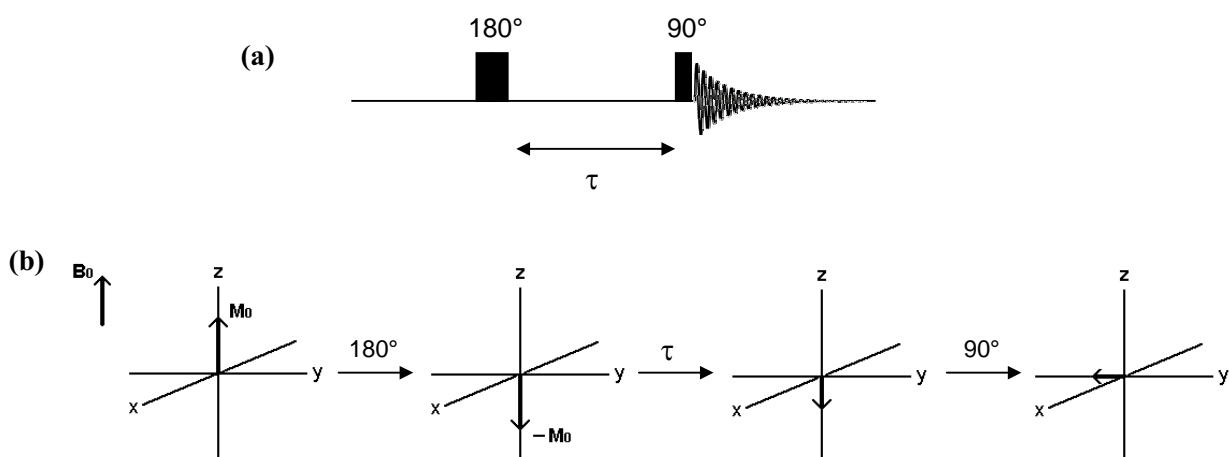
Figure 7.10: **(a)** The pulse sequence of a generalised inversion recovery experiment, and **(b)** the corresponding vector representation.

Quantitatively, T_1 can be calculated from the following equation;

$$M = M_0 \, (1 - 2e^{-\tau / T_1})$$

where $\mathbf{M_0}$ is the magnetisation at thermal equilibrium and $\mathbf{M}$ is the observed magnetisation [345,614]. By performing a number of experiments with a range of τ delays, the decay rate of $\mathbf{M_z}$ can be established.

7.7.2 Transverse Relaxation

Immediately after a 90° pulse, the z-component of the magnetisation vector is zero and there exists a transverse magnetisation, $\mathbf{M_y}$. The nuclear spins now precess about the z-axis in the xy-plane. The precessing spins gradually lose their phase coherence, either gradually since this precession is dependent upon the Larmor frequency of each spin which is different for magnetically inequivalent nuclei, or abruptly when they change spin state as in longitudinal relaxation. In addition, even the minute inhomogeneity of the applied magnetic field causes the magnetisation from nuclei in different areas of the sample to dephase. Over time $\mathbf{M_y}$ becomes smaller, and since this is the direction in which magnetisation is recorded, the induced signal decays also. This constitutes the transverse relaxation. T_1 is always greater than or equal to T_2 since it is not possible for the magnetisation to return to its equilibrium value in the z-axis until the transverse magnetisation has disappeared.

Measurement of the T_2 relaxation time can be achieved using a spin-echo type pulse sequence [604,605]. A 90° pulse is employed to tip the magnetisation into the xy-plane, which decays according to T_2 over the period τ. A subsequent 180° pulse is applied to invert the magnetisation, which then refocusses to reach an echo maximum during the second τ delay (Figure 7.11).

(a)

(b)
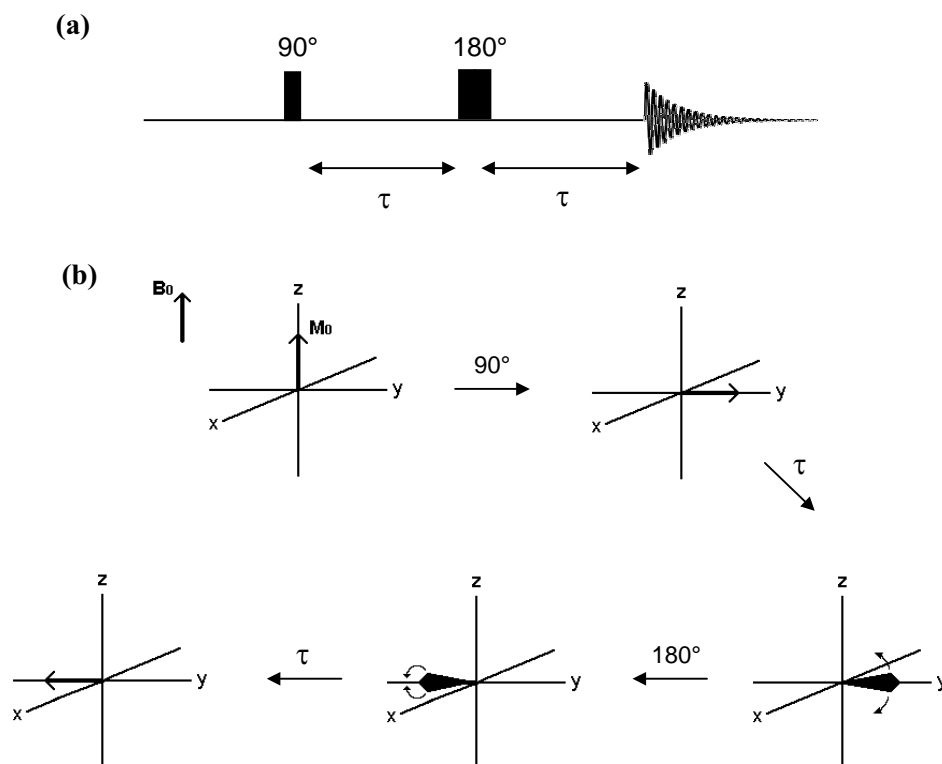
Figure 7.11: **(a)** The pulse sequence of a generalised spin-echo experiment, and **(b)** the corresponding vector representation.

In the absence of relaxation, the echo at time 2τ would have the same size as the initial signal after the 90° pulse. However, since the magnetisation is undergoing spin-spin relaxation in this time, the echo amplitude will decrease according to the equation;

$$M = M_0 \, e^{-\tau / T_2}$$

where **M_0** is the magnetisation at immediately after the initial 90º pulse and **M** is the observed magnetisation [345,614]. Thus, T_2 can be determined by the combination of a number of spin-echo experiments in which the value of τ is varied.

7.7.3 NMR Relaxation Measurements in Membranes

A number of dynamic processes occur in lipid bilayers which are amenable to study using solid state NMR spectroscopy. As discussed previously, the averaging ^{2}H quadrupolar interaction can detect molecular motions in the order of approximately 10-100 kHz, whereas the averaging ^{31}P CSA is effective for probing rates of 4-6 kHz (Sections 7.4 and 7.5 respectively). In addition to this, relaxation measurements are sensitive to molecular motion of the lipids on the nanosecond to millisecond time scale [615].

The longitudinal relaxation time can provide insight into the lipid molecular motions occurring on a time scale from a few nanoseconds to several microseconds. This includes rapid conformational changes of lipid acyl chains and polar head groups such as fast *trans*-gauche isomerisation of acyl chains (10^{-10}-10^{-9} seconds), as well as rotation about the long axis (10^{-9}-10^{-8} seconds) and lateral diffusion of the lipids (10^{-8}-10^{-7} seconds) [616-618]. The transverse relaxation time is effective for measuring slower, collective lipid motions in the bilayer, whose correlation times depend on membrane size and thickness but typically occur with time scales in the millisecond range [616,619-621]

A number of motional changes over a range of time scales can be induced in a lipid membrane upon interaction with a peptide or protein. NMR relaxation studies therefore provide a sensitive probe for studying the dynamics resulting from perturbation of the phospholipid bilayers by peptides [606,616,622].

~ CHAPTER 8 ~

Solid State NMR Studies of Membrane Active Antibacterial Peptides

8.1 Introduction

8.1.1 Antibacterial Peptides

Innate immunity forms a first line of defence against infection by the numerous pathogenic microorganisms which are continually seeking a susceptible host. Antimicrobial peptides are widely distributed throughout nature, and represent an ancient and pervasive component of this innate defence mechanism. They were initially identified in invertebrates [623], and later also in vertebrates including humans [624], and even exist in microbes themselves [625]. Several hundred antimicrobial peptides have been characterised to date, and their sequences are available along with a comprehensive list of reviews and publications [624].

Antibacterial peptides are an important form of defence against pathogens, especially for plants and invertebrates which lack developed and adaptive immune responses. However, even vertebrates with versatile immune systems have a need for antibacterial peptides. Often a series of different peptides are produced, each with a different spectrum of activity, to quickly and effectively counteract a broad range of invading microorganisms [626]. These molecules are rapidly synthesised at low metabolic cost, and require limited genetic information [309]. In addition, they are easily stored in large quantities and are readily available for immediate release upon infection [627].

Traditional therapeutics target the receptors and enzymes which are components of the bacterial biochemical machinery. Consequently, mutations which are induced over successive generations cause this machinery to become unrecognisable to the antibiotic, and hence these organisms acquire resistance to treatment [628]. Indeed, many strains of bacteria have emerged that are resistant to currently used antibiotics [629,630]. However, the large majority of antibacterial peptides appear to act via a specific, but not

receptor-mediated, permeabilisation of the target microbial membrane (Section 8.1.2). Since no mutatable proteins are involved, development of resistance is more difficult. Furthermore, the rate with which the peptides kill bacteria means there is less time for the adaptive process to occur [631]. This confers considerable potential for the development of antibacterial peptides as novel therapeutic agents.

Although the sequences of antimicrobial peptides are enormously diverse, they can be broadly classified based on their primary and secondary structure, and to date scientific interest has been directed principally toward three such classes [632]. The first group comprises Cys-containing peptides with at least one intramolecular disulfide bond. β-sheet structures generally predominate for these peptides [12], with examples including the tachyplesins from the horseshoe crab [633], and the human defensins [624].

Tachyplesin I   KWCFRVCYRGICYRRCR–NH$_2$

Defensin HNP-1   ACYCRIPACIAGERRYGTCIYQGRLWAFCC–OH
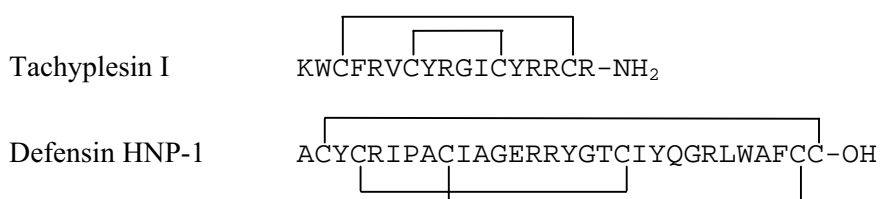
The second group contains peptides with an unusual bias in certain amino acids, typically Pro, Arg, Trp or His [632]. These molecules have an extended helical structure and include bovine indolicidin [634] and porcine PR-39 [635].

Indolicidin   ILPWKWPWWPWRR–NH$_2$

PR-39   RRRPRPPYLPRPRPPPFFPPRLPPRIPPGFPPRFPPRFP–NH$_2$
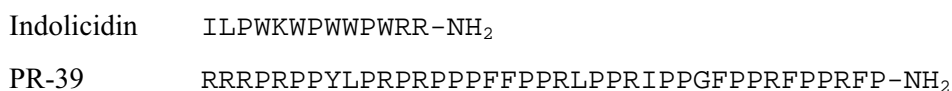
The final group consists of linear peptides, which are amongst the most abundant and widespread in nature [636]. The insect-derived cecropins [637] and the amphibian magainin peptides [638] are examples of this group. These peptides are typically small, cationic and adopt amphipathic α-helical structures, and are variably active against a wide range of pathogens including bacteria, fungi and protozoa. The following chapter is focused principally on peptides from this structural class.

Cecropin A   KWKLFKKIEKVGQNIRDGIIKAGPAVAVVGQATQIAK–NH$_2$

Magainin 1   GIGKFLHSAGKFGKAFVGEIMKS–OH
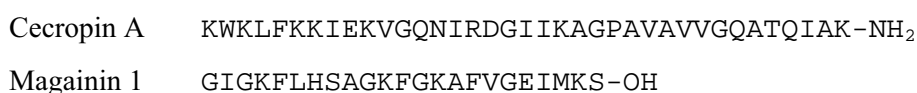
8.1.2 Mechanism of Action

Understanding the mechanism of membrane disruption by antibacterial peptides is fundamental for their future application as pharmaceuticals. Consequently, many studies have attempted to elucidate the mechanism by which such membrane active antimicrobial peptides kill their target microorganism. Although the details of membrane permeation are still not clear, it has been conclusively shown that peptide-lipid interactions rather than receptor-mediated recognition processes are major factors which influence the function of most linear antibacterial peptides (see [639], and references cited therein). Several models have been proposed in recent years to account for the available evidence, of which the 'barrel-stave' and 'carpet' mechanisms have been most widely applied.

In the barrel-stave model [640-642], peptides that are initially unstructured aggregate at the membrane surface, where they then adopt a defined secondary structure such as an amphipathic α-helix. Subsequent insertion into the lipid bilayer occurs via formation of a transmembrane barrel-like pore, in which the peptides are arranged perpendicular to the plane of the bilayer. Individual peptides are organised such that their hydrophobic surfaces face the core of the bilayer, and their hydrophilic surfaces line the central pore. Theoretically, as little as three peptide molecules could form these pores, however progressive recruitment of additional peptide monomers leads to an increase in pore size [643]. Indeed, functional studies have revealed that peptides such as pardaxin [644], alamethicin [645], and the helix α5 of δ-endotoxin [646] lyse both bacteria and erythrocytes by the barrel-stave mechanism.

Most antibacterial peptides are highly cationic along their lengths, and hence arranging such peptides into a barrel structure would result in considerable electrostatic repulsion. Furthermore, the pores would be expected to be anion-selective, which is not always the case [647]. These ideas led to the development of the toroidal model [648,649], whereby lipids are interspersed between the peptides of the pore, such that the negatively charged head groups are associated with the positive charges of the peptide side chains and the aqueous pore interior. As a consequence, the pores formed by this process are more capacious than those expected by the barrel-stave mechanism, and allow for the passage of larger molecules across the bilayer [648].

In addition, a minimum of 20 residues is required to span the membrane entirely if the peptide adopts an α-helical form. However, a modified version of the barrel-stave model has been proposed in which shorter peptides can dimerise end-on to effect complete penetration [650]. Gramicidin A has been shown to act in this manner [651].

Contact between the hydrophobic region of the membrane and the polar face of a single amphipathic α-helix is highly unfavourable. Therefore, a critical process in the barrel-stave mechanism involves the initial aggregation of the peptide monomers in their membrane bound state, which allows for the peptides to associate such that the polar side chains can be shielded from the hydrophobic lipid membrane core [652]. Thus, evidence of aggregation suggests the barrel-stave mechanism is acting [643].

In contrast, the carpet mechanism [642,643,653] was first proposed to describe the mode of action of dermaseptin S [33], and has since been used to rationalise the action of numerous antimicrobial peptides including the cecropins [637], LL-37 [654] and caerin 1.1 [312]. By this model, positively charged lytic peptides are electrostatically attracted to the surface of the negatively charged target membrane where they bind in a parallel orientation, and cover it in a carpet or detergent-like manner. In order for this to occur, the peptides must adopt an amphipathic structure in which the hydrophobic face is directed towards the lipid acyl chains, while the hydrophilic face maintains interactions with the lipid head groups. Above a critical concentration, strain on the bilayer curvature causes permeation of the membrane, and the membrane degrades into micelle-like complexes. An intermediate step may occur in this model prior to the collapse of the membrane whereby transient holes are formed, as described in the toroidal model for pore formation [652], or in the two-state model [655].

Self-aggregation is not necessary for the carpet mechanism, and the peptides are instead more likely to be interspersed between the lipid head groups due to electrostatic repulsion between the cationic side-chains. The presence of negatively charged lipids is important in this case, as they help to reduce the repulsive electrostatic forces between positively charged peptides [554]. Any peptide may act via the carpet mechanism provided the net charge is overall strongly positive, and a certain level of hydrophobicity and basicity is preserved [656].

On the whole, for the barrel-stave, toroidal and carpet mechanisms, disruption of normal membrane function ultimately leads to cell death. These models are represented pictorially in Figure 8.1. Nevertheless, none of the models described at present satisfy all of the available evidence for every antibacterial peptide, suggesting that a ubiquitous mechanism may not exist. Instead, it is likely that the predominance of a specific mechanism is determined by both the structural features of the peptide, and the influence of the target membrane on binding and permeabilisation [657].
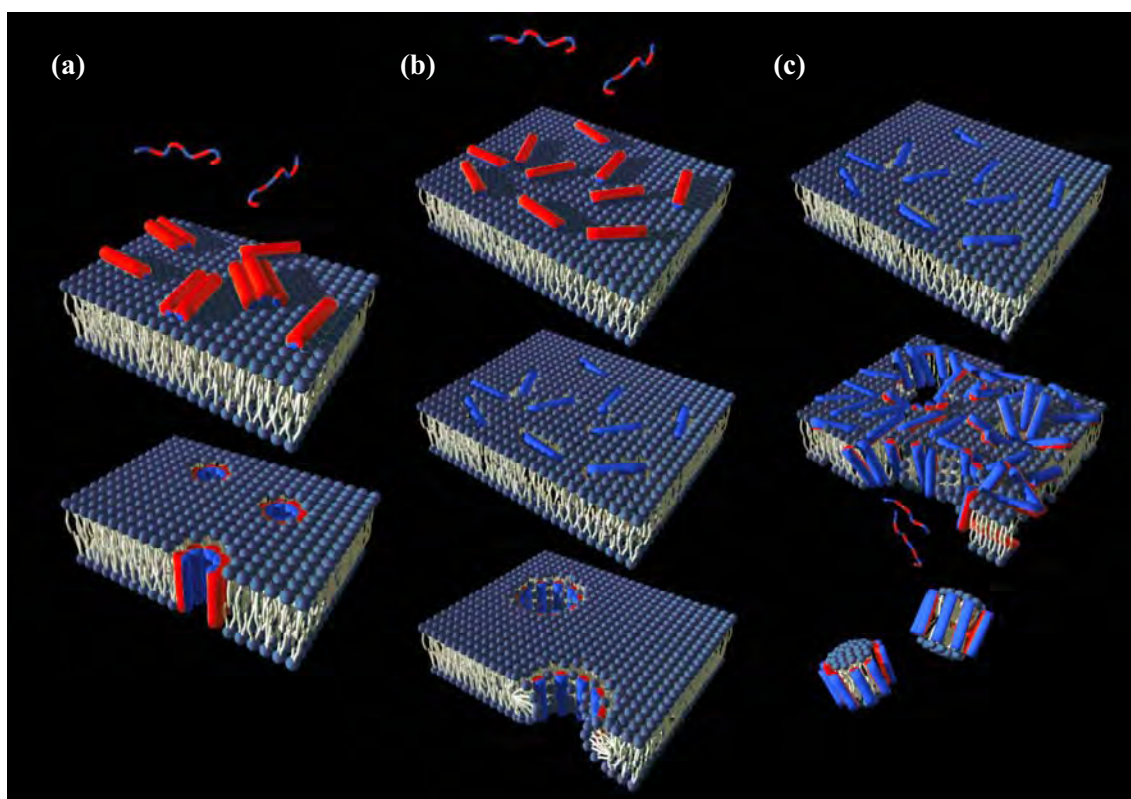
Figure 8.1: **(a)** Barrel-stave mechanism; peptides aggregate on the membrane surface as α-helices before inserting into the bilayer to form pores, **(b)** toroidal mechanism; peptides insert into the bilayer to form pores in which lipid molecules are interspersed between the peptides, and **(c)** carpet mechanism; peptides integrate into the membrane surface until a threshold concentration is reached and the membrane deteriorates. Peptides in helical form are represented by cylinders, with hydrophilic and hydrophobic regions of the peptides coloured blue and red respectively. Figure adapted from [658].

8.1.3 Target Membranes

Antibacterial peptides display varying degrees of specificity. For example, some exhibit broad-spectrum antibiotic activity against a range of microorganisms, while others are active against only a select few. In addition, some peptides are lethal to prokaryotic or tumourigenic cells at concentrations that are harmless to normal cells. A number of marked dissimilarities occur between bacterial and mammalian cells which may contribute to specificity, including differences in the cell surface, lipid composition and membrane potential. Peptides that are specific for bacterial cell membranes are candidates for therapeutic use as they would not damage host cells, and therefore factors controlling specificity are of particular interest.

The primary difference in cytoplasmic membranes between prokaryotic and eukaryotic cells is the composition and topological arrangement of lipids. The outer leaflets of mammalian cells are comprised entirely of neutral, zwitterionic phospholipids, primarily phosphatidylcholine and sphingomyelin [659,660]. In contrast, bacterial cytoplasmic membranes contain a large proportion of anionic phospholipids, including phosphatidylglycerol and cardiolipin [653,661]. Furthermore, bacteria have a cell wall that surrounds the cytoplasmic membrane which acts to provide additional strength and rigidity to the cell [9,662], and varies significantly for Gram-positive and Gram-negative bacteria.

The cell wall in Gram-positive bacteria is a single layer, consisting predominately of peptidoglycan and teichoic acids [663], the latter of which are phosphate-containing polysaccharides that further contribute to the negative charge at the surface of these microorganisms. However, the peptidoglycan layer only accounts for a small portion of the Gram-negative cell wall, which is also devoid of teichoic acids. Instead, Gram-negative bacteria possess an additional outer phospholipid membrane that sits on top of the thin peptidoglycan layer. Lipopolysaccharides take the place of phospholipids in the outer half of the outer membrane, and again are a factor in the anionic nature of Gram-negative bacteria [662,664]. A comparison of the cell walls for both Gram-positive and Gram-negative bacteria is given in Figure 8.2.

(a)

Peptidoglycan

Teichoic acids

Lipopolysaccharide

(b)

Outer
membrane

Protein

Peptidoglycan

Plasma
membrane

Plasma
membrane

Protein
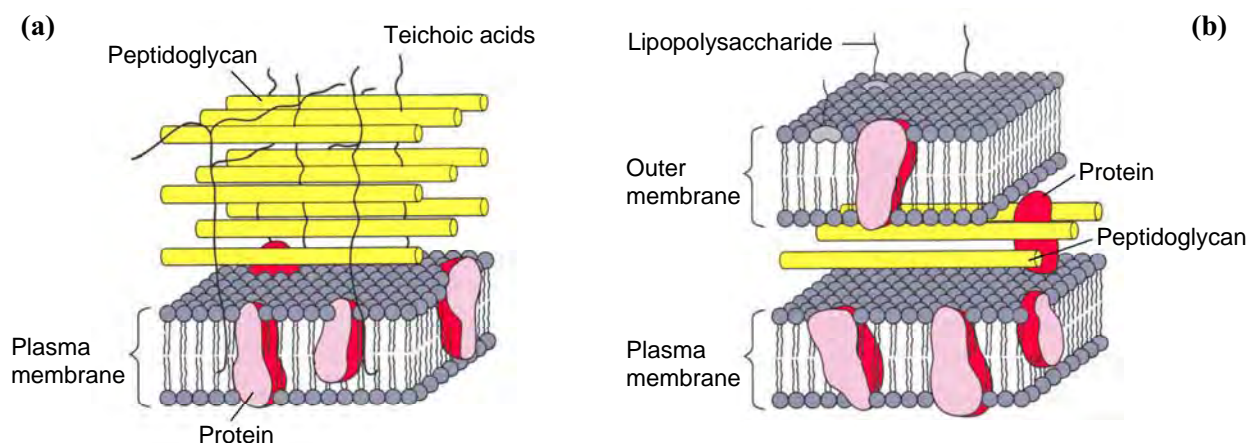
Figure 8.2: The external composition of **(a)** Gram-positive bacteria, and **(b)** Gram-negative bacteria. Figure adapted from [9].

Antibacterial peptides typically bind and permeate anionic lipid vesicles more readily than neutral vesicles [637,656,665,666]. In addition, Gram-positive bacteria with more anionic teichoic acids demonstrate increased susceptibility to lysis upon treatment with basic peptides [663]. Thus the relative insensitivity of eukaryotic cells to antimicrobial peptides is generally ascribed to differences in surface charge. A correlation also exists between the lysis of the inner membrane of Gram-negative bacterium and their acidic lipid content [667]. Increasing the ionic strength of the medium reduces the binding and bioactivity of the peptide, suggesting that electrostatic interactions are the basis for preference towards acidic membranes [668,669].

While many peptides are active against both Gram-positive and Gram-negative bacteria, some are selectively active against one or the other. This may be a consequence of how well the peptides interact with the respective bacterial cell walls. For example, the susceptibility of Gram-negative cells to antibacterial peptides has been associated with factors that facilitate the transport of peptides across the outer membrane, such as the charge, concentration and location of lipopolysaccharides in the outer membrane, as well as the general outer membrane molecular architecture [670-672].

In addition, divalent Mg^{2+} ions form cross-links between the lipopolysaccharides of Gram-negative bacteria, and act to neutralise the charges and stabilise the outer membrane [673]. Cationic antibacterial peptides are believed to compete for binding sites and displace these Mg^{2+} ions [674,675], breaking down the cross-links and disrupting the integrity of the outer membrane. This allows access to the cytoplasmic membrane, in a process known as 'self-promoted uptake' [675]. Conversely, a qualitative examination of specificity versus aggregation tendency suggests that peptides which self-aggregate on the cell surface are prevented from crossing the outer membrane, and in fact have their antibacterial activity hindered [637,676]. There is also evidence that the rate of permeabilisation of Gram-positive bacteria is slower than that of Gram-negative bacteria, indicating the peptidoglycan layer is a significant obstacle for activity towards Gram-positive cells [677].

Mammalian cell membranes contain high levels of sterols such as cholesterol, while those of bacteria contain none [659]. Cholesterol is known to influence membrane fluidity [678,679], and it has been suggested that the reorientation of peptides necessary for permeabilisation is somewhat prevented by higher levels of cholesterol, delaying cells lysis [680]. The formation of hydrogen bonds between glutamates and cholesterol has also been implicated in the reduction of antibiotic activity [680]. In addition, the membrane potentials of bacterial cells are on the order of -70 mV, while in mammalian cells these are negligible (approximately -9 mV) [681]. Membrane potentials are also known to facilitate pore formation, possibly by interacting with the helix dipole to force the peptide into a transmembrane alignment [554,641], and also affect the partitioning of polypeptides between aqueous and lipid phases [682], the peptide bilayer penetration depth, and peptide conformation [683]. Consequently, these factors may also contribute to prokaryote specificity for some membrane active peptides.

Certain antibacterial peptides are also lethal towards cancer cells [36,59,684], and are often active at concentrations that are harmless to normal cells [685]. This ability to differentiate between tumourigenic and normal cells may be due to a loss of lipid asymmetry, and therefore a more anionic character, in the outer leaflet of cancer cells [686]. In addition, selectivity may also be related to the larger negative membrane potential associated with many types of tumour cells [685,686].

8.1.4 Antibacterial Efficacy

The efficacy of α-helical antibacterial peptides is modulated to a certain degree by structural properties of the peptide itself, and can be used as a starting point for the rational design of antibacterial peptide therapeutics. Numerous studies have described the influence of factors such as helicity, hydrophobicity, amphipathicity, hydrophilic angle and charge state on the permeabilising effect and antibacterial activity of α-helical peptides [636,657,687]. Although the individual importance of each of these features is difficult to determine, as they are often inter-related, some general trends can be observed.

Early studies aimed towards enhancing antibacterial peptides were directed at increasing peptide helicity, and although these studies typically indicated that replacing helix destabilising residues with those that were helix promoting improved antibacterial efficacy, a quantitative correlation was rarely found [637,688,689]. This is most likely due to the fact that altering peptide helicity often involves amino acid substitutions that impact other structural features of the peptide [657,690,691]. However, D-amino acid substitutions locally disturb helix formation while retaining sequence, hydrophobicity and charge [657]. Using this method, a correlation between decreasing helicity and membrane disruption can be observed [692], which is significantly more pronounced for membranes with little or no negative charge [693]. Thus, while the antibacterial activity may decrease somewhat as helical structure is disrupted, haemolytic activity decreases by a greater amount since erythrocytes have neutral membranes. In fact, a non-helical peptide may retain antibacterial function but lose all haemolytic activity, provided it has a high net positive charge [694,695].

The relationship between helicity and antibacterial activity is further complicated by the class of α-helical peptides that form helix-bend-helix structures, such as caerin 1.1 [312], cecropin A [696], and melittin [697]. The flexible hinge is usually a result of Pro, or one or more Gly residues present in the sequence, which are known to disrupt helical structure [698]. Generally, the N-terminal helix of these peptides is amphipathic, while the C-terminal helix is hydrophobic [696,699,700], and the hinge allows the two helices to move independently. The importance of the hinge region has

been demonstrated repeatedly. For instance, replacing Pro residues in caerin 1.1 with Ala results in strikingly decreased activity relating to a reduction in central flexibility [314]. It is likely that the additional flexibility allows insertion of the hydrophobic C-terminal helix into the bilayer, while the more amphipathic N-terminus remains parallel to the surface of the membrane, thereby facilitating the transition to transmembrane helix bundles [650,701].

The hydrophobicity of an antibacterial peptide is typically described by the average of the numeric hydrophobicity values of all residues [702,703], and measures the degree of peptide affinity for hydrophobic phases such as the lipid acyl chains of membranes. In general, hydrophobicity appears to have little effect on peptide binding or efficiency of permeabilisation in negatively charged membranes [704]. However, an increase in hydrophobicity can be associated with an enhanced binding, and in turn improved membrane lytic activity, for zwitterionic bilayers [704]. Therefore, while antimicrobial activity is not significantly influenced by this parameter, cytotoxicity towards neutral mammalian cells is drastically enhanced [705-707]. Thus, selectivity for prokaryotes is reduced.

Amphipathicity is a measure of the spatial separation between hydrophilic and hydrophobic side chains within a peptide. A useful quantitative measure of this property is the hydrophobic moment (μ), often calculated as the mean vector sum of the hydrophobicities of each residue perpendicular to the axis of the helix, with large values of μ indicating a high degree of amphipathicity [708]. Amphipathicity is regarded in some cases as the most important structural determinant of antibacterial efficacy [687], and allows the peptide to insert into the lipid bilayer, keeping the hydrophilic face in contact with polar groups and water phases while the hydrophobic face can interact with lipid acyl side chains. Peptides incorporating varying degrees of amphipathicity have therefore been used to demonstrate a correlation between hydrophobic moment and antimicrobial activity [677,709,710]. This is reinforced by the finding that membrane binding is improved by increasing μ, while permeabilising efficiency is essentially unaffected [711]. The hydrophobic moment plays a more substantial role for neutral lipid membranes, confirming the predominant influence of hydrophobic peptide-lipid interactions. Consequently, an increase in antibacterial activity is often noted in parallel

with an increase in haemolytic activity [677,710,712], meaning that the specificity for bacterial membranes is reduced with increasing μ [711].

Plotting the sequence of an amphipathic, helical peptide on a Schiffer-Edmundson wheel allows the angle subtended by the hydrophilic face to be determined. This angle can be varied while keeping the mean hydrophobicity and hydrophobic moment approximately constant, and is thought to influence the location of the peptide in the membrane upon binding [657]. It has been suggested that peptides with a small hydrophilic angle typically associate to form transmembrane pores, while peptides with equivalent hydrophobic and hydrophilic faces tend to orient parallel to membrane surfaces [713]. Furthermore, the value of the hydrophilic angle differentially affects peptide-membrane affinity and membrane permeabilisation ability [714,715]. This is because the peptides are energetically better able to bind to the membrane surface when the hydrophilic angle is around 180°, however this large angle results in unfavourable electrostatic interactions that prevent the peptides from inserting into the bilayer [657]. In particular this serves to highlight the different structural requirements for binding and lytic activity. Moreover, both antimicrobial and haemolytic activity present a positive correlation with an increase of the hydrophilic angle, and a decrease in specificity is observed against bacteria compared to erythrocytes [714,716].

Most naturally occurring cell-lytic peptides are cationic due to an abundance of Lys or Arg [630]. This charge is particularly important for antibacterial efficacy since it allows for the recognition and enhanced binding of these peptides with the anionic bacterial cell membrane, and hence allows for improved prokaryotic selectivity [657,694]. Charge may also play a role in determining specificity between bacterial subtypes. For example, increasing the number of Lys residues in caerin 1.1 improves antibacterial activity against Gram-negative organisms, yet diminishes that against Gram-positive (unpublished data). However, increasing the net charge of the peptide will not improve activity if the charged residues are placed such that other structural features, including amphipathicity and helicity, are disrupted [657,717]. Furthermore, when the positive charge becomes too high, the membrane activity of the peptides may actually decrease, since strong electrostatic interactions anchor the peptide to the lipid head group region [657], or because the repulsion between the positively charged side chains impedes the

formation of pores [653]. A highly cationic peptide is more likely to orient parallel to the membrane surface, presumably because it is energetically unfavourable to contain the charged residues within the hydrophobic lipid environment [718].

In summary, peptides with a moderately high positive charge, a large hydrophobic moment and a small hydrophilic angle tend to have improved selectivity against bacteria, and a preference for a carpet-like mechanism of action. On the contrary, peptides with a relatively low positive charge, a small amphipathic moment, and high intrinsic hydrophobicity show increased activity towards both microbial and host membranes, and a predisposition to form barrel-stave-like pores [652]. Table 8.1 shows an overview of the qualitative effects that structural features can have on the activity of antibacterial peptides. However, because these factors are often mutually dependent, it is difficult to predict the antimicrobial activity, selectivity, and mode of action of any given peptide.

Table 8.1: Relationship between the structural features of a linear, α-helical antibacterial peptide, and characteristics of membrane activity.

| | **Increasing:** | | | | |
	Helicity	**H**[a]	**μ**[b]	**ϕ**[c]	**Charge (+)**
Binding	↑	↑[f]	↑	↑	↑
Permeabilising Efficiency[d]	↑[f]	≈	≈	↓	↓
Antibacterial Activity	↑	↑	↑	↑	↑
Hemolytic Activity	↑	↑	↑	↑	↓
Specificity[e]	↓	↓	↓	↓	↑

[a] Hydrophobicity (H), calculated from the Eisenberg consensus sequence [702].
[b] Hydrophobic moment (μ) per residue [703].
[c] Hydrophilic angle (ϕ). Increasing here means from 0° to 180°.
[d] The ability of an already bound peptide to then permeabilise the membrane.
[e] The ratio of antibacterial activity to haemolytic activity.
[f] For neutral lipids**.**

8.1.5 Antibacterial Peptides from Australian Amphibians

Since the bombinin antimicrobial peptides were first identified from the skin of *Bombina variegata* in 1969 [719], the skin of amphibians has been considered as a valuable source of antimicrobial peptides. This was further reinforced by the characterisation of magainins from the secretions of the African clawed frog *Xenopus laevis* [31], which initiated a serious screening of frog and toad skins for the isolation of new peptides exhibiting activity against bacteria, fungus, virus and tumour cells.

To date, more than eighty antibacterial peptides have been identified and fully characterised from the skin secretions of approximately twenty species of Australian frogs [28]. Antibacterial peptides isolated from the secretions of these animals do not contain Cys residues or have an excess of any particular amino acid [80], and often have no mammalian analogues. They are typically small, containing less than forty amino acids, and are cationic due to the presence of Lys and Arg residues. All peptides examined so far have been shown to form amphipathic α-helices, with many having a kinked region of greater flexibility in the middle of the structure [28,80].

Recently, the interaction of a series of antimicrobial peptides from different species of Australian tree frogs with zwitterionic phospholipid model membranes has been investigated using NMR and circular dichroism spectroscopy [608,720]. These peptides were namely aurein 1.2, citropin 1.1, caerin 1.1 and maculatin 1.1, the sequences of which are given below. Both aurein 1 and citropin 1 peptides adopt short, linear, amphipathic helices in membrane-like media, [59,65], while solution structures of selected caerin 1 and maculatin 1 peptides suggests these form two well-constructed α-helices along their length, which are separated by a short central hinge region initiated by Pro15 [313,721].

Aurein 1.2	`GLFDIIKKIAESF-NH`$_2$
Citropin 1.1	`GLFDVIKKVASVIGGL-NH`$_2$
Caerin 1.1	`GLLSVLGSVAKHVLPHVVPVIAEHL-NH`$_2$
Maculatin 1.1	`GLFGVLAKVAAHVVPAIAEHF-NH`$_2$

In previous studies, bicelles and DMPC multilayers were used as models for neutral erythrocyte membranes, and NMR and circular dichroism results suggest that the antimicrobial peptides partially inserted into the membranes with a tilted orientation, and in an α-helical conformation. The effects on the model membrane systems indicated limited interaction with the phospholipid head groups, in addition to some disordering of the membranes with the shorter peptides and ordering by the longer peptides. The peptides did not appear to insert deeply into the neutral membranes and are thought to be located predominantly in the aqueous region of the membrane bilayer. These results were more consistent with the carpet mechanism of action, and possibly explain why these peptides preferentially lyse bacterial rather than eukaryotic cells [608,720].

Although these peptides do disrupt neutral bilayers, additional work is needed in mixed lipid systems which more accurately mimic bacterial cell membranes, and may better take into account the electrostatic interactions involved in membrane binding and permeation. Thus, in order to further understand the antibacterial activity of such peptides, similar studies using anionic phospholipids were proposed. Since phosphatidylglycerols are known to be the most abundant anionic phospholipids in bacterial cells [722], 1,2-dimyristoylphosphatidylglycerol (DMPG, Figure 8.3) is a suitable model for bacterial membranes. Furthermore, DMPG forms ordered bilayer structures in a similar manner to DMPC [723], allowing for ease of comparison between these two systems.
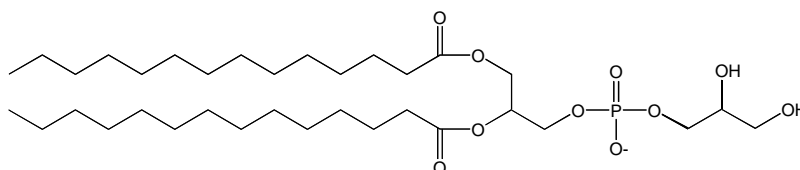
Figure 8.3: The structure of the bilayer-forming lipid DMPG.

The following chapter summarises the solid state NMR investigations carried out for the Australian amphibian peptides citropin 1.1, and maculatin 1.1, using anionic lipid membrane model systems.

8.2 Results

8.2.1 Structure Activity Relationship

The antibacterial activity of citropin 1.1 and maculatin 1.1 has been investigated previously [65,721], the results of which are summarised in Table 8.2. Selected synthetic modifications of citropin 1.1 have also been included here to demonstrate the importance of charge on antibacterial efficacy.

Table 8.2: Antibiotic activities of citropin 1.1 and maculatin 1.1, along with selected synthetic modifications [65,721]. MIC is the minimum concentration required for pathogen growth inhibition. Where no figure is indicated, MIC is > 100 μg.ml^{-1}. The first and second groups of bacteria are Gram-positive and Gram-negative respectively.

Peptide	Sequence
Maculatin 1.1	GLFGVLAKVAAHVVPAIAEHF-NH$_2$
Citropin 1.1	GLFDVIKKVASVIGGL-NH$_2$
Mod. 1	GLF**A**VIKKVASVIGGL-NH$_2$
Mod. 2	GLFDVI**A**KVASVIGGL-NH$_2$
Mod. 3	GLFDVI**AA**VASVIGGL-NH$_2$
Mod. 4	GLFDVIKKVASVI**K**GL-NH$_2$
Mod. 5	GLFDVIKKVAS**K**IGGL-NH$_2$

Organism	MIC (μg.ml^{-1})						
	Mac 1.1	**Cit 1.1**	**Mod. 1**	**Mod. 2**	**Mod. 3**	**Mod. 4**	**Mod. 5**
Bacillus cereus	50	50	25	100		50	
Leuconostoc lactis	3	6	3	25		3	12
Listeria innocua	100	25	25	25		25	50
Micrococcus luteus	12	12	12	100		25	
Staphylococcus aureus	6	25	25	100		25	
Staphylococcus epidermidis	12	12	12	100		25	100
Streptococcus uberis	3	25	25	100		25	100
Eschericha coli				100		50	100
Pasteurella multocida	50					100	

Both citropin 1.1 and maculatin 1.1 are positively charged at neutral pH, and the importance of this charge is particularly evident from the data in Table 8.2. The first modification, where Asp4 is replaced with Ala in citropin 1.1, results in a peptide with increased positive charge, increased hydrophobicity and reduced amphipathicity. Nevertheless, the observed spectrum of activity is essentially the same as the natural peptide. This suggests that the increased charge compensates for the reduced amphipathicity.

Replacing Lys7 of citropin 1.1 with Ala (mod. 2) results in a peptide with a reduced charge, but similar hydrophobicity and amphipathicity to mod. 1. The dramatic drop in efficacy noted for the Ala7 analogue is therefore likely to be a direct consequence of the decrease in positive charge. Furthermore, as seen for mod. 3, replacing both Lys7 and Lys8 with Ala entirely negates the antibacterial activity. Conversely, when Gly14 is exchanged for Lys (mod. 4), the activity against Gram-negative bacteria increases in parallel with the positive charge of the molecule. However, replacing Val12 with Lys (mod. 5) reduces that activity. Therefore, basic residues seem to increase antibiotic activity, but only when positioned in the hydrophilic zone of the peptide.

These modifications illustrate the importance of cationic nature to the activity of citropin 1.1, and the potential role for electrostatic interactions in membrane binding of the positively charged amphibian peptides.

8.2.2 ^{31}P NMR Spectroscopy

To investigate the effect of the amphibian peptides on the head groups of the lipids, static ^{31}P spectra were acquired on unoriented d_{54}-DMPC/DMPG multilayers in which d_{54}-DMPC and DMPG were present in a 1:1 molar ratio, both with and without peptide (15:1 lipid/peptide ratio). The resulting spectra are shown in Figure 8.4.

Figure 8.4: ^{31}P NMR spectra obtained for unoriented bilayers containing d_{54}-DMPC/DMPG **(a)** alone, **(b)** in the presence of maculatin 1.1, and **(c)** in the presence of citropin 1.1, at a lipid/peptide ratio of 15:1 and 28 °C.

The ^{31}P NMR spectrum for d_{54}-DMPC/DMPG alone reveals an axial symmetric line shape with a CSA of approximately -41 ppm, which is consistent with that expected for uniaxially mobile phospholipids in randomly oriented lipid bilayers [555,585]. A single powder pattern is observed in this case, suggesting that the lipid species are well dispersed within the bilayer with no evidence of lateral phase separation, and that the lipid aggregates exceed 1 μM, typical of multilamellar vesicle (MLV) suspensions [585,724].

The spectral line shape remains dominated by the effective CSA of the lipid phosphates upon addition of either maculatin 1.1 or citropin 1.1, indicating the integrity of the bilayer is for the most part maintained in the presence of the peptides. However, a decrease in CSA to -35 ppm and -32 ppm was noted for the maculatin/lipid and citropin/lipid samples respectively, inferring the head groups are more disordered in the presence of the peptides. Furthermore, the relative spectral intensity distribution is altered upon addition of both peptides, with in increase in intensity noted at 0 ppm. This is consistent with enhanced isotropic motions, as a result of peptide induced membrane disruption.

Static ^{31}P NMR experiments were repeated on samples that had been refrigerated at 4 °C for several weeks. A substantial change was observed for the citropin 1.1 sample, which now featured three contributing spectral signals (Figure 8.5). It is possible that citropin 1.1 is inducing some phase separation of the d_{54}-DMPC and DMPG lipids. Alternatively, this may be attributed to the formation of unordered lipid bilayers with $\sigma_{\parallel}$ near -6 ppm, as well as an isotropic phase (approximately 0 ppm), both in addition to the regular lamellar phase. This did not occur for the control d_{54}-DMPC/DMPG sample, or to a significant extent for the maculatin 1.1 sample, and suggests that citropin 1.1 is most efficient in inducing non-lamellar phases over time.
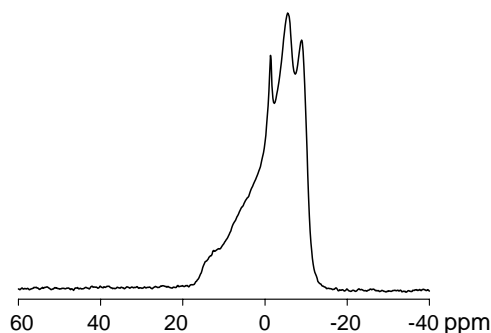
Figure 8.5: ^{31}P NMR spectra obtained for unoriented bilayers containing d_{54}-DMPC/DMPG in the presence of citropin 1.1, at a lipid/peptide ratio of 15:1 and 28 °C, obtained after several weeks of refrigeration.

8.2.3 ^{31}P NMR Relaxation Studies

^{31}P relaxation studies were carried out for the anionic phospholipid system with both maculatin 1.1 and citropin 1.1. Maximum intensity was measured for the ^{31}P spectra, and relaxation times T_1 and T_2 were determined by fitting a single exponential to a plot of signal intensity against the delay time τ, for inversion recovery and spin-echo experiments respectively (Section 7.7). An example of this data fitting is given for the control d_{54}-DMPC/DMPG sample in Figure 8.6.
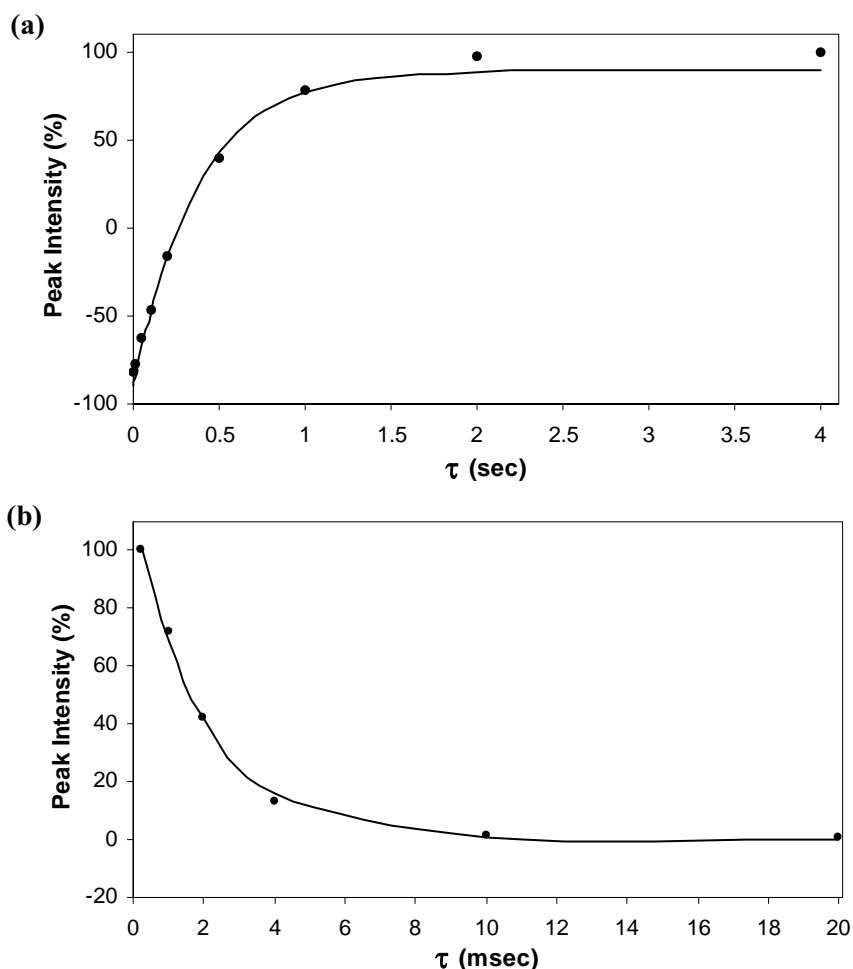
Figure 8.6: ^{31}P NMR **(a)** longitudinal, and **(b)** transverse relaxation measurements for d_{54}-DMPC/DMPG lipids at 28 ºC.

The relaxation times are altered upon addition of the peptides to the lipid bilayers as shown in Table 8.3. Longitudinal relaxation rates are controlled primarily by rapid conformational changes, while transverse relaxation measurements are sensitive to differences in slow collective membrane motions (Section 7.7.3). T_1 becomes shorter upon addition of both maculatin 1.1, and in particular citropin 1.1, indicating the peptides are enhancing the intensity of fast motions on the MHz time scale. Changes to T_2 confirm these peptides do in fact interact with the surface of the model membranes, and also alter the slow rate motions of the phospholipid head groups. An increase in T_2 is consistent with a less efficient relaxation mechanism on the millisecond time scale.

Table 8.3: ^{31}P NMR relaxation times for d_{54}-DMPC/DMPG lipids, with the addition of amphibian antibacterial peptides at a lipid/peptide ratio of 15:1 and 28 °C.

Sample	T$_1$ (ms)	Δ T$_1$ (ms)	Δ T$_1$ (%)	T$_2$ (ms)	Δ T$_2$ (ms)	Δ T$_2$ (%)
d_{54}-DMPC/DMPG	374	-	-	2.0	-	-
d_{54}-DMPC/DMPG + maculatin 1.1	341	-33	-9	3.0	1.0	+50
d_{54}-DMPC/DMPG + citropin 1.1	202	-172	-46	2.6	0.6	+30

8.2.4 ^{2}H NMR Spectroscopy

^{2}H NMR spectra were obtained for the d_{54}-DMPC/DMPG (1:1 molar ratio) phospholipid bilayers in the absence and presence of the amphibian peptides (15:1 lipid/peptide ratio), and are shown in Figure 8.7. The spectra are typical of unoriented bilayer dispersions in which the lipid acyl chains are perdeuterated [557,593], and consist of the superimposition of Pake doublets for each deuteron in the chain. Compared with the d_{54}-DMPC/DMPG control sample, peaks in the spectrum of the peptide-containing MLVs are less well-defined. The decrease in resolution indicates that the motion of the lipids side chains has changed, and suggests the presence of the peptide affects the packing of the deuterated acyl chains.
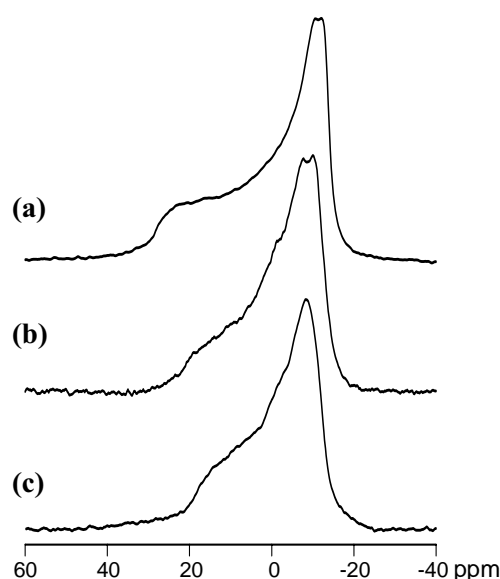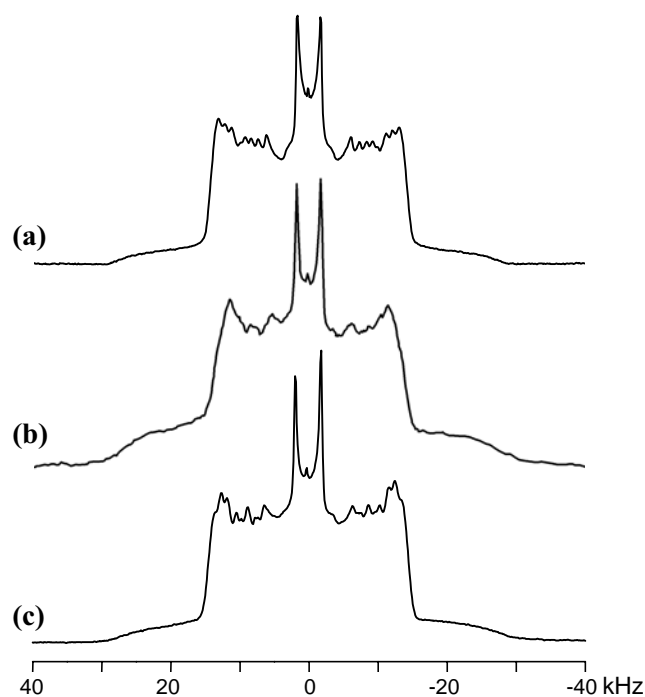

Figure 8.7: ^{2}H NMR spectra obtained for unoriented bilayers containing d_{54}-DMPC/DMPG **(a)** alone, **(b)** in the presence of maculatin 1.1, and **(c)** in the presence of citropin 1.1, at a lipid/peptide ratio of 15:1 and 28 °C.

The spectra were dePaked and carbon-deuterium bond order parameters (S_{CD}) were calculated from the splitting [725] (Section 7.5). No attempt was made to individually assign overlapped peaks, and instead these deuterons are given a single splitting value. Order profiles for ^2H are plotted against carbon position in Figure 8.8, where it can be seen that the segmental order parameters for the peptide-lipid samples have increased relative to those of the d_{54}-DMPC/DMPG sample alone. These results indicate that the acyl chains are more ordered in the presence of the peptides, and slightly more so for citropin 1.1.
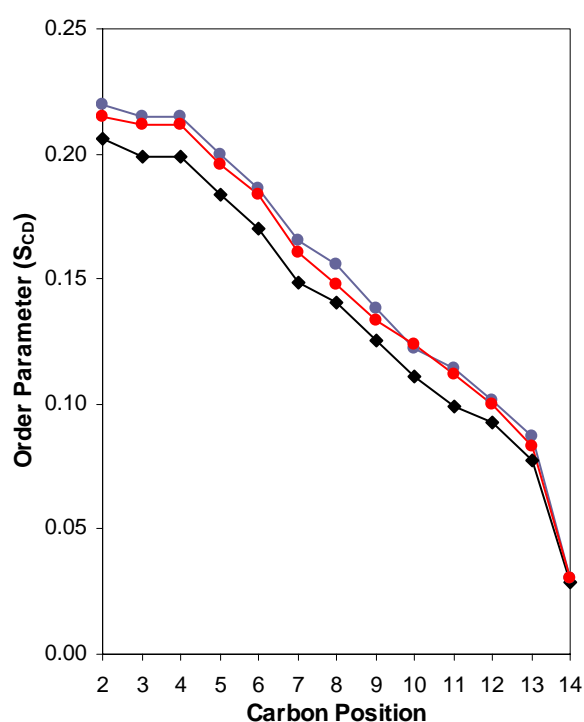
Figure 8.8: Plot of the carbon-deuterium bond order parameters (S_{CD}) against acyl chain carbon position for unoriented d_{54}-DMPC/DMPG bilayers alone (black), and in the presence of maculatin 1.1 (red) or citropin 1.1 (blue), at a 15:1 lipid/peptide ratio and 28 °C.

These conclusions are further evident after quantitative analysis of the splittings (Table 8.4). The relative change in order parameters for both peptide samples is greater for citropin 1.1, with the change in splittings ranging from 8% to 15%. The difference in segmental order also tends to be greater towards the ends of the acyl chains, suggesting the peptides induce more order in the bilayer centre compared with the polar head group region.

Table 8.4: ^{2}H quadrupolar splittings measured for d_{54}-DMPC/DMPG bilayers both alone and in the presence of maculatin 1.1 or citropin 1.1, at a 15:1 lipid/peptide ratio and 28 °C.

Carbon Position	^{2}H Quadrupolar Splittings (kHz)			Relative Change from Lipid Alone (%)	
	DMPC/DMPG	+ Maculatin 1.1	+ Citropin 1.1	Maculatin 1.1	Citropin 1.1
2	26.0	27.0	27.6	4	6
3	25.1	26.6	27.0	6	8
4	25.1	26.6	27.0	6	8
5	23.1	24.7	25.1	7	9
6	21.4	23.2	23.4	8	10
7	18.7	20.3	20.9	8	12
8	17.7	18.7	19.6	5	11
9	15.8	16.9	17.5	7	10
10	14.0	15.6	15.4	11	10
11	12.5	14.1	14.4	13	15
12	11.7	12.6	12.8	8	10
13	9.8	10.5	11.0	7	12
14	3.6	3.8	3.8	5	5

8.2.5 ^{15}N NMR Spectroscopy

Cross-polarisation MAS ^{15}N NMR spectra obtained at 28 °C of dry powder samples with selectively labelled citropin 1.1 and maculatin 1.1 are shown in Figure 8.9. An isotropic chemical shift of approximately 85 ppm was observed for the labelled residue Gly15 of citropin 1.1, while residue Ala10 of maculatin 1.1 demonstrated an isotropic shift of approximately 100 ppm. In both instances these shifts are indicative of an α-helical conformation [726-728].
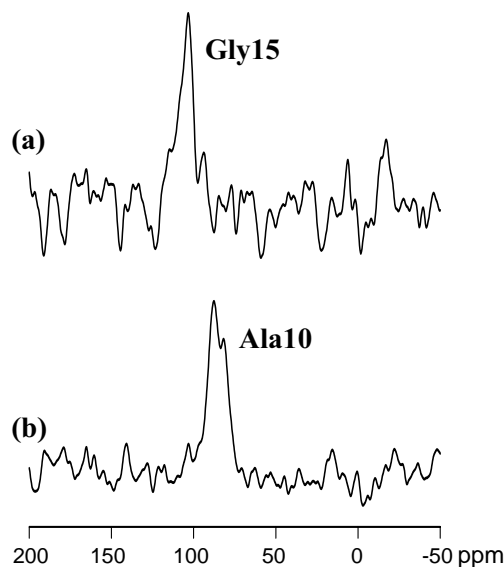
Figure 8.9: MAS ^{15}N NMR spectra of selectively labelled **(a)** maculatin 1.1, and **(b)** citropin 1.1 in d_{54}-DMPC/DMPG unoriented bilayers at a 15:1 lipid/peptide ratio. Approximately 40,000 scans were recorded at 28 ºC.

Attempts were made to obtain ^{15}N NMR spectra for these peptides in hydrated bilayers, and in all cases were ineffective. Cross-polarisation parameters for ^{15}N can be difficult to optimise because of the length of time it takes to obtain a ^{15}N signal. However, since the same experiments were successful for the dry peptide powders, this may imply the peptides are relatively mobile in the fluid bilayers, resulting in inefficient cross-polarisation [729].

8.3 Discussion

Solid state NMR spectroscopy has been used to investigate the effect of maculatin 1.1 and citropin 1.1 on d_{54}-DMPC/DMPG bilayers, in an attempt to further probe the antibacterial activity of these peptides using a lipid system more representative of the bacterial cell membrane.

Citropin 1.1 is thought to adopt a linear α-helical structure in lipid environments, as determined using solution NMR methods [65]. Similarly, maculatin 1.1 exists in a helical conformation, with a pronounced flexible kink at Pro15 that may enable better amphipathic distribution of residues, and a more precise interaction with the membrane surface [312,721]. These structures can be represented by Schiffer-Edmundson helical wheel projections as shown in Figure 8.10, where the amphipathic nature of each peptide is evident.
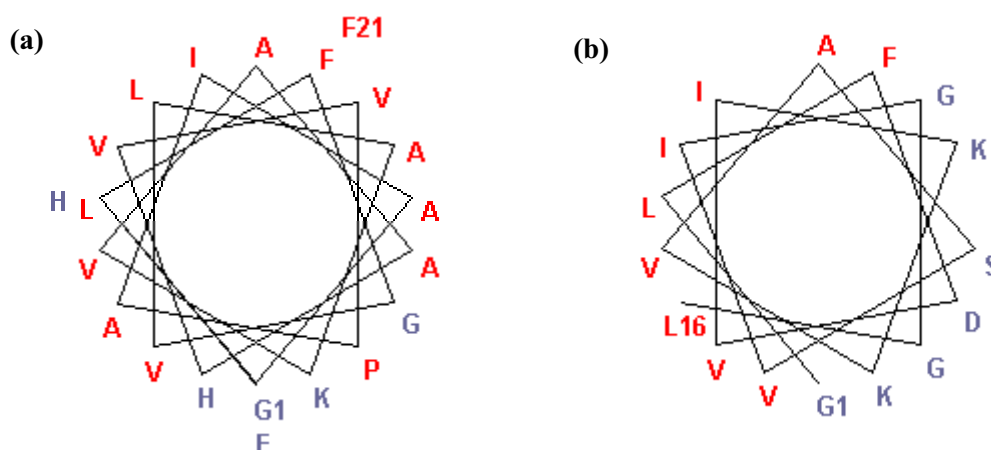
Figure 8.10: Schiffer-Edmundson helical wheel projections of **(a)** maculatin 1.1, and **(b)** citropin 1.1. Hydrophilic residues are coloured blue, while hydrophobic residues are coloured red.

Table 8.5 summarises selected physical characteristics of both maculatin 1.1 and citropin 1.1. Here it can be seen that these peptides are positively charged at neutral pH, which may facilitate electrostatic attraction to the acidic lipids of bacterial cell membranes. They are also hydrophobic, which would allow them to insert into the hydrophobic region of a bilayer. Citropin 1.1 is less hydrophobic than maculatin 1.1, and its predicted hydrophilic angle is greater. Peptides with hydrophilic angles around

180° bind to lipid bilayers with high affinity but are less able to permeabilise the membranes once bound [657]. Citropin 1.1 might therefore be expected to bind more strongly to bacterial membranes, while maculatin 1.1 might have greater permeabilising activity.

Table 8.5: Structural parameters of citropin 1.1 and maculatin 1.1.

Peptide	Hydrophobicity[a]	Hydrophobic Moment[b]	Hydrophilic Angle	Charge
Citropin 1.1	0.05	0.37	140°	+2
Maculatin 1.1	0.16	0.25	80°	+1

[a] Mean residue hydrophobicity as calculated from the consensus sequence of Eisenberg [702].
[b] Hydrophobic moment (μ) per residue [703].

The structure-activity relationship described for citropin 1.1 in Section 8.2.1 clearly demonstrates that the positive charge and the extent of amphipathicity are critical for antibacterial efficacy. It is therefore postulated that the way in which such peptides behave in an anionic membrane environment may be different to that observed previously using zwitterionic membrane models, and that lipid-peptide binding interactions would be enhanced.

The static ^{31}P NMR results on unoriented d_{54}-DMPC/DMPG bilayers suggest the lipids remain in the lamellar phase when either maculatin 1.1 or citropin 1.1 is present. However, a significant reduction in CSA was noted, which may reflect an increase in head group disorder, or a change in the phosphate head group environment [585,592,600]. This implies that both peptides do in fact interact with the bilayer in the region of the lipid head groups, and is further supported by the results of the ^{31}P relaxation studies. The changes to longitudinal and transverse relaxation times recorded in Table 8.3 are indicative of a decline in the spectral density of collective, segmental motions, and an increase in the spectral density of the faster motions attributable to intramolecular rearrangements upon association with the antibacterial peptides [730].

The change in CSA observed here is of a similar direction and magnitude reported in analogous experiments using d_{54}-DMPC alone [608]. However, in comparison with this study, a more pronounced difference in spectral line shape was noted. For the d_{54}-DMPC/DMPG system, a greater increase in relative intensity of the isotropic ^{31}P NMR resonance near 0 ppm is an indication of membrane disruption by the antimicrobial peptides, since lysis results in an increased amount of small, fast tumbling phospholipid structures [720,724]. This suggests the amphibian peptides may be relatively more destructive to anionic lipid membranes.

Citropin 1.1 was also found to induce the formation of additional lipid phases in d_{54}-DMPC/DMPG at approximately 4 ºC over an extended period of time. Even with DMPC bilayers alone, three phases have been observed in some samples as a consequence of membrane disruption by aurein 1.2, citropin 1.1 and maculatin 1.1[†] (unpublished data obtained in collaboration with Assoc. Prof. F. Separovic, University of Melbourne). This is compatible with the carpet mechanism, whereby the bilayer structure disintegrates and segments break off as micelles [554]. Alternatively, it could indicate a toroidal mechanism since the phospholipids involved in the pore structures should give rise to an isotropic signal [731]. However, in the case of DMPC/DMPG mixed bilayers it may be that an anionic DMPG enriched phase is produced near the positively charged peptide. It would be worthwhile to further investigate the induction of isotropic phases by these peptides in a systematic manner, to probe the time course of this transition and determine the biological relevance.

Cross-polarisation MAS ^{15}N NMR spectra of phospholipid powders gave chemical shifts consistent with helical conformations for both maculatin 1.1 and citropin 1.1. Although unstructured in water, the results presented here indicate that, even in the dry state, these peptides favour α-helical structure in an anionic lipid environment. The structural transition from disordered (in solution) to helical (in the membrane bound state) must be a direct consequence of the immersion of the peptides into the less polar environment of the membrane interface. The difficulty in obtaining ^{15}N spectra for the peptides in hydrated bilayers despite several attempts is most likely due to high

---

[†] Macroscopic phase transitions in the presence of magainin have also been described [Bechinger, B. (2005) Detergent-like properties of magainin antibiotic peptides: A ^{31}P solid-state NMR spectroscopy study. *Biochim. Biophys. Acta.* 1712:101-108].

molecular mobility, leading to poor cross-polarisation efficiency, and would need to be addressed in order to obtain suitable ^{15}N spectra for the hydrated systems.

To further investigate the mechanism of action of maculatin 1.1 and citropin 1.1 in acidic membranes, it would be desirable to determine the orientation of the peptides with respect to the bilayer. ^{15}N NMR studies may be applicable using mechanically oriented lipids (Section 7.6), but to improve the sensitivity it would be preferable to employ greater amounts of labelled peptides than were used in the present study.

Both maculatin 1.1 and citropin 1.1 were found to increase the order of the lipid acyl chains in unoriented model membranes, with the ordering effect greater toward the centre of the lipid bilayers, and more pronounced for citropin 1.1. A disordering effect has been reported for surface oriented peptides [600,729,732,733], which are thought to insert into the lipid-water interface and laterally separate the lipids, giving the acyl chains greater spatial freedom. In contrast, a transmembrane configuration or greater membrane penetration may either increase or decrease ^{2}H bond order parameters depending on specific interactions between the peptide and acyl chain segments [720,733,734]. Since the ordering effect of both maculatin 1.1 and citropin 1.1 occurred along the whole lipid chain, it may be that these peptides are oriented perpendicular to the bilayer plane in d_{54}-DMPC/DMPG lipids. Furthermore, the ordering observed for d_{54}-DMPC in the presence of citropin 1.1 or maculatin 1.1 could also indicate a lateral separation of d_{54}-DMPC and DMPG, as has been described for in-plane oriented cationic peptides in mixed anionic lipid membranes [Mason, A.J., Martinez, A., Glaubitz, C., Danos, O., Kichler, A. and Bechinger B. (2006) The antibiotic and DNA-transfecting peptide LAH4 selectively associates with, and disorders, anionic lipids in mixed membranes. *FASEB J.* 20:320-2].

These results differ somewhat from previous reports using neutral lipids only. For example, Marcotte *et al.* indicate an increase in disorder for d_{54}-DMPC acyl chains in the presence of citropin 1.1, and an ordering effect for the longer maculatin 1.1, using mechanically aligned lipid bilayers [720]. Moreover, Balla *et al.* describe a decrease in quadrupolar splitting for both maculatin 1.1 and citropin 1.1 in unoriented as well as aligned d_{54}-DMPC bilayers, although to a lesser extent for maculatin 1.1 [608]. The

clear ordering effect observed for the peptides in the present study, which is contrary to the previous data, might be evidence for the transition from a location at the surface of zwitterionic lipids to a predominant transmembrane orientation in anionic lipids.

Support for a pore-forming mechanism of action for maculatin 1.1 in acidic lipids is provided by attenuated total reflection infrared Fourier transform infrared (ATR-FTIR) studies, and deuterium exchange experiments [735]. Using these methods, nearly 70% of maculatin 1.1 molecules were found to insert into DMPG liposomes, at an angle of approximately 35° to the membrane normal, and a predominant α-helical structure. Under the same conditions, less than 5% of the peptide inserted into DMPC liposomes, and a range of secondary structures were present in similar proportion. This also substantiates a possible difference in the mechanism by which the peptides exert their effects in either zwitterionic or anionic lipids.

Solution structure studies indicate citropin 1.1 to be approximately 20 Å in length in TFE/H$_2$O [65], and maculatin 1.1 to be close to 30 Å [721]. Since the average thickness of a bacterial membrane is also 30 Å [722], the length of maculatin 1.1 is sufficient to span the bilayer in a channel forming mechanism. Citropin 1.1 on the other hand is not long enough to form barrel-stave type channels, yet it is still feasible for this peptide to form toroidal model pores if the bilayer lipids are capable of stabilising the ends of the shorter pores.

The enhanced interaction for maculatin 1.1 and citropin 1.1 associated with negatively charged lipids may also be sufficient to explain why these peptides show a lack of activity against Gram-negative bacteria, and are selectively active towards prokaryote cells. However, other factors such as the presence of the outer layer may also contribute. For example, lipopolysaccharides present in the outer leaflet of the membrane may also directly influence the binding and membrane disrupting capabilities of these peptides. Relatively few studies have investigated the interactions between antibacterial peptides and such lipopolysaccharides due to problems with obtaining suitable model membrane systems [736]. Nevertheless, by continually increasing the complexity of the model membranes used, we become closer to understanding the basis for selectivity and efficacy in these antibacterial peptides.

8.4 Experimental Procedures

8.4.1 Sample Preparation

Peptides were synthesised commercially by Mimotopes (Clayton, Victoria) using L-amino acids and standard N-α-Fmoc solid phase techniques [331], and were shown to be greater than 90% pure by HPLC and ESI-MS. ^{15}N-L-amino acids were specifically incorporated at Gly14 of citropin 1.1 and Ala10 of maculatin 1.1 for ^{15}N NMR spectroscopy. Phospholipids were purchased from either Avanti Polar Lipids (Alabaster, USA) or Sigma (St. Louis, USA), and used as received.

Each peptide (typically 5 mg) was co-dissolved in a small amount of chloroform/methanol (9:1 v/v) with a 1:1 molar mixture of d_{54}-DMPC and DMPG, giving an overall lipid/peptide molar ratio of 15:1. The solvent was evaporated under a stream of N_2, and the samples were lyophilised. NMR spectra were acquired for the dry samples prior to hydration, where 40 µL of water was added to each sample. The samples were then submitted to at least three cycles of freeze-thawing followed by vortex mixing until a viscous, translucent dispersion was obtained. They were then transferred to a 5 mm NMR tube for analysis. Control samples of d_{54}-DMPC/DMPG were prepared in a similar manner without the addition of peptide.

8.4.2 NMR Spectroscopy

NMR experiments were performed on a Varian Inova-300 spectrometer, using a 5 mm Doty MAS probe. ^{31}P proton decoupled experiments were carried out at a frequency of 121.5 MHz, using a single 90º pulse for excitation, and were referenced to H_3PO_4 (0 ppm). For the investigation of maculatin 1.1 and citropin 1.1, 2048 scans were recorded with a spectral width of 62.5 kHz, a 90° pulse length of 8 µs and 1.5 second recycle delay. 2048 data points were acquired, then zero-filled to 4096. Line broadening of 100 Hz was applied to all spectra.

Deuterium quadrupole echo spectra were recorded at 46.1 MHz and 28 ºC, and referenced to D_2O (0 ppm). A 90° pulse of 5-6 µs with an echo spacing of 40 µs and a recycle delay of 500 ms were used. Typically, 100 k scans were recorded over a spectral width of 200 kHz with either 2048 or 4096 data points, and a line broadening of either 100 or 200 Hz was applied to the spectra. ^2H solid state spectra were dePaked using an algorithm developed by Dr. John Gehman (Department of Chemistry, University of Melbourne) based on that described by Sternin *et al*. [596] and Whittall *et al*. [737].

^{15}N NMR spectra of powder samples were obtained using cross-polarisation experiments with proton decoupling [563]. Data was acquired at 30.4 MHz, and recorded for spinning samples (4-5 kHz) at ambient temperature. A cross-polarisation contact time of 1.5 ms, 90° proton pulse of 8.3 µs and a recycle delay of 1.5 seconds were used over a spectral width of 30 kHz, and a 100 Hz line broadening applied. 2048 points were acquired for 40 k scans (and zero filled to 8k). ^{15}N spectra were referenced to the ammonium signal of $^{15}NH_4NO_3$ (0 ppm).

An inversion recovery pulse sequence ($\pi - \tau - \pi/2$) with τ values between 0.001 and 4 seconds was used for measurement of longitudinal relaxation times, while transverse relaxation was investigated with a spin-echo experiment ($\pi/2 - \tau - \pi$) with τ values between 0.2 and 20 ms. Relaxation times were then determined by fitting a single exponential to a plot of signal intensity against the decay time τ, using the program Origin (Microcal Software, Inc., version 4.10). Errors are estimated as the root mean square of the fitting of an exponential curve to the experimental data, and are in the order of 10%.

~ CHAPTER 9 ~

Structure and Activity of Cupiennin 1a

9.1 Introduction

9.1.1 *Cupiennius salei*

The neotropical wandering spider *Cupiennius salei* is a large, nocturnal hunting spider distributed throughout Central America, located as far north as Veracruz state in Mexico and extending to Honduras in the south (Figure 9.1). It is restricted to altitudes ranging from 200-1,250 meters, and resides in the tropical rain forests of this region [104]. The spider is brown with small, light spots on the abdomen and many dark longitudinal stripes, predominantly on the carapace. The legs, patella and femurs are also striped with lighter circles, while the underbody is red-yellow with thin black vertical stripes under the abdomen (Figure 9.1). Females can reach up to 35 mm in body length and have a 100 mm leg span, while males are typically smaller and less brightly coloured [104].
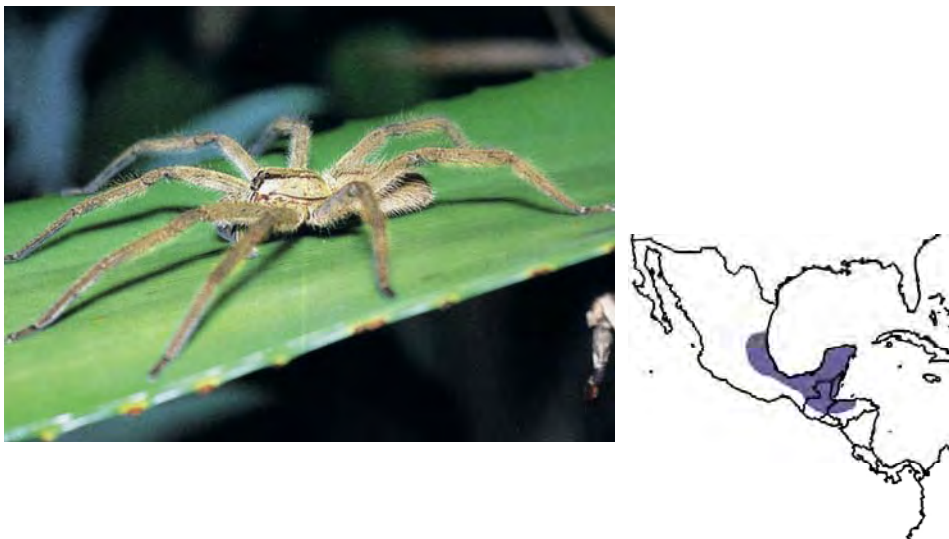
Figure 9.1: Appearance and geographical distribution of *Cupiennius salei* [104].

Since it was realised in the mid 1950s that *C. salei* is large, easy to breed and an ideal model spider, this species has been reared in numerous zoological institutes. Today nearly 200 publications are available on the behaviour and physiology of *C. salei*, making it the best studied spider species known [95].

9.1.2 *Cupiennius salei* Venom Composition

The venom of *C. salei* is a natural insecticide, causing a rapid and dose dependent paralysis of prey up to a critical lethal dose [104]. Three classes of molecules comprise the venom, and can be categorised on the basis of molecular weights. The first group consists of low molecular weight compounds, including ions, free amino acids, amines and polyamines. The following ion concentrations have been determined: Na^+ 8.9 mM, K^+ 215 mM and Ca^{2+} 4.0 mM [116]. Most of the free amino acids occur at concentrations below 25 $pmol.\mu L^{-1}$, with the exception of Gly and taurine [95]. Among the amines, histamine is the most common, and polyamines such as putrescine and cadaverine can be detected in low quantities [116]. Currently, no acylpolyamines have been identified in the venom of *C. salei*.

The second group includes mainly proteins with masses between 25 and 27 kDa. Of these, a highly active hyaluronidase has been reported, which is a spreading factor used to accelerate toxin transport into the tissue [116,117]. However, no proteolytic activity is detectable in the venom within a one-hour assay, and even under extreme test conditions, only very low levels of proteolytic enzymes are observable [116]. The final group comprises peptides with masses generally in the range of 2-8 kDa. To date, toxicological information and sequence data for the neurotoxins CSTX-1 and CSTX-9, and the neurotoxic two-chain enhancer peptide CSTX-13 have been reported [95,738]. Furthermore, the antimicrobial and cytolytic cupiennins have been identified [117], and are the basis of this present study.

The role of these highly cationic, Cys-free antibacterial peptides in the venom of *C. salei* may be twofold. Firstly, the cheliceral claws which first penetrate the prey are heavily exposed to external pathogens, and thus the venom glands are easily accessible to bacteria via the venom duct [739]. Consequently, the antibacterial peptides may be

involved in protection of the venom apparatus against infection. In addition, there is evidence that the cytolytic activity of these peptides may afford the neurotoxins better access to their intracellular targets, dramatically enhancing insecticidal efficacy [740]. Thus, after venom injection into prey, these peptides may act in synergy with the CSTX peptides to augment the paralytic effect of the neurotoxins.

9.1.3 The Cupiennin Peptides

The cupiennin 1 family is currently comprised of four peptides, the sequences of which are given below [95]. All peptides consist of 35 amino acids, and are characterised by a hydrophobic N-terminal region and a C-terminus composed primarily of polar or charged residues. Cupiennin 1a occurs in the crude venom at a concentration of 1.2 mM, while cupiennin 1b is 12 times less abundant and cupiennin 1c and 1d are only present in trace amounts [95]. In addition, four peptides have thus far been assigned to the cupiennin 2 family, however this group has not been well characterised to date and the sequences have not been reported. These peptides were initially assigned to the CSTX family [116], but were subsequently renamed upon isolation of the cupiennin 1 peptides.

Cupiennin 1a	GFGALFKFLAKKVAKTVAKQAAKQGAKYVVNKQME-NH$_2$
Cupiennin 1b	GF**S**ALFKFLAKKVAKTVAKQAAKQGAKY**IA**NKQME-NH$_2$
Cupiennin 1c	GF**S**ALFKFLAKKVAKTVAKQAAKQGAKY**IA**NKQTE-NH$_2$
Cupiennin 1d	GF**S**ALFKFLAKKVAKTVAKQAAKQGAKYV**A**NK**H**ME-NH$_2$

The cupiennin 1 peptides are active against both Gram-positive and Gram-negative bacteria with MIC values in the low micromolar range, and also exhibit cytolytic activity towards human erythrocytes. In addition, these peptides demonstrate insecticidal properties in the *Drosophila* bioassay, although are significantly less efficacious than the CSTX neurotoxins. A summary of the biological activity of the cupiennin 1 peptides can be found in Table 9.1. Cupiennin 2a (formerly CSTX-4) also shows wide-spectrum antibacterial activity in the low micromolar range, however is two to three times less effective in the *Drosophila* insecticidal bioassay [95].

Table 9.1: Biological activity of the cupiennin 1 peptides [117]. Where no figure is given, activity was not tested**.** The first and second groups of bacteria are Gram-positive and Gram-negative respectively.

	Cupiennin 1a	Cupiennin 1b	Cupiennin 1d
Antimicrobial Activity[a] (MIC, μM)			
S. aureus	0.3 - 0.6		0.6 - 1.3
E. faecalis	2.5 - 5.0		1.3 - 2.5
E. coli	0.3 - 0.6		0.8 - 0.2
P. aeruginosa	0.3 - 0.6		0.2 - 0.3
Hemolysis (EC$_{50}$, μM)			
	24.4		
Insecticide Bioassay (LD$_{50}$, pmol.mg^{-1} fly)			
	5.9	4.7	6.4

[a] The minimum inhibitory concentration (MIC, μM) is expressed as a final concentration interval [a]-[b], where [a] is the highest concentration at which bacteria are growing and [b] is the lowest concentration causing 100% growth inhibition.

Sequence analysis of the cupiennin 1 peptides suggests a unique structure distinctly different from that of other potentially helical cationic peptides isolated thus far. Following the polar N-terminal region, the cupiennin 1 family is characterised by six repeats of four amino acids, defined by the following; position 1 is always Lys, position 2 is variable, position 3 is always a hydrophobic amino acid or Gly, and in position 4 is either Ala or Val. Using cupiennin 1a as a model, when represented by a Schiffer-Edmundson helical wheel projection, the amphipathic nature of this peptide is not clearly evident in an α-helical form (Figure 9.2a). However, using a helical net projection in which the helix is effectively 'cut open' and projected on the plane surface with the x axis representing the circumference of the helix and the y axis representing the distance along the helix, it is apparent that the cupiennins show a unique amphipathic motif in which the N-terminus is connected by a spiral band of Lys and polar amino acids to the C-terminus (Figure 9.2b)

Figure 9.2: **(a)** Schiffer-Edmundson helical wheel projection of cupiennin 1a, and **(b)** net projection of cupiennin 1a. Hydrophilic residues are coloured blue, while hydrophobic residues are coloured red.

Furthermore, structure-activity relationship studies conducted previously for cupiennin 1d suggest that the hydrophobic N-terminal segment primarily determines the antibiotic effects and insecticidal properties of these peptides, while the polar C-terminus seems to modulate peptide accumulation at negatively charged cell surfaces via electrostatic interactions [741]. Interestingly, the mean hydrophobicity values and hydrophobic moment of the cupiennin peptides are particularly low in comparison with other antimicrobial peptides [117]. Since these factors play a significant role in the modulation of antibacterial efficacy (Section 8.1.4), either the hydrophobicity of the N-terminal region is sufficient to induce membrane disruption, or the high activity is related to specific structural features of these membrane bound peptides based on their unique distribution of charged and hydrophobic residues.

In order to probe the unusual structural features of the cupiennins, the solution structure of cupiennin 1a was determined using NMR spectroscopy and RMD calculations in aqueous TFE. Following this, solid state NMR methods were used to study the behaviour of this peptide in a lipid environment, to gain further insight into the mechanism of action of the cupiennins. The results of these investigations, as well as the newly discovered nNOS inhibitory activity are described in subsequent sections.

9.2 Results

9.2.1 NMR Spectroscopy

Circular dichroism spectra have been recorded previously for cupiennin 1a, and suggest this peptide is unstructured in water but adopts an α-helical conformation in a 1:1 v/v aqueous TFE mixture [117]. Based on these results, NMR studies were undertaken using this solvent system. NMR spectra were acquired for cupiennin 1a in aqueous TFE, and proton chemical shifts were assigned using standard sequential assignment methods [489] and a combination of NOESY, TOCSY and COSY experiments as outlined in Section 4.4. Partial TOCSY and NOESY spectra are shown in Figure 9.3, where labelled cross-sections for each amino acid are indicated.

For the most part the amide cross-sections are well resolved, with the exception of those in the regions of 8.15 ppm and 7.95 ppm. In these areas some of the cross-sections are very close together, and in such cases assignments were conclusively determined by examination of appropriate 3-bond correlations in the COSY spectrum. Amide proton chemical shifts were assigned in sequential order primarily using the d_{NN} NOE cross-peaks found in the NH region of the NOESY spectrum. Breaks in the sequence result where adjacent residues contain amide protons of similar shift, in which case the cross-peak appears too close to the diagonal for clear resolution. For example, amide shifts for Asn31 and Lys32 are almost coincident, and hence the cross-peak occurs too close to the diagonal to be seen distinctly. In such instances, other characteristic signals including $d_{\alpha N}$, $d_{\beta N}$ and $d_{\alpha\beta(i, \ i+3)}$ peaks were used to confirm the position of residues within the sequence.
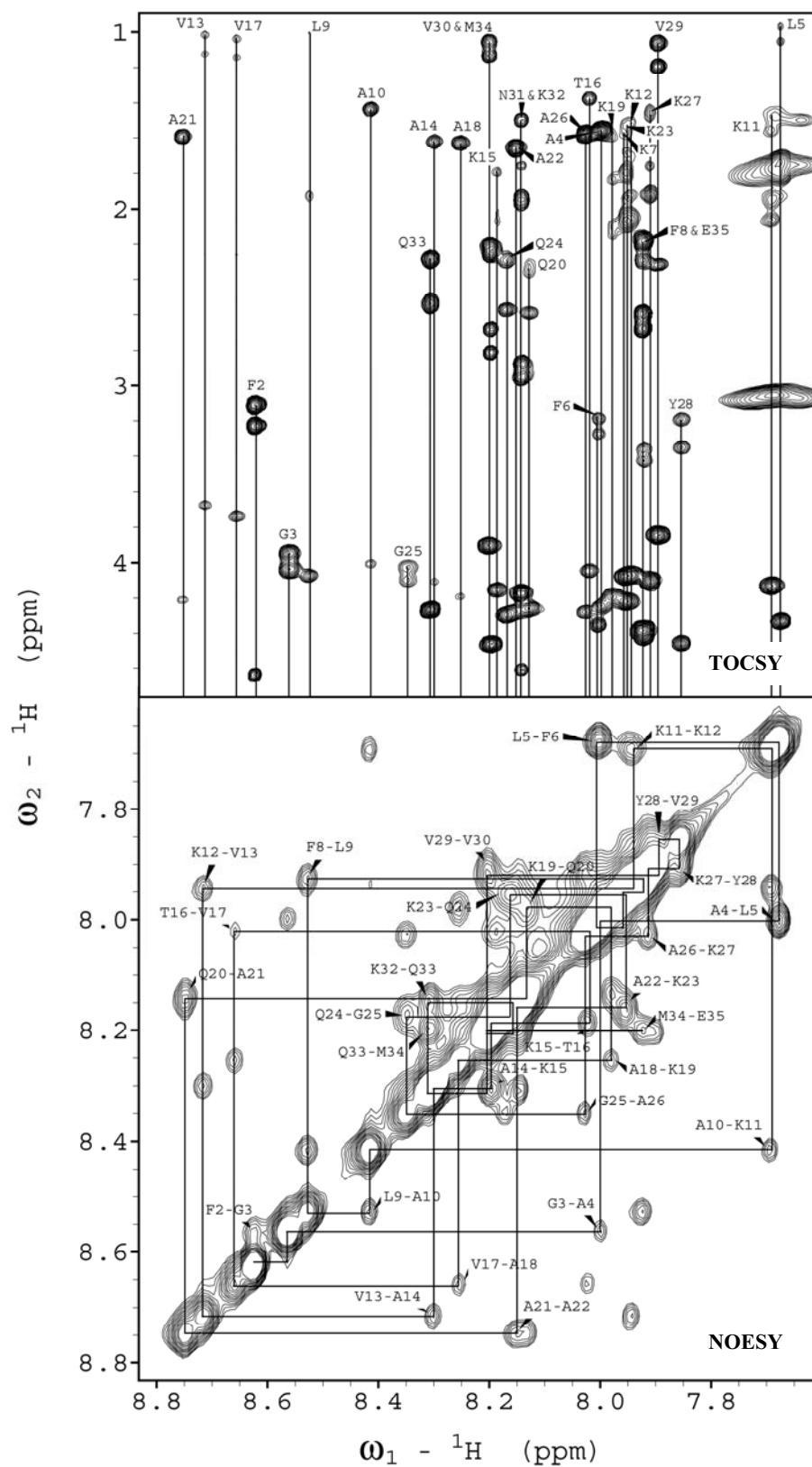
Figure 9.3: Partial TOCSY and NOESY spectra of cupiennin 1a in TFE/H$_2$O (1:1 v/v). Vertical lines connect resonances of the same spin system. NOEs between sequential amide protons are indicated in the NOESY spectrum.

αC resonances were identified by direct investigation of the αH/αC region of a HSQC spectrum, which is illustrated in Figure 9.4. A summary of all assigned proton and αC resonances is given in Table 9.2.
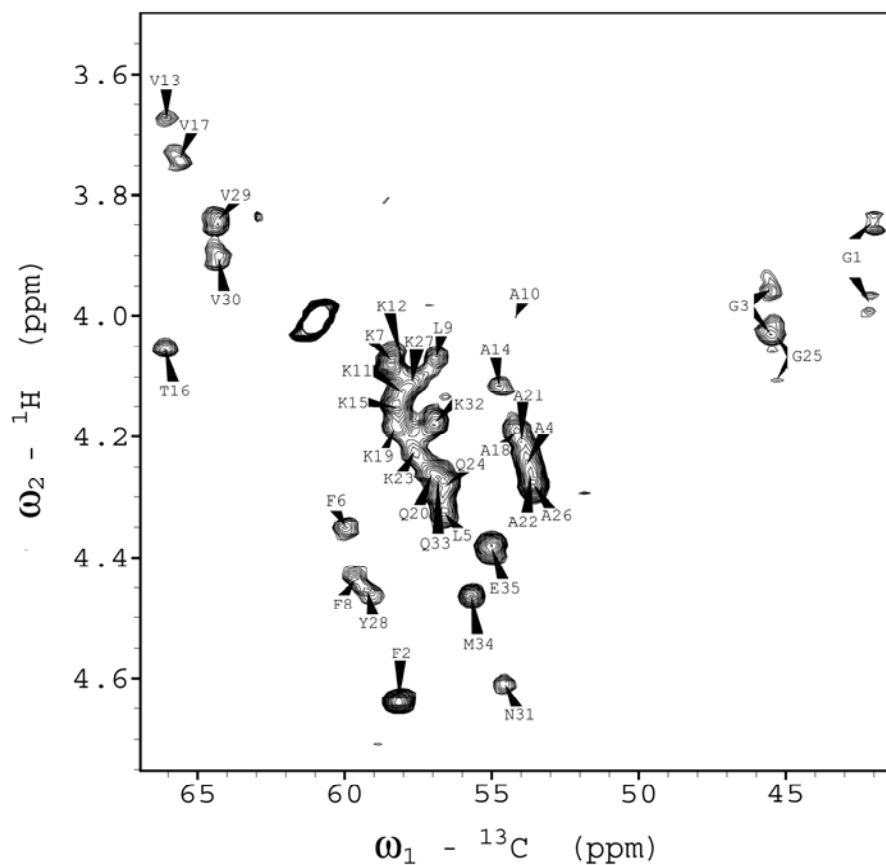
Figure 9.4: αH/αC region of the HSQC spectrum of cupiennin 1a in TFE/H$_2$O (1:1 v/v).

Table 9.2: ^{1}H and ^{13}C chemical shifts for cupiennin 1a in TFE/H$_2$O (1:1 v/v). n.o. indicates resonance was not observed.

Residue					
				Chemical shift (ppm)	
	NH	**αH**	**βH**	**Other H**	**αC**
Gly1	n.o.	3.96, 3.85			42.1
Phe2	8.63	4.64	3.22, 3.11	H2, H6 7.30	58.2
				H3, H5 7.39	
				H4 7.36	
Gly3	8.57	4.03, 3.95			45.5
Ala4	8.00	4.25	1.56		53.8
Leu5	7.68	4.33	1.81	γ-CH 1.72	56.5
				δ-CH$_3$ 1.05, 0.97	
Phe6	8.01	4.35	3.28, 3.19	H2, H6 7.29	60.0
				H3, H5 7.41	
				H4 7.37	
Lys7	7.96	4.08	2.03, 1.94	γ-CH$_2$ 1.52, 1.42	58.4
				δ-CH$_2$ 1.79	
				ε-CH$_2$ 3.07	
				ε-NH$_3^+$ n.o.	
Phe8	7.93	4.43	3.43, 3.35	H2, H6 7.36	59.7
				H3, H5 7.40	
				H4 7.30	
Leu9	8.53	4.07	1.92, 1.69	γ-CH$_2$ 1.96	56.9
				δ-CH$_3$ 1.01	
Ala10	8.42	4.01	1.44		54.2
Lys11	7.70	4.13	2.06	γ-CH$_2$ 1.62	58.0
				δ-CH$_2$ 1.96	
				ε-CH$_2$ 3.06	
				ε-NH$_3^+$ n.o.	
Lys12	7.94	4.07	2.03	γ-CH$_2$ 1.43	58.1
				δ-CH$_2$ 1.92	
				ε-CH$_2$ 3.04	
				ε-NH$_3^+$ n.o.	
Val13	8.72	3.67	2.27	γ-CH$_3$ 1.13, 1.02	66.1
Ala14	8.30	4.11	1.63		54.7
Lys15	8.19	4.15	2.08, 2.01	γ-CH$_2$ 1.62	58.2
				δ-CH$_2$ 1.79	
				ε-CH$_2$ 3.07	
				ε-NH$_3^+$ n.o.	
Thr16	8.02	4.05	4.61	γ-CH$_3$ 1.37	66.1
Val17	8.66	3.74	2.26	γ-CH$_3$ 1.14, 1.04	65.6
Ala18	8.25	4.19	1.63		54.1

Table 9.2 (continued):

Residue	Chemical shift (ppm)				
	NH	**α-CH**	**β-CH**	**Other H**	**α-C**
Lys19	7.98	4.19	2.15, 2.09	γ-CH$_2$ 1.63	58.2
				δ-CH$_2$ 1.84	
				ε-CH$_2$ 3.09	
				ε-NH$_3^+$ n.o.	
Gln20	8.13	4.26	2.36, 2.30	γ-CH$_2$ 2.59	57.0
				δ-NH$_2$ 7.25, 6.72	
Ala21	8.75	4.21	1.59		54.0
Ala22	8.15	4.28	1.65		53.7
Lys23	7.95	4.22	2.08	γ-CH$_2$ 1.58	57.6
				δ-CH$_2$ 1.83, 1.77	
				ε-CH$_2$ 3.09	
				ε-NH$_3^+$ n.o.	
Gln24	8.17	4.29	2.29	γ-CH$_2$ 2.57	56.7
				δ-NH$_2$ 7.31, 6.74	
Gly25	8.35	4.10, 4.02			45.4
Ala26	8.03	4.28	1.58		53.6
Lys27	7.92	4.10	1.92	γ-CH$_2$ 1.58	57.4
				δ-CH$_2$ 1.75	
				ε-CH$_2$ 3.06	
				ε-NH$_3^+$ n.o.	
Tyr28	7.86	4.46	3.35, 3.19	H2, H6 7.25	59.2
				H3, H5 6.92	
Val29	7.90	3.84	2.32	γ-CH$_3$ 1.20, 1.06	64.3
Val30	8.20	3.90	2.20	γ-CH$_3$ 1.14, 1.06	64.3
Asn31	8.15	4.61	2.95, 2.88	γ-NH$_2$ 7.54, 6.73	54.6
Lys32	8.15	4.17	1.96, 1.94	γ-CH$_2$ 1.50	57.0
				δ-CH$_2$ 1.76	
				ε-CH$_2$ 3.06	
				ε-NH$_3^+$ n.o.	
Gln33	8.31	4.27	2.28	γ-CH$_2$ 2.53	56.8
				δ-NH$_2$ 7.18, 6.62	
Met34	8.20	4.46	2.26	γ-CH$_2$ 2.81, 2.68	55.7
				ε-CH$_3$ 2.24	
Glu35	7.93	4.38	2.29, 2.19	γ-CH$_2$ 2.68, 2.59	55.0
				CONH$_2$ 7.31, 7.00	

9.2.2 Secondary Shifts

Random coil chemical shifts determined in water were obtained from the literature [371]. The chemical shift differences between observed resonances and random coil values, $\Delta\delta$, were smoothed over a window of n ± 2 residues and plotted against the amino acid sequence for αH and αC resonances. NH secondary shifts were plotted unsmoothed.

Figure 9.5 demonstrates a distinct upfield shift from random coil values for αH resonances along the majority of the sequence, consistent with the peptide having predominantly helical structure. The exception to this is in the vicinity of Gln24, and the N and C-termini. In these regions the resonances are random-coil like, suggesting the peptide is more flexible. Flexibility at the ends of the peptide is anticipated, since the first and last four residues are less involved in the intramolecular hydrogen bonding network responsible for maintaining secondary structure, and hence are not as efficiently restrained in a helical state [377]. However, the observed flexibility towards the centre of the peptide suggests it may adopt a helix-hinge-helix type structure.
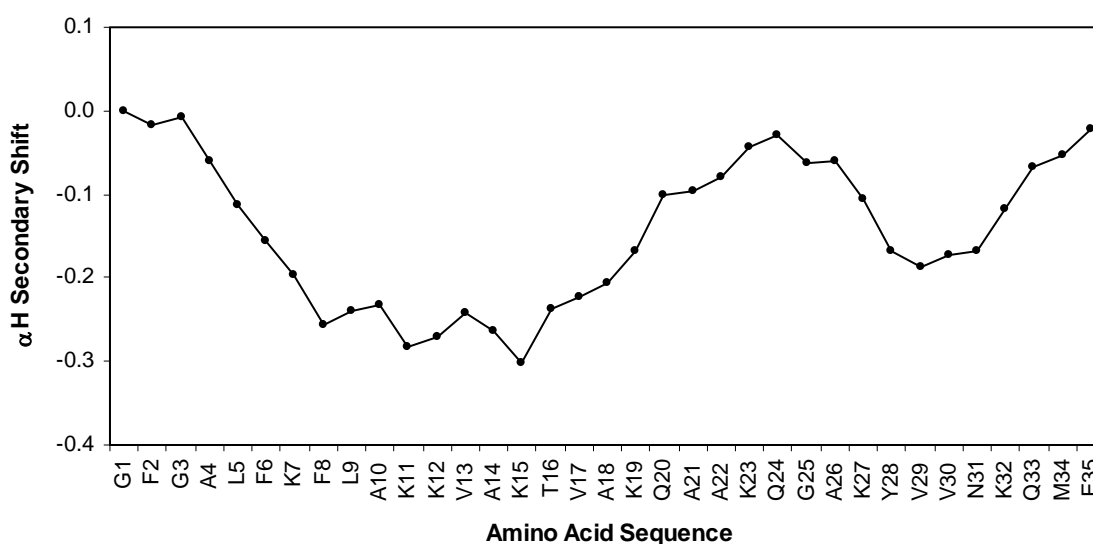
Figure 9.5: αH ^{1}H secondary shifts of cupiennin 1a in TFE/H_2O (1:1 v/v), smoothed over n ± 2 residues. Negative values indicate an upfield shift from random coil resonances, while positive values indicate a shift downfield.

This is further supported by the αC secondary shifts (Figure 9.6) in which two distinct helical regions can be identified by their significant downfield shifts. Δδ values tend more towards random coil shifts for residues at the N- and C-termini, as well as those surrounding Gln24.
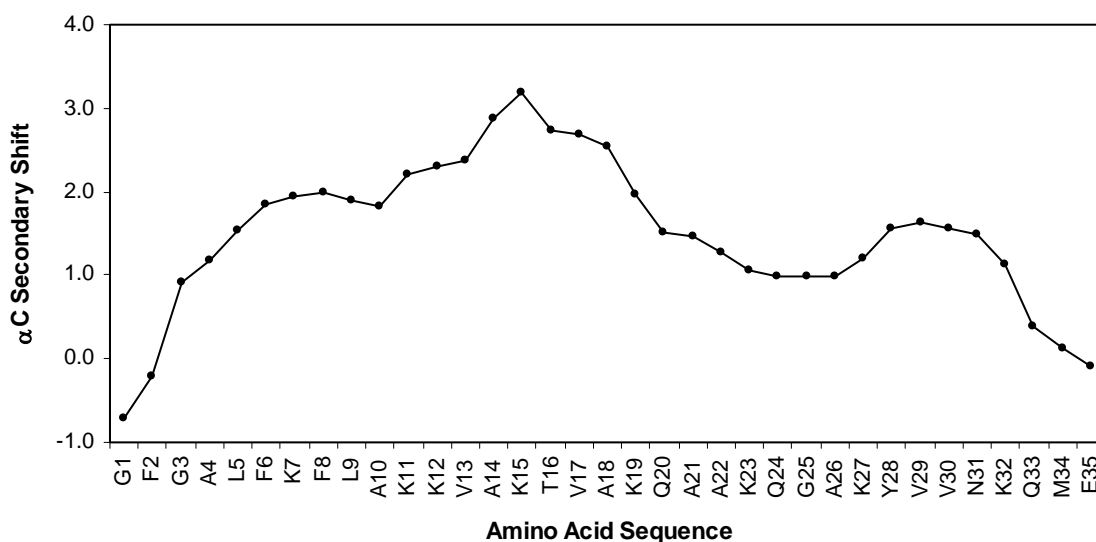
Figure 9.6: αC ^{13}C secondary shifts of cupiennin 1a in TFE/H$_2$O (1:1 v/v), smoothed over n ± 2 residues. Negative values indicate an upfield shift from random coil resonances, while positive values indicate a shift downfield.

The magnitude of unsmoothed NH Δδ values deviates periodically over 3-4 residues, with hydrophobic residues generally producing resonances further downfield compared with those which are hydrophilic (Figure 9.7). This pattern is characteristic of an amphipathic α-helix, and results due to differences in hydrogen bond lengths on either face of the peptide [377]. A general upfield trend is also noted for the NH Δδ values at the N terminus. This is again indicative of helical structure since it is accounted for by the presence of a helix dipole [372]. The 'zig-zag' trend in the graph of NH secondary shifts is maximal between residues Lys7 and Ala22, suggesting the helix is most well-defined in this region.
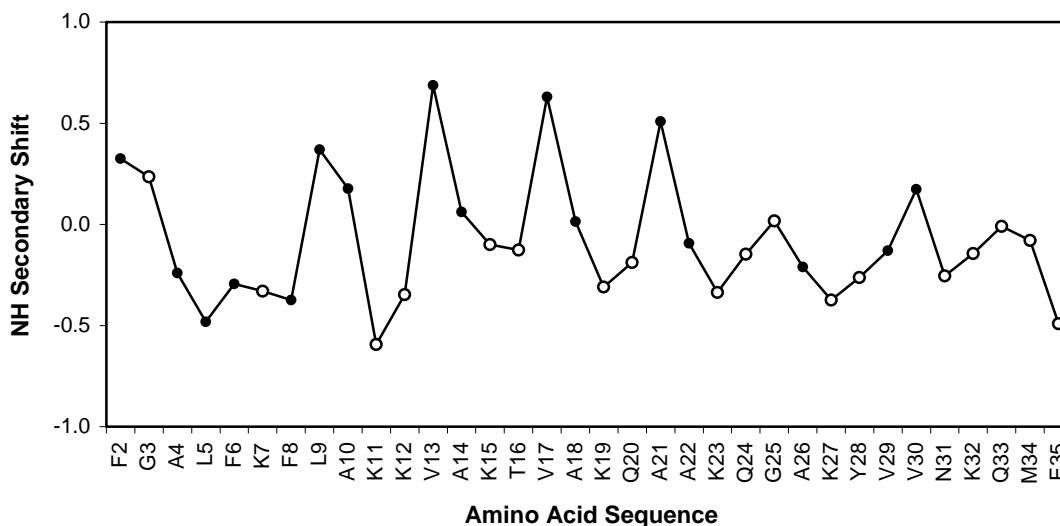
Figure 9.7: NH ^{1}H secondary shifts of cupiennin 1a in TFE/H$_2$O (1:1 v/v). Negative values indicate an upfield shift from random coil values, while positive values indicate a shift downfield. Hydrophilic residues are represented by open symbols.

9.2.3 NOE Connectivities

The diagnostic NOE connectivities used in structure calculations for cupiennin 1a are given in Figure 9.8. Here the strong series of d$_{NN}$ signals already seen in Figure 9.3 are noted, in addition to a number of weaker d$_{NN(i, i+2)}$ NOEs. Sequential d$_{\alpha N}$ and d$_{\beta N}$ NOEs also occur along the majority of the sequence. A significant number of medium-range NOEs are present from three and four residues apart, particularly d$_{\alpha N(i, i+3)}$ d$_{\alpha N(i, i+3)}$ and d$_{\alpha \beta(i, i+3)}$ signals. Also evident in this figure is the relatively large degree of assignment ambiguity, resulting from resonance overlap.

The pattern of observed NOEs and their intensities is generally consistent with the peptide having helical structure along the majority of the sequence. However, the reduction in medium-range NOEs at both the N and C termini, as well as in the region from Ala21 to Ala26 suggest these areas may have a more extended or random conformation. This is further support for a helix-hinge-helix type structure in cupiennin 1a.

241
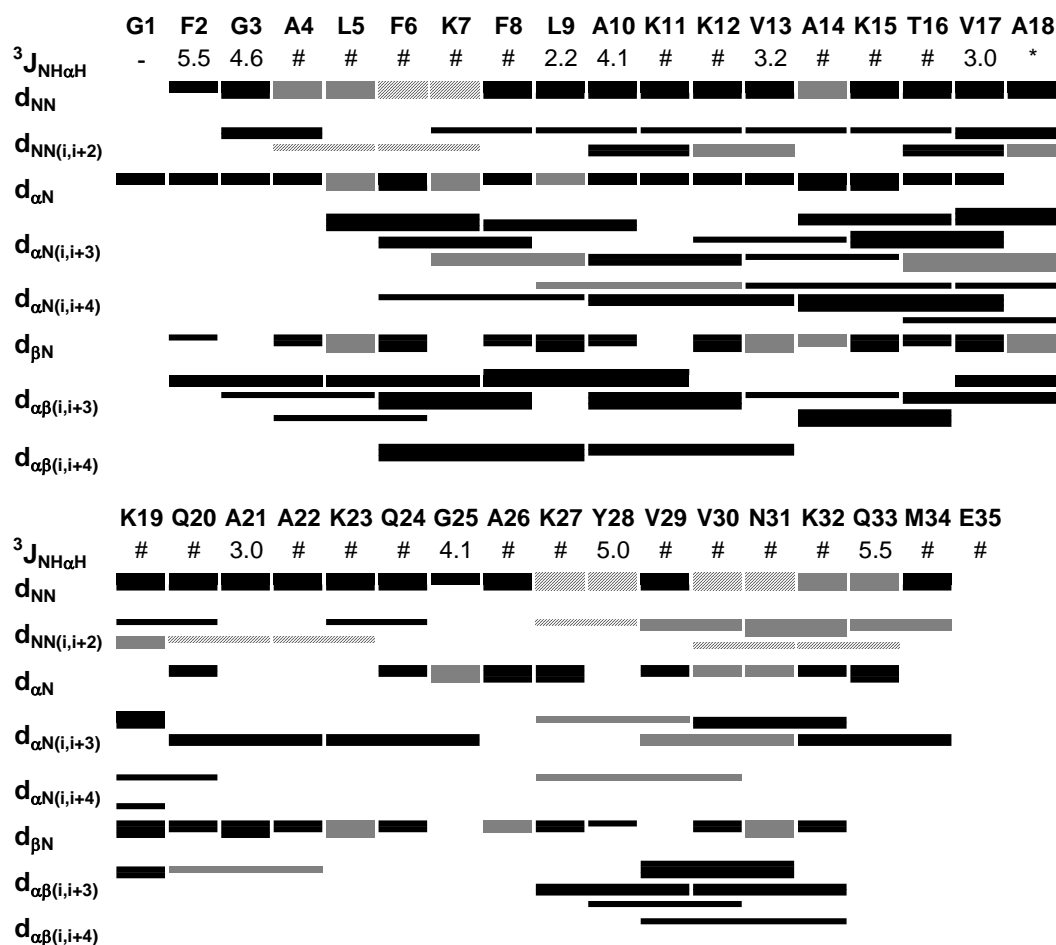
Figure 9.8: A summary of NOEs used in structure calculations for cupiennin 1a in TFE/H$_2$O (1:1 v/v). The thickness of the bars indicate the relative strength of the signal (strong < 3.1 Å, medium 3.1-3.7 Å, weak > 3.7 Å). Grey shaded boxes represent ambiguous NOEs, while striped boxes represent signals too close to the diagonal for clear observation. ^{3}J$_{NH\alpha H}$ values are indicated where possible. * indicates that no coupling constant was detected, while # indicates the coupling constant could not be reliably assigned due to overlap.

9.2.4 Coupling Constants

The ^{3}J$_{NH\alpha H}$ coupling constants as determined from the NH region of the high-resolution 1D ^{1}H spectra are also given in Figure 9.8. The splitting was not resolved for one NH signal, while the majority of the remaining signals were overlapped such that the coupling constants could not be reliably determined. Attempts at measuring the ^{3}J$_{NH\alpha H}$ values from DQF-COSY spectra were also made using the method of Kim and Prestegard [383], however the line-widths were too broad to determine these accurately. Nevertheless, ten ^{3}J$_{NH\alpha H}$ values could be measured, all of which were less than 6 Hz. These values are therefore consistent with α-helical structure.

9.2.5 Structure Calculations

Following assignment of all cross-peaks in the NOESY spectrum of cupiennin 1a according to the methodology described in Chapter 4, the volume of each NOE signal was converted to a distance restraint using the procedure of Nilges *et al.* [384]. This process generated a total of 646 non-redundant distance restraints. Of these, 143 were ambiguous, and were managed by the application of sum-averaging methods. No long-range NOE signals were observed between amino acids greater than five residues apart. This is consistent with a lack of intermolecular association, and hence implies the peptide is monomeric in these conditions. A comparison of the distance restraints for cupiennin 1a resulting after eight iterations of ARIA structure calculations is given in Table 9.3. A total of ten dihedral angle restraints were also employed during the structure calculations.

Table 9.3: Experimental restraints derived from the NOESY spectrum of cupiennin 1a in TFE/H_2O (1:1 v/v).

	Number of Restraints
Sequential NOEs	146
Medium-range NOEs	135
Long-range NOEs	0
Intra-residue NOEs	222
Ambiguous NOEs	143
Total	646

The conclusions derived from examination of NMR spectral data were confirmed by the structural calculations. Sixty final structures were generated by the ARIA RMD and SA protocol, of which the twenty with lowest potential energy were chosen for analysis. Figure 9.9 shows the twenty lowest energy structures of cupiennin 1a in TFE/H_2O, aligned over selected backbone residues. Superimposing the N-terminal helix (residues 3-21) leads to a 'fraying' of the C-terminal helix (residues 28-34). Similarly, superimposing the C-terminal helix causes the N-terminal helix to become indiscriminate. Clearly, cupiennin 1a adopts two well-defined helices, separated by a more flexible hinge region.

(a)

(b)
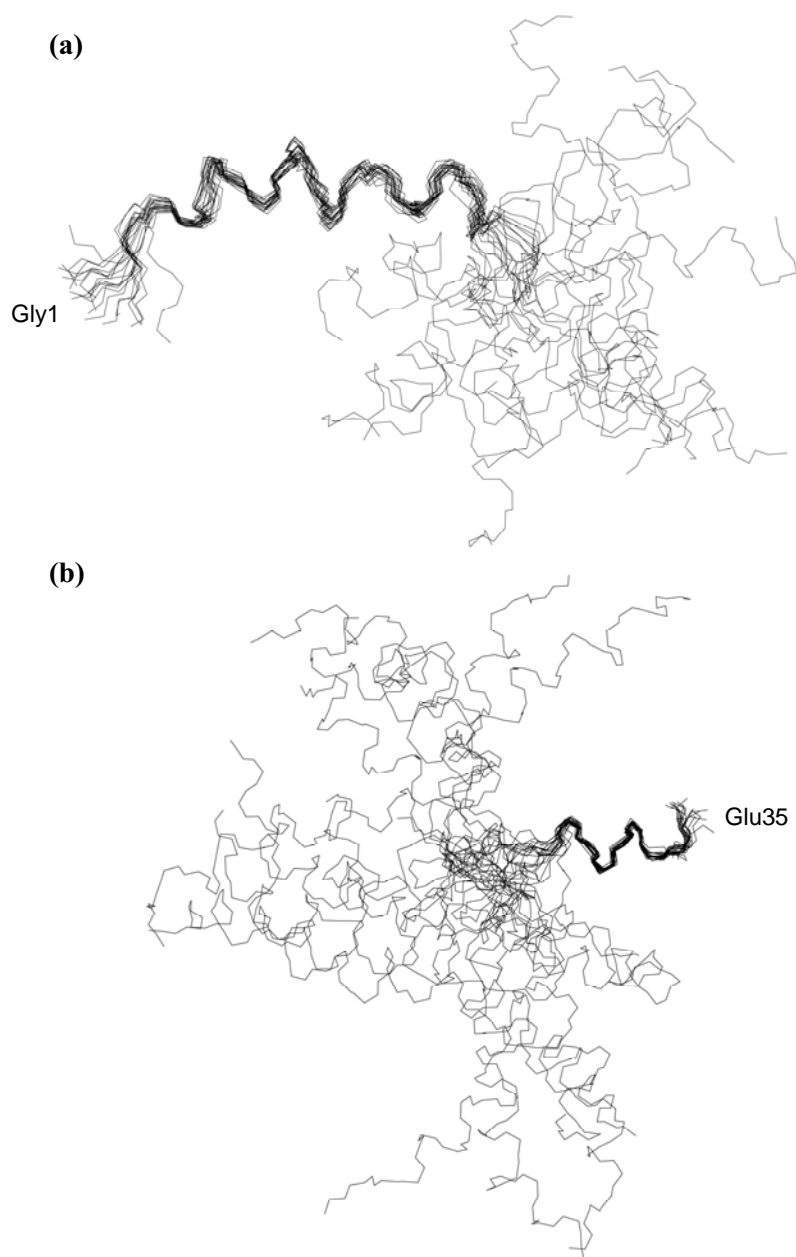
Figure 9.9: 20 most stable calculated structures of cupiennin 1a in TFE/H$_2$O (1:1 v/v), superimposed over the backbone atoms of residues **(a)** 3-21, and **(b)** 28-34.

The extent of structural disorder towards the centre of the molecule is illustrated further in Figure 9.10, which shows the backbone angular order parameters for all residues. Here it can be seen that residues Gly3-Ala21 as well as Tyr28-Lys32 are well-defined (S > 0.9 for both ϕ and ψ), however the remaining residues are poorly defined with low S values, particularly in the vicinity of Gln24.
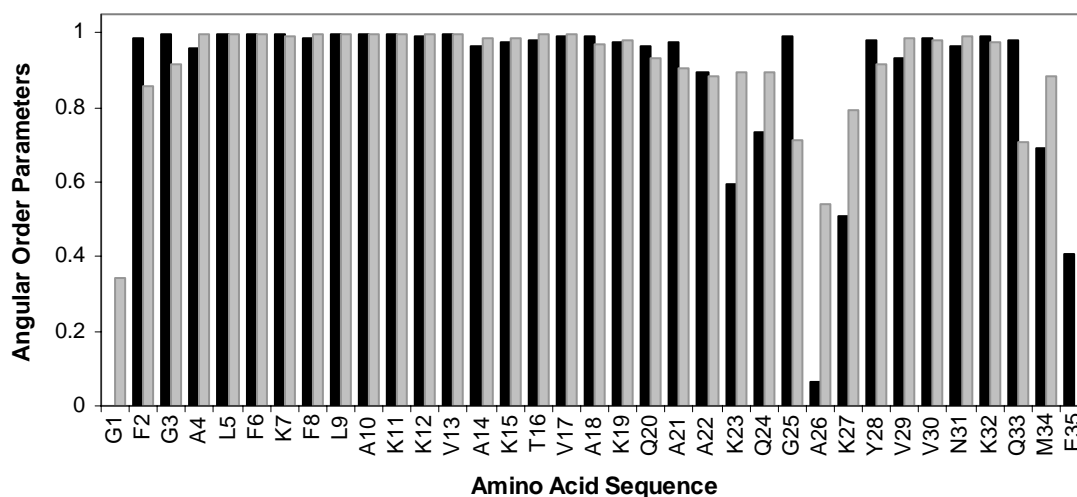
Figure 9.10: Plot of the angular order parameters $S\phi$ (black) and $S\psi$ (grey) for the individual residues of cupiennin 1a in TFE/H$_2$O (1:1 v/v).

A Ramachandran plot of the average ϕ and ψ angles for cupiennin 1a shows that the majority of residues fall within the favoured region for α-helical structure. Residues Phe2, Gln20 and Ala26 are exceptions, with dihedral angles consistent with that of a β-sheet. However, these residues are in regions which are less structured, and hence it is not surprising that there may be some deviation from a helical conformation.
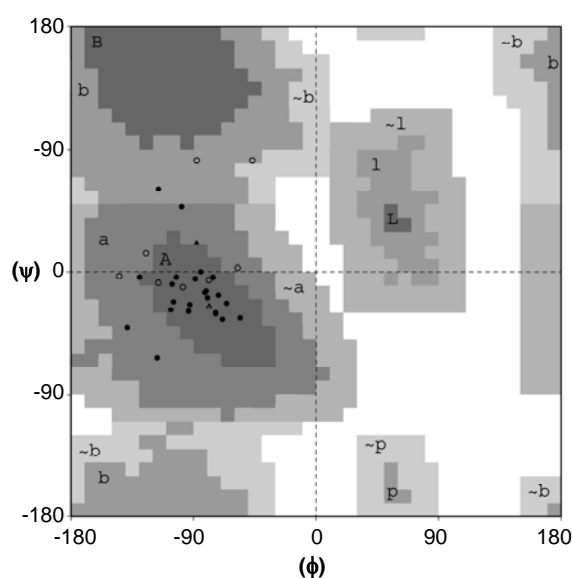
Figure 9.11: Ramachandran plot for cupiennin 1a in TFE/H$_2$O (1:1 v/v). Favourable regions for α-helices are labelled A, allowable and generous regions are labelled a and ~a respectively. Gly residues are indicated by Δ, remaining residues are indicated by $\circ$, and well-defined residues are indicated by filled symbols.

The energy and structural statistics for cupiennin 1a in TFE/H_2O are given in Table 9.4. Final structures demonstrate only minor deviation from idealised covalent geometry ($\leq$ 0.05 Å for bonds, $\leq$ 5° for angles and impropers). Just seven of the distance restraints were violated at greater than 0.3 Å, suggesting the resultant structures adequately satisfy the NMR derived data, and hence are likely to be an accurate representation of this peptide in solution.

Table 9.4: Structural statistics for cupiennin 1a following RMD/SA calculations.

Energies (kcal.mol^{-1})	
E_{total}	25.45 $\pm$ 1.48
E_{bond}	0.38 $\pm$ 0.05
E_{angle}	12.35 $\pm$ 0.33
$E_{improper}$	0.75 $\pm$ 0.09
E_{VDW}	10.62 $\pm$ 1.09
E_{NOE}	1.33 $\pm$ 0.33
E_{cdih}	0.00
Well-defined residues	3-21, 28-32
RMSD from mean geometry (Å)	
Backbone atoms of well-defined residues (3-21)	0.85 $\pm$ 0.27
Heavy atoms of well-defined residues (3-21)	1.34 $\pm$ 0.32
Backbone atoms of well-defined residues (28-32)	0.21 $\pm$ 0.06
Heavy atoms of well-defined residues (28-32)	1.18 $\pm$ 0.46
All backbone atoms	4.27 $\pm$ 1.11
All heavy atoms	5.17 $\pm$ 1.18

RMSD values were calculated for the structure ensemble over the entire peptide, as well as both well-defined regions, and are also given in Table 9.4. The large inconsistency in structures as a result of the flexible hinge region is reflected by particularly high RMSD values over the whole molecule. However, calculating the RMSD for the helical domains only indicates that the structures in this ensemble agree very well with each other over the well-defined regions. This provides further evidence for the model of two rigid helices separated by a flexible linker.

The most energetically stable calculated structure of cupiennin 1a in TFE/H_2O is shown in Figure 9.12. Here the helix-hinge-helix structure is again clearly evident. This representation also shows that the N-terminal helix is amphipathic, with obvious hydrophobic and hydrophilic faces, while the C-terminus is essentially a hydrophilic helix.
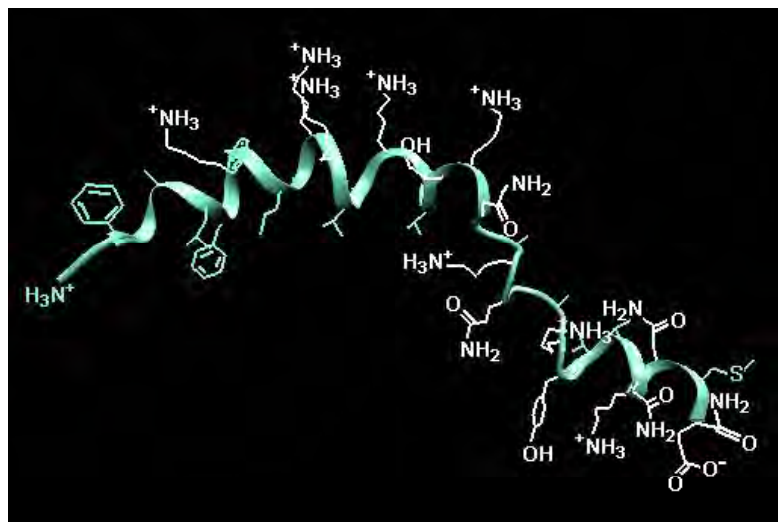
Figure 9.12: The lowest calculated potential energy structure of cupiennin 1a in TFE/H_2O (1:1 v/v). Hydrophobic groups are shown in green and hydrophilic groups in white.

9.2.6 ^{31}P NMR Spectroscopy

The effect of cupiennin 1a on the phospholipid head group behaviour was studied using static ^{31}P solid state NMR spectroscopy. Spectra were collected for unoriented d_{54}-DMPC and d_{54}-DMPC/DMPG (2:1 molar ratio) multilayers, both with and without cupiennin 1a (40:1 lipid/peptide ratio) at 30 ºC. These are displayed in Figure 9.13, where it can be seen that the shapes of the spectra are consistent with the formation of hydrated lipid bilayers, with the phospholipids rotating rapidly about their director axes. This is a good indication that the samples are in fact MLV dispersions [585,724].

Figure 9.13: ^{31}P spectra of unoriented bilayers containing **(a)** d_{54}-DMPC, **(b)** d_{54}-DMPC in the presence of cupiennin 1a (40:1 lipid/peptide ratio), **(c)** d_{54}-DMPC/DMPG, and **(d)** d_{54}-DMPC/DMPG in the presence of cupiennin 1a (40:1 lipid/peptide ratio), each at 30 ºC.

The ^{31}P CSA ($\Delta\sigma$) for d_{54}-DMPC alone is -47 ppm, which is reasonable for a pure lipid multilayer sample [555,585] and consistent with that reported previously for d_{54}-DMPC above the gel to L$_\alpha$ phase transition temperature [608]. $\Delta\sigma$ decreased to -40 ppm upon addition of cupiennin 1a, inferring the head groups are more disordered in the presence of this peptide. This is likely to be a result of the peptide perturbing the packing of the bilayer phospholipids, causing an increase in the average area occupied by each lipid molecule [555].

The single CSA value for d_{54}-DMPC/DMPG bilayers supports a direct interaction between the head groups of these lipids, and no lateral phase separation in this binary lipid mixture over the NMR time scale. The CSA of -39 ppm observed for the d_{54}-DMPC/DMPG sample is much smaller than the CSA of d_{54}-DMPC alone, and is typical of a mixed lipid system. Upon addition of cupiennin 1a, the signal is resolved into two contributing powder patterns resulting from each of the lipid species. Deconvolution of the resulting spectra allows for the CSA of each lipid to be determined independently, with that of DMPG showing a significant decrease as a result of peptide addition. This suggests cupiennin 1a interacts preferentially with the anionic lipids, and gives rise to some degree of phase separation within the bilayer.

A summary of the ^{31}P CSA values for each lipid system is given in Table 9.5.

248

Table 9.5: ^{31}P chemical shift anisotropy values for d_{54}-DMPC and d_{54}-DMPC/DMPG unoriented bilayers, with the addition of cupiennin 1a at a lipid/peptide ratio of 40:1 and 30 °C.

Sample	^{31}P CSA (ppm)	
	Control	**+ Cupiennin 1a**
DMPC Bilayers		
d_{54}-DMPC	-47	-40
Mixed Lipid Bilayers		
d_{54}-DMPC	-39	-41
DMPG	-39	-29

9.2.7 ^{31}P NMR Relaxation Studies

The effect of cupiennin 1a on the motion of the lipid bilayers was monitored by measurement of ^{31}P relaxation rates. Magic angle spinning ($\nu_r \sim 6$ kHz) was employed to give high-resolution spectra. Under these conditions the spectrum of d_{54}-DMPC MLVs contains a single narrow signal at -0.51 ppm, while the individual contributions from d_{54}-DMPC at -0.51 ppm and DMPG at 0.50 ppm are well resolved, and their intensities reflect the molar ratio (i.e. 2:1) of each lipid in the d_{54}-DMPC/DMPG mixture (Figure 9.14). Upon addition of cupiennin 1a at a lipid/peptide ratio of 40:1, there is no change in the number of peaks, or the line shapes and chemical shifts of the NMR signals in either model membrane system, indicating the membrane surface charge density is largely unaffected by peptide binding [420].
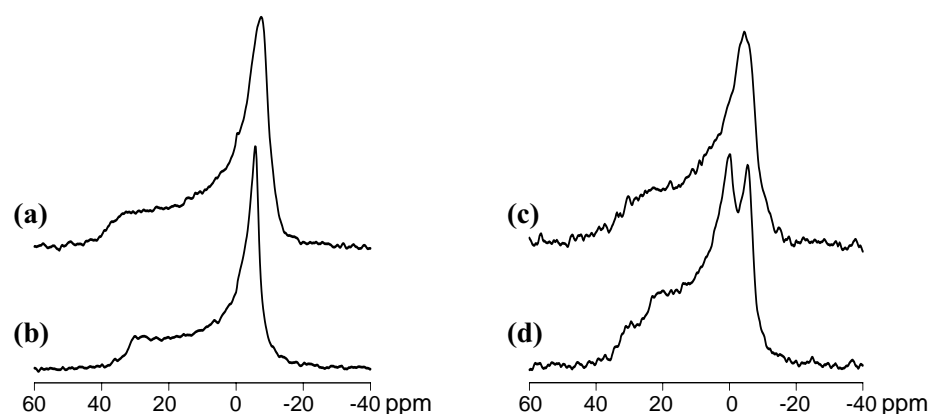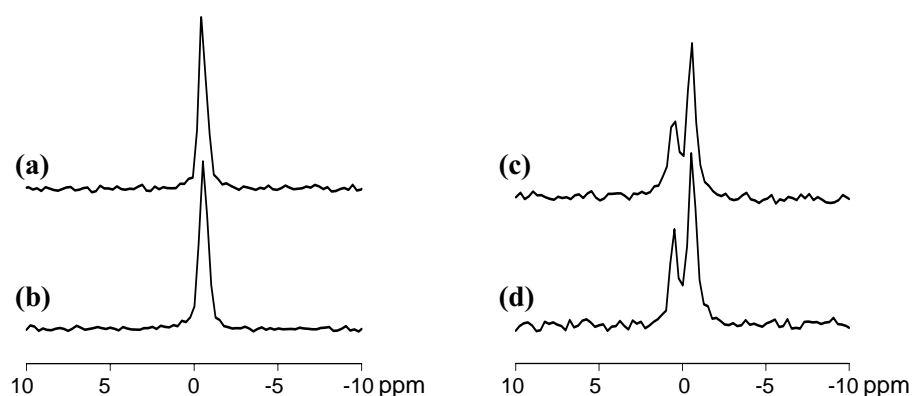

Figure 9.14: Magic angle spinning ^{31}P NMR spectra of unoriented bilayers containing **(a)** d_{54}-DMPC, **(b)** d_{54}-DMPC in the presence of cupiennin 1a (40:1 lipid/peptide ratio), **(c)** d_{54}-DMPC/DMPG, and **(d)** d_{54}-DMPC/DMPG in the presence of cupiennin 1a (40:1 lipid/peptide ratio), each at 30 °C.

Relaxation times were determined by fitting a single exponential to a plot of signal intensity against the decay time τ, for both longitudinal and transverse relaxation experiments. As an example, Figure 9.15 shows the data fitting for the d_{54}-DMPC lipid multilayers.
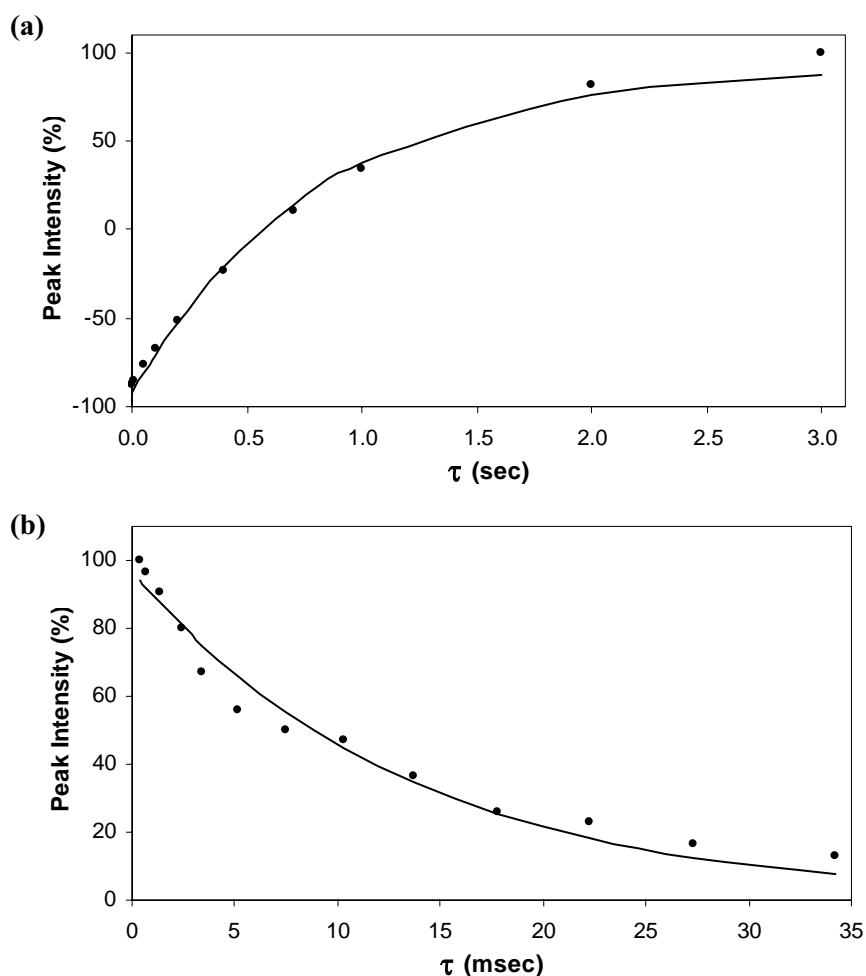
Figure 9.15: ^{31}P NMR **(a)** longitudinal, and **(b)** transverse relaxation measurements for unoriented d_{54}-DMPC lipid bilayers at 30 °C.

Longitudinal relaxation rates are controlled by the availability of molecular vibrations at a relevant frequency (in the order of MHz). Therefore, if T_1 is longer, the peptide is depressing the intensity of motion on this time scale, with the converse also true [615]. Table 9.6 contains T_1 values for the ^{31}P NMR signals in the MAS experiments. Upon addition of cupiennin 1a to d_{54}-DMPC MLVs, the value of T_1 decreases by approximately 11%. However, in the case of the mixed lipid vesicles, addition of cupiennin 1a is associated with slower longitudinal relaxation of both signals, and

moreover the relative change in T_1 is much greater. The difference between relaxation properties of DMPC and mixed lipid multilayers upon peptide addition indicates cupiennin 1a interacts differently with zwitterionic and anionic membrane surfaces, in particular the lipid head groups.

Table 9.6: ^{31}P longitudinal NMR relaxation times for d_{54}-DMPC and d_{54}-DMPC/DMPG lipids, with the addition of cupiennin 1a at a lipid/peptide ratio of 40:1 and 30 ºC.

Sample	[31]P T_1 (ms)		ΔT_1 (ms)	ΔT_1 (%)
	Control	**+ Cupiennin 1a**		
DMPC Bilayers				
d_{54}-DMPC	931	834	-98	-11
Mixed Lipid Bilayers				
d_{54}-DMPC	448	551	103	+23
DMPG	522	679	158	+30

Transverse relaxation measurements of the ^{31}P signal provide insight into the slow molecular motions within the headgroup region of the lipids on the millisecond time scale. In the case of d_{54}-DMPC MLVs, addition of cupiennin 1a caused an increase in the rate of transverse relaxation by approximately 19%. Conversely, upon addition of peptide to the mixed lipid system the T_2 of both lipids increased, albeit to a lesser extent (Table 9.7). Changes to T_2 after the addition of cupiennin 1a confirms the peptide does in fact interact with the surface of both model membranes, and disturbs the slow rate motions of the phospholipid head groups. However, a difference in relaxation properties of the lipids in the presence of cupiennin 1a again indicates the peptide is interacting differently with the neutral and charged membrane surfaces.

Table 9.7: ^{31}P transverse NMR relaxation times for d_{54}-DMPC and d_{54}-DMPC/DMPG lipids, with the addition of cupiennin 1a at a lipid/peptide ratio of 40:1 and 30 ºC.

Sample	^{31}P T$_2$ (ms)		Δ T$_2$ (ms)	Δ T$_2$ (%)
	Control	**+ Cupiennin 1a**		
DMPC Bilayers				
d_{54}-DMPC	13.5	11.0	-2.5	-19
Mixed Lipid Bilayers				
d_{54}-DMPC	4.6	5.3	0.7	+15
DMPG	6.0	6.6	0.6	+10

9.2.8 ^{2}H NMR Spectroscopy

Deuterated DMPC was used to investigate the effects of cupiennin 1a on lipid order and chain mobility. Static ^{2}H NMR spectra were obtained at 30 ºC for both the d_{54}-DMPC and d_{54}-DMPC/DMPG (2:1 molar ratio) phospholipid bilayers in the absence and presence of cupiennin 1a (40:1 lipid/peptide ratio), as shown in Figure 9.16. The spectra consist of superimposed Pake doublets typical of a bilayer forming chain-perdeuterated lipid above its gel to L$_\alpha$ phase transition temperature, with rounding at the outer edges representative of dispersed lipids forming MLVs. The isotropic peak present in these spectra is most likely due to residual deuterium in the buffer component of the samples.
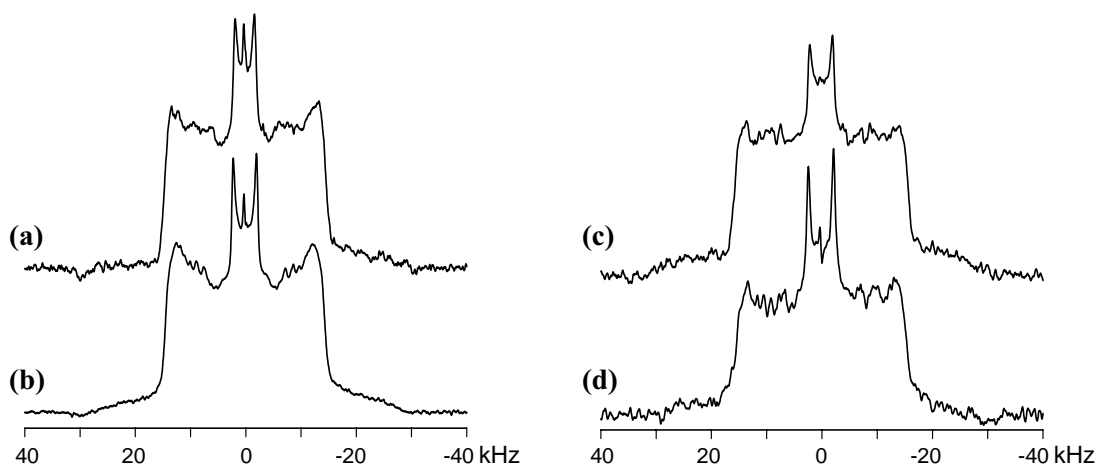
Figure 9.16: ^{2}H NMR spectra of unoriented bilayers containing **(a)** d_{54}-DMPC, **(b)** d_{54}-DMPC in the presence of cupiennin 1a (40:1 lipid/peptide ratio), **(c)** d_{54}-DMPC/DMPG, and **(d)** d_{54}-DMPC/DMPG in the presence of cupiennin 1a (40:1 lipid/peptide ratio), each at 30 ºC.

Further changes to the ^{2}H spectra upon addition of cupiennin 1a suggest the peptide interacts with the lipids in a manner which perturbs the motions of the acyl chains. The order parameters for each C-^{2}H bond were calculated after dePaking the spectra. The broad peaks at the outer edges of the spectra are due to the overlap of the doublets from the deuterons on carbons nearer to the phospholipid head group. No attempt was made to resolve such peaks, and instead these deuterons were assigned a single splitting value. Thus, the assignments are only approximate for some of the deuterium resonances. Order profiles for ^{2}H at different carbon positions along the chain deuterated DMPC are shown in Figure 9.17.
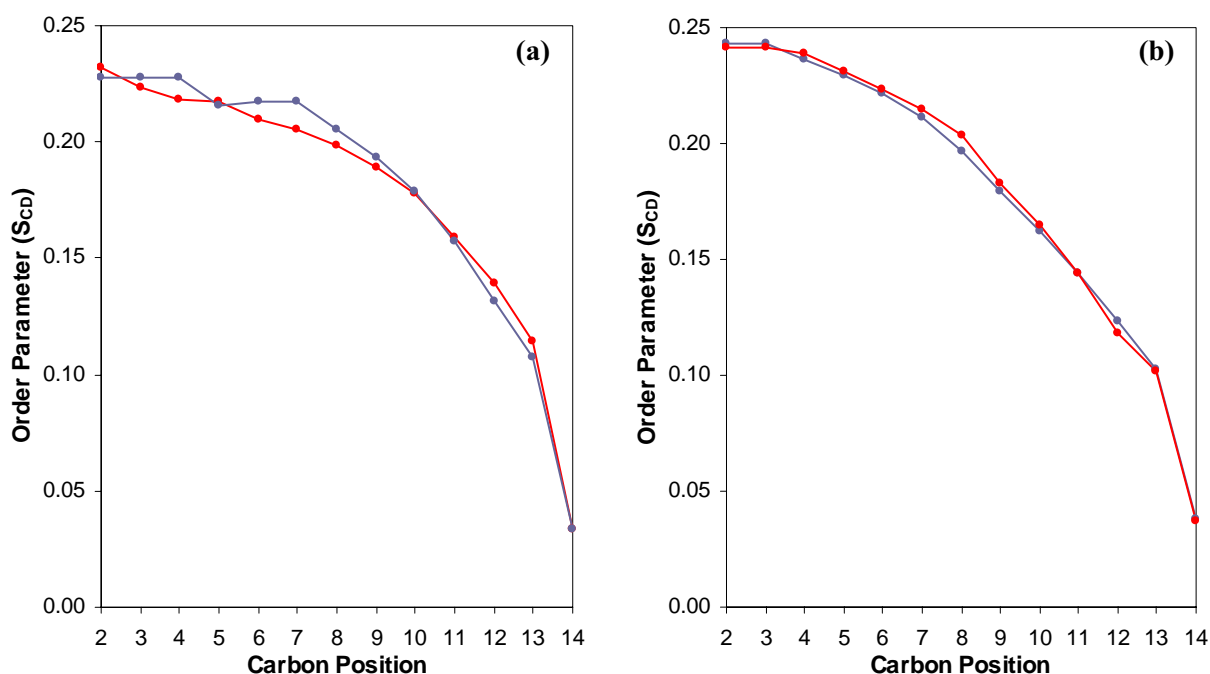
Figure 9.17: Plot of the carbon-deuterium bond order parameters (S_{CD}) against acyl chain carbon position for **(a)** unoriented d_{54}-DMPC bilayers alone (blue), and in the presence of cupiennin 1a (red) at a 40:1 lipid/peptide ratio and 30 °C, and **(b)** unoriented d_{54}-DMPC/DMPG bilayers alone (blue), and in the presence of cupiennin 1a (red) at a 40:1 lipid/peptide ratio and 30 °C.

The extent of ordering slightly decreased along the majority of the acyl chain for d_{54}-DMPC multilayers in the presence of cupiennin 1a, in particular for the region from carbon 3-9, while from C_{11} to the terminal methyl group the chain is slightly more ordered upon addition of peptide. In contrast, the segmental order was affected to a lesser degree by the addition of cupiennin 1a to the d_{54}-DMPC/DMPG system, and in an

opposing manner. A slight reduction in order was noted in the region running from C_3-C_{11}, along with a small ordering effect from C_{11} to the terminal methyl group. The difference in the order parameter changes between the zwitterionic and anionic lipid membranes suggests that the hydrophobic core of the bilayers are affected differently, and that the mechanism by which cupiennin 1a interacts with the lipids is somewhat dissimilar in each system. However, the differences caused by cupiennin 1a are very small, and may not be significant given the errors associated with measurement of the order parameters.

9.2.9 nNOS Activity

Cupiennin 1a was tested for the ability to inhibit nNOS, using an assay that measures the conversion of ^{3}H-arginine to ^{3}H-citrulline by this enzyme. The results of this investigation can be seen in Figure 9.18, where it is evident that cupiennin 1a produces a dose-dependent inhibition of nNOS. From this data, the IC_{50} value and Hill slope are calculated to be 7.2 $\mu g.mL^{-1}$ and 11.8 respectively.
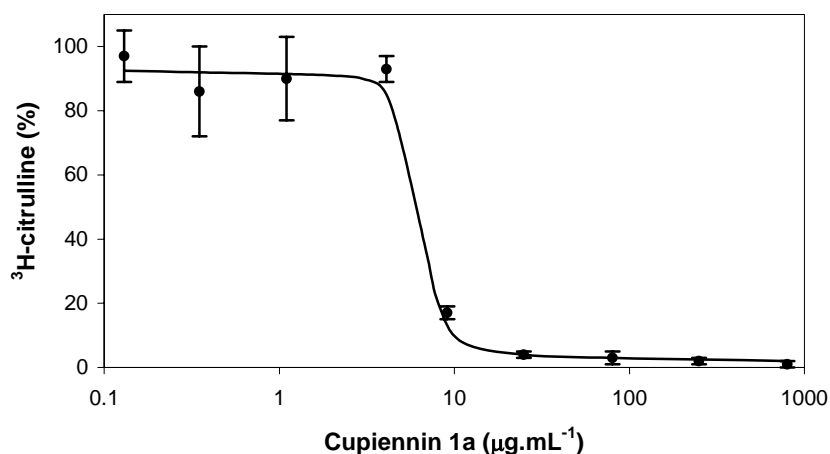
Figure 9.18: Concentration-response curve for the inhibition of nNOS by cupiennin 1a.

To determine if cupiennin 1a is interacting with CaM to inhibit the action of nNOS in a similar manner to that of the amphibian peptides described in Chapter 5, a ^{15}N HSQC titration was performed. Increasing quantities of unlabelled cupiennin 1a were added to ^{15}N labelled Ca_4-CaM, and a high-resolution ^{15}N HSQC spectrum was recorded after each addition. The chemical shift changes were then tracked by overlaying each of the spectra, as can be seen in Figure 9.19. Chemical shift changes were considered to be significant when greater than 0.5 ppm in the nitrogen dimension and greater than 0.05 ppm in the hydrogen dimension [492].
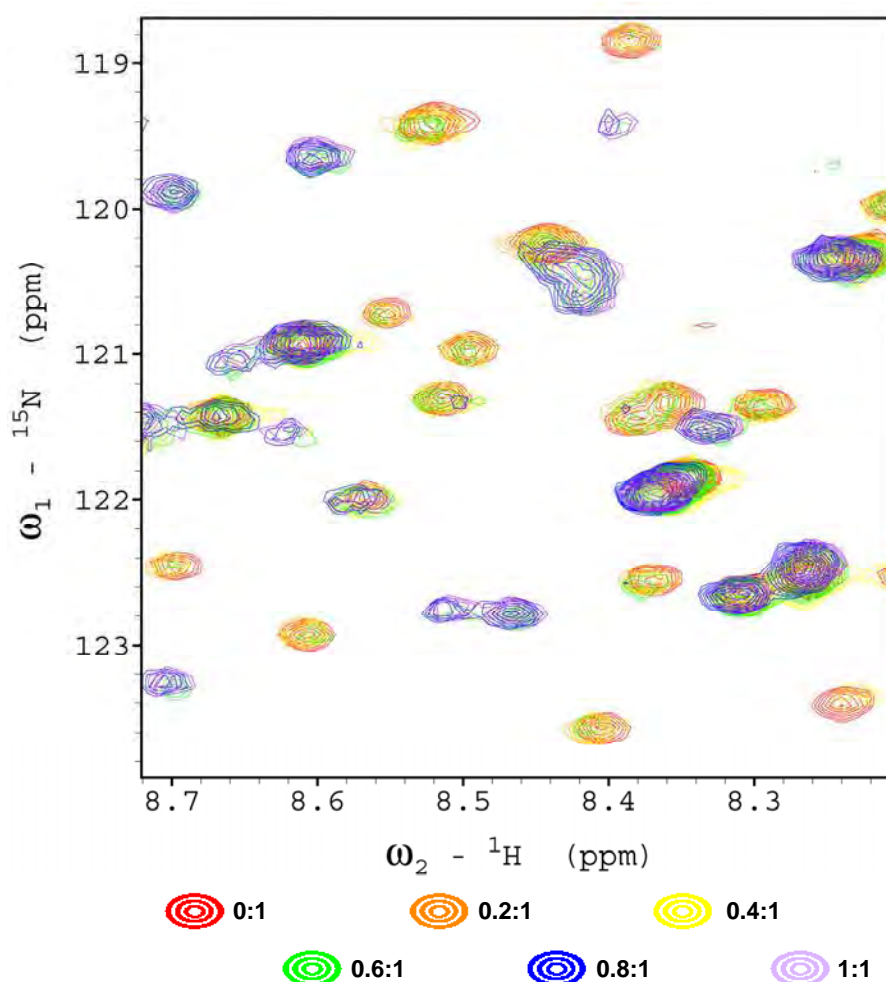
Figure 9.19:   Partial overlaid ^{15}N HSQC spectra for the titration of CaM with cupiennin 1a. The legend is shown below the spectrum, indicating the peptide/protein ratio.

Evidence of complex formation is apparent after addition of only 0.4 equivalents of cupiennin 1a, with the titration series showing distinct chemical shift changes for a significantly large number of residues throughout the CaM sequence. Peak intensities for the bound and unbound conformers at 0.6 equivalents of peptide are comparable, indicating a 1:1 stoichiometry and providing evidence of slow exchange binding. The protein was fully bound and giving rise to a completely new set of chemical shifts at a 1:1 molar concentration, with continued addition of peptide to 2:1 equivalents having no further effect on the chemical shifts (data not shown). The peak intensities for the bound and unbound conformations are approximately equal upon full saturation, further indicating that the complex is stable on the NMR time scale and exists in a slow exchange regime.

9.3 Discussion

9.3.1 Structure Analysis

The cytolytic nature of cupiennin 1a may afford this peptide with a dual role in the venom of *C. salei*, similar to that described for a number of venomous arthropods [136]. Disruption of bacterial cell membranes imparts antibacterial activity, and in turn provides a defensive mechanism capable of preventing infection of the venom apparatus. Similarly, the ability to lyse eukaryote cells facilitates immobilisation of prey, by allowing other venom components improved access to their site of action. The balance between these functions for all of the dual-role peptides depends on specificity of action, and is governed by structural features of the peptide (Section 8.1). In the case of cupiennin 1a, this balance appears to be dominated by the antibacterial effect.

The results of solution NMR studies presented in Sections 9.2.1 through 9.2.5 indicate cupiennin 1a forms a helix-hinge-helix structure in aqueous TFE. TFE acts as a membrane mimicking solvent by promoting the formation of intramolecular hydrogen bonds [34, 35], and therefore it is likely that the structures determined here persist in a bilayer environment. This is further supported by results of previous circular dichroism experiments, which show the peptides are unstructured in aqueous buffer but adopt α-helical structures in the presence of TFE as well as DMPC vesicles [117,741].

Often regions of flexibility in peptides with a helix-hinge-helix motif are initiated by Pro, or less commonly Gly, which are known to disrupt helical structure [698]. While Gly does possess an amide proton available for hydrogen bonding, its small side-chain, consisting of a single proton, allows for increased conformational freedom compared with other residues. Thus, kinks can occur where this amino acid is present, particularly when multiple Gly residues are in close proximity. This is consistent with the role of Gly in globular proteins, where it often facilitates a reversal in the chain direction [742].

In the case of cupiennin 1a, only one Gly residue is present in the hinge region (Gly25). It is likely that this, along with the specific physical interactions between the neighbouring residues (such as steric hindrance, electrostatic and hydrophobic forces) contribute to the disorder noted in the region of residues 22-27. This is further supported by the fact that a number of secondary structure prediction methods, including the GOR method of Garnier *et al.* [117,743], are able to predict an extended structure for this region of cupiennin 1a based on the primary sequence alone.

The N-terminal helix is well-defined over residues 3-21, and as can be seen from Figure 9.12 and the Schiffer-Edmundson projection given in Figure 9.20, this helix exhibits a high degree of amphipathicity, particularly when compared with the molecule overall. In contrast, the C-terminal helix is essentially hydrophilic. As a result, it is likely that each helix has a different functional influence on the antibacterial activity of this peptide. Furthermore, the flexibility imparted by the central hinge would allow each helix to orient independently, thereby enhancing the membrane binding and permeabilising ability of this peptide.
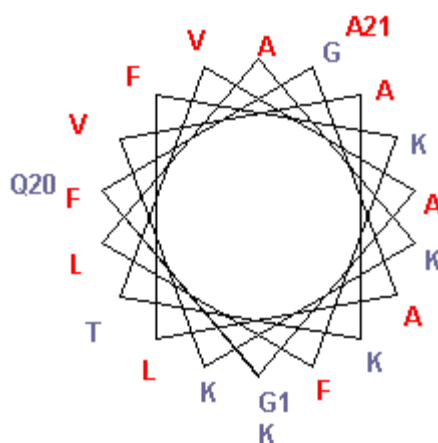
Figure 9.20: Schiffer-Edmundson helical wheel projection of cupiennin 1a, residues 1-21. Hydrophilic residues are coloured blue, while hydrophobic residues are coloured red.

The structure-activity relationship of the cupiennin peptides has been investigated previously by the synthesis and analysis of three truncated cupiennin 1d analogues [741]. Deletion of nine residues at the C-terminus gave a peptide with reduced cationic charge, reduced hydrophilic angle, and increased hydrophobicity, and caused a decrease in antibacterial efficacy, particularly towards Gram-positive bacteria. Additional elimination of the N-terminal pentapeptide entirely negated both the antimicrobial and haemolytic activity. This is consistent with what is now known of the structure of cupiennin 1a. Accordingly, it can be proposed that the cytolytic activity of the cupiennin peptides depends primarily on the amphipathic N-terminus, which is capable of inserting into the membrane, and is modulated by the C-terminus via electrostatic interactions with the cell surface [741].

9.3.2 Antibacterial Activity

The effects of cupiennin 1a on the dynamic properties of lipid membranes were further investigated using ^{31}P and ^{2}H solid state NMR spectroscopy, in two model membrane systems representing prokaryotic (anionic, d_{54}-DMPC/DMPG) and eukaryotic (zwitterionic, d_{54}-DMPC) cells.

The line shapes observed for static ^{31}P NMR spectra indicate that the lipids remain organised in a bilayer structure in the presence of cupiennin 1a, at a lipid/peptide ratio of 40:1 and at 30 °C. However, in neutral model membranes cupiennin 1a appears to have some interaction with the phospholipid head group, since the observed CSA is decreased. This is typically due to an increase in head group disorder, or may also relate to a change in head group environment [585,592,600].

In contrast, the ^{31}P spectra clearly indicate that cupiennin 1a disrupts d_{54}-DMPC/DMPG bilayers into two predominant species. The fact that the CSA of d_{54}-DMPC in the mixed lipid system is not significantly changed, while that of DMPG is drastically reduced, suggests that cupiennin 1a is preferentially interacting with the negatively charged lipids. This is not surprising given the cationic nature of the peptide. Therefore, this phase separation is consistent with the formation of cupiennin 1a/DMPG lateral domains, surrounded by a DMPC-rich, DMPG-depleted lateral bilayer phase.

Furthermore, the higher degree of association with anionic phospholipids implies the interaction of cupiennin 1a with bacterial cell membranes is primarily electrostatic in nature.

^{31}P relaxation data indicate that addition of cupiennin 1a to zwitterionic d_{54}-DMPC lipid bilayers causes a decrease in both longitudinal, and in particular, transverse relaxation times. This suggests that the peptide is enhancing the motion of the lipids, allowing for a more efficient relaxation process to occur. This subtle increase in lipid motion would also result in a slight decrease in ordering for both the lipid head groups and the acyl chains, and therefore agrees well with both the static ^{31}P and ^{2}H solid state data for this system.

T_1 and, to a lesser extent, T_2 are increased upon addition of cupiennin 1a to anionic d_{54}-DMPC/DMPG MLVs for both lipid types. This is presumably caused by a reduction in the fast axis rotational motion of the lipids as a result of peptide binding, and indicates that a strong interaction exists between the peptide and the d_{54}-DMPC/DMPG phospholipid bilayers [606]. Given that the change in relaxation times for d_{54}-DMPC differs in direction depending on the lipid composition of the membrane, it is important to consider the interaction between d_{54}-DMPC and DMPG together. Since electrostatic interactions are clearly involved in binding, it is probable that cupiennin 1a associates with DMPG directly and restricts the head group motion. In turn, the d_{54}-DMPC head group motion is indirectly affected by the interaction between the two lipids [606].

Cupiennin 1a was found to primarily decrease the order of the lipid acyl chains in d_{54}-DMPC MLVs, with a slight increase in order noted towards the bilayer centre. When a peptide is incorporated in the bilayer surface region, it acts as a spacer between the lipid head groups and provides more freedom of movement for the acyl chains, thereby decreasing their order [733,744]. In view of the fact that the disordering effect of cupiennin 1a is not apparent over the entire acyl chain, it appears unlikely for this peptide to adopt a predominant surface orientation in zwitterionic lipids.

For the d_{54}-DMPC/DMPG model membranes, the cupiennin 1a appeared to have negligible effect on the order parameters for each C-^{2}H bond. Since an overall increase in disorder was not observed along the acyl chain, it is again unlikely that the peptide intercalates between the phospholipid head groups at the surface of the bilayer. However, as only the DMPC lipid acyl chains were labelled with deuterium in this study, it may be that the entire picture is not being represented, particularly since cupiennin 1a clearly interacts preferentially with the anionic lipids. It would therefore be of interest to repeat these experiments using chain perdeuterated DMPG, to determine the influence of the peptide on each lipid type in the model membrane. Nevertheless, the ^{2}H solid state spectra again support a different mode of interaction between cupiennin 1a and either the zwitterionic or anionic lipids.

Based on the solution structures calculated in this study, the length of the N-terminal helix of cupiennin 1a is close to 30 Å, which is also the average thickness of a bacterial cell membrane [722]. The length of this helix is therefore sufficient to span the bilayer, and is also consistent with a pore-forming mechanism in which this segment would adopt a transmembrane orientation.

Given the limited data available, it is difficult to provide a detailed description of the mechanism by which cupiennin 1a exerts its cytolytic effects. However, it is clear that this mechanism is subtly different in neutral and charged membranes, and the strong interaction between cupiennin 1a and anionic lipids may account for the observed specificity of this peptide, whereby the antibacterial efficacy is significantly more pronounced than the haemolytic activity. It is proposed that in neutral membranes, the amphipathic N-terminal helix becomes buried within the core of the bilayer, acting as a driving force for pore formation and membrane disruption. In contrast, electrostatic interactions between the polar C-terminal helix and the anionic lipid head groups are expected to significantly disrupt the cell surface. The flexible hinge region of the peptide can allow for the C-terminal portion to remain as an effective anchor at the membrane surface, while the N-terminal domain inserts into the hydrophobic region of the bilayer to form a structured pore.

To obtain more detailed evidence for the mechanism of action of cupiennin 1a, it is necessary to determine the location of the peptide within the membrane. This can be achieved using solid state NMR methods, with ^{15}N labelled peptide in an oriented model membrane system (Section 7.6). Labelling each end of the helix-hinge-helix structure independently would allow for direct observation of the orientation of both N- and C-terminal helices. This could potentially give support for the proposed model of membrane lysis, and the importance of the helix-hinge-helix motif in this peptide.

9.3.3 Inhibition of Nitric Oxide Synthesis

After the secondary structure determination of cupiennin 1a was complete, it became apparent that a marked similarity existed with that of splendipherin and frenatin 3 [72,405,482], despite little sequence homology between the primary structures of these peptides. Since the amphibian peptides are known to be potent nNOS inhibitors, it was decided to test cupiennin 1a for this property. Results of such testing indicate this peptide inhibits nNOS with an IC_{50} value of 7.2 $\mu g.mL^{-1}$. In fact, cupiennin 1a is currently one of the most potent peptide inhibitors of this enzyme identified to date.

The Hill slope calculated from the concentration-response curve for the inhibition of nNOS by cupiennin 1a is 11.8, which is noticeably larger in magnitude compared with those measured for the amphibian peptides described in Chapter 5, and may imply a different mode of inhibition. However, the chemical shift changes occurring in the ^{15}N HSQC spectrum of CaM upon addition of peptide indicate strong binding, with a 1:1 stoichiometry. It can therefore be concluded that it is also via interaction with CaM that cupiennin 1a inhibits nNOS.

Binding of peptides to Ca_4-CaM appears to require the peptide to adopt an amphipathic α-helical conformation. As seen from the NMR solution structure analysis presented here, the N-terminal region of cupiennin 1a demonstrates a propensity to form such a structure. However, in addition to this, electrostatic interactions strongly contribute to binding, and therefore the extent of positive charge has also been related to binding affinity [316,469]. This is consistent with the fact that synthetic analogues of citropin 1.1 that are designed with increased cationic nature demonstrate improved

nNOS inhibition [483]. Due to the particularly large number of Lys residues in cupiennin 1a and an overall charge of +8, it is of no surprise that this peptide binds with high affinity to CaM, and in turn has such a low IC_{50} value for the inhibition of nNOS.

Since the N-terminal helix of cupiennin 1a is clearly more amphipathic than the C-terminus, and also has a greater positive charge, it seems reasonable to postulate that CaM is more likely to bind to this region of the peptide. However, the data presented here does not give any indication as to the kind of fold that CaM adopts during binding with cupiennin 1a. Although the resonances in the CaM spectrum were not assigned, the fact that significant chemical shift changes occur for a relatively large number of signals indicates that a substantial change in conformation occurs upon binding, rather than localised structural differences at the binding interfaces. Further experiments are necessary to investigate the structure of the association complex formed between Ca_4-CaM and cupiennin 1a, and to fully understand the mechanism at work.

The multifaceted activity of cupiennin 1a is no doubt an added benefit for *C. salei*. In addition to the antibacterial properties demonstrated for this family of peptides, the inhibition of nNOS would drastically influence numerous processes which rely on NO as a neurotransmitter. CaM is not only the regulatory protein for the NOS isoforms, but also for calcineurin, other kinase phosphorylating enzymes and adenylate cyclase [745]. Ca_4-CaM is also involved in regulation of the eukaryote cytoskeleton [745], and bacteria have recently been shown to possess NOS enzymes [746,747]. Therefore, the likelihood is that the active cupiennin peptides will interfere with many cellular functions at once, causing maximum inconvenience and deterrence to any attacker or pathogen, and provide rapid immobilisation of prey.

9.4 Experimental Procedures

9.4.1 Solution State NMR Spectroscopy

Cupiennin 1a was provided by Dr Lucia Kuhn-Nentwig, of the University of Bern, Switzerland. The isolation, primary structure determination and subsequent synthesis of this peptide have been described previously [117]. Solution structure studies were carried out in aqueous TFE, with the sample prepared by dissolving cupiennin 1a (5.3 mg, 1.3 μmol) in d_3-TFE/H_2O (1:1 v/v, 0.7 mL), to give a final concentration of 2.0 mM. pH was recorded using a Eutech Cyberscan pH 500 Meter with an AEP 331 glass-body pH probe (183 x 4 mm, thin stem), and measured to be 2.55.

A Varian Inova-600 NMR spectrometer was used for acquisition of all NMR spectra, with a ^{1}H frequency of 600 MHz and a ^{13}C frequency of 150 MHz. Experiments were carried out at 25 ˚C, and referenced to the methylene protons of residual unlabelled TFE (3.918 ppm). Referencing of the ^{13}C dimension of the HSQC spectrum was achieved using the ^{13}CH$_2$ signal of TFE (60.975 ppm). Suppression of the water signal was accomplished using presaturation methods during a 1 second relaxation delay between scans. Gradient methods for suppression were used in the DQF-COSY experiment [507].

High-resolution 1D ^{1}H NMR spectra were acquired for cupiennin 1a in aqueous TFE, with 0.038 Hz per point digital resolution. TOCSY, DQF-COSY and NOESY experiments were collected in the phase sensitive mode. Typically, 64 time-averaged scans were acquired per increment with a total of 200 increments for each experiment, and the FID in t_2 consisting of 2048 data points over a spectral width of 5795.4 Hz. The NOESY spectrum was acquired with a mixing time of 250 ms, while the TOCSY pulse sequence included an 80 ms MLEV-17 spin-lock [361]. The HSQC experiment was recorded with an interpulse delay of $1/2J_{CH}$ = 3.6 ms, corresponding to J_{CH} = 140 Hz. 128 increments, each comprising 64 transients, were acquired over 2048 data points in the directly detected ^{1}H, F_2 dimension. A spectral with of 25641.0 Hz was used in the ^{13}C, F_1 dimension.

2D spectra were processed using VNMR software (VNMRJ, version 1.1D). Data matrices were multiplied by a Gaussian function in both dimensions before zero-filling to 4096 data points prior to Fourier transformation.

9.4.2 Structure Calculations

[1]H resonances in the NOESY spectrum were assigned using Sparky software (version 3.111) and a standard sequential assignment procedure [360]. Each of the cross-peaks was integrated, and the volumes converted to distance restraints using the method of Nilges *et al.* [384]. For each symmetric pair of cross-peaks, the peak of larger volume was used. $J_{NH\alpha H}$ values were measured from the high-resolution 1D ^{1}H NMR spectrum for cupiennin 1a, and dihedral angles were restrained as follows: $^3J_{NH\alpha H} < 5$ Hz, $\phi = -60° \pm 30°$; 5 Hz $< ^3J_{NH\alpha H} < 6$ Hz, $\phi = -60° \pm 40°$. For $^3J_{NH\alpha H}$ values ≥ 6 Hz, ϕ angles were not restrained. The absence of resolved splitting for an NH resonance implies that its $^3J_{NH\alpha H}$ value is < 5 Hz.

Structures were generated from random starting conformations using ARIA (version 1.2) [391] implemented with CNS (version 1.1) [548]. The standard RMD and SA protocol was used as described in Chapter 4, with floating stereospecific assignments implemented [401]. A single ARIA run consisted of eight iterations, using optimised parameters based on those described by Pari *et al.* [549]. In the final iteration, sixty structures were calculated, from which the twenty with lowest potential energy were selected for analysis. 3D structures were viewed using VMD software (version 1.8.2) [550] and the program MOLMOL (version 2k.2) [551].

9.4.3 Solid State NMR Spectroscopy

Phospholipids were purchased from either Avanti Polar Lipids (Alabaster, USA) or Sigma (St. Louis, USA), and used without further purification. Cupiennin 1a (1 mg, 0.26 μmoles) was co-dissolved in a small amount of chloroform/methanol (1:1 v/v) with either d_{54}-DMPC alone or d_{54}-DMPC/DMPG (2:1 molar ratio) to give an overall lipid/peptide molar ratio of 40:1. The solvent was evaporated under a stream of N_2, and

the samples dried under vacuum for several hours to ensure complete solvent removal. The samples were then re-suspended in 52 μL water, and submitted to five cycles of freeze-thawing followed by vortex mixing until a viscous transparent gel was obtained. They were then transferred to a 5mm NMR rotor for MAS experiments, or a 5 mm NMR tube for static analysis. Control samples of d_{54}-DMPC and d_{54}-DMPC/DMPG were prepared in a similar manner without the addition of peptide.

All NMR experiments were performed on a Varian Inova-300 spectrometer, using a 5 mm Doty MAS probe. ^{31}P proton decoupled experiments were carried out at an operating frequency of 121.5 MHz, using a single 90º pulse for excitation, and were referenced to H_3PO_4 (0 ppm). Spectra were recorded at 30 ºC, and typical operating parameters were as follows; 90º pulse duration, 3.8 μs; repetition delay, 2 seconds; sweep width, 62.5 kHz. Generally 12 k scans were recorded for static spectra which were processed with 100 Hz of line broadening.

Deuterium quadrupole echo spectra were recorded at 46.1 MHz over a spectral width of 200 kHz. Typical operating conditions were as follows; 90º pulse, 5 μs; echo spacing, 40 μs; recycle delay, 400 ms; number of data points, 4080; number of scans, 110 k; line broadening, 200 Hz. Deuterium spectra were referenced to D_2O (0 ppm). ^{2}H solid state spectra were dePaked using an algorithm developed by Dr. John Gehman, of the Department of Chemistry, University of Melbourne, based on that described by Sternin *et al*. [596] and Whittal *et al*. [737].

^{31}P longitudinal relaxation times were measured under MAS conditions (4-6 kHz) using the inversion recovery pulse sequence ($\pi - \tau - \pi/2$) with τ values between 0.001 and 3 seconds. Transverse relaxation times were measured with a spin-echo experiment ($\pi/2 - \tau - \pi$) with τ values between 0.171 and 17.1 ms to observe the decay in spectral intensity. Relaxation times were determined by fitting a single exponential to a plot of signal intensity against the decay time τ, using the program Origin (Microcal Software, Inc., version 4.10). Errors are estimated as the root mean square of the fitting of an exponential curve to the experimental data, and are in the order of 10%.

9.4.4 nNOS Bioactivity Testing

nNOS inhibition testing was conducted by the Australian Institute of Marine Science, (Townsville, Queensland). Inhibition was measured and analysed by monitoring the conversion of ^{3}H-arginine to ^{3}H-citrulline by nNOS, using methods reported previously [72].

9.4.5 ^{15}N HSQC Titration

^{15}N labelled CaM was supplied by Dr. Margit Apponyi of the Department of Chemistry, at the University of Adelaide. Details of the bacterial expression and purification of this protein have been described previously [482]. CaM samples used for the titration series contained CaM (3.16 mg, 1.89×10^{-7} moles), potassium chloride (100 mM), calcium chloride (6.2 mM) and 10% D_2O in aqueous solution at pH 6.3. Sodium azide (0.02%) was added as a preservative [505].

Cupiennin 1a (1.44 mg, 3.79×10^{-7} moles) was dissolved in water, adjusted to pH 6.3 using sodium hydroxide, then divided into aliquots such that successive additions would give the desired peptide/CaM ratio as given in Table 9.8. The aliquots were then lyophilised, and the dried peptide portions added to the CaM sample in sequence. pH was re-adjusted back to 6.3 with the addition of small quantities of hydrochloric acid or sodium hydroxide solutions as required.

Table 9.8: Quantities of cupiennin 1a used for titration with CaM.

Step	Cupiennin 1a (mg)	Concentration (mM)	Cupiennin 1a:CaM
1	0	0	0:1
2	0.144	0.076	0.2:1
3	0.288	0.113	0.4:1
4	0.432	0.151	0.6:1
5	0.576	0.189	0.8:1
6	0.720	0.378	1:1
7	1.440	0.756	2:1

Spectra were recorded using a Varian Inova-600 NMR spectrometer, with a ^{1}H frequency of 600 MHz and a ^{13}C frequency of 150 MHz. Experiments were conducted at 25 ˚C, and referenced to DSS at 0 ppm in ^{1}H, while the ^{15}N dimension was centred at 120 ppm. The standard gNhsqc pulse sequence from the VNMR library was used, with 256 increments, each comprising 16 transients, acquired over 2048 data points. A spectral width of 7197.5 Hz was used in the ^{1}H dimension and 2200 Hz in the ^{15}N dimension. Resultant spectra were processed using NMRPipe [506], and viewed with Sparky software (version 3.111).

~ CHAPTER 10 ~

Summary

10.1 *L. caerulea - L. splendida* Hybrids

Interspecific breeding of two species of Australian tree frogs has produced five healthy adult female hybrids. mtDNA and peptide profile analysis confirms the putative hybrids are indeed the offspring of a male *L. caerulea* and female *L. splendida*. Monthly collection of the host-defence skin peptides of all five hybrids over a nine-month period show the peptide profiles to be identical for each hybrid, and invariant over the period of investigation. The peptide profile of the hybrid frogs includes the neuropeptide caerulein, as well as members of the caerin and caeridin peptide families.

The skin secretions of the *L. caerulea - L. splendida* hybrids contain some peptides which are common to only one parent, some which are common to both parents, and three novel peptides not previously identified in any species of amphibian studied to date. Of the novel peptides, caerins 2.6 and 2.7 show narrow-spectrum antibacterial activity against selected Gram-positive bacteria, while caerin 2.6 also demonstrates inhibition of nNOS with an IC_{50} value of 15.8 μM. In addition, caerin 5.1 has been characterised, and shows little sequence homology with any amphibian peptides previously isolated. The role of this peptide in the amphibian skin remains unknown.

The appearance of novel peptides in the hybrids may be due to the inheritance of peptides from parents of populations that to date have not had their skin peptide profiles characterised, or to changes in the regulation of peptide expression. If the latter is in fact the case and novel peptides can be generated by interspecific hybridisation, this is potentially a creative evolutionary pathway.

10.2 Amphibian Peptides and the Binding of Calmodulin

Frogs of the genus *Litoria* typically possess in their glandular secretion at least one peptide that is able to inhibit the formation of NO by the enzyme nNOS. CaM is a protein cofactor required for activation of this enzyme, and it has been assumed for quite some time that the active peptides bind to CaM and induce a conformational change which prevents the association of this cofactor with nNOS. This has been conclusively demonstrated using ESI-MS, which has allowed for the identification of a number of peptide-CaM complexes in the gas phase. In all cases the non-covalent assemblies are formed with a 1:1:4 calmodulin/peptide/Ca^{2+} stoichiometry.

Charge state analysis and H/D exchange experiments suggest CaM undergoes a significant conformational change to a more compact structure upon complex formation, consistent with previous binding models. The relative affinity of representative peptides from each of the three nNOS inhibitor groups was investigated using both competitive binding methods and in source dissociation experiments. Both techniques suggest the order of CaM binding strength is in the order caerin 1.8 > citropin 1.1 (mod. 18) > splendipherin. This correlates well with that observed previously in the solution state, and justifies the use of mass spectrometry for analysis of physiologically relevant systems in the gas phase.

NMR spectroscopy has been employed to further probe the caerin 1.8-CaM complex. Caerin 1.8 was specifically labelled with ^{15}N at the amide positions of residues Val5, Leu6, Ile21 and Ala22, and was shown to adopt a random structure in aqueous solution. The interaction between caerin 1.8 and Ca_4-CaM was monitored by performing a ^{15}N HSQC titration, which confirmed complex formation with a slow exchange binding regime. Marked spectral differences were observed for the labelled residues at the N-terminus of the bound peptide, but not for those at the C-terminus, suggesting only the N-terminal end of caerin 1.8 is directly involved in complex formation with Ca_4-CaM. Furthermore, this region of the peptide appears to undergo a conformational change from random structure to an α-helix upon binding.

Overall, the amphibian peptides appear to bind to CaM in a way that is consistent with previously reported CaM-peptide binding interactions.

10.3 *Crinia* Neuropeptides

Recently a number of small, disulfide-contaning neuropeptides of the signiferin and riparin families have been characterised from the skin secretion of frogs of the *Crinia* genus. Of these, signiferin 1 and riparin 1.1 are both ten residue peptides with similar primary sequences, however appear to have a significantly different spectrum of bioactivity. Although both act at CCK_2 receptors, signiferin 1 is smooth muscle active while riparin 1 is not, and instead causes proliferation of lymphocytes. As a step towards understanding the molecular basis of the biological activity of these peptides, the 3D structures of both signiferin 1 and riparin 1.1 were determined using NMR spectroscopy and RMD calculations, in an aqueous TFE solvent system.

Both signiferin 1 and riparin 1.1 adopt similar β-turn type structures involving residues 5-8, as a result of the structural constraints imparted by the disulfide bridge. Analysis of the dihedral angles suggests both can be classified into the 'open' class of β-turns. Differences in primary structure occur principally in the turn region of the peptides, while a significant variation is also observed in the secondary structure of the N-terminal end. Differences in these 3D structures may be responsible for altered interaction or activation of the CCK_2 receptor, and in turn account for the variation in biological activity noted for signiferin 1 and riparin 1.1.

10.4 Antibiotic Amphibian Peptides

Many frog and toad species have glandular secretions which contain antibiotic peptides, often with a range of differing activity to afford greater protection against one or several bacteria. It is well established that such peptides typically exert their effects by disruption of the bacterial cell membrane, in either a carpet-like or pore forming mechanism. This has been confirmed previously for the peptides maculatin 1.1 and citropin 1.1, both isolated from the skin secretions of Australian frogs of the genus *Litoria*. However, earlier mechanistic studies for these peptides have predominantly utilised zwitterionic lipids, which may not provide an adequate model of the bacterial cell membrane.

In this study DMPG lipids, which are anionic in nature, have been incorporated with DMPC into unoriented lipid bilayers to more accurately represent bacterial cell membranes. The effects of maculatin 1.1 and citropin 1.1 on the dynamic properties of the lipids were then determined using ^{31}P, ^{2}H and ^{15}N solid state NMR spectroscopy in an attempt to further understand their mechanism of action.

Although the peptides are unstructured in water, ^{15}N NMR spectra for both maculatin 1.1 and citropin 1.1 were consistent with the peptides adopting α-helical structures in dry d_{54}-DMPC/DMPG powders. ^{31}P static spectra and relaxation measurements imply a direct interaction between the peptides and the head group region of the lipids, consistent with that observed in neutral membranes. However, this interaction may be more disruptive in anionic lipids as evidenced by the increase in isotropic signal. Furthermore, interpretation of ^{2}H order parameters suggests both maculatin 1.1 and citropin 1.1 have an ordering effect on the lipid acyl chains. This is in direct contrast with previous reports using only zwitterionic lipids.

While both maculatin 1.1 and citropin 1.1 do not appear to insert deeply into neutral DMPC membranes, it is possible that the presence of negative charges in the lipid head group causes a functional change from a surface location to a transmembrane orientation. Further NMR studies using labelled peptides in oriented systems are required in order to better determine the location of the molecules in the bilayer, and confirm the proposed mechanism of action for the cationic amphibian peptides in bacterial cell membranes.

10.5 Cupiennin 1a

The solution structure of the 35 residue, basic antibacterial peptide cupiennin 1a, isolated from the venom of the neotropical wandering spider *Cupiennius salei*, has been investigated in an attempt to shed light on its mechanism of action. Using NMR spectroscopy and RMD calculations, this peptide was found to adopt a helix-hinge-helix structure in the membrane mimicking solvent mixture TFE/H$_2$O. The hinge is thought to play a role in allowing the amphipathic N-terminal helix and polar C-terminal helix

to orient independently upon membrane binding, in order to achieve maximal antibacterial efficacy.

Solid state ^{31}P and ^{2}H NMR was used to further study the effects of cupiennin 1a on the dynamic properties of lipid membranes, using both zwitterionic d_{54}-DMPC and anionic d_{54}-DMPC/DMPG MLVs. In d_{54}-DMPC alone, cupiennin 1a causes a decrease in the ^{31}P CSA indicating some interaction with the lipid head groups, and a decrease in order over the entire acyl chain. In contrast, for the mixed lipid system cupiennin 1a appears to induce lateral separation of the two lipids as evidenced by the ^{31}P spectra, in which the peptide preferentially interacts with DMPG. Little effect was observed on the acyl chain order parameters in the d_{54}-DMPC/DMPG model membranes. Furthermore, ^{31}P NMR relaxation measurements confirm the lipid motions are differentially influenced by cupiennin 1a depending upon the membrane composition.

It is therefore likely that subtle differences exist in the mechanism by which cupiennin 1a causes membrane lysis in either prokaryotic or eukaryotic cells, and may explain the specific spectrum of observed activity. Additional studies are necessary to confirm the orientation of both the N- and C-terminal helices of the helix-hinge-helix motif within lipid bilayers, and glean further information on the mechanism of action of this peptide.

The secondary structure of cupiennin 1a bears significant resemblance to amphibian peptides such as frenatin 3 and splendipherin, which are known to bind to CaM and effect the inhibition of nNOS. Cupiennin 1a was therefore tested for this property, and in addition to its antibacterial activity, was found to potently inhibit the formation of NO by nNOS with an IC$_{50}$ value of 7.2 µg.mL^{-1} and a Hill slope of 11.8. To confirm the inhibitory effect of this peptide was also due to binding of the enzyme cofactor CaM, a ^{15}N HSQC titration was performed in which increasing quantities of unlabelled cupiennin 1a were sequentially added to ^{15}N labelled Ca^{2+}-CaM. This peptide was found to bind in slow exchange with CaM, in a 1:1 stoichiometry. The proportion of residues experiencing significant chemical shift perturbations was large, suggesting that CaM undergoes a considerable conformational transformation upon binding.

10.6 Conclusion

The research presented in this thesis demonstrates the extreme diversity of biologically active peptides isolated from venoms, toxins and host-defence systems, both in structure and in biological function. The use of proteomic approaches and techniques such as mass spectrometry and NMR spectroscopy has given new dimensions to toxinology, substantially increasing the possibilities for understanding and applying this diverse pharmacopeia for the benefit of future generations.

~ REFERENCES ~

1. Wood, W.F., Sollers, B.G., Dragoo, G.A. and Dragoo, J.W. (2002) Volatile components in defensive spray of the hooded skunk, *Mephitis macroura. J. Chem. Ecol.* 28:1865-1870.

2. Lee, N.P. and Arriola, E.R. (1999) Poison ivy, oak, and sumac dermatitis. *West. J. Med.* 171:354-355.

3. Markland, F.S. (1998) Snake venoms and the hemostatic system. *Toxicon.* 36:1749-1800.

4. Rash, L.D. and Hodgson, W.C. (2002) Pharmacology and biochemistry of spider venoms. *Toxicon.* 40:225-254.

5. Rang, H.P., Dale, M.M. and Ritter, J.M. (1995) *Pharmacology. 3rd ed.* Churchill Livingstone, Edinburgh.

6. Frokjaer, S. and Hovgaard, L. (eds.) (2000) *Pharmaceutical Formulation Development of Peptides and Proteins.* Taylor and Francis, London.

7. Zubay, G. (1983) *Biochemistry.* Addison-Wesley, Reading.

8. Elliot, W.H. and Elliot, D.C. (2001) *Biochemistry and Molecular Biology. 2nd ed.* Oxford University Press, Oxford.

9. Campbell, N.A. (1996) *Biology. 4th ed.* Benjamin Cummings Pub. Co., California.

10. Sherwood, L. (1993) *Human Physiology. From Cells to Systems. 2nd ed.* West Pub. Co., Minneapolis.

11. Terry, A., Poulter, L., Williams, D., Nutkins, J., Giovannini, M., Moore, C. and Gibson, B. (1988) The cDNA sequence coding for prepro-PGS (prepro-magainins) and aspects of the processing of this prepro-polypeptide. *J. Biol. Chem.* 263:5745-5751.

12. Boman, H.G. (2000) Innate immunity and the normal microflora. *Immunol. Rev.* 173:5-16.

13. Mann, M. and Jensen, O.N. (2003) Proteomic analysis of post-translational modifications. *Nat. Biotechnol.* 21:255-261.

14. Wold, F. and Moldave, K. (1984) *Post-translational Modifications.* Academic Press, Orlando.

15. Ganz, T. (1994) Biosynthesis of defensins and other antimicrobial peptides. In *Antimicrobial Peptides. Ciba Foundation Symposium 186,* (eds. Marsh, J. and Goode, J.A.) pp. 62-71. John Wiley and Sons, London.

16. Bevins, C.L. and Zasloff, M. (1990) Peptides from frog skin. *Annu. Rev. Biochem.* 59:395-414.

17. Vanhoye, D., Brustion, F., Nicolas, P. and Amiche, M. (2003) Antimicrobial peptides from hylid and ranin frogs originated from a 150-million-year-old ancestral precursor with a conserved signal peptide but hypermutable antimicrobial domain. *Eur. J. Biochem.* 270:2068-2081.

18. Tedford, H.W., Sollod, B.L., Maggio, F. and King, G.F. (2004) Australian funnel-web spiders: Master insecticide chemists. *Toxicon.* 43:601-618.

19. Lazarus, L.H. and Attila, M. (1993) The toad, ugly and venomous, wears yet a precious jewel in his skin. *Prog. Neurobiol.* 41:473-507.

20. Tyler, M.J. (1987) Frog and cane toad skin secretions. In *Toxic Plants and Animals. A Guide for Australia.,* (ed. Covacevich, J.) pp. 329-339. Queensland Museum, Brisbane.

21. Erspamer, V., Erspamer, G.F., Severini, C., Potenza, R.L., Barra, D., Mignogna, G. and Bianchi, A. (1993) Pharmacological studies of 'sapo' from the frog *Phyllomedusa bicolor* skin: A drug used by the Peruvian Matses Indians in shamanic hunting practices. *Toxicon.* 31:1099-1111.

22. Daly, J., Caceres, J., Moni, R., Gusovsky, F., Moos, M., Seamon, K., Milton, K. and Myers, C. (1992) Frog secretions and hunting magic in the upper Amazon: Identification of a peptide that interacts with an adenosine receptor. *Proc. Natl. Acad. Sci.* 89:10960-10963.

23. Erspamer, V. (1994) Bioactive secretions in the amphibian integument. In *Amphibian Biology: The Integument,* (ed. Heatwole, H.) pp. 178-350. Surrey, Beatty and Sons, Chipping Norton.

24. Cei, J.M., Erspamer, V. and Rosechini, M. (1967) Taxonomic and evolutionary significance of biogenic amines and polypeptides occurring in amphibian skin. I. Neotropical *leptodactylid* frogs. *Syst. Zool.* 16:328-342.

25. Cunha Filho, G.A., Schwartz, C.A., Resck, I.S., Murta, M.M., Lemos, S.S., Castro, M.S., Kyaw, C., Pires, J., Osmindo R. and Leite, J.R.S. (2005) Antimicrobial activity of the bufadienolides marinobufagin and telocinobufagin isolated as major components from skin secretion of the toad *Bufo rubescens. Toxicon.* 45:777-782.

26. Daly, J.W. (1998) Thirty years of discovering arthropod alkaloids in amphibian skin. *J. Nat. Prod.* 61:162-172.

27. Erspamer, V. and Melchiorri, P. (1980) Active polypeptides: From amphibian skin to the gastrointestinal tract and brain of mammals. *Trends Pharmacol. Sci.* 1:391-395.

28. Pukala, T.L., Bowie, J.H., Maselli, V.M., Musgrave, I.F. and Tyler, M.J. (2006) Host-defence peptides from the glandular secretions of amphibians: Structure and activity. *Nat. Prod. Rep.* 23:368-393.

29. Mensah-Dwumah, M. and Daly, J.W. (1978) Pharmacological activity of alkaloids from poison-dart frogs (Dendrobatidae). *Toxicon.* 16:189-194.

30. Zasloff, M., Martin, B. and Chen, H. (1988) Antimicrobial activity of synthetic magainin peptides and several analogues. *Proc. Natl. Acad. Sci.* 85:910-913.

31. Zasloff, M. (1987) Magainins, a class of antimicrobial peptides from *Xenopus* skin: Isolation, characterization of two active forms, and partial cDNA sequence of a precursor. *Proc. Natl. Acad. Sci.* 84:5449-5453.

32. Bowie, J.H., Chia, B.C.S. and Tyler, M.J. (1998) Host defence peptides from the skin glands of Australian amphibians: A powerful chemical arsenal. *Pharmacol. News.* 5:16-21.

33. Pouny, Y., Rapaport, D., Mor, A., Nicolas, P. and Shai, Y. (1992) Interaction of antimicrobial dermaseptin and its fluorescently labeled analogues with phospholipid membranes. *Biochem.* 31:12416-12423.

34. Jacob, L.S. and Zasloff, M. (1994) Potential therapeutic applications of magainins and other antimicrobial agents of animal origin. In *Antimicrobial Peptides. Ciba Foundations Symposium 186,* (eds. Marsh, J. and Goode, J.A.) pp. 197-223. John Wiley and Sons, London.

35. Grenard, S. (1994) Frogs and toads. In *Medical Herpetology,* pp. 2-127. Reptiles and Amphibian Magazine, Pottsville.

36. Baker, M.A., Maloy, W.L., Zasloff, M. and Jacob, L.S. (1993) Anticancer efficacy of magainin 2 and analogue peptides. *Cancer Res.* 53:3052-3057.

37. Bannon, A.W., Decker, M.W., Holladay, M.W., Curzon, P., Donnelly-Roberts, D., Puttfarcken, P.S., Bitner, R.S., Diaz, A., Dickenson, A.H., Porsolt, R.D., Williams, M. and Arneric, S.P. (1998) Broad-spectrum, non-opioid analgesic activity by selective modulation of neuronal nicotinic acetylcholine receptors. *Science.* 279:77-80.

38. Anastasi, A., Erspamer, V. and Endean, R. (1968) Isolation and amino acid sequence of caerulein, the active decapeptide of the skin of *Hyla caerulea. Arch. Biochem. Biophys.* 125:57-68.

39. Livermore, D. (2004) Can better prescribing turn the tide of resistance? *Nat. Rev. Microbiol.* 2:73-78.

40. Boman, H.G. (1995) Peptide antibiotics and their role in innate immunity. *Annu. Rev. Immunol.* 13:91-92.

41. Waugh, R.J., Stone, D.J.M., Bowie, J.H., Wallace, J.C. and Tyler, M.J. (1993) Peptides from Australian frogs. The structures of the caerins and caeridins from *Litoria gilleni. J. Chem. Res. (S).* 139:(M)937-961.

42. Stone, D.J.M., Waugh, R.J., Bowie, J.H., Wallace, J.C. and Tyler, M.J. (1993) Peptides from Australian frogs. The structures of the caerins from *Litoria caerulea. J. Chem. Res. (S).* 138:(M)910-936.

43. Cei, J.M. (1985) Taxonomic and evolutionary significance of peptides in amphibian skin. *Peptides.* 6:13-16.

44. Low, B.S. (1972) Evidence from paratoid-gland secretions. In *Evolution in the genus Bufo,* (ed. Blair, W.F.) pp. 244-264. University of Texas Press, Austin.

45. Myers, C.W., Daly, J.W., Garroffo, H.M., Wisnieski, A. and Cover, J.F.J. (1995) Discovery of the Costa Rican poison frog *Dendrobates granuliferus* in sympatry with *Dendrobates pumilo*, and comments on taxonomic use of skin alkaloids. *Am. Mus. Novit.* 3144:1-21.

46. Dessauer, H.C. and Nevo, E. (1969) Geographic variation of blood and liver proteins in cricket frogs. *Biochem. Genet.* 3:171-188.

47. Toledo, R.C. and Jared, C. (1995) Cutaneous granular glands and amphibian venoms. *Comp. Biochem. Physiol. A.* 111:1-29.

48. Dockray, G. and Hopkins, C. (1975) Caerulein secretion by dermal glands in *Xenopus laevis*. *J. Cell Biol.* 64:724-733.

49. Giovannini, M.G., Poulter, L., Gibson, B.W. and Williams, D.H. (1987) Biosynthesis and degradation of peptides derived from *Xenopus laevis* prohormones. *Biochem. J.* 243:113-120.

50. Flucher, B.E., Lenglachner-Bachinger, C., Pohlhammer, K., Adam, H. and Mollay, C. (1986) Skin peptides in *Xenopus laevis* morphological requirements for precursor processing in developing and regenerating granular skin glands. *J. Cell Biol.* 103:2299-2309.

51. Sjoberg, E. and Flock, A. (1976) Innervation of skin glands in the frog. *Cell Tissue Res.* 172:81-91.

52. Erspamer, V., Erspamer, G.F., Mazzanti, G. and Endean, R. (1984) Active peptides in the skins of one hundred amphibian species from Australia and Papua New Guinea. *Comp. Biochem. Physiol. C.* 77:99-108.

53. Roseghini, M., Erspamer, W. and Endean, R. (1976) Indole-, imidazole- and phenyl-alkylamines in the skin of one hundred amphibian species from Australia and Papua New Guinea. *Comp. Biochem. Physiol. C.* 54:31-43.

54. Campbell, A. (ed.) (1999) *Declines and Disappearances of Australian Frogs.* Biodiversity Group, Environment Australia, Canberra.

55. Gibson, B.W., Poulter, L., Williams, D.H. and Maggio, J.E. (1986) Novel peptide fragments originating from PGLa and the caerulein and xenopsin precursors from *Xenopus laevis*. *J. Biol. Chem.* 261:5341-5349.

56. Tyler, M.J., Stone, D.J.M. and Bowie, J.H. (1992) A novel method for the release and collection of dermal, glandular secretions from the skin of frogs. *J. Pharm. Toxicol. Methods.* 28:199-200.

57. Barker, J., Grigg, G.C. and Tyler, M.J. (1995) *A Field Guide to Australian Frogs.* Surrey Beatty and Sons, Chipping Norton.

58. Apponyi, M.A., Pukala, T.L., Brinkworth, C.S., Maselli, V.M., Bowie, J.H., Tyler, M.J., Booker, G.W., Wallace, J.C., Carver, J.A., Separovic, F., Doyle, J. and Llewellyn, L.E. (2004) Host-defence peptides of Australian anurans: structure, mechanism of action and evolutionary significance. *Peptides.* 25:1035-1054.

59. Rozek, T., Wegener, K.L., Bowie, J.H., Olver, I.N., Carver, J.A., Wallace, J.C. and Tyler, M.J. (2000) The antibiotic and anticancer active aurein peptides from the Australian bell frogs *Litoria aurea* and *Litoria raniformis*. The solution structure of aurein 1.2. *Eur. J. Biochem.* 267:5330-5341.

60. Wabnitz, P.A., Bowie, J.H., Tyler, M.J., Wallace, J.C. and Smith, B.P. (2000) Differences in the skin peptides of the male and female Australian tree frog *Litoria splendida* - the discovery of the aquatic male sex pheromone splendipherin, together with Phe8 caerulein and a new antibiotic peptide caerin 1.10. *Eur. J. Biochem.* 267:269-275.

61. Steinborner, S.T., Waugh, R.J., Bowie, J.H. and Tyler, M.J. (1997) New caerin antibacterial peptides from the skin glands of the Australian tree frog *Litoria xanthomera*. 2. Sequence determination using mass spectrometry and associated techniques. *Rapid Commun. Mass Spectrom.* 11:997-1000.

62. Steinborner, S.T., Waugh, R.J., Bowie, J.H., Wallace, J.C., Tyler, M.J. and Ramsay, S.L. (1997) New caerin antibacterial peptides from the skin glands of the Australian tree frog *Litoria xanthomera*. *J. Pept. Sci.* 3:181-185.

63. Steinborner, S.T., Currie, G.J., Bowie, J.H., Wallace, J.C. and Tyler, M.J. (1998) New antibiotic caerin 1 peptides from the skin secretion of the Australian tree frog *Litoria chloris* - comparison of the activities of the caerin 1 peptides from the genus *Litoria*. *Int. J. Peptide Protein Res.* 51:121-126.

64. Brinkworth, C.S., Bowie, J.H., Tyler, M.J. and Wallace, J.C. (2002) A comparison of the host defence skin peptides of the New Guinea tree frog (*Litoria genimaculata)* and the fringed tree frog (*Litoria eucnemis*). The link between the caerin and the maculatin antimicrobial peptides. *Aust. J. Chem.* 55:605-610.

65. Wegener, K.L., Wabnitz, P.A., Carver, J.A., Bowie, J.H., Chia, B.C.S., Wallace, J.C. and Tyler, M.J. (1999) Host defence peptides from the skin glands of the Australian Blue Mountains tree frog *Litoria citropa*. Solution structure of the antibacterial peptide citropin 1.1. *Eur. J. Biochem.* 265:627-637.

66. Pukala, T.L., Bertozzi, T., Donnellan, S.C., Bowie, J.H. and Tyler, M.J. (2006) Host-defence peptide profiles of the skin secretions of interspecific hybrid tree frogs and their parents, female *Litoria splendida* and male *Litoria caerulea*. *FEBS J.* 273:3511-3519.

67. Wegener, K.L., Brinkworth, C.S., Bowie, J.H., Wallace, J.C. and Tyler, M.J. (2001) Bioactive dahlein peptides from the skin secretions of the Australian aquatic frog *Litoria dahlii*: Sequence determination by electrospray mass spectrometry. *Rapid Commun. Mass Spectrom.* 15:1726-1734.

68. Raftery, M.J., Bradford, A.M., Bowie, J.H., Wallace, J.C. and Tyler, M.J. (1993) Peptides from Australian frogs - the structures of the dynastins from the banjo frogs *Limnodynastes interioris*, *Limnodynastes dumerilii* and *Limnodynastes terraereginae*. *Aust. J. Chem.* 46:833-842.

69. Bradford, A.M., Raftery, M.J., Bowie, J.H., Wallace, J.C. and Tyler, M.J. (1993) Peptides from Australian frogs - the structures of the dynastins from *Limnodynastes salmini* and fletcherin from *Limnodynastes fletcheri*. *Aust. J. Chem.* 46:1235-1244.

70.   Wabnitz, P.A., Bowie, J.H., Wallace, J.C. and Tyler, M.J. (1999) Peptides from the skin glands of the Australian buzzing tree frog *Litoria electrica*. Comparison with the skin peptides of the red tree frog *Litoria rubella*. *Aust. J. Chem.* 52:639-645.

71.   Waugh, R.J., Raftery, M.J., Bowie, J.H., Wallace, J.C. and Tyler, M.J. (1996) The structures of the frenatin peptides from the skin secretions of the giant tree frog, *Litoria infrafrenata*. *J. Pept. Sci.* 2:117-124.

72.   Doyle, J., Llewellyn, L.E., Brinkworth, C.S., Bowie, J.H., Wegener, K.L., Rozek, T., Wabnitz, P.A., Wallace, J.C. and Tyler, M.J. (2002) Amphibian peptides that inhibit neuronal nitric oxide synthase: The isolation of lesueurin from the skin secretion of the Australian stony creek frog *Litoria lesueuri*. *Eur. J. Biochem.* 269:100-109.

73.   Rozek, T., Waugh, R.J., Steinborner, S.T., Bowie, J.H., Tyler, M.J. and Wallace, J.C. (1998) The maculatin peptides from the skin glands of the tree frog *Litoria genimaculata* - a comparison of the structures and antibacterial activities of maculatin 1.1 and caerin 1.1. *J. Peptide Sci.* 4:111-115.

74.   Steinborner, S.T., Wabnitz, P.A., Waugh, R.J., Bowie, J.H., Gao, C.W., Tyler, M.J. and Wallace, J.C. (1996) The structures of new peptides from the Australian red tree frog *Litoria rubella* - the skin peptide profile as a probe for the study of evolutionary trends of amphibians. *Aust. J. Chem.* 49:955-963.

75.   Steinborner, S.T., Gao, C.W., Raftery, M.J., Waugh, R.J., Blumenthal, T., Bowie, J.H., Wallace, J.C. and Tyler, M.J. (1994) The structures of four tryptophyllin and three rubellidin peptides from the Australian red tree frog *Litoria rubella*. *Aust. J. Chem.* 47:2099-2108.

76.   Maselli, V.M., Bilusich, D., Bowie, J.H. and Tyler, M.J. (2006) Host-defence skin peptides of the Australian streambank froglet *Crinia riparia*: Isolation and sequence determination by positive and negative ion electrospray mass spectrometry. *Rapid Commun. Mass Spectrom.* 20:797-803.

77.   Brinkworth, C.S., Bowie, J.H., Bilusich, D. and Tyler, M.J. (2005) The rothein peptides from the skin secretion of Roth's tree frog *Litoria rothii*. Sequence determination using positive and negative ion electrospray mass spectrometry. *Rapid Commun. Mass Spectrom.* 19:2716-2724.

78.   Maselli, V.M., Brinkworth, C.S., Bowie, J.H. and Tyler, M.J. (2004) Host-defence skin peptides of the Australian common froglet *Crinia signifera*: Sequence determination and negative ion electrospray mass spectra. *Rapid Commun. Mass Spectrom.* 18:2155-2161.

79.   Bradford, A.M., Raftery, M.J., Bowie, J.H., Tyler, M.J., Wallace, J.C., Adams, G.W. and Severini, C. (1996) Novel uperin peptides from the dorsal glands of the Australian floodplain toadlet *Uperoleia inundata*. *Aust. J. Chem.* 49:475-484.

80.   Bowie, J.H., Wegener, K.L., Chia, B.C.S., Wabnitz, P.A., Carver, J.A., Tyler, M.J. and Wallace, J.C. (1999) Host defence antibacterial peptides from skin secretions of Australian amphibians. The relationship between structure and activity. *Protein Pept. Lett.* 6:259-269.

81.   VanCompernolle, S.E., Taylor, R.J., Oswald-Richter, K., Jiang, J., Youree, B.E., Bowie, J.H., Tyler, M.J., Conlon, J.M., Wade, D., Aiken, C., Dermody, T.S., KewalRamani, V.N., Rollins-Smith, L.A. and Unutmaz, D. (2005) Antimicrobial peptides from amphibian skin potently inhibit human immunodeficiency virus infection and transfer of virus from dendritic cells to T cells. *J. Virol.* 79:11598-11606.

82.   Woodhams, D., Rollins-Smith, L., Carey, C., Reinert, L., Tyler, M. and Alford, R. (2006) Population trends associated with skin peptide defenses against chytridiomycosis in Australian frogs. *Oecologia.* 146:531-540.

83.   Zetler, G. (1985) Caerulein and its analogues: Neuropharmacological properties. *Peptides.* 6:33-46.

84.   Erspamer, V. and Melchiorri, P. (1983) Actions of amphibian skin peptides on the central nervous system and anterior pituitary. In *Neuroendocrine Perspectives,* (eds. Muller, E.E. and MacLeod, R.M.) pp. 37-106. Elsevier, Amsterdam.

85.   Wabnitz, P.A., Bowie, J.H., Tyler, M.J., Wallace, J.C. and Smith, B.P. (1999) Animal behaviour - aquatic sex pheromone from a male tree frog. *Nature.* 401:444-445.

86.   Waugh, R.J., Stone, D.J.M., Bowie, J.H., Wallace, J.C. and Tyler, M.J. (1993) Peptides from Australian frogs. Structures of the caeridins from *Litoria caerulea*. *J. Chem. Soc. Perkin Trans.* 1:573-576.

87.   Nutkins, J.C. and Williams, D.H. (1989) Identification of highly acidic peptides from processing of the skin prepropeptides of *Xenopus laevis*. *Eur. J. Biochem.* 181:97-102.

88.   Platnick, N.I. (1997) *Advances in Spider Taxonomy, 1992–1995: With Redescriptions 1940–1980.* New York Entomological Society and The American Museum of Natural History, New York.

89.   King, G.F. (2004) The wonderful world of spiders: Preface to the special Toxicon issue on spider venoms. *Toxicon.* 43:471-475.

90.   Minton, S.A. (1974) *Venom Diseases.* Thomas Pub., Springfield.

91.   Bettini, S. and Brignoli, P.M. (1978) Review of the spider families. In *Handbook of Experimental Pharmacology 48. Arthropod Venoms,* (ed. Bettini, S.) pp. 101-120. Springer-Verlag, New York.

92.   Foelix, R.F. (1982) *Biology of Spiders.* Harvard University Press, Cambridge.

93.   Corzo, G. and Escoubas, P. (2003) Pharmacologically active spider peptide toxins. *Cell. Mol. Life Sci.* 60:2409-2426.

94.   Escoubas, P., Diochot, S. and Corzo, G. (2000) Structure and pharmacology of spider venom neurotoxins. *Biochimie.* 82:893-907.

95.   Kuhn-Nentwig, L., Schaller, J. and Nentwig, W. (2004) Biochemistry, toxicology and ecology of the venom of the spider *Cupiennius salei* (Ctenidae). *Toxicon.* 43:543-553.

96.   Grishin, E. (1999) Polypeptide neurotoxins from spider venoms. *Eur. J. Biochem.* 264:276-280.

97. Grishin, E.V. (1998) Black widow spider toxins: The present and the future. *Toxicon.* 36:1693-1701.

98. Jackson, J.R.H., Krapcho, K.J., Johnson, J.H. and Kral, R.M. (1993) Insecticidally effective spider toxin. *USA Patent No. 5457178.*

99. Jackson, J.R.H., DelMar, E., Johnson, J.H. and Kral, R.M. (1998) Insecticidally effective peptides isolatable from *Phidippus* spider venom. *USA Patent No. 5756459.*

100. Oerke, E. (1994) Estimated crop losses due to pathogens, animal pests and weeds. In *Crop Production and Crop Protection - Estimated Losses in Major Food and Cash Crops.,* (eds. Oerke, E., Dehne, H., Schonbeck, R. and Weber, A.) pp. 72-78. Elsevier, Amsterdam.

101. Gratz, N.G. (1999) Emerging and resurging vector-borne diseases. *Annu. Rev. Entomol.* 44:51-75.

102. Mueller, A.L., Artman, L.D., Balandrin, M.F., Brady, E., Chien, Y., Delmar, E.G., George, K., Kierstead, A., Marriott, T.B., Moe, S.T., Newman, M.K., Raszkiewicz, J.L., Sanguinetti, E.L., VanWagenen, B.C. and Wells, D. (1999) NPS 1506, a novel NMDA receptor antagonist and neuroprotectant: Review of preclinical and clinical studies. *Ann. N.Y. Acad. Sci.* 890:450-457.

103. Malli, H., Kuhn-Nentwig, L., Imboden, H., Moon, M. and Wyler, T. (2000) Immunocytochemical localization and secretion process of the toxin CSTX-1 in the venom gland of the wandering spider *Cupiennius salei* (Araneae: Ctenidae). *Cell Tissue Res.* 299:417-426.

104. Barth, F.G. (2002) *A Spiders World. Senses and Behaviour.* Springer-Verlag, Berlin.

105. Boeve, J., Kuhn-Nentwig, L., Keller, S. and Nentwig, W. (1995) Quantity and quality of venom released by a spider (*Cupiennius salei*, Ctenidae). *Toxicon.* 33:1347-1357.

106. Malli, H., Kuhn-Nentwig, L., Imboden, H. and Nentwig, W. (1999) Effects of size, motility and paralysation time of prey on the quantity of venom injected by the hunting spider *Cupiennius salei*. *J. Exp. Biol.* 202:2083-2089.

107. Meadows, P.E. and Russell, F.E. (1970) Milking of arthropods. *Toxicon.* 8:311-312.

108. Bascur, L., Yevenes, I. and Adrian, H. (1980) An electric method to obtain *Loxosceles* spider venom. *Toxicon.* 18:224.

109. Smith, C.W. and Micks, D.W. (1968) A comparative study of the venom and other components of three species of *Loxosceles*. *Am. J. Trop. Med. Hyg.* 17:651-656.

110. Escoubas, P. and Rash, L. (2004) Tarantulas: Eight-legged pharmacists and combinatorial chemists. *Toxicon.* 43:555-574.

111. Quistad, G.B. and Skinner, W.S. (1994) Isolation and sequencing of insecticidal peptides from the primitive hunting spider, *Plectreurys tristis* (Simon). *J. Biol. Chem.* 269:11098-11101.

112. Sheumack, D.D., Claassens, R., Whiteley, N.M. and Howden, M.H.H. (1985) Complete amino acid sequence of a new type of lethal neurotoxin from the venom of the funnel-web spider *Atrax robustus*. *FEBS Lett.* 181:154-156.

113. Brown, M.R., Sheumack, D.D., Tyler, M.I. and Howden, M.E.H. (1988) Amino acid sequence of versutoxin, a lethal neurotoxin from the venom of the funnel-web spider *Atrax vertusus*. *Biochem. J.* 250:401-401.

114. Adams, M.E., Bindokas, V.P., Hasegawa, L. and Venema, V.J. (1990) Omega-agatoxins: Novel calcium channel antagonists of two subtypes from funnel-web spider (*Agelenopsis aperta*) venom. *J. Biol. Chem.* 265:861-867.

115. Skinner, W.S., Adams, M.E., Quistad, G.B., Kataoka, H., Cesarin, B.J., Enderlin, F.E. and Schooley, D.A. (1989) Purification and characterization of two classes of neurotoxins from the funnel web spider, *Agelenopsis aperta*. *J. Biol. Chem.* 264:2150-2155.

116. Kuhn-Nentwig, L., Schaller, J. and Nentwig, W. (1994) Purification of toxic peptides and the amino acid sequence of CSTX-1 from the multicomponent venom of *Cupiennius salei* (Araneae: Ctenidae). *Toxicon.* 32:287-302.

117. Kuhn-Nentwig, L., Müller, J., Schaller, J., Walz, A., Dathe, M. and Nentwig, W. (2002) Cupiennin 1, a new family of highly basic antimicrobial peptides in the venom of the spider *Cupiennius salei* (Ctenidae). *J. Biol. Chem.* 277:11208-11216.

118. Stapleton, A., Blankenship, D.T., Ackermann, B.L., Chen, T.M., Gorder, G.W., Manley, G.D., Palfreyman, M.G., Coutant, J.E. and Cardin, A.D. (1990) Curtatoxins. Neurotoxic insecticidal polypeptides isolated from the funnel-web spider *Hololena curta*. *J. Biol. Chem.* 265:2054-2059.

119. Sutton, K.G., Siok, C., Stea, A., Zamponi, G.W., Heck, S.D., Volkmann, R.A., Ahlijanian, M.K. and Snutch, T.P. (1998) Inhibition of neuronal calcium channels by a novel peptide spider toxin, DW13.3. *Mol. Pharmacol.* 54:407-418.

120. Swartz, K.J. and MacKinnon, R. (1995) An inhibitor of the Kv2.1 potassium channel isolated from the venom of a Chilean tarantula. *Neuron.* 15:941-949.

121. Suchyna, T.M., Johnson, J.H., Hamer, K., Leykam, J.F., Gage, D.A., Clemo, H.F., Baumgarten, C.M. and Sachs, F. (2000) Identification of a peptide toxin from *Grammostola spatulata* spider venom that blocks cation-selective stretch-activated channels. *J. Gen. Physiol.* 115:583-598.

122. Sanguinetti, M.C., Johnson, J.H., Hammerland, L.G., Kelbaugh, P.R., Volkmann, R.A., Saccomano, N.A. and Mueller, A.L. (1997) Heteropodatoxins: Peptides isolated from spider venom that block Kv4.2 potassium channels. *Mol. Pharmacol.* 51:491-498.

123. Zhou, P., Xie, X., Li, M., Yang, D., Xie, Z., Zong, X. and Liang, S. (1997) Blockade of neuromuscular transmission by huwentoxin-I, purified from the venom of the Chinese bird spider *Selenocosmia huwena*. *Toxicon.* 35:39-45.

124. Peng, K., Shu, Q., Liu, Z. and Liang, S. (2002) Function and solution structure of huwentoxin-IV, a potent neuronal tetrodotoxin (TTX)-sensitive sodium channel antagonist from Chinese bird spider *Selenocosmia huwena*. *J. Biol. Chem.* 277:47564-47571.

125. Yan, L. and Adams, M.E. (1998) Lycotoxins, antimicrobial peptides from venom of the wolf spider *Lycosa carolinensis*. *J. Biol. Chem.* 273:2059-2066.

126. Corzo, G., Villegas, E., Gomez-Lagunas, F., Possani, L.D., Belokoneva, O.S. and Nakajima, T. (2002) Oxyopinins, large amphipathic peptides isolated from the venom of the wolf spider *Oxyopes kitabensis* with cytolytic properties and positive insecticidal cooperativity with spider neurotoxins. *J. Biol. Chem.* 277:23627-23637.

127. Corzo, G., Escoubas, P., Stankiewicz, M., Pelhate, M., Kristensen, C.P. and Nakajima, T. (2000) Isolation, synthesis and pharmacological characterization of δ-palutoxins IT, novel insecticidal toxins from the spider *Paracoelotes luctuosus* (Amaurobiidae). *Eur. J. Biochem.* 267:5783-5795.

128. Cordeiro, M.D., Diniz, C.R., do Carmo Valentim, A., von Eickstedt, V.R.D., Gilroy, J. and Richardson, M. (1992) The purification and amino acid sequences of four Tx2 neurotoxins from the venom of the Brazilian 'armed' spider *Phoneutria nigriventer* (Keys). *FEBS Lett.* 310:153-156.

129. Kushmerick, C., Kalapothakis, E., Beirao, P.S.L., Penaforte, C.L., Prado, V.F., Cruz, J.S., Diniz, C.R., Cordeiro, M.N., Gomez, M.V., Romano-Silva, M.A. and Prado, M.A.M. (1999) *Phoneutria nigriventer* toxin Tx3-1 blocks A-type K^+ currents controlling Ca^{2+} oscillation frequency in GH3 cells. *J. Neurochem.* 72:1472-1481.

130. Reis, H.J., Prado, M.A.M., Kalapothakis, E., Cordeiro, M.N., Diniz, C.R., DeMarco, L.A., Gomez, M.V. and Romano-Silva, M.A. (1999) Inhibition of glutamate uptake by a polypeptide toxin (phoneutriatoxin 3-4) from the spider *Phoneutria nigriventer*. *Biochem. J.* 343:413-418.

131. Branton, W.D., Rudnick, M.S., Zhou, Y., Eccleston, E.D., Fields, G.B. and Bowers, L.D. (1993) Fatty acylated toxin structure. *Nature.* 365:496-497.

132. Marvin, L., De, E., Cosette, P., Gagnon, J., Molle, G. and Lange, C. (1999) Isolation, amino acid sequence and functional assays of SGTx1. The first toxin purified from the venom of the spider *Scodra griseipes*. *Eur. J. Biochem.* 265:572-579.

133. Newcomb, R., Palma, A., Fox, J., Gaur, S., Lau, K., Chung, D., Cong, R., Bell, J.R., Horne, B., Nadasdi, L. and Ramachandran, J. (1995) SNX-325, a novel calcium antagonist from the spider *Segestria florentina*. *Biochem.* 34:8341-8347.

134. Pallaghy, P.K., Nielsen, K.J., Craik, D.J. and Norton, R.S. (1994) A common structural motif incorporating a cystine knot and a triple-stranded beta-sheet in toxic and inhibitory polypeptides. *Protein Sci.* 3:1833-1839.

135. Lewis, J.L. and Garcia, M.L. (2003) Therapeutic potential of venom peptides. *Nat. Rev. Drug Disov.* 2:790-802.

136. Kuhn-Nentwig, L. (2003) Antimicrobial and cytolytic peptides of venomous arthropods. *Cell Mol. Life Sci.* 60:2651-2668.

137. Xu, K., Ji, Y. and Qu, X. (1989) Purification and characterization of an antibacterial peptide from venom of *Lycosa singoriensis*. *Acta Zool. Sinica.* 35:300-305.

138. Thomson, J.J. (1913) *Rays of Positive Electricity and Their Application to Chemical Analyses.* Longmans, Green and Co., London.

139. Mattauch, J. and Herzog, R. (1934) About a new mass spectrograph. *Z. Physik.* 89:786-795.

140. Beynon, J.H., Cooks, R.G., Amy, J.W., Baitinger, W.E. and Ridley, T.Y. (1973) Design and performance of a mass-analyzed ion kinetic energy (MIKE) spectrometer. *Anal. Chem.* 45:1023A-1031A.

141. Stephens, W.E. (1946) A pulsed mass spectrometer with time dispersion. *Phys. Rev.* 69:691.

142. Cotter, R.J. (1994) Time-of-flight mass spectrometry. In *Time-of-Flight Mass Spectrometry,* (ed. Cotter, R.J.) pp. 16-48. American Chemical Society, Washington.

143. Dawson, P.H. (1976) *Quadrupole Mass Spectrometry and its Applications.* Elsevier, Amsterdam.

144. Yost, R.A. and Enke, C.G. (1978) Selected ion fragmentation with a tandem quadrupole mass spectrometer. *J. Am. Chem. Soc.* 100:2274-2275.

145. Paul, W. (1990) Electromagnetic traps for charged and neutral particles. *Angew. Chem. Int. Ed.* 29:739-748.

146. Cooks, R.G. and Kaiser, R.E. (1990) Quadrupole ion trap mass spectrometry. *Acc. Chem. Res.* 23:213-219.

147. Dempster, A.J. (1918) A new method of positive ray analysis. *Phys. Rev.* 11:316-325.

148. Harrison, A.G. and Cotter, R.J. (1990) Methods of ionization. *Methods Enzymol.* 193:3-36.

149. Rose, M.E. (1982) *Mass Spectrometry for Chemists and Biochemists.* Cambridge University Press, Cambridge.

150. Munson, M.S.B. and Field, F.H. (1966) Chemical ionization mass spectrometry. 1. General introduction. *J. Am. Chem. Soc.* 88:2621-2630.

151. Harrison, A.G. (1983) *Chemical Ionization Mass Spectrometry.* CRC Press, Boca Raton.

152. Karas, M., Bachmann, D., Bahr, U. and Hillenkamp, F. (1987) Matrix-assisted ultraviolet laser desorption of non-volatile compounds. *Int. J. Mass Spectrom. Ion Processes.* 78:53-68.

153. Karas, M. and Hillenkamp, F. (1988) Laser desorption ionization of proteins with molecular masses exceeding 10 000 daltons. *Anal. Chem.* 60:2299A-2301A.

154. Tanaka, K., Waki, H., Ido, Y., Akita, S., Yoshida, Y., Yoshida, T. and Matsuo, T. (1988) Protein and polymer analyses up to *m/z* 100 000 by laser ionization time-of-flight mass spectrometry. *Rapid Commun. Mass Spectrom.* 2:151-153.

155. Griffiths, W.J., Jonsson, A.P., Liu, S., Rai, D.K. and Wang, Y. (2001) Electrospray and tandem mass spectrometry in biochemistry. *Biochem. J.* 355:545-561.

156. Morris, H.R., Paxton, T., Dell, A., Langhorne, J., Berg, M., Bordoli, R.S., Hoyes, J. and Bateman, R.H. (1996) High sensitivity collisionally-activated decomposition tandem mass spectrometry on a novel quadrupole/orthogonal-acceleration time-of-flight mass spectrometer. *Rapid Commun. Mass Spectrom.* 10:889-896.

157. Wysocki, V.H., Resing, K.A., Zhang, Q. and Chen, G. (2005) Mass spectrometry of peptides and proteins. *Methods.* 35:211-222.

158. Steel, C. and Henchman, M. (1998) Understanding the quadrupole mass filter through computer simulation. *J. Chem. Ed.* 75:1049-1054.

159. Lane, C.S. (2005) Mass spectrometry-based proteomics in the life sciences. *Cell. Mol. Life Sci.* 62:848-869.

160. Cooks, R.G., Beynon, J.H., Caprioli, R.M. and Lester, G.R. (1973) *Metastable Ions.* Elsevier, Amsterdam.

161. de Hoffmann, E. (1996) Tandem mass spectrometry: A primer. *J. Mass Spectrom.* 31:129-137.

162. Shukla, A.K. and Futrell, J.H. (2000) Tandem mass spectrometry: Dissociation of ions by collisional activation. *J. Mass Spectrom.* 35:1069-1090.

163. Cooks, R.G. (1978) *Collision Spectroscopy.* Plenum Press, New York.

164. Haynes, R. and Gross, M.L. (1990) Collision-induced dissociation. *Methods Enzymol.* 193:237-263.

165. Shukla, A.K. and Futrell, J.H. (1993) Collisional activation and dissociation of polyatomic ions. *Mass Spectrom. Rev.* 12:211-255.

166. Cooks, R.G. (2005) Collision-induced dissociation: Readings and commentary. *J. Mass Spectrom.* 30:1215-1221.

167. Mamyrin, B.A. (1994) Laser assisted reflectron time-of-flight mass spectrometry. *Int. J. Mass Spectrom. Ion Processes.* 131:1-19.

168. Mamyrin, B.A., Krataev, V.I., Shmikk, D.V. and Zagulin, V.A. (1973) The mass-reflectron, a new nonmagnetic time-of-flight mass spectrometer with high resolution. *Sov. Phys. JETP.* 37:45-48.

169. Chernushevich, I.V., Loboda, A.V. and Thompson, B.A. (2001) An introduction to quadrupole-time-of-flight mass spectrometry. *J. Mass Spectrom.* 36:849-865.

170. Dole, M., Mach, L.L., Hines, R.L., Mobley, R.C., Ferguson, L.D. and Alice, M.B. (1968) Molecular beams of macroions. *J. Chem. Phys.* 49:2210-2247.

171. Fenn, J.B., Mann, M., Meng, C.K., Wong, S.F. and Whitehouse, C.M. (1990) Electrospray ionization - principles and practice. *Mass Spectrom. Rev.* 9:37-70.

172. Fenn, J.B., Mann, M., Meng, C.K., Wong, S.F. and Whitehouse, C.M. (1989) Electrospray ionization for mass spectrometry of large biomolecules. *Science.* 246:64-71.

173. Yamashita, M. and Fenn, J.B. (1984) Electrospray ion source. Another variation on the free-jet theme. *J. Phys. Chem.* 88:4451-4459.

174. Yamashita, M. and Fenn, J.B. (1984) Negative ion production with the electrospray ion source. *J. Phys. Chem.* 88:4671-4675.

175. Whitehouse, C.M., Dreyer, R.N., Yamashita, M. and Fenn, J.B. (1985) Electrospray interface for liquid chromatographs and mass spectrometers. *Anal. Chem.* 57:675-679.

176. Fuerstenau, S.D., Benner, W.H., Thomas, J.J., Brugidou, C., Bothner, B. and Siuzdak, G. (2001) Mass spectrometry of an intact virus. *Angew. Chem. Int. Ed.* 40:541-544.

177. Felitsyn, N., Peschke, M. and Kebarle, P. (2002) Origin and number of charges observed on multiply-protonated native proteins produced by ESI. *Int. J. Mass Spectrom.* 219:39-62.

178. Taylor, G.I. (1964) Disintegration of water drops in an electric field. *Proc. Royal Soc. Lond. A*. 280:383-397.

179. Kebarle, P. (2000) A brief overview of the present status of the mechanisms involved in electrospray mass spectrometry. *J. Mass Spectrom.* 35:804-817.

180. Kebarle, P. and Ho, Y. (1997) On the mechanism of electrospray mass spectrometry. In *Electrospray Ionization Mass Spectrometry,* pp. 3-63. John Wiley and Sons, New York.

181. Smith, D.P.H. (1986) The electrohydrodynamic atomisation of liquids. *IEEE Trans. Ind. Appl.* 22:527-535.

182. Rayleigh, J.W.S. (1882) On the equilibrium of liquid conducting masses charged with electricity. *Philos. Mag.* 44:184-186.

183. Taflin, D.C., Ward, T.L. and Davis, E.J. (1988) Electrified droplet fission and the Rayleigh limit. *Langmuir.* 5:376 - 384.

184. Nehring, H., Thiebes, S., Bütfering, L. and Röllgen, F.W. (1993) Cluster ion formation in thermospray mass spectrometry of ammonium salts. *Int. J. Mass Spectrom. Ion Processes.* 128:123-132.

185. Iribarne, J.V. and Thomson, B.A. (1976) On the evaporation of small ions from charged droplets. *J. Chem. Phys.* 64:2287-2294.

186. Loo, J.A. (1997) Studying noncovalent protein complexes by electrospray ionization mass spectrometry. *Mass Spectrom. Rev.* 16:1-23.

187. Mann, M., Hendrickson, R.C. and Pandey, A. (2001) Analysis of proteins and proteomics by mass spectrometry. *Annu. Rev. Biochem.* 70:437-473.

188. Pramanik, B.N., Bartner, P.L., Mirza, U.A., Liu, Y. and Ganguly, A.K. (1998) Electrospray ionization mass spectrometry for the study of non-covalent complexes: An emerging technology. *J. Mass Spectrom.* 33:911-920.

189. Ashcroft, A.E. (2005) Recent developments in electrospray ionisation mass spectrometry: Noncovalently bound protein complexes. *Nat. Prod. Rep.* 22:452-464.

190. Fenn, J.B., Meng, C.K. and Mann, M. (1990) Multiply charged ions and a method for determining the molecular weight of large molecules, especially biopolymers, by electrospray mass spectrometry. *USA Patent No. 9014148.*

191. Mann, M., Meng, C.K. and Fenn, J.B. (1989) Interpreting mass spectra of multiply charged ions. *Anal. Chem.* 61:1702-1708.

192. Ferrige, A.G., Seddon, M.J., Green, B.N., Jarvis, S.A., Skilling, J. and Staunton, J. (1992) Disentangling electrospray spectra with maximum entropy. *Rapid Commun. Mass Spectrom.* 6:707-711.

193. Cech, N.B. and Enke, C.G. (2001) Practical implications of some recent studies in electrospray ionization fundamentals. *Mass Spectrom. Rev.* 20:362-387.

194. Iavarone, A.T., Jurchen, J.C. and Williams, E.R. (2000) Effects of solvent on the maximum charge state and charge state distribution of protein ions produced by electrospray ionization. *J. Am. Soc. Mass Spectrom.* 11:976-985.

195. Herskovitis, T.T., Gadegbeku, B. and Jaillet, H. (1970) On the structural stability and solvent denaturation of proteins. 1. Denaturation by the alcohols and glycols. *J. Biol. Chem.* 245:2588-2598.

196. Dill, K.A. and Shortle, D. (1991) Denatured states of proteins. *Annu. Rev. Biochem.* 60:795-825.

197. Fink, A.L. and Painter, B. (1987) Characterization of the unfolding of ribonuclease A in aqueous methanol solvents. *Biochem.* 26:1665-1671.

198. Babu, K.R. and Douglas, D.J. (2000) Methanol-induced conformations of myoglobin at pH 4.0. *Biochem.* 39:14702-14710.

199. Mant, C.T. and Hodges, R.S. (1991) *High Performance Liquid Chromatography of Peptides and Proteins. Separation, Analysis and Conformation.* CRC Press, Boca Raton.

200. García, M.C. (2005) The effect of the mobile phase additives on sensitivity in the analysis of peptides and proteins by high-performance liquid chromatography-electrospray mass spectrometry. *J. Chromatog. B.* 825:111-123.

201. Yoshida, T. (2004) Peptide separation by hydrophilic-interaction chromatography: A review. *J. Biochem. Biophys. Methods.* 60:265-280.

202. Henschen, A., Hupe, K., Lottspeich, F. and Voelter, W. (1985) *High Performance Liquid Chromatography in Biochemistry.* VCH Publishers, Weinheim.

203. Williams, D.H. and Fleming, I. (1995) *Spectroscopic Methods in Organic Chemistry.* McGraw-Hill Book Co., London.

204. Biemann, K. and Martin, S.A. (1987) Mass spectrometric determination of the amino acid sequence of peptides and proteins. *Mass Spectrom. Rev.* 6:1-76.

205. Williams, D.H., Bradley, C.V., Santikarn, S. and Bojesen, G. (1982) Fast-atom-bombardment mass spectrometry. A new technique for the determination of molecular weights and amino acid sequences of peptides. *Biochem. J.* 201:105-117.

206. Tsaprailis, G., Nair, H., Somogyi, A., Wysocki, V.H., Zhong, W., Futrell, J.H., Summerfield, S.G. and Gaskell, S.J. (1999) Influence of secondary structure on the fragmentation of protonated peptides. *J. Am. Chem. Soc.* 121:5142-5154.

207. Nair, H., Somogyi, A. and Wysocki, V.H. (1996) Effect of alkyl substitution at the amide nitrogen on amide bond cleavage: Electrospray ionization/surface-induced dissociation fragmentation of substance P and two alkylated analogues. *J. Mass Spectrom.* 31:1141-1148.

208. Medzihradszky, K.F. (2005) In-solution digestion of proteins for mass spectrometry. *Methods Enzymol.* 405:50-65.

209. Lee, T.D. and Shively, J.E. (1990) Enzymatic and chemical digestion of proteins for mass spectrometry. *Methods Enzymol.* 193:361-373.

210. Bodanszky, M. (1988) *Peptide Chemistry. A Practical Textbook.* Springer-Verlag, Berlin.

211. Mentele, R., Eckerskorn, C., Kellerman, J., Straupat, K. and Hagmann, J. (1997) *Swiss-Prot Accession No. Q7M135.*

212. Wada, Y. and Kadoya, M. (2003) In-gel digestion with endoproteinase LysC. *J. Mass Spectrom.* 38:117-118.

213. Schweppe, R.E., Haydon, C.E., Lewis, T.S., Resing, K.A. and Ahn, N.G. (2003) The characterization of protein post-translational modifications by mass spectrometry. *Acc. Chem. Res.* 36:453-461.

214. Bradbury, A.F. and Smyth, D.G. (1991) Peptide amidation. *Trends Biochem. Sci.* 16:112-115.

215. Merkler, D.J. (1994) C-terminal amidated peptides: Production by the in vitro enzymatic amidation of glycine-extended peptides and the importance of the amide to bioactivity. *Enzyme Microb. Technol.* 16:450-456.

216. Bradbury, A.F. and Smyth, D.G. (1987) Biosynthesis of the C-terminal amide in peptide hormones. *Biosci. Rep.* 7:907-916.

217. Moore, K.L. (2003) The biology and enzymology of protein tyrosine O-sulfation. *J. Biol. Chem.* 278:24243-24246.

218. Hemmerich, S., Verdugo, D. and Rath, V.L. (2004) Strategies for drug discovery by targeting sulfation pathways. *Drug Discovery Today.* 9:967-975.

219. Edman, P. and Begg, G. (1967) A protein sequenator. *Eur. J. Biochem.* 1:80-91.

220. Hunkapiller, M.W., Hewick, R.M., Dreyer, W.J. and Hood, L.E. (1983) High-sensitivity sequencing with a gas-phase sequenator. *Methods Enzymol.* 91:399-413.

221. Gevaert, K. and Vandekerckhove, J. (2000) Protein identification methods in proteomics. *Electrophoresis.* 21:1145-1154.

222. Veenstra, T.D. (1999) Electrospray ionization mass spectrometry in the study of biomolecular non-covalent interactions. *Biophys. Chem.* 79:63-79.

223. Loo, J.A., He, J.X. and Cody, W.L. (1998) Higher order structure in the gas phase reflects solution structure. *J. Am. Chem. Soc.* 120:4542-4543.

224. Rogniaux, H., Van Dorsselaer, A., Barth, P., Biellmann, J.F., Barbanton, J., van Zandt, M., Chevrier, B., Howard, E., Mitschler, A. and Potier, N. (1999) Binding of aldose reductase inhibitors: Correlation of crystallographic and mass spectrometric studies. *J. Am. Chem. Soc. Mass Spectrom.* 10:635-647.

225. Edmonds, C.G., Loo, J.A., Barinaga, C.J., Udseth, H.R. and Smith, R.D. (1989) Capillary electrophoresis-electrospray ionization-mass spectrometry. *J. Chromatog. A.* 474:21-37.

226. Smith, R.D., Lightwahl, K.J., Winger, B.E. and Loo, J.A. (1992) Preservation of noncovalent associations in electrospray ionization mass spectrometry: Multiply charged polypeptide and protein dimers. *Org. Mass Spectrom.* 27:811-821.

227. Covey, T.R., Bonner, R.F., Shushan, B.I., Henion, J. and Boyd, R.K. (1988) The determination of protein, oligonucleotide and peptide molecular weights by ion-spray mass spectrometry. *Rapid Commun. Mass Spectrom.* 2:249-256.

228. Ganem, B., Li, Y.T. and Henion, J.D. (1991) Detection of noncovalent receptor-ligand complexes by mass spectrometry. *J. Am. Chem. Soc.* 113:6294-6296.

229. Katta, V. and Chait, B.T. (1991) Observation of the heme-globin complex in native myoglobin by electrospray-ionization mass spectrometry. *J. Am. Chem. Soc.* 113:8534-8535.

230. Veenstra, T.D. (1999) Electrospray ionization mass spectrometry: A promising new technique in the study of protein/DNA complexes. *Biochem. Biophys. Res. Commun.* 257:1-5.

231. Smith, D.L. and Zhang, Z. (1994) Probing noncovalent structural features of proteins by mass spectrometry. *Mass Spectrom. Rev.* 13:411-429.

232. Przybylski, M. and Glocker, M.O. (1996) Electrospray mass spectrometry of biomacromolecular complexes with noncovalent interactions: New analytical perspectives for supramolecular chemistry and molecular recognition processes. *Angew. Chem. Int. Ed.* 35:807-826.

233. Loo, J.A. (2000) Electrospray ionization mass spectrometry: A technology for studying noncovalent macromolecular complexes. *Int. J. Mass Spectrom.* 200:177-186.

234. Fitzgerald, M.C., Chernushevich, I., Standing, K.G., Whitman, C.P. and Kent, S.B.H. (1996) Probing the oligomeric structure of an enzyme by electrospray ionization time-of-flight mass spectrometry. *Proc. Natl. Acad. Sci.* 93:6851-6856.

235. Hernandez, H. and Robinson, C.V. (2001) Dynamic protein complexes: Insights from mass spectrometry. *J. Biol. Chem.* 276:46685-46688.

236. Loo, J.A., Ogorzalek Loo, R.R., Udseth, H.R., Edmonds, C.G. and Smith, R.D. (1991) Solvent-induced conformational changes of polypeptides probed by electrospray-ionization mass spectrometry. *Rapid Commun. Mass Spectrom.* 5:101-105.

237. Konermann, L. and Douglas, D.J. (1998) Equilibrium unfolding of proteins monitored by electrospray ionization mass spectrometry: Distinguishing two-state from multi-state transitions. *Rapid Commun. Mass Spectrom.* 12:435-442.

238. Hunter, C.L., Mauk, A.G. and Douglas, D.J. (1997) Dissociation of heme from myoglobin and cytochrome b_5: Comparison of behavior in solution and the gas phase. *Biochem.* 36:1018-1025.

239. Gao, J., Cheng, X., Chen, R., Sigal, G.B., Bruce, J.E., Schwartz, B.L., Hofstadler, S.A., Anderson, G.A., Smith, R.D. and Whitesides, G.M. (1996) Screening derivatized peptide libraries for tight binding inhibitors to carbonic anhydrase II by electrospray ionization-mass spectrometry. *J. Med. Chem.* 39:1949-1955.

240. Suckau, D., Shi, Y., Beu, S., Senko, M., Quinn, J., Wampler FM, I. and McLafferty, F. (1993) Coexisting stable conformations of gaseous protein ions. *Proc. Natl. Acad. Sci.* 90:790-793.

241. Feng, R., Castelhano, A.L., Billedeau, R. and Zhengyu, Y. (1995) Study of noncovalent enzyme-inhibitor complexes and metal binding stoichiometry of matrilysin by electrospray ionization mass spectrometry. *J. Am. Soc. Mass Spectrom.* 6:1105-1111.

242. Cheng, X., Gao, Q., Smith, R.D., Jung, K. and Switzer, C. (1996) Comparison of 3,5- and 2,5-linked DNA duplex stabilities by electrospray ionization mass spectrometry. *J. Chem. Soc. Chem. Commun.* 6:747-748.

243. Robinson, C.V., Chung, E.W., Kragelund, B.B., Knudsen, J., Aplin, R.T., Poulsen, F.M. and Dobson, C.M. (1996) Probing the nature of noncovalent interactions by mass spectrometry. A study of protein-CoA ligand binding and assembly. *J. Am. Chem. Soc.* 118:8646-8653.

244. Wu, Q., Gao, J., Joseph-McCarthy, D., Sigal, G.B., Bruce, J.E., Whitesides, G.M. and Smith, R.D. (1997) Carbonic anhydrase-inhibitor binding: From solution to the gas phase. *J. Am. Chem. Soc.* 119:1157-1158.

245. Rostum, A.A., Sunde, M., Richardson, S.J., Schreiber, G., Jarvis, S., Bateman, R., Dobson, C.M. and Robinson, C.V. (1998) Dissection of multi-protein complexes using mass spectrometry: Subunit interactions in transthyretin and retinol-binding protein complexes. *Proteins.* 2:3-11.

246. Hoaglund-Hyzer, C.S., Counterman, A.E. and Clemmer, D.E. (1991) Anhydrous protein ions. *Chem. Rev.* 99:3037-3080.

247. Daniel, J.D., Friess, S.D., Rajagopalan, S., Wendt, S. and Zenobi, R. (2002) Quantitative determination of noncovalent binding interactions using soft ionization mass spectrometry. *Int. J. Mass Spectrom.* 216:1-27.

248. Smith, R.D., Loo, J.A., Ogorzalek Loo, R.R., Busman, M. and Udseth, H.R. (1991) Principles and practice of electrospray ionization - mass spectrometry for large polypeptides and proteins. *Mass Spectrom. Rev.* 10:359-451.

249. Le Blanc, J.C.Y., Wang, J., Guevremont, R. and Siu, K.W.M. (1994) Electrospray mass spectra of protein cations formed in basic solutions. *Org. Mass Spectrom.* 29:587-593.

250. Fernandez de la Mora, J. (2000) Electrospray ionization of large multiply charged species proceeds via Dole's charged residue mechanism. *Anal. Chim. Acta.* 406:93-104.

251. Schnier, P.D., Gross, D.S. and Williams, E.R. (1995) On the maximum charge state and proton transfer reactivity of peptide and protein ions formed by electrospray ionization. *J. Am. Soc. Mass Spectrom.* 6:1086-1097.

252. Greig, M.J., Gaus, H., Cummins, L.L., Sasmor, H. and Griffey, R.H. (1995) Measurement of macromolecular binding using electrospray mass spectrometry. Determination of dissociation constants for oligonucleotide:serum albumin complexes. *J. Am. Chem. Soc.* 117:10765-10766.

253. Lim, H., Hsieh, Y.L., Ganem, B. and Henion, J. (1995) Recognition of cell-wall peptide ligands by vancomycin group antibiotics: Studies using ion spray mass spectrometry. *J. Mass Spectrom.* 30:708-714.

254. Jorgensen, T.J.D., Roepstorff, P. and Heck, A.J.R. (1998) Direct determination of solution binding constants for noncovalent complexes between bacterial cell wall peptide analogues and vancomycin group antibiotics by electrospray ionization mass spectrometry. *Anal. Chem.* 70:4427-4432.

255. Kempen, E.C. and Brodbelt, J.S. (2000) A method for the determination of binding constants by electrospray ionization mass spectrometry. *Anal. Chem.* 72:5411-5416.

256. Schwartz, B.L., Bruce, J.E., Anderson, G.A., Hofstadler, S.A., Rockwood, A.L., Smith, R.D., Chilkoti, A. and Stayton, P.S. (1995) Dissociation of tetrameric ions of noncovalent streptavidin complexes formed by electrospray ionization. *J. Am. Soc. Mass Spectrom.* 6:459-465.

257. Penn, S.G., Fei, H., Kirk Green, M. and Lebrilla, C.B. (1997) The use of heated capillary dissociation and collision-induced dissociation to determine the strength of noncovalent bonding interactions in gas-phase peptide-cyclodextrin complexes. *J. Am. Chem. Soc. Mass Spectrom.* 8:244-252.

258. Rockwood, A.L., Busman, M., Udseth, H.R. and Smith, R.D. (1991) Thermally induced dissociation of ions from electrospray mass spectrometry. *Rapid Commun. Mass Spectrom.* 5:582-585.

259. Loo, J.A., Udseth, H.R., Smith, R.D. and Futrell, J.H. (1988) Collisional effects on the charge distribution of ions from large molecules, formed by electrospray-ionization mass spectrometry. *Rapid Commun. Mass Spectrom.* 2:207-210.

260. Li, Y., Hsieh, Y.L., Henion, J.D., Ocain, T.D., Schiehser, G.A. and Ganem, B. (1994) Analysis of the energetics of gas-phase immunophilin-ligand complexes by ion spray mass spectrometry. *J. Am. Chem. Soc.* 116:7487-7493.

261. Smith, D.L., Deng, Y. and Zhang, Z. (1997) Probing the non-covalent structure of proteins by amide hydrogen exchange and mass spectrometry. *J. Mass Spectrom.* 32:135-146.

262. Busenlehner, L.S. and Armstrong, R.N. (2005) Insights into enzyme structure and dynamics elucidated by amide H/D exchange mass spectrometry. *Arch. Biochem. Biophys.* 433:34-46.

263. Hoofnagle, A.N., Resing, K.A. and Ahn, N.G. (2003) Protein analysis by hydrogen exchange mass spectrometry. *Annu. Rev. Biochem.* 32:1-25.

264. Yan, X., Watson, J., Ho, P.S. and Deinzer, M.L. (2004) Mass spectrometric approaches using electrospray ionization charge states and hydrogen-deuterium exchange for determining protein structures and their conformational changes. *Mol. Cell. Proteomics.* 3:10-23.

265. Bai, Y., Milne, J.S., Mayne, L. and Englander, S.W. (1993) Primary structure effects on peptide group hydrogen exchange. *Proteins.* 17:75-86.

266. Maity, H., Lim, W.K., Rumbley, J.N. and Englander, S.W. (2003) Protein hydrogen exchange mechanism: Local fluctuations. *Protein Sci.* 12:153-160.

267. Fregeau Gallagher, N.L., Sailer, M., Niemezura, W.P., Nakashima, T.T., Stiles, M.E. and Vederas, J.C. (1997) Three-dimensional structure of leucocin A in trifluoroethanol and dodecylphosphocholine micelles: Spatial location of residues critical for biological activity in type IIa bacteriocins from lactic acid bacteria. *Biochem.* 36:15062-15072.

268. Evans, J.N.S. (1995) *Biomolecular NMR Spectroscopy.* Oxford University Press, Oxford.

269. Mandell, J.G., Falick, A.M. and Komives, E.A. (1998) Identification of protein-protein interfaces by decreased amide proton solvent accessibility. *Proc. Natl. Acad. Sci.* 95:14705-14710.

270. Ehring, H. (1999) Hydrogen exchange electrospray ionization mass spectrometry studies of structural features of proteins and protein/protein interactions. *Anal. Biochem.* 267:252-259.

271. Baerga-Ortiz, A., Hughes, C.A., Mandell, J.G. and Komives, E.A. (2002) Epitope mapping of a monoclonal antibody against human thrombin by H/D-exchange mass spectrometry reveals selection of a diverse sequence in a highly conserved protein. *Protein Sci.* 11:1300-1308.

272. Deng, Y. and Smith, D.L. (1998) Identification of unfolding domains in large proteins by their unfolding rates. *Biochem.* 37:6256-6262.

273. Gro{szlig}, M., Robinson, C.V., Mayhew, M., Hartl, F.U. and Radford, S.E. (1996) Significant hydrogen exchange protection in GroEL-bound DHFR is maintained during iterative rounds of substrate cycling. *Protein Sci.* 5:2506-2513.

274. McCammon, M.G., Scott, D.J., Keetch, C.A., Greene, L.H., Purkey, H.E., Petrassi, H.M., Kelly, J.W. and Robinson, C.V. (2002) Screening transthyretin amyloid fibril inhibitors: Characterization of novel multiprotein, multiligand complexes by mass spectrometry. *Structure.* 10:851-863.

275. Hoofnagle, A.N., Resing, K.A., Goldsmith, E.J. and Ahn, N.G. (2001) Changes in protein conformational mobility upon activation of extracellular regulated protein kinase-2 as detected by hydrogen exchange. *Proc. Natl. Acad. Sci.* 98:956-961.

276. Resing, K.A. and Ahn, N.G. (1998) Deuterium exchange mass spectrometry as a probe of protein kinase activation. Analysis of wild-type and constitutively active mutants of MAP kinase kinase-1. *Biochem.* 37:463-475.

277. Mandell, J.G., Baerga-Ortiz, A., Akashi, S., Takio, K. and Komives, E.A. (2001) Solvent accessibility of the thrombin-thrombomodulin interface. *J. Mol. Biol.* 306:575-589.

278. Burke, J.M. and Arnold, M.J. (2001) Genetics and fitness of hybrids. *Annu. Rev. Genet.* 35:31-52.

279. Arnold, M.L. (1997) *Natural Hybridization and Evolution.* Oxford University Press, New York.

280. Arnold, M.L. and Hodges, S.A. (1995) Are natural hybrids fit or unfit relative to their parents? *Trends Ecol. Evol.* 10:67-71.

281. Woodruff, D.S. (1973) Natural hybridization and hybrid zones. *Syst. Zool.* 22:213-218.

282. Arnold, M.J. (1992) Natural hybridization as an evolutionary process. *Annu. Rev. Ecol. Syst.* 23:237-261.

283. Mayr, E. (1966) The breakdown of isolating mechanisms (hybridization). In *Animal Species and Evolution,* pp. 110-135. Harvard University Press, Cambridge.

284. Dowling, T.E. and Secor, C.L. (1997) The role of hybridization and introgression in the diversification of animals. *Annu. Rev. Ecol. Syst.* 28:593-619.

285. Harrison, R.G. (1993) *Hybrid Zones and the Evolutionary Process.* Oxford University Press, New York.

286. Wynn, A.H. (1986) Linkage disequilibrium and a contact zone in *Plethodon cinereus* on the Del-Mar-Va peninsula. *Evolution.* 40:44-54.

287. Barton, N.H. (2001) The role of hybridization in evolution. *Mol. Ecol.* 10:551-568.

288. Lewontin, R.C. and Birch, L.C. (1966) Hybridization as a source of variation for adaptation to new environments. *Evolution.* 20:315-336.

289. DeMarais, B., Dowling, T., Douglas, M., Minckley, W. and Marsh, P. (1992) Origin of *Gila seminuda* (Teleostei: Cyprinidae) through introgressive hybridization: Implications for evolution and conservation. *Proc. Natl. Acad. Sci.* 89:2747-2751.

290. Rieseberg, L.H. (1997) Hybrid origins of plant species. *Annu. Rev. Ecol. Syst.* 28:359-389.

291. Voss, S.R. and Shaffer, H.B. (1996) What insights into the developmental traits of urodeles does the study of interspecific hybrids provide? *Int. J. Dev. Biol.* 40:885-893.

292. Fitzpatrick, B.M. and Shaffer, H.B. (2004) Environment-dependent admixture dynamics in a tiger salamander hybrid zone. *Evol. Int. J. Org. Evol.* 58:1282-1293.

293. Alexandrino, J., Baird, S.J., Lawson, L., Macey, J.R., Moritz, C. and Wake, D.B. (2005) Strong selection against hybrids at a hybrid zone in the *Ensatina* ring species complex and its evolutionary implications. *Evol. Int. J. Org. Evol.* 59:1334-1347.

294. Weisrock, D.W., Kozak, K.H. and Larson, A. (2005) Phylogeographic analysis of mitochondrial gene flow and introgression in the salamander, *Plethodon shermani. Mol. Ecol.* 14:1457-1472.

295. Sequeira, F., Alexandrino, J., Rocha, S., Arntzen, J.W. and Ferrand, N. (2005) Genetic exchange across a hybrid zone within the Iberian endemic golden-striped salamander, *Chioglossa lusitanica*. *Mol. Ecol.* 14:245-254.

296. Voros, J., Alcobendas, M., Martinez-Solano, I. and Garcia-Paris, M. (2005) Evolution of *Bombina bombina* and *Bombina variegata* (Anura: Discoglossidae) in the Carpathian Basin: A history of repeated mt-DNA introgression across species. *Mol. Phylogent. Evol.* 38:705-718.

297. Masta, S.E., Sullivan, B.K., Lamb, T. and Routman, E.J. (2002) Molecular systematics, hybridization and phylogeography of the *Bufo americanus* complex in Eastern North America. *Mol. Phylogent. Evol.* 24:302-314.

298. Szymura, J.M. and Barton, N.H. (1986) Genetic analysis of a hybrid zone between the firebellied toads, *Bombina bombina* and *B. variegata,* near Cracow in southern Poland. *Evolution.* 40:1141-1159.

299. Hillis, D.M. (1988) Systematics of the *Rana pipiens* complex: Puzzle and paradigm. *Annu. Rev. Ecol. Syst.* 19:39-63.

300. Littlejohn, M.J. and Watson, G.F. (1985) Hybrid zones and homogamy in Australian frogs. *Ann. Rev. Ecol. Syst.* 16:85-112.

301. Spolsky, C. and Uzzell, T. (1986) Evolutionary history of the hybridogenetic hybrid frog *Rana esculenta* as deduced from mtDNA analyses. *Mol. Biol. Evol.* 3:44-56.

302. Graf, J. and Polls-Pelaz, M. (1989) Evolutionary genetics of the *Rana esculenta* complex. In *Evolution and Ecology of Unisexual Vertebrates,* (eds. Dawley, R.M. and Bogart, J.P.) pp. 289-302. University of the State of New York, New York.

303. Lamb, T. and Avise, J.C. (1987) Morphological variability in genetically defined categories of anuran hybrids. *Evolution.* 41:157-165.

304. Wake, D.B., Yang, S.Y. and Papenfuss, T.J. (1980) Natural hybridization and its evolutionary implications in Guatemalan Plethodontid salamanders of the genus *Bolitoglossa*. *Herpetologica.* 36:335-345.

305. Simmaco, M., Mignogna, G., Barra, D. and Bossa, F. (1994) Antimicrobial peptides from skin secretions of *Rana esculenta*. Molecular cloning of cDNAs encoding esculentin and brevinins and isolation of new active peptides. *J. Biol. Chem.* 269:11956-11961.

306. Ali, M.F., Knoop, F.C., Vaudry, H. and Conlon, J.M. (2003) Characterization of novel antimicrobial peptides from the skins of frogs of the *Rana esculenta* complex. *Peptides.* 24:955-961.

307. Cogger, H. (1983) *Reptiles and Amphibians of Australia.* Reed Books, Frenchs Forest.

308. Clyne, D. (1969) *Australian Frogs.* Periwinkle Books, Melbourne.

309. Barra, D., Simmaco, M. and Boman, H.G. (1998) Gene-encoded peptide antibiotics and innate immunity. Do 'animalcules' have defence budgets? *FEBS Lett.* 430:130-134.

310. Stone, D.J.M., Waugh, R.J., Bowie, J.H., Wallace, J.C. and Tyler, M.J. (1992) Peptides from Australian frogs. Structures of the caerins and caeridin 1 from *Litoria splendida. J. Chem. Soc. Perkin Trans.* 1:3173-3178.

311. Wabnitz, P.A., Walters, H., Tyler, M.J., Wallace, J.C. and Bowie, J.H. (1998) First record of host defence peptides in tadpoles. The magnificent tree frog *Litoria splendida. J. Pept. Res.* 52:477-483.

312. Wong, H., Bowie, J.H. and Carver, J.A. (1997) The solution structure and activity of caerin 1.1, an antimicrobial peptide from the Australian green tree frog, *Litoria splendida. Eur. J. Biochem.* 247:545-557.

313. Wegener, K.L., Carver, J.A. and Bowie, J.H. (2003) The solution structures and activity of caerin 1.1 and caerin 1.4 in aqueous trifluoroethanol and dodecylphosphocholine micelles. *Biopolymers.* 69:42-59.

314. Pukala, T.L., Brinkworth, C.S., Carver, J.A. and Bowie, J.H. (2004) Investigating the importance of the flexible hinge in caerin 1.1: Solution structures and activity of two synthetically modified caerin peptides. *Biochem.* 43:937-944.

315. Segrest, J.P., De Loof, H., Dohlman, J.G., Brouillette, C.G. and Anantharamaiah, G.M. (1990) Amphipathic helix motif: Classes and properties. *Proteins Struct. Funct. Genet.* 8:103-117.

316. O'Neil, K.T. and DeGrado, W.F. (1990) How calmodulin binds its targets: Sequence independent recognition of amphiphilic α-helices. *Trends Biochem. Sci.* 15:59-64.

317. Watterson, D.M. and Vincenzi, F.F. (eds.) (1980) *Calmodulin and Cell Functions.* New York Academy of Sciences, New York.

318. Chen, X.J. and Butow, R.A. (2006) The organisation and ineritance of the mitochondrial genome. *Nat. Rev. Genet.* 6:815-825.

319. Borst, P. (1972) Mitochondrial nucleic acids. *Annu. Rev. Biochem.* 41:333-376.

320. Hutchinson, C.A., Newbold, J.E., Potter, S.S. and Edgell, M.H. (1974) Maternal inheritance of mammalian mitochondrial DNA. *Nature.* 251:536-538.

321. Dawid, I.B. and Blackler, A.W. (1972) Maternal and cytoplasmic inheritance of mitochondrial DNA in *Xenopus. Dev. Biol.* 29:152-161.

322. Giles, R.E., Blanc, H., Cann, H.M. and Wallace, D.C. (1980) Maternal inheritance of human mitochondrial DNA. *Proc. Natl. Acad. Sci.* 77:6715-6719.

323. Pakendorf, B. and Stoneking, M. (2005) Mitochondrial DNA and human evolution. *Annu. Rev. Genomics Hum. Genet.* 6:165-183.

324. Michalak, P. and Noor, M.A.F. (2003) Genome-wide patterns of expression in *Drosophila* pure species and hybrid males. *Mol. Biol. Evol.* 20:1070-1076.

325. Nielsen, M.G., Wilson, K.A., Raff, E.C. and Raff, R.A. (2000) Novel gene expression patterns in hybrid embryos between species with different modes of development. *Evol. Dev.* 2:133-144.

326. Kocher, T.D., Thomas, W.K., Meyer, A., Edwards, S.V., Paabo, S.F., Villablanca, F.X. and Wilson, A.C. (1989) Dynamics of mtDNA evolution in animals: Amplification and sequencing with conserved primers. *Proc. Natl. Acad. Sci.* 86:6196-6200.

327. Donnellan, S.C., Hutchinson, M.N. and Saint, K.M. (1999) Molecular evidence for the phylogeny of Australian gekkonoid lizards. *Biol. J. Linnean Soc.* 67:97-118.

328. Kimura, M. (1980) A simple method for estimating evolutionary rates of base substitutions through comparative studies of nucleotide sequences. *J. Mol. Evol.* 16:111-120.

329. Swafford, D. (1998) *PAUP*. Phylogenetic Analysis Using Parsimony and Other Methods. Version 4b10.* Sinauer Associates, Sunderland.

330. National Health and Medical Research Council. (2004) *Australian Code of Practice for the Care and Use of Animals for Scientific Purposes. 7th ed.* Australian Government, Canberra.

331. Maeji, N.J., Bray, A.M., Valerio, R.M. and Wang, W. (1995) Larger scale multipin peptide synthesis. *J. Pept. Res.* 8:33-38.

332. Jorgensen, J.H., Cleeland, W.A., Craig, G., Doern, M., Ferraro, J., Finegold, C.M., Hansen, S.L., Jenkins, S.G., Novick, W.J., Pfaller, M.S., Preston, D.A., Reller, L.B. and Swanson, J.M. (1993) Methods for dilution antimicrobial susceptibility tests for bacteria that grow aerobically, 3rd approved standard. Document M7-A3. *National Committee for Clinical Laboratory Standards.* 33:1-12.

333. Chen, T., Scott, C., Tang, L., Zhou, M. and Shaw, C. (2005) The structural organization of aurein precursor cDNAs from the skin secretion of the Australian green and golden bell frog, *Litoria aurea*. *Regul. Pept.* 128:75-83.

334. Jacobson, B., Anderson, W.A. and Arnold, J.T. (1954) A proton magnetic resonance study of the hydration of deoxyribonucleic acid. *Nature.* 17:772-773.

335. Saunders, M., Wishnia, A. and Kirkwood, J.G. (1957) The nuclear magnetic resonance spectrum of ribonuclease. *J. Am. Chem. Soc.* 70:3289-3290.

336. Gronenborn, A.M. and Clore, G.M. (1990) Protein structure determination in solution by two-dimensional and three-dimensional nuclear magnetic resonance spectroscopy. *Anal. Chem.* 62:2-15.

337. Wüthrich, K. (1989) Protein structure determination in solution by nuclear magnetic resonance spectroscopy. *Science.* 243:45-50.

338. Greenfield, N.J. (1996) Methods to estimate the conformation of proteins and polypeptides from circular dichroism data. *Analyt. Biochem.* 235:1-10.

339. Kelly, S.M., Jess, T.J. and Price, N.D. (2005) How to study proteins by circular dichroism. *Biochim. Biophys. Acta.* 1715:119-139.

340. Baumeister, W. and Steven, A.C. (2000) Macromolecular electron microscopy in the era of structural genomics. *Trends Biochem. Sci.* 25:624-631.

341. Chiu, W., Baker, M.L., Jiang, W. and Zhou, Z.H. (2002) Deriving folds of macromolecular complexes through electron cryomicroscopy and bioinformatics approaches. *Curr. Opin. Struct. Biol.* 12:263-269.

342. Blundell, T.L. and Johnson, L.N. (1976) *Protein Crystallography.* Academic Press, New York.

343. Glusker, J.P. (1981) *Structural Crystallography in Chemistry and Biology.* Hutchinson Ross Pub. Co., Stroudsburg.

344. Wider, G. (2000) Structure determination of biological macromolecules in solution using nuclear magnetic resonance spectroscopy. *Biotechniques.* 29:1278-1294.

345. Wüthrich, K. (1976) *NMR in Biological Research: Peptides and Proteins.* North-Holland Pub. Co., Amsterdam.

346. Macomber, R.S. (1998) *A Complete Introduction to Modern NMR Spectroscopy.* John Wiley and Sons, New York.

347. Friebolin, H. (1991) *Basic One- and Two-Dimensional NMR Spectroscopy.* VCH Publishers, Weinheim.

348. Clore, G.M. and Gronenborn, A.M. (1989) Determination of three-dimensional structures of proteins and nucleic acids in solution by nuclear magnetic resonance spectroscopy. *Crit. Rev. Biochem. Mol. Biol.* 24:479-564.

349. Aue, W.P., Bartholdi, E. and Ernst, R.R. (1976) Two dimensional spectroscopy. Application to nuclear magnetic resonance. *J. Chem. Phys.* 64:2229-2246.

350. Sørensen, O.W., Eich, G.W., Levitt, M.H., Bodenhausen, G. and Ernst, R.R. (1983) Product operator formalism for the description of NMR pulse experiments. *Progr. NMR. Spectrosc.* 16:163-192.

351. Kriwacki, R.W. and Pitner, T.P. (1989) Current aspects of practical two-dimensional (2D) nuclear magnetic resonance (NMR) spectroscopy: Applications to structure elucidation. *Pharm. Res.* 6:531-554.

352. Rance, M., Sørensen, O.W., Bodenhausen, G., Wagner, G., Ernst, R.R. and Wüthrich, K. (1983) Improved spectral resolution in COSY ^{1}H NMR spectra of proteins via double quantum filtering. *Biochem. Biophys. Res. Commun.* 117:479-485.

353. Marion, D. and Wüthrich, K. (1983) Application of phase sensitive two-dimensional correlated spectroscopy (COSY) for measurements of [1]H-^{1}H spin-spin coupling constants in proteins. *Biochem. Biophys. Res. Commun.* 113:967-974.

354. Bax, A. (1989) Two-dimensional NMR and protein structure. *Annu. Rev. Biochem.* 58:223-256.

355. Davis, D.G. and Bax, A. (1985) Assignment of complex ^{1}H NMR spectra via two-dimensional homonuclear Hartmann-Hahn spectroscopy. *J. Am. Chem. Soc.* 107:2820-2821.

356. Bax, A. (1989) Homonuclear Hartmann-Hahn experiments. *Methods Enzymol.* 176:151-168.

357. Hartmann, S.R. and Hahn, E.L. (1962) Nuclear double resonance in the rotating frame. *Phys. Rev.* 128:2042-2053.

358. Levitt, M.H., Suter, D. and Ernst, R.R. (1986) Spin dynamics and thermodynamics in solid-state NMR cross polarisation. *J. Chem. Phys.* 84:4243-4255.

359. Braunschweiler, L. and Ernst, R.R. (1983) Coherance transfer by isotropic mixing: Application to proton correlation spectroscopy. *J. Magn. Reson.* 53:521-528.

360. Wüthrich, K. (1986) *NMR of Proteins and Nucleic Acids.* John Wiley and Sons, New York.

361. Griesinger, C., Otting, G., Wüthrich, K. and Ernst, R.R. (1988) Clean TOCSY for ^{1}H spin system identification in macromolecules. *J. Am. Chem. Soc.* 110:7870-7872.

362. Maudsley, A.A. and Ernst, R.R. (1977) Indirect magnetisation of magnetic resonance by heteronuclear two-dimensional spectroscopy. *Chem. Phys. Lett.* 50:368-372.

363. Bax, A. (1981) An improved method for heteronuclear chemical shift correlation by two-dimensional NMR. *J. Magn. Reson.* 42:501-505.

364. Bax, A. (1983) Broadband homonuclear decoupling in heteronuclear shift correlation NMR spectroscopy. *J. Magn. Reson.* 53:517-520.

365. Neuhaus, D. and Williamson, M.P. (1989) *The Nuclear Overhauser Effect in Structural and Conformational Analysis.* VCH Publishers, New York.

366. Braun, W., Bosch, C., Brown, L.R., Go, N. and Wüthrich, K. (1981) Combined use of proton-proton Overhauser enhancements and a distance geometry algorithm for determination of polypeptide conformations. Application to micelle-bound glucagon. *Biochim. Biophys. Acta.* 667:377-396.

367. Jeener, J. (1979) Investigation of exchange processes by two-dimensional NMR spectroscopy. *J. Chem. Phys.* 71:4546-4553.

368. Clore, G.M. and Gronenborn, A.M. (1998) New methods of structure refinement for macromolecular structure determination by NMR. *Proc. Natl. Acad. Sci.* 95:5891-5898.

369. Wagner, R. and Berger, S. (1996) Gradient-selected NOESY - a fourfold reduction of the measurement time for the NOESY experiment. *J. Magn. Reson. A.* 123:119-121.

370. Kalk, A. and Berendsen, H.J.C. (1976) Proton magnetic relaxation and spin diffusion in proteins. *J. Magn. Res.* 24:343-366.

371. Wishart, D.S., Bigam, C.G., Holm, A., Hodges, R.S. and Sykes, B.D. (1995) H-1, C-13 and N-15 random coil NMR chemical shifts of the common amino acids. 1. Investigations of nearest-neighbor effects. *J. Biomol. NMR.* 5:67-81.

372. Wishart, D.S., Sykes, B.D. and Richards, F.M. (1991) Relationship between nuclear magnetic resonance chemical shift and protein secondary structure. *J. Mol. Biol.* 222:311-333.

373. Pastore, A. and Saudek, V. (1990) The relationship between chemical shift and secondary structure in proteins. *J. Magn. Res.* 90:165-176.

374. Dalgarno, D.C., Levine, B.A. and Williams, R.J.P. (1983) Structural information from NMR secondary chemical shifts of peptide α C-H protons in proteins. *Biosci. Rep.* 3:443-452.

375. Hol, W.G.J. (1985) The role of the α-helix dipole in protein function and structure. *Prog. Biophys. Mol. Biol.* 45:149-195.

376. Kuntz, I.D., Kosen, P.A. and Craig, E.C. (1991) Amide chemical shifts in many helices in peptides and proteins are periodic. *J. Am. Chem. Soc.* 113:1406-1408.

377. Zhou, N.E., Zhu, B., Sykes, B.D. and Hodges, R.S. (1992) Relationship between amide proton chemical shifts and hydrogen bonding in amphipathic α-helical peptides. *J. Am. Chem. Soc.* 114:4320-4326.

378. Blundell, T., Barlow, D., Borkakoti, N. and Thornton, J. (1983) Solvent-induced distortions and the curvature of α-helices. *Nature.* 306:281-283.

379. Wüthrich, K., Billeter, M. and Braun, W. (1984) Polypeptide secondary structure determination by nuclear magnetic resonance observation of short proton-proton distances. *J. Mol. Biol.* 180:715-740.

380. Karplus, M. (1959) Contact electron-spin coupling of nuclear magnetic moments. *J. Chem. Phys.* 30:11-15.

381. Pardi, A., Billeter, M. and Wüthrich, K. (1984) Calibration of the angular dependence of the amide proton-Cα coupling constants, $^3J_{HN\alpha}$, in a globular protein. *J. Mol. Biol.* 180:741-751.

382. Richardson, J.S. (1981) The anatomy and taxonomy of protein structure. *Adv. Protein Chem.* 34:167-339.

383. Kim, Y. and Prestegard, J.H. (1989) Measurement of vicinal couplings from cross peaks in COSY spectra. *J. Magn. Reson.* 84:9-13.

384. Nilges, M., Macias, M.J., Odonoghue, S.I. and Oschkinat, H. (1997) Automated NOESY interpretation with ambiguous distance restraints - the refined NMR solution structure of the pleckstrin homology domain from β-spectrin. *J. Mol. Biol.* 269:408-422.

385. Nilges, M. and O'Donoghue, S.I. (1998) Ambiguous NOEs and automated NOE assignment. *Prog. Nucl. Magn. Reson. Spectrosc.* 32:107-139.

386. Brünger, A.T., Adams, P.D., Clore, G.M., DeLano, W.L., Gros, P., Grosse-Kunstleve, R.W., Jiang, J., Kuszewski, J., Nilges, M., Pannu, N.S., Read, R.J., Rice, L.M., Simpson, T. and Warren, G.L. (1989) Crystallography & NMR system: A new software suite for macromolecular structure determination. *Acta Cryst. D.* 54:905-921.

387. Mal, T.K., Bagby, S. and Ikura, M. (2002) Protein structure calculation from NMR data. In *Calcium-Binding Protein Protocols,* (ed. Vogel, H.J.) pp. 267-283. Humana Press, Totowa.

388. Kaptein, R., Boelens, R., Scheek, R.M. and van Gunsteren, W.F. (1988) Protein structures from NMR. *Biochem.* 27:5389-5395.

389. Barsukov, I.L. and Lian, L. (1993) Structure determination from NMR data. I. Analysis of NMR data. In *NMR of Macromolecules: A Practical Approach,* (ed. Roberts, G.C.K.) pp. 315-357. Oxford University Press, New York.

390. Habeck, M., Rieping, W., Linge, J.P. and Nilges, M. (2004) NOE assignment with ARIA 2.0 - the nuts and bolts. In *Protein NMR Techniques,* (ed. Downing, A.K.) pp. 379-402. Humana Press, Totowa.

391. Linge, J.P., Habeck, M., Rieping, W. and Nilges, M. (2003) ARIA: Automated NOE assignment and NMR structure calculation. *Bioinformatics.* 19:315-316.

392. Williamson, M.P., Havel, T.F. and Wüthrich, K. (1985) Solution conformation of proteinase inhibitor IIA from bull seminal plasma by ^{1}H nuclear magnetic resonance and distance geometry. *J. Mol. Biol.* 182:295-315.

393. Havel, T.F. (1991) An evaluation of computational strategies for use in the determination of protein structure from distance constraints obtained by nuclear magnetic resonance. *Prog. Biophys. Mol. Biol.* 56:43-78.

394. Nilges, M. (1995) Calculation of protein structures with ambiguous distance restraints. Automated assignment of ambiguous NOE crosspeaks and disulphide connectivities. *J. Mol. Biol.* 245:645-660.

395. Güntert, P., Berndt, K.D. and Wüthrich, K. (1993) The program ASNO for computer-supported collection of NOE upper distance constraints as input for protein structure determination. *J. Biomol. NMR.* 3:601-606.

396. Nilges, M. (1993) A calculation strategy for the structure determination of symmetric dimers by ^{1}H NMR. *Proteins: Struct. Funct. Genet.* 17:297-309.

397. Fletcher, C.M., Jones, D.N.M., Diamond, R. and Neuhaus, D. (1996) Treatment of NOE constraints involving equivalent or nonstereoassigned protons in calculations of biomacromolecular structures. *J. Biomol. NMR.* 8:292-310.

398. Güntert, P., Werner, B., Gilleter, M. and Wüthrich, K. (1989) Automated stereospecific proton NMR assignments and their impact on the precision of protein structure determinations in solution. *J. Am. Chem. Soc.* 111:3997-4004.

399. Driscoll, P.C., Gronenborn, A.M. and Clore, G.M. (1989) The influence of stereospecific assignments on the determination of three-dimensional structures of proteins by nuclear magnetic resonance spectroscopy: Application to the sea anemone protein BDS-I. *FEBS Lett.* 243:223-233.

400. Zuiderweg, E.R.P., Boelens, R. and Kaptein, R. (1985) Stereospecific assignments of ^{1}H-NMR methyl lines and conformation of valyl residues in the *lac* repressor headpiece. *Biopolymers.* 24:601-611.

401. Folmer, R.H.A., Hilbers, C.W., Konings, R.N.H. and Nilges, M. (1997) Floating stereospecific assignment revisited - application to an 18 kDa protein and comparison with J-coupling data. *J. Biomol. NMR.* 9:245-258.

402. Weber, P.L., Morrison, R. and Hare, D. (1988) Determining stereo-specific ^{1}H nuclear magnetic resonance assignments from distance geometry calculations. *J. Mol. Biol.* 204:483-487.

403. Williamson, M.P. and Madison, V.S. (1990) Three-dimensional structure of porcine C5a$_{desArg}$ from proton nuclear magnetic resonance data. *Biochem.* 29:2895-2905.

404. Mulhern, T.D., Howlett, G.J., Reid, G.E., Simpson, R.J., McColl, D.J., Anders, R.F. and Norton, R.S. (1995) Solution structure of a polypeptide containing four heptad repeat units from a merozoite surface antigen of *Plasmodium falciparum. Biochem.* 34:3479-3491.

405. Brinkworth, C.S., Carver, J.A., Wegener, K.L., Doyle, J., Llewellyn, L.E. and Bowie, J.H. (2003) The solution structure of frenatin 3, a neuronal nitric oxide synthase inhibitor from the giant tree frog, *Litoria infrafrenata. Biopolymers.* 70:424-434.

406. Nilges, M., Clore, G.M. and Gronenborn, A.M. (1988) Determination of three-dimensional structures of proteins from interproton distance data by dynamical simulated annealing from a random array of atoms - circumventing problems associated with folding. *FEBS Lett.* 239:129-136.

407. Brünger, A.T., Clore, G.M., Gronenborn, A.M. and Karplus, M. (1986) Three-dimensional structure of proteins determined by molecular dynamics with interproton distance restraints: Application to crambin. *Proc. Natl. Acad. Sci.* 83:3801-3805.

408. Clore, G.M., Gronenborn, A.M., Brunger, A.T. and Karplus, M. (1985) Solution conformation of a heptadecapeptide comprising the DNA binding helix F of the cyclic AMP receptor protein of *Escherichia coli*: Combined use of 1H nuclear magnetic resonance and restrained molecular dynamics. *J. Mol. Biol.* 186:435-455.

409. Kaptein, R., Zuiderweg, E.R.P., Scheek, R.M., Boelens, R. and van Gunsteren, W.F. (1985) A protein structure from nuclear magnetic resonance data: lac repressor headpiece. *J. Mol. Biol.* 182:179-182.

410. Karplus, M. and Petsko, G.A. (1990) Molecular dynamics simulations in biology. *Nature.* 347:631-639.

411. Haile, J.M. (1992) *Molecular Dynamics Simulation - Elementary Methods.* John Wiley and Sons, New York.

412. Nabburs, S.B., Spronk, C.A.E.M., Vriend, G. and Vuister, G.W. (2004) Concepts and tools for NMR restraint analysis and validation. *Concepts Mag. Reson. A.* 22:90-105.

413. Laskowski, R.A. (2003) Structural quality assurance. In *Structural Bioinformatics,* (eds. Bourne, P.E. and Weissig, H.) pp. 273-303. John Wiley and Sons, New Jersey.

414. Morris, A.L., MacArthur, M.W., Hutchinson, E.G. and Thornton, J.M. (1992) Stereochemical quality of protein structure coordinates. *Proteins: Struct. Funct. Genet.* 12:345-364.

415. Hyberts, S.G., Goldberg, M.S., Havel, T.F. and Wagner, G. (1992) The solution structure of eglin C based on measurements of many NOEs and coupling constants and its comparison with X-ray structures. *Protein Sci.* 1:736-751.

416. Pallaghy, P.K., Duggan, B.M., Pennington, M.W. and Norton, R.S. (1993) Three-dimensional structure in solution of the calcium channel blocker ω-conotoxin. *J. Mol. Biol.* 234:405-420.

417. Ramachandran, G.N., Ramakrishnan, C. and Sasisekharan, V. (1963) Stereochemistry of polypeptide chain configurations. *J. Mol. Biol.* 7:95-99.

418. Epand, R.M. and Vogel, H.J. (1999) Diversity of antimicrobial peptides and their mechanisms of action. *Biochim. Biophys. Acta.* 1462:11-28.

419. Bechinger, B. (2000) Understanding peptide interactions with the lipid bilayer: A guide to membrane protein engineering. *Curr. Opin. Chem. Biol.* 4:639-644.

420. Bonev, B., Watts, A., Bokvist, M. and Grobner, G. (2001) Electrostatic peptide-lipid interactions of amyloid-β peptide and pentalysine with membrane surfaces monitored by ^{31}P MAS NMR. *Phys. Chem. Chem. Phys.* 3:2904-2910.

421. Inooka, H., Ohtaki, T., Kitahara, O., Ikegami, T., Endo, S., Kitada, C., Ogi, K., Onda, H., Fujino, M. and Shirakawa, M. (2001) Conformation of a peptide ligand bound to its G-protein coupled receptor. *Nat. Struct. Biol.* 8:161-165.

422. Moroder, L. and Romano, R. (1994) Synthesis, conformational and biological properties of lipophilic derivatives of gastrin and cholecystokinin peptides. *Pure App. Chem.* 66:2111-2114.

423. Lauterwein, J., Bosch, C., Brown, L.R. and Wüthrich, K. (1979) Physicochemical studies of the protein-lipid interactions in melittin-containing micelles. *Biochim. Biophys. Acta.* 556:244-264.

424. Mendz, G.L., Moore, W.J., Brown, L.R. and Martenson, R.E. (1984) Interaction of myelin basic protein with micelles of dodecylphosphocholine. *Biochem.* 23:6041-6046.

425. Rajan, R. and Balaram, P. (1996) A model for the interaction of trifluoroethanol with peptides and proteins. *Int. J. Pept. Protein Res.* 48:328-336.

426. Nelson, J.W. and Kallenbach, N.R. (1986) Stabilisation of the ribonuclease S-peptide α-helix by trifluoroethanol. *Proteins: Struct. Funct. Genet.* 1:211-217.

427. Gesell, J., Zasloff, M. and Opella, S.J. (1997) Two-dimensional ^{1}H NMR experiments show that the 23-residue magainin antibiotic peptide is an alpha-helix in dodecylphosphocholine micelles, sodium dodecylsulfate micelles, and trifluoroethanol/water solution. *J. Biomol. NMR.* 9:127-135.

428. Marion, D., Zasloff, M. and Bax, A. (1988) A two-dimensional NMR study of the antimicrobial peptide magainin 2. *FEBS Lett.* 227:21-26.

429. Santiveri, C.M., Pantoja-Uceda, D., Rico, M. and Jiméne, M.A. (2005) β-Hairpin formation in aqueous solution and in the presence of trifluoroethanol: A ^{1}H and ^{13}C NMR conformational study of designed peptides. *Biopolymers.* 79:150-162.

430. Yu, K., Kim, Y., Kang, S., Park, N. and Shin, J. (2000) Relationship between the tertiary structures of mastoparan B and its analogs and their lytic activities studied by NMR spectroscopy. *J. Pept. Res.* 55:51-62.

431. Hong, D.P., Hoshino, M., Kuboi, R. and Goto, Y. (1999) Clustering of fluorine-substituted alcohols as a factor responsible for their marked effects on proteins and peptides. *J. Am. Chem. Soc.* 121:8427-8433.

432. Hirota, N., Mizuno, K. and Goto, Y. (1998) Group additive contributions to the alcohol-induced alpha-helix formation of melittin - implication for the mechanism of the alcohol effects on proteins. *J. Mol. Biol.* 275:365-378.

433. Dong, A., Matsuura, J., Manning, M.C. and Carpenter, J.F. (1998) Intermolecular β-sheet results from trifluoroethanol-induced nonnative α-helical structure in β-sheet predominant proteins - infrared and circular dichroism spectroscopic study. *Arch. Biochem. Biophys.* 355:275-281.

434. Sönnichsen, F.D., Van Eyk, J.A., Hodges, R.S. and Sykes, B.D. (1992) Effect of trifluoroethanol on protein secondary structure: An NMR and CD study using a synthetic actin peptide. *Biochem.* 31:8790-8798.

435. Schönbrunner, N., Wey, J., Engels, J., Georg, H. and Kiefhaber, T. (1996) Native-like β-structure in a trifluoroethanol-induced partially folded state of the all-β-sheet protein tendamistat. *J. Mol. Biol.* 260:432-445.

436. Reiersen, H. and Rees, A.R. (2000) Trifluoroethanol may form a solvent matrix for assisted hydrophobic interactions between peptide side chains. *Protein Eng.* 13:739-743.

437. Kuwata, K., Hoshino, M., Era, S., Batt, C.A. and Goto, Y. (1998) α - β transition of α-lactoglobulin as evidenced by heteronuclear NMR. *J. Mol. Biol.* 283:731-739.

438. Narhi, L.O., Philo, J.S., Li, T., Zhang, M., Samal, B. and Arakawa, T. (1996) Induction of α-helix in the β-sheet protein tumor necrosis factor-α: Thermal- and trifluoroethanol-induced denaturation at neutral pH. *Biochem.* 35:11447-11453.

439. Jesson, J.P., Meakin, P. and Kneissel, G. (1973) Homonuclear decoupling and peak elimination in Fourier transform nuclear magnetic resonance. *J. Am. Chem. Soc.* 95:618-620.

440. Wider, G., Hosur, R.J. and Wüthrich, K. (1983) Suppression of the solvent resonance in 2D NMR spectra of proteins in H_2O solution. *J. Magn. Reson.* 52:130-135.

441. Smallcombe, S.H., Patt, S.L. and Kiefer, P.A. (1995) WET solvent suppression and its application to LC NMR and high-resolution NMR spectroscopy. *J. Magn. Reson.* 117:295-303.

442. Ogg, R.J., Kingsley, P.B. and Taylor, J.S. (1994) WET, a T1- and B1-insensitive water-suppression method for in vivo localised ^{1}H NMR spectroscopy. *J. Magn. Reson. B.* 104:1-10.

443. Piotto, M., Saudek, V. and Sklenár, V. (1992) Gradient-tailored excitation for single-quantum NMR spectroscopy of aqueous solutions. *J. Biomol. NMR.* 2:661-665.

444. Liu, M., Mao, X., Ye, C., Huang, H., Nicholson, J.K. and Lindon, J.C. (1998) Improved WATERGATE pulse sequences for solvent suppression in NMR spectroscopy. *J. Magn. Reson.* 132:125-129.

445. Lincoln, J., Hoyle, C.H.V. and Burnstock, G. (1997) Synthesis and properties of nitric oxide. In *Nitric Oxide in Health and Disease,* pp. 12-26. Cambridge University Press, Cambridge.

446. Moncada, S. and Higgs, E.A. (1995) Molecular mechanisms and therapeutic strategies related to nitric oxide. *FASEB J.* 9:1319-1330.

447. Billiar, T.R. (1995) Nitric oxide, novel biology with clinical relevance. *Ann. Surg.* 221:339-349.

448. Nathan, C.F. and Hibbs, J.B. (1991) Role of nitric oxide synthesis in macrophage antimicrobial activity. *Curr. Opin. Immunol.* 3:65-70.

449. Lancaster, J.R. (1997) A tutorial on the diffusibility and reactivity of free nitric oxide. *Nitric Oxide.* 1:18-30.

450. Ignaro, L.J. (1990) Biosynthesis and metabolism of endothelium-derived nitric oxide. *Annu. Rev. Pharmacol. Toxicol.* 30:535-560.

451. Kerwin, J.F. (1995) Nitric oxide: A new paradigm for second messengers. *J. Med. Chem.* 38:4343-4362.

452. Pfeilschifter, J., Eberhardt, W., Hummel, R., Kunz, D., Muhl, H., Nitsch, D., Pluss, C. and Walker, G. (1996) Therapeutic strategies for the inhibition of inducible nitric oxide synthase - potential for a novel class of anti-inflammatory agents. *Cell Biol. Int.* 20:51-58.

453. Stuehr, D.J. (1999) Mammalian nitric oxide synthases. *Biochim. Biophys. Acta.* 1411:217-230.

454. Marletta, M.A. (1993) Nitric oxide synthase structure and mechanism. *J. Biol. Chem.* 268:12231-12234.

455. Alderton, W.K., Copper, C.E. and Knowles, R.G. (2001) Nitric oxide synthases: Structure, function and inhibition. *Biochem. J.* 357:593-615.

456. Andrew, P.J. and Mayer, B. (1999) Enzymatic function of nitric oxide synthases. *Cardiovascular Res.* 43:521-531.

457. Nathan, C. and Xie, Q. (1994) Regulation of biosynthesis of nitric oxide. *J. Biol. Chem.* 269:13725-13728.

458. Schmidt, H.H.H.W., Pollock, J.S., Nankane, M., Forstermann, U. and Murad, F. (1992) Ca^{2+}/calmodulin-regulated nitric oxide synthases. *Cell Calcium.* 13:427-434.

459. Means, A.R., Tash, J.S. and Chafouleas, J.G. (1982) Physiological implications of the presence, distribution and regulation of calmodulin in eukaryotic cells. *Phys. Rev.* 62:1-39.

460. Barbato, G., Ikura, M., Kay, L.E., Pastor, R.W. and Bax, A. (1992) Backbone dynamics of calmodulin studied by ^{15}N relaxation using inverse detected two-dimensional NMR spectroscopy: The central helix is flexible. *Biochem.* 31:5269-5278.

461. Chattopadhyaya, R., Meador, W.E., Means, A.R. and Quiocho, F.A. (1992) Calmodulin structure refined at 1.7 Å resolution. *J. Mol. Biol.* 228:1177-1192.

462. Williams, R.J.P. (1992) Calcium and calmodulin. *Cell Calcium.* 13:355-362.

463. Babu, Y.S., Bugg, C.E. and Cook, W.J. (1988) Structure of calmodulin refined at 2.2 Å resolution. *J. Mol. Biol.* 204:191-204.

464. Watanabe, Y., Hu, Y. and Hidaka, H. (1996) Identification of a specific amino acid cluster in the calmodulin-binding domain of the neuronal nitric oxide synthase. *FEBS Lett.* 403:75-78.

465. Matsubara, M., Hayashi, N., Titani, K. and Taniguchi, H. (1997) Circular dichroism and ^{1}H NMR studies on the structures of peptides derived from the calmodulin-binding domains of inducible and endothelial nitric-oxide synthase in solution and in complex with calmodulin. *J. Biol. Chem.* 272:23050-23056.

466. Abu-Soud, H., Yoho, L. and Stuehr, D. (1994) Calmodulin controls neuronal nitric-oxide synthase by a dual mechanism. Activation of intra- and interdomain electron transfer. *J. Biol. Chem.* 269:32047-32050.

467. Abu-Soud, H. and Stuehr, D. (1993) Nitric oxide synthases reveal a role for calmodulin in controlling electron transfer. *Proc. Natl. Acad. Sci.* 90:10769-10772.

468. Gachhui, R., Presta, A., Bentley, D.F., Abu-Soud, H.M., McArthur, R., Brudvig, G., Ghosh, D.K. and Stuehr, D.J. (1996) Characterization of the reductase domain of rat neuronal nitric oxide synthase generated in the methylotrophic yeast *Pichia pastoris*. *J. Biol. Chem.* 271:20594-20602.

469. Cox, J.A., Comte, M., Fitton, J.E. and DeGrado, W.F. (1985) The interaction of calmodulin with amphiphilic peptides. *J. Biol. Chem.* 260:2527-2534.

470. Vetter, S.W. and Leclerc, E. (2003) Novel aspects of calmodulin target recognition and activation. *Eur. J. Biochem.* 270:404-414.

471. Ikura, M., Clore, G.M., Gronenborn, A.M., Zhu, G., Klee, C.B. and Bax, A. (1992) Solution structure of a calmodulin-target peptide complex by multidimensional NMR. *Science.* 256:632-638.

472. Persechini, A. and Kretsinger, R.H. (1988) Towards a model of the calmodulin-myosin light-chain kinase complex: Implications for calmodulin function. *J. Cardiovasc. Pharmacol.* 12 (Suppl. 5):S1-S12.

473. Rhoads, A. and Friedberg, F. (1997) Sequence motifs for calmodulin recognition. *FASEB J.* 11:331-340.

474. Mirzoeva, S., Weigand, S., Lukas, T.J., Shuvalova, L., Anderson, W.F. and Watterson, D.M. (1999) Analysis of the functional coupling between calmodulin's calcium binding and peptide recognition properties. *Biochem.* 38:3936-3947.

475. Roth, S.M., Schmeider, D.M., Strobel, L., van Berkum, M., Means, A. and Wand, A.J. (1991) Structure of the smooth muscle myosin light-chain kinase calmodulin-binding domain peptide bound to calmodulin. *Biochem.* 30:10078-10084.

476. Meador, W.E., Means, A.R. and Quiocho, F.A. (1992) Target enzyme recognition by calmodulin: 2.4 Å structure of a calmodulin peptide complex. *Science.* 257:1251-1255.

477.   Elshorst, B., Hennig, M., Forsterling, H., Diener, A., Maurer, M., Schulte, P., Schwalbe, H., Griesinger, C., Krebs, J., Schmid, H., Vorherr, T. and Carafoli, E. (1999) NMR solution structure of a complex of calmodulin with a binding peptide of the Ca^{2+} pump. *Biochem.* 38:12320-12332.

478.   Renteria, R.C. and Constantine-Paton, M. (1999) Nitric oxide in the retinotectal system: A signal but not a retrograde messenger during map refinement and segregation. *J. Neurosci.* 19:7066-7076.

479.   Gobbetti, A. and Zeran, M. (1999) Hormonal and cellular brain mechanisms regulating the amplexus of male and female water frog (*Rana esculenta*). *J. Neuroendocrinol.* 11:589-596.

480.   Molero, M., Hernandez, I.M., Lobo, P., Cardenas, P., Romero, R. and Chacin, J. (1998) Modulation by nitric oxide of gastric acid secretion in toads. *Acta Physiol. Scand.* 164:229-236.

481.   Guerini, D. (1997) Calcineurin: Not just a simple protein phosphatase. *Biochem. Biophys. Res. Commun.* 235:271-275.

482.   Apponyi, M.A. (2006) *Amphibian Skin Peptides Which Inhibit nNOS: Structure and Binding Studies Using Heteronuclear NMR.* Chemistry Ph.D. Thesis. The University of Adelaide

483.   Doyle, J., Brinkworth, C.S., Wegener, K.L., Carver, J.A., Llewellyn, L.E., Olver, I.N., Bowie, J.H., Wabnitz, P.A. and Tyler, M.J. (2003) nNOS inhibition, antimicrobial and anticancer activity of the amphibian skin peptide, citropin 1.1 and synthetic modification: The solution structure of a modified citropin 1.1. *Eur. J. Biochem.* 270:1141-1153.

484.   Maclean, M.J., Brinkworth, C.S., Bilusich, D., Bowie, J.H., Doyle, J.R., Llewellyn, L.E. and Tyler, M.J. (2006) New caerin antibiotic peptides from the skin secretion of the dainty green tree frog *Litoria gracilenta*. Identification using positive and negative ion electrospray mass spectrometry. *Toxicon.* 47:664-675.

485.   Hill, T.J., Lafitte, D., Wallace, J.I., Cooper, H.J., Tsvetkov, P.O. and Derrick, P.J. (2000) Calmodulin-peptide interactions: Apocalmodulin binding to the myosin light chain kinase target-site. *Biochem.* 39:7284-7290.

486.   Lafitte, D., Heck, A.J.R., Hill, T.J., Jumel, K., Harding, S.E. and Derrick, P.J. (1999) Evidence of noncovalent dimerization of calmodulin. *Eur. J. Biochem.* 261:337-344.

487.   Hu, P., Qi-Zhuang, Y. and Loo, J.A. (1994) Calcium stoichiometry determination for calcium binding proteins by electrospray ionization mass spectrometry. *Anal. Chem.* 66:4190-4194.

488.   Chowdhury, S.K. and Chait, B.T. (1990) Analysis of mixtures of closely related forms of bovine trypsin by electrospray ionization mass spectrometry: Use of charge state distributions to resolve ions of the different forms. *Biochem. Biophys. Res. Commun.* 173:927-931.

489.   Wüthrich, K. and Wider, G. (1982) Sequential resonance assignments as a basis for determination of spatial protein structures by high resolution proton nuclear magnetic resonance. *J. Mol. Biol.* 155:311-319.

490. Szilagyi, L. and Jardetzky, O. (1989) α-Proton chemical shifts and secondary structure in proteins. *J. Magn. Res.* 83:441-449.

491. Wright, P.E., Dyson, H.J. and Lerner, R.A. (1988) Conformation of peptide fragments of proteins in aqueous solution: Implications for initiation of protein folding. *Biochem.* 27:7167-7175.

492. Schon, O., Friedler, A., Freund, S. and Fersht, A.R. (2004) Binding of p53-derived ligands to MDM2 induces a variety of long range conformational changes. *J. Mol. Biol.* 336:197-202.

493. Le, H. and Oldfield, E. (1994) Correlation between ^{15}N NMR chemical shifts in proteins and secondary structure. *J. Biomol. NMR.* 4:341-348.

494. Wagner, G., Pardi, A., Wuthrich, K. (1983) Hydrogen bond length and ^{1}H NMR chemical shifts in proteins. *J. Am. Chem. Soc.* 105:5948-5949.

495. Prêcheur, B., Munier, H., Mispelter, J., Bârzu, O. and Craescu, C. (1992) ^{1}H and ^{15}N NMR characterization of free and bound states of an amphipathic peptide interacting with calmodulin. *Biochem.* 31:229-236.

496. Craescu, C., Bouhss, A., Mispelter, J., Diesis, E., Popescu, A., Chiriac, M. and Bârzu, O. (1995) Calmodulin binding of a peptide derived from the regulatory domain of *Bordetella perussis* adenylate cyclase. *J. Biol. Chem.* 270:7088-7096.

497. Lafitte, D., Benezech, V., Bompart, J., Laurent, F., Bonnet, P.A., Chapat, J.P., Grassy, G. and Calas, B. (1997) Characterization of low affinity complexes between calmodulin and pyrazine derivatives by electrospray ionisation mass spectrometry. *J. Mass Spectrom.* 32:87-93.

498. Nemirovskiy, O., Ramanthan, R. and Gross, M.L. (1997) Investigation of calcium-induced, noncovalent association of calmodulin with melittin by electrospray ionization mass spectrometry. *J. Am. Soc. Mass Spectrom.* 8:809-812.

499. Schumacher, M.A.F.R.A., Bachinger, H.P. and Adelman, J.P. (2001) Structure of the gating domain of a Ca^{2+}-activated K^{+} channel complexed with Ca^{2+}/calmodulin. *Nature.* 410:1120-1124.

500. Wintrode, P.L. and Privalov, P.L. (1997) Energetics of target peptide recognition by calmodulin: A calorimetric study. *J. Mol. Biol.* 266:1050-1062.

501. Watt, S.J., Oakley, A., Shiel, M. and Beck, J. (2005) Comparison of negative and positive ion electrospray ionization mass spectra of calmodulin and its complex with trifluoperazine. *Rapid Commun. Mass Spectrom.* 19:2123-2130.

502. O'Neil, K.T. and DeGrado, W.F. (1989) The interaction of calmodulin with fluorescent and photoreactive model peptides: Evidence for a short interdomain separation. *Proteins.* 6:284-293.

503. Crouch, T.H. and Klee, C.B. (1980) Positive cooperative binding of calcium to bovine brain calmodulin. *Biochem.* 19:3692-3698.

504. Nemirovskiy, O., Giblin, D.E. and Gross, M.L. (1999) Electrospray ionization mass spectometry and hydrogen/deuterium exchange for probing the interaction of calmodulin with calcium. *J. Am. Chem. Soc. Mass Spectrom.* 10:711-718.

505. Ikura, M., Kay, L.E. and Bax, A. (1990) A novel approach for sequential assignment of ^{1}H, ^{13}C and ^{15}N spectra of larger proteins: Heteronuclear triple-resonance three-dimensional NMR spectroscopy. Application to calmodulin. *Biochem.* 29:4659-4667.

506. Delaglio, F., Grzesiek, S., Vuister, G.W., Zhu, G., Pfeifer, J. and Bax, A. (1995) NMRPipe: A multidimensional spectral processing system based on UNIX pipes. *J. Biomol. NMR.* 6:277-293.

507. John, B.K., Plant, D., Webb, P. and Hurd, R.E. (1992) Effective combination of gradients and crafted RF pulses for water suppression in biological samples. *J. Magn. Res.* 98:200-206.

508. Tyler, M.J. (1978) *Amphibians of South Australia.* D.J. Woolman, Adelaide.

509. Maselli, V.M. (2006) *Amphibian Neuropeptides: Isolation, Sequence Determination and Bioactivity*. Chemistry Ph.D. Thesis, The University of Adelaide

510. Noble, F., Wank, S.A., Crawley, J.N., Bradwejn, J., Seroogy, K.B., Hamon, M. and Roques, B.P. (1999) Structure, distribution and functions of cholecystokinin receptors. *Pharm. Rev.* 51:745-781.

511. Reeve, J.R. (ed.) (1994) *Cholecystokinin.* New York Academy of Sciences, New York.

512. Dockray, G., Dimaline, R. and Varro, A. (2005) Gastrin: Old hormone, new functions. *Pflügers Arch.* 449:344-355.

513. Wank, S.A. (1995) Cholecystokinin receptors. *Am. J. Physiol.* 269:628-646.

514. Patel, M. and Spraggs, C.F. (1992) Functional comparisons of gastrin/cholecystokinin receptors in isolated preparations of gastric mucosa and ileum. *Br. J. Pharmacol.* 106:275-282.

515. Bitar, K.N. and Makhlouf, G.M. (1982) Receptors on smooth muscle cells: Characterization by contraction and specific antagonists. *Am. J. Physiol.* 242:400-407.

516. Sacerdote, P., Wiedermann, C.J., Wahl, L.M., Pert, C.B. and Ruff, M.R. (1991) Visualization of cholecystokinin receptors on a subset of human monocytes and in rat spleen. *Peptides.* 12:167-176.

517. Fourmy, D., Escrieut, C., Archer, E., Gales, C., Gigoux, V., Maigret, B., Moroder, L., Silvente-Poirot, S., Martinez, J., Fehrentz, J. and Pradayrol, L. (2002) Structure of cholecystokinin receptor binding sites and mechanism of activation/inactivation by agonists/antagonists. *Pharmacol. Toxicol.* 91:313-320.

518. Escherich, A., Lutz, J., Escrieut, C., Fourmy, D., van Neuren, A.S., Müller, G., Schafferhans, A., Klebe, G. and Moroder, L. (2000) Peptide/benzodiazepine hybrids as ligands of CCK_A and CCK_B receptors. *Biopolymers.* 56:55-76.

519. De Luca, S., Ragone, R., Bracco, C., Digilio, G., Aloj, L., Tesauro, D., Saviano, M., Pedone, C. and Morelli, G. (2003) A cyclic CCK8 analogue selective for the cholecystokinin type A receptor: Design, synthesis, NMR structure and binding measurements. *Chem. Biochem.* 4:1176-1187.

520. Hamm, H.E. (1998) The many faces of G protein signalling. *J. Biol. Chem.* 273:669-672.

521. Ji, T.H., Grossmann, M. and Ji, I. (1998) G protein-coupled receptors. 1. Diversity of receptor-ligand interactions. *J. Biol. Chem.* 273:17299-17302.

522. Iyengar, R. and Hildebrandt, J.D. (eds.) (2002) *G protein pathways.* Academic Press, San Diego.

523. Palczewski, K., Kumasaka, T., Hori, T., Behnke, C.A., Motoshima, H., Fox, B.A., Trong, I.L., Teller, D.C., Okada, T., Stenkamp, R.E., Yamamoto, M. and Miyano, M. (2000) Crystal structure of rhodopsin: A G protein-coupled receptor. *Science.* 289:739-745.

524. Ji, Z., Hadac, E.M., Henne, R.M., Patel, S.A., Lybrand, T.P. and Miller, L.J. (1997) Direct identification of a distinct site of interaction between the carboxyl-terminal residue of cholecystokinin and the type A cholecystokinin receptor using photoaffinity labeling. *J. Biol. Chem.* 272:24393-24401.

525. Kopin, A.S., McBride, E.W., Quinn, S.M., Kolakowski, L.F. and Beinborn, M. (1995) The role of the cholecystokinin-B/gastrin receptor transmembrane domains in determining affinity for subtype-selective ligands. *J. Biol. Chem.* 270:5019-5023.

526. Silvente-Poirot, S., Escrieut, C. and Wank, S.A. (1998) Role of the extracellular domains of the cholecystokinin receptor in agonist binding. *Mol. Pharmacol.* 54:364-371.

527. Jagerschmidt, A., Guillaume, N., Roques, B.P. and Noble, F. (1998) Binding sites and transduction process of the cholecystokinin B receptor: Involvement of highly conserved aromatic residues of the transmembrane domains evidenced by site-directed mutagenesis. *Mol. Pharmacol.* 53:878-885.

528. Galés, C., Poirot, M., Taillefer, J., Maigret, B., Martinez, J., Moroder, L., Escrieut, C., Pradayrol, L., Fourmy, D. and Silvente-Poirot, S. (2003) Identification of tyrosine 189 and asparagine 358 of the cholecystokinin 2 receptor in direct interaction with the crucial C-terminal amide of cholecystokinin by molecular modeling, site-directed mutagenesis, and structure/affinity studies. *Mol. Pharmacol.* 63:973-982.

529. Anders, J., Bluggel, M., Meyer, H.E., Kuhne, R., ter Laak, A.M., Korjo, E. and Farenholz, F. (1999) Direct identification of the agonist binding site in the human brain cholecystokinin_B receptor. *Biochem.* 38:6043-6055.

530. Silvente-Poirot, S. and Wank, S.A. (1996) A segment of five amino acids in the second extracellular loop of the cholecystokinin-B receptor is essential for selectivity of the peptide agonist gastrin. *J. Biol. Chem.* 271:14698-14706.

531. Silvente-Poirot, S., Escrieut, C., Galés, C., Fehrentz, J.A., Escherich, A., Wank, S.A., Martinez, J., Moroder, L., Maigret, B., Bouisson, M., Vaysse, N. and Fourmy, D. (1999) Evidence for a direct interaction between the penultimate C-terminal aspartic acid of cholecystokinin and histidine 207 located in the second extracellular loop of the cholecystokinin B receptor. *J. Biol. Chem.* 274:23191-23197.

532. Dong, M., Ding, X., Pinon, D.I., Hadac, E.M., Oda, R.P., Landers, J.P. and Miller, L.J. (1999) Structurally related peptide agonist, partial agonist, and antagonist occupy a similar binding pocket within the cholecystokinin receptor. *J. Biol. Chem.* 274:4778-4785.

533. Conlon, J.M., Kolodziejek, J. and Nowotny, N. (2004) Antimicrobial peptides from ranid frogs: Taxonomic and phylogenetic markers and a potential source of new therapeutic agents. *Biochim. Biophys. Acta.* 1696:1-14.

534. Erspamer, W., Erspamer, G.F. and Cei, J.M. (1986) Active peptides in the skins of two hundred and thirty American amphibian species. *Comp. Biochem. Physiol.* 85C:125-137.

535. Marenah, L., Flatt, P.R., Orr, D.F., Shaw, C. and Abdel-Wahab, Y.H.A. (2005) Characterization of naturally occurring peptides in the skin secretion of the *Rana pipiens* frog reveal pipinin-1 as the novel insulin-releasing agent. *J. Pept. Res.* 66:204-210.

536. Sai, K., Jagannadham, M., Vairamani, M., Raju, N., Devi, A., Nagaraj, R. and Sitaram, N. (2001) Tigerinins: Novel antimicrobial peptides from the Indian frog *Rana tigerina*. *J. Biol. Chem.* 276:2701-2707.

537. MacArthur, M.W. and Thornton, J.M. (1991) Influence of proline residues on protein conformation. *J. Mol. Biol.* 218:397-412.

538. Jabs, A., Weiss, M.S. and Hilgenfeld, R. (1999) Non-proline cis peptide bonds in proteins. *J. Mol. Biol.* 286:291-304.

539. Rose, G.D., Gierasch, L.M. and Smith, J.S. (1985) Turns in peptides and proteins. *Adv. Protein Chem.* 37:1-109.

540. Chou, K. (2000) Prediction of tight turns and their types in proteins. *Anal. Biochem.* 286:1-16.

541. Venkatachalam, C.M. (1968) Stereochemical criteria for polypeptides and proteins. V. Conformation of a system of three linked peptide units. *Biopolymers.* 6:1425-1436.

542. Lewis, P.N., Momany, F.A. and Scheraga, H.A. (1973) Chain reversals in proteins. *Biochim. Biophys. Acta.* 303:211-229.

543. Fournié-Zaluski, M.C., Belleny, J., Lux, B., Durieux, C., Gérard, G., Gacel, G., Maigret, B. and Roques, B.P. (1986) Conformational analysis of neuronal cholecystokinin CCK$_{26,33}$ and related fragments by ^{1}H NMR spectroscopy, fluorescence transfer measurements and calculations. *Biochem.* 25:3778-3787.

544. Charpentier, B., Pelaprat, D., Durieux, C., Dor, A., Reibaud, M., Blanchard, J.C. and Roques, B.P. (1988) Cyclic cholecystokinin analogues with high selectivity for central receptors. *Proc. Natl. Acad. Sci.* 85:1968-1972.

545. Charpentier, B., Dor, A., Roy, P., England, P., Pham, H., Durieux, C. and Roques, B.P. (1989) Synthesis and binding affinities of cyclic and related linear analogs of CCK8 selective for central receptors. *J. Med. Chem.* 32:1184-1190.

546. Archer-Lahlou, E., Escrieut, C., Clerc, P., Martinez, J., Moroder, L., Logsdon, C., Kopin, A., Seva, C., Dufresne, M., Pradayrol, L., Maigret, B. and Fourmy, D. (2005) Molecular mechanism underlying partial and full agonism mediated by the human cholecystokinin-1 receptor. *J. Biol. Chem.* 280:10664-10674.

547. Huang, S., Fortune, K., Wank, S., Kopin, A. and Gardner, J. (1994) Multiple affinity states of different cholecystokinin receptors. *J. Biol. Chem.* 269:26121-26126.

548. Brünger, A.T. (1988) Crystallographic refinement by simulated annealing - application to a 2.8 Å resolution structure of aspartate aminotransferase. *J. Mol. Biol.* 203:803-816.

549. Pari, K., Mueller, G.A., DeRose, E.F., Kirby, T.W. and London, R.E. (2003) Solution structure of the RNase H domain of the HIV-1 reverse transcriptase in the presence of magnesium. *Biochem.* 42:639-650.

550. Humphrey, W., Dalke, A. and Schulten, K. (1996) VMD - visual molecular dynamics. *J. Mol. Graphics.* 14:33-38.

551. Koradi, R., Billeter, M. and Wüthrich, K. (1996) MOLMOL - a program for display and analysis of macromolecular structures. *J. Mol. Graphics.* 14:51-55.

552. Fyfe, C.A. (1983) *Solid State NMR for Chemists.* CFC Press, Ontario.

553. Brown, S.P. and Emsley, L. (2003) Solid-State NMR. In *Handbook of Spectroscopy,* (eds. Vo-Dinh, T. and Gauglitz, G.) pp. 269-326. Wiley, Weinheim.

554. Bechinger, B. (1999) The structure, dynamics and orientation of antimicrobial peptides in membranes by multidimensional solid-state NMR spectroscopy. *Biochim. Biophys. Acta.* 1462:157-183.

555. Smith, I.C.P. and Ekiel, I.H. (1984) Phosphorus-31 NMR of phospholipids in membranes. In *Phosphorus-31 NMR. Principles and Applications,* (ed. Garenstein, D.G.) pp. 447-475. Academic Press Inc., London.

556. Kentgens, A.P.M. (1997) A practical guide to solid-state NMR of half-integer quadrupolar nuclei with some applications to disordered systems. *Geoderma.* 80:271-306.

557. Davis, J.H. (1983) The description of membrane lipid conformation, order and dynamics by ^{2}H-NMR. *Biochim. Biophys. Acta.* 737:117-171.

558. Sanders, C.R., Hare, B.J., Howard, K.P. and Prestegard, J.H. (1994) Magnetically-oriented phospholipid micelles as a tool for the study of membrane-associated molecules. *Prog. Nucl. Magn. Reson. Spectrosc.* 26:421-444.

559. Pake, G.E. (1948) Nuclear resonance absorption in hydrated crystals: Fine structure of the proton line. *J. Chem. Phys.* 16:327-336.

560. Laws, D., Bitter, H.L. and Jerschow, A. (2002) Solid-state NMR spectroscopic methods in chemistry. *Angew. Chem. Int. Ed.* 41:3096-3129.

561. Opella, S.J. (1982) Solid state NMR of biological systems. *Ann. Rev. Phys. Chem.* 33:533-562.

562. Hodgkinson, P. and Emsley, L. (1999) The accuracy of distance measurements in solid-state NMR. *J. Magn. Reson.* 139:46-56.

563. Pines, A., Gibby, M.C. and Waugh, J.S. (1973) Proton enhanced nuclear magnetic resonance of dilute spins in solids. *J. Chem. Phys.* 59:569-590.

564. Bloch, F. (1956) Dynamical theory of nuclear induction. *Phys. Rev.* 102:104-135.

565. Andrew, E.G., Bradbury, A. and Eades, R.G. (1959) Removal of dipolar broadening of nuclear magnetic resonance spectra of solids by specimen rotation. *Nature.* 183:1802-1803.

566. Lowe, I.J. (1959) Free induction decays of rotating solids. *Phys. Rev. Lett.* 2:285-287.

567. Roberts, J.E. and Griffin, R.G. (1987) Solid state NMR techniques. In *Phosphorus NMR in Biology,* (ed. Burt, C.T.) pp. 63-94. CRC Press, Florida.

568. Herzfeld, J. and Berger, A.E. (1980) Sideband intensities in NMR spectra of samples spinning at the magic angle. *J. Chem. Phys.* 73:6021-6030.

569. Finean, J.B. and Michell, R.H. (1981) Isolation, composition and general structure of membranes. In *Membrane Structure,* (eds. Finean, J.B. and Michell, R.H.) pp. 1-36. Elsevier, Amsterdam.

570. Rouser, G., Nelson, G.J., Fleischer, S. and Simon, G. (1968) Lipid composition of animal cell membranes, organelles and organs. In *Biological Membranes: Physical Fact and Function,* (ed. Chapman, D.) pp. 5-69. Academic Press, London.

571. Rogers, H.J., Perkins, H.R. and Ward, J.B. (1980) *Microbial Cell Walls and Membranes.* Chapman and Hall, London.

572. Kobayashi, T., Gu, F. and Gruenberg, J. (1998) Lipids, lipid domains and lipid-protein interactions in endocytic membrane traffic. *Semin. Cell Dev. Biol.* 9:517-526.

573. Jahn, R. (1999) Membrane fusion and exocytosis. *Ann. Rev. Biochem.* 68:863-911.

574. van Meer, G. and Sprong, H. (2004) Membrane lipids and vesicular traffic. *Curr. Opin. Cell Biol.* 16:373-378.

575. Dowhan, W. and Bogdanov, M. (2002) Functional role of lipids in membranes. In *Biochemistry of Lipids, Lipoproteins and Membranes, 4 ed.* (eds. Vance, D.E. and Vance, J.E.) pp. 1-35. Elsevier Science, Amsterdam.

576. Luzzati, V. (1968) X-ray diffraction studies of lipid-water systems. In *Biological Membranes: Physical Fact and Function,* (ed. Chapman, D.) pp. 71-123. Academic Press, London.

577. Luzzati, V. and Husson, F. (1962) The structure of the liquid-crystalline phases of lipid-water systems. *J. Cell Biol.* 12:207-219.

578. Singer, S.G. and Nicolson, G.L. (1972) The fluid mosaic model of the structure of cell membranes. *Science.* 175:720-731.

579. Seelig, J. (1984) Lipid polymorphism, reverse micelles, and phosphorus-31 nuclear magnetic resonance. In *Reverse Micelles,* (eds. Luisi, P.L. and Straub, B.E.) pp. 209-220. Plenum Pub. Co., New York.

580. Bocian, D.F. and Chan, S.I. (1978) NMR studies of membrane structure and dynamics. *Ann. Rev. Phys. Chem.* 29:307-335.

581. Lodish, H., Berk, A., Zipursky, L.S., Matsudaira, P., Baltimore, D. and Darnell, J. (2000) *Cellular Energetics: Glycolysis, Aerobic Oxidation, and Photosynthesis. 4th ed.* W. H. Freeman, New York.

582. Davis, J.H. and Auger, M. (1999) Static and magic angle spinning NMR of membrane peptides and proteins. *Prog. Nucl. Magn. Reson. Spectrosc.* 35:1-84.

583. Seelig, J. and Niederberger, W. (1974) Two pictures of a lipid bilayer. A comparison between deuterium label and spin-label experiments. *Biochem.* 13:1585-1588.

584. Yeagle, P.L. (1987) ^{31}P NMR and the phospholipid headgroups of membranes. In *Phosphorus NMR in Biology,* (ed. Burt, C.T.) pp. 95-113. CRC Press, Florida.

585. Seelig, J. (1978) ^{31}P nuclear magnetic resonance and the head group structure of phospholipids in membranes. *Biochim. Biophys. Acta.* 515:105-140.

586. Bechinger, B., Aisenbrey, C. and Bertani, P. (2004) The alignment, structure and dynamics of membrane-associated polypeptides by solid-state NMR spectroscopy. *Biochim. Biophys. Acta.* 1666:190-204.

587. Thayer, A.M. and Kohler, S.J. (1981) Phosphorus-31 nuclear magnetic resonance spectra characteristic of hexagonal and isotropic phospholipid phases generated from phosphatidylethanolamine in the bilayer phase. *Biochem.* 20:6831-6834.

588. Cullis, P.R. and deKruijff, B. (1979) Lipid polymorphism and the functional roles of lipids in biological membranes. *Biochim. Biophys. Acta.* 559:399-420.

589. Niederberger, W. and Seelig, J. (1976) Phosphorus-31 chemical shift anisotropy in unsonicated phospholipid bilayers. *J. Am. Chem. Soc.* 98:3704-3706.

590. Seelig, A. and Seelig, J. (1974) The dynamic structure of fatty acyl chains in a phospholipid bilayer measured by deuterium magnetic resonance. *Biochem.* 13:4839-4845.

591. Tulloch, A.P. (1979) Synthesis of deuterium and carbon-13 labelled lipids. *Chem. Phys. Lipids.* 24:391-406.

592. Seelig, J. and Seelig, A. (1980) Lipid conformation in model membranes and biological membranes. *Quart. Rev. Biophys.* 13:19-61.

593. Lafleur, M., Fine, B., Sternin, E., Cullis, P.R. and Bloom, M. (1989) Smoothed orientational order profile of lipid bilayers by [2]H-nuclear magnetic resonance. *Biophys. J.* 56:1037-1041.

594. Sanders, C.R. and Schwonek, J.P. (1992) Characterization of magnetically orientable bilayers in mixtures of dihexanoylphosphatidylcholine and dimyristoyl-phosphatidylcholine by solid-state NMR. *Biochem.* 31:8898-8905.

595. Bloom, M., Davis, J.H. and MacKay, A.L. (1981) Direct determination of the oriented sample NMR spectrum from the powder spectrum for systems with local axial symmetry. *Chem. Phys. Lett.* 80:198-202.

596. Sternin, E., Bloom, M. and MacKay, A.L. (1983) De-Pake-ing of NMR spectra. *J. Magn. Reson.* 55:274-282.

597. Burnett, L.J. and Muller, B.H. (1971) Deuteron quadrupole coupling constants in three solid deuterated paraffin hydrocarbons: C_2D_6, C_4D_{10}, C_6D_{14}. *J. Chem. Phys.* 55:5829-5831.

598. Boden, N., Jones, S.A. and Sixl, F. (1991) On the use of deuterium nuclear magetic resonance as a probe of chain packing in lipid bilayers. *Biochem.* 30:2146-2155.

599. Lafleur, M., Cullis, P.R., Fine, B. and Bloom, M. (1990) Comparison of the orientational order of lipid chains in the L_α and H_{II} Phases. *Biochem.* 29:8325-8333.

600. Yamaguchi, S., Huster, D., Waring, A., Lehrer, R.I., Kearney, W., Tack, B.F. and Hong, M. (2001) Orientation and dynamics of an antimicrobial peptide in the lipid bilayer by solid-state NMR spectroscopy. *Biophys. J.* 81:2203-2214.

601. Bechinger, B., Zasloff, M. and Opella, S.J. (1992) Structure and interactions of magainin antibiotic peptides in lipid bilayers: A solid-state nuclear magnetic resonance investigation. *Biophys. J.* 62:12-14.

602. Banerjee, U., Zidovetzki, R., Birge, R.R. and Chan, S.I. (1985) Interaction of alamethicin with lecithin bilayers: A ^{31}P and ^2H NMR study. *Biochem.* 24:7621-7627.

603. de Planque, M.R.R., Greathouse, D.V., Koeppe, R.E., Schafer, H., Marsh, D. and Killian, J.A. (1998) Influence of lipid/peptide hydrophobic mismatch on the thickness of diacylphosphatidylcholine bilayers. A ^2H NMR and ESR study using designed transmembrane α-helical peptides and gramicidin A. *Biochem.* 37:9333-9345.

604. Carr, H.Y. and Purcell, E. (1954) Effects of diffusion on free precession in nuclear magnetic resonance experiments. *Phys. Rev.* 94:630-638.

605. Hahn, E. (1950) Spin echos. *Phys. Rev.* 80:580-594.

606. Lu, J., Damodaran, K., Blazyk, J. and Lorigan, G.A. (2005) Solid-state nuclear magnetic resonance relaxation studies of the interaction mechanism of antimicrobial peptides with phospholipid bilayer systems. *Biochem.* 44:10208-10217.

607. Bechinger, B., Zasloff, M. and Opella, S.J. (1993) Structure and orientation of the antibiotic peptide magainin in membranes by solid-state nuclear magnetic resonance spectroscopy. *Protein Sci.* 2:2077-2084.

608. Balla, M.S., Bowie, J.H. and Separovic, F. (2004) Solid-state NMR study of antimicrobial peptides from Australian frogs in phospholipid membranes. *Eur. Biophys. J.* 33:109-116.

609. Vogt, B., Ducarme, P., Schinzel, S., Brasseur, R. and Bechinger, B. (2000) The topology of lysine-containing amphipathic peptides in bilayers by circular dichroism, solid-state NMR and molecular modelling. *Biophys. J.* 79:2644-2656.

610. Marassi, F.M., Opella, S.J., Juvvadi, P. and Merrifield, R.B. (1999) Orientation of cecropin A helices in phospholipid bilayers determined by solid-state NMR spectroscopy. *Biophys. J.* 77:3152-3155.

611. Brender, J.R., Taylor, D.M. and Ramamoorthy, A. (2001) Orientation of amide-nitrogen-15 chemical shift tensors in peptides: A quantum chemical study. *J. Am. Chem. Soc.* 123:914-922.

612. Wu, C.H., Ramamoorthy, A., Gierasch, L.M. and Opella, S.J. (1995) Simultaneous characterization of the amide ^{1}H chemical shift, ^{1}H-^{15}N dipolar, and ^{15}N chemical shift interaction tensors in a peptide bond by three-dimensional solid-state NMR spectroscopy. *J. Am. Chem. Soc.* 117:6148-6149.

613. Mai, W., Hu, W., Wang, C. and Cross, T.A. (1993) Orientational constraints as three-dimensional structural constraints from chemical shift anisotropy: The polypeptide backbone of gramicidin A in a lipid bilayer. *Protein Sci.* 2:532-542.

614. McCain, D. (1987) ^{31}P nuclear spin relaxation. In *Phosphorus NMR in Biology,* (ed. Burt, C.T.) pp. 25-61. CRC Press, Florida.

615. Cornell, B.A., Hiller, R.G., Raison, J., Separovic, F., Smith, R., Vary, J.C. and Morris, C. (1983) Biological membranes are rich in low-frequency motion. *Biochim. Biophys. Acta.* 732:473-478.

616. Watts, A. (1998) Solid-state NMR approaches for studying the interaction of peptides and proteins with membranes. *Biochim. Biophys. Acta.* 1376:297-318.

617. Mayer, C., Grobner, G., Muller, K., Weisz, K. and Kothe, G. (1990) Orientation-dependent deuteron spin-lattice relaxation times in bilayer membranes: Characterization of the overall lipid motion. *Chem. Phys. Lett.* 165:155-161.

618. Meier, P., Ohmes, E. and Kothe, G. (1986) Multipulse dynamic nuclear magnetic resonance of phospholipid membranes. *J. Chem. Phys.* 85:3598-3614.

619. Bloom, M. and Sternin, E. (1987) Transverse nuclear spin relaxation in phospholipid bilayer membranes. *Biochem.* 26:2101-2105.

620. Simatos, G.A., Forward, K.B., Morrow, M.R. and Keough, K.M.W. (1990) Interaction between perdeuterated dimyristoylphosphatidylcholine and low molecular weight pulmonary surfactant protein SP-C. *Biochem.* 29:5807-5814.

621. Pinheiro, T.J.T., Duer, M.J. and Watts, A. (1997) Phospholipid headgroup dynamics in DOPG-d5-cytochrome C complexes as revealed by 2H and 31P NMR: The effects of a peripheral protein on collective lipid fluctuations. *Solid State NMR.* 8:55-64.

622. Cornell, B.A., Davenport, J.B. and Separovic, F. (1982) Low-frequency motion in membranes. The effect of cholesterol and proteins. *Biochim. Biophys. Acta.* 689:337-345.

623. Boman, H.G. (1991) Antibacterial peptides: Key components needed in immunity. *Cell.* 65:205-207.

624. Smet, K. and Contreras, R. (2005) Human antimicrobial peptides: Defensins, cathelicidins and histatins. *Biotechnol. Lett.* 27:1337-1347.

625. Putsep, K., Branden, C., Boman, H.G. and Normark, S. (1999) Antibacterial peptides from *H. pylori. Nature.* 398:671-672.

626. Mor, A., Hani, K. and Nicolas, P. (1994) The vertebrate peptide antibiotics dermaseptins have overlapping structural features but target specific microorganisms. *J. Biol. Chem.* 269:31635-31641.

627. Moore, K.S., Bevins, C.L., Brasseur, M.M., Tomassini, N., Turner, K., Eck, H. and Zasloff, M. (1991) Antimicrobial peptides in the stomach of *Xenopus laevis. J. Biol. Chem.* 266:19851-19857.

628. Mazel, D. and Davies, J. (1999) Antibiotic resistance in microbes. *Cell. Mol. Life Sci.* 56:742-754.

629. Hiramatsu, K., Aritaka, N., Hanaki, H., Kawasaki, S., Hosoda, Y., Hori, S., Fukuchi, Y. and Kobayashi, I. (1997) Dissemination in Japanese hospitals of strains of *Staphylococcus aureus* heterogeneously resistant to vancomycin. *Lancet.* 350:1670-1673.

630. Hancock, R.E.W. (1997) Peptide antibiotics. *Lancet.* 349:418-422.

631. Sitaram, N. and Nagaraj, R. (2002) The therapeutic potential of host-defense antimicrobial peptides. *Curr. Drug Targets.* 3:259-267.

632. Boman, H.G. (2003) Antibacterial peptides: Basic facts and emerging concepts. *J. Int. Med.* 254:197-215.

633. Iwanaga, S., Muta, T., Shigenaga, T., Seki, N., Kawano, K., Katsu, T. and Kawabata, S. (1994) Structure-function relationships of tachyplesins and their analogues. In *Antimicrobial Peptides. Ciba Foundations Symposium 186,* (eds. Marsh, J. and Goode, J.A.) pp. 160-175. John Wiley and Sons, London.

634. Rozek, A., Friedrich, C.L. and Hancock, R.E.W. (2000) Structure of the bovine antimicrobial peptide indolicidin bound to dodecylphosphocholine and sodium dodecyl sulfate micelles. *Biochem.* 39:15765-15774.

635. Epand, R.M. and Vogel, H.J. (1999) Diversity of antimicrobial peptides and their mechanisms of action. *Biochim. Biophys. Acta.* 1462:11-28.

636. Tossi, A., Sandri, L. and Giangaspero, A. (2000) Amphipathic, α-helical antimicrobial peptides. *Biopolymers.* 55:4-30.

637. Gazit, E., Boman, A., Boman, H.G. and Shai, Y. (1995) Interaction of the mammalian antibacterial peptide cecropin P1 with phospholipid vesicles. *Biochem.* 34:11479-11488.

638. Simmaco, M., Mignogna, G. and Barra, D. (1998) Antimicrobial peptides from amphibian skin: What do they tell us? *Biopolymers.* 47:435-450.

639. Marsh, J. and Goode, J.A. (eds.) (1994) *Antimicrobial Peptides. Ciba Foundation Symposium 186.* John Wiley and Sons, London.

640. Ehrenstein, G. and Lecar, H. (1977) Electrically gated ionic channels in lipid bilayers. *Quart. Rev. Biophys.* 10:1-34.

641. Sansom, M.S.P. (1991) The biophysics of peptide models of ion channels. *Prog. Biophys. Mol. Biol.* 55:139-235.

642. Oren, Z. and Shai, Y. (1998) Mode of action of linear amphipathic α-helical antimicrobial peptides. *Biopolymers.* 47:451-463.

643. Epand, R.M., Shai, Y.C., Segrest, J.P. and Anantharamaiah, G.M. (1995) Mechanisms for the modulation of membrane bilayer properties by amphipathic helical peptides. *Biopolymers.* 37:319-338.

644. Rapaport, D. and Shai, Y. (1991) Interaction of fluorescently labeled pardaxin and its analogues with lipid bilayers. *J. Biol. Chem.* 266:23769-23775.

645. Sansom, M.S.P. (1993) Alamethicin and related peptaibols - model ion channels. *Eur. Biophys. J.* 22:105-124.

646. Gazit, E., Bach, D., Kerr, I.D., Samson, M.S., Chejanovsky, N. and Shai, Y. (1994) The α-5 segment of *Bacillus thuringiensis* δ-endotoxin: In vitro activity, ion channel formation and molecular modelling. *Biochem.* 304:895-902.

647. Cruciani, R.A., Barker, J.L., Durell, S.R., Raghunathan, G., Guy, H.R., Zasloff, M. and Stanley, E.F. (1992) Magainin 2, a natural antibiotic from frog skin, forms ion channels in lipid bilayer membranes. *Eur. J. Biochem.* 226:287-296.

648. Ludtke, S.J., He, K., Heller, W.T., Harroun, T.A., Yang, L. and Huang, H.W. (1996) Membrane pores induced by magainin. *Biochem.* 35:13723-13728.

649. Matsuzaki, K. (1998) Magainins as paradigm for the mode of action of pore forming polypeptides. *Biochim. Biophys. Acta.* 10:391-400.

650. Andreu, D., Ubach, J., Boman, A., Wahlin, B., Wade, D., Merrifield, R.B. and Boman, H.G. (1992) Shortened cecropin A-melittin hybrids - significant size reduction retains potent antibiotic activity. *FEBS Lett.* 296:190-194.

651. Arseniev, A.S., Barsukov, I.F., Bystrov, V.F., A.L., L. and Ovchinnikov, Y.A. (1985) ^{1}H-NMR study of gramicidin A transmembrane ion channels. *FEBS Lett.* 186:168-174.

652. Shai, Y. (1999) Mechanism of the binding, insertion and destabilization of phospholipid bilayer membranes by α-helical antimicrobial and cell non-selective membrane-lytic peptides. *Biochim. Biophys. Acta.* 1462:55-70.

653. Matsuzaki, K. (1999) Why and how are peptide-lipid interactions utilized for self-defense? Magainins and tachyplesins as archetypes. *Biochim. Biophys. Acta.* 1462:1-10.

654. Oren, Z., Lerman, J.C., Gudmundsson, G.H., Agerberth, B. and Shai, Y. (1999) Structure and organisation of the human antimicrobial peptide LL-37 in phospholipid membranes: Relevance to the molecular basis for its non-cell-selective activity. *Biochem. J.* 341:501-513.

655. Huang, H.W. (2000) Action of antimicrobial peptides: Two-state model. *Biochem.* 39:8347-8352.

656. Oren, Z., Hong, J. and Shai, Y. (1997) A repertoire of novel antibacterial diastereomeric peptides with selective cytolytic activity. *J. Biol. Chem.* 272:14643-14649.

657. Dathe, M. and Wieprecht, T. (1999) Structural features of helical antimicrobial peptides: Their potential to modulate activity on model membranes and biological cells. *Biochim. Biophys. Acta.* 1462:71-87.

658. Wegener, K.L. (2001) *Amphibian peptides: Their structures and bioactivities*. Chemistry Ph.D. Thesis, The University of Adelaide

659. Gennis, R.B. (1989) The structure and properties of membrane lipids. In *Biomembranes: Molecular Structure and Function,* pp. 154-158. Springer-Verlag, New York.

660. Ghosh, A.K., Rukmini, R. and Chattopadhyay, A. (1997) Modulation of tryptophan environment in membrane-bound melittin by negatively charged phospholipids: Implications in membrane organization and function. *Biochem.* 36:14291-14305.

661. Lugtenberg, B. and Van Alphen, L. (1983) Molecular architecture and functioning of the outer membrane of *Escherichia coli* and other Gram-negative bacteria. *Biochim. Biophys. Acta.* 737:51-115.

662. Rogers, H.J., Perkins, H.R. and Ward, J.B. (1980) *Microbial Cell Walls and Membranes*. pp. 1-22. Chapman and Hall, New York.

663. Peschel, A., Otto, M., Jack, R.W., Kalbacher, H., Jung, G. and Gotz, F. (1999) Inactivation of the *dlt* operon in *Staphylococcus aureus* confers sensitivity to defensins, protegrins and other antimicrobial peptides. *J. Biol. Chem.* 274:8405-8410.

664. Cano, R.J. and Colome, J.S. (1986) *Microbiology*. West Pub. Co., St. Paul.

665. Gazit, E., Lee, W.J., Brey, P.T. and Shai, Y.C. (1994) Mode of action of the antibacterial cecropin B2 - a spectrofluorometric study. *Biochem.* 33:10681-10692.

666. Nakajima, Y., Qu, X. and Natori, S. (1987) Interaction between liposomes and sarcotoxin IA, a potent antibacterial protein of *Sarcophaga peregrina* (Flesh Fly). *J. Biol. Chem.* 262:1665-1669.

667. Matsuzaki, K., Sugishita, K., Harada, M., Fujii, N. and Miyajima, K. (1997) Interactions of an antimicrobial peptide, magainin 2, with outer and inner membranes of Gram-negative bacteria. *Biochim. Biophys. Acta.* 1327:119-130.

668. Skerlavaj, B., Romeo, D. and Gennaro, R. (1990) Rapid membrane permeabilization and inhibition of vital functions of Gram-negative bacteria by bactenecins. *Infect. Immun.* 58:3724-3730.

669. Matsuzaki, K., Harada, M., Funakoshi, S., Fujii, N. and Miyajima, K. (1991) Physiochemical determinants for the interactions of magainins 1 and 2 with acidic lipid bilayers. *Biochim. Biophys. Acta.* 1063:162-170.

670. Rana, F.R., Macias, E.A., Sultany, C.M., Modzrakowski, M.C. and Blazyk, J. (1991) Interactions between magainin 2 and *Salmonella typhimurium* outer membranes: Effect of lipopolysaccharide structure. *Biochem.* 30:5858-5866.

671. Zhang, L., Scott, M.G., Yan, H., Mayer, L.D. and Hancock, R.E. (2000) Interaction of polyphemusin I and structural analogs with bacterial membranes, lipopolysaccharide, and lipid monolayers. *Biochem.* 39:14504-14514.

672. Allende, D. and McIntosh, T.J. (2003) Lipopolysaccharides in bacterial membranes act like cholesterol in eukaryotic plasma membranes in providing protection against melittin-induced bilayer lysis. *Biochem.* 42:1101-1108.

673. Nikaido, H. and Hancock, R.E.W. (1986) Outer membrane permeability of *Pseudomonas aeruginosa*. In *The Bacteria: A Treatise on Structure and Function,* (eds. Gunsalus, I.C., Sokatch, J.R. and Ornstan, L.N.) pp. 145-183. Academic Press, New York.

674. Sawyer, J.G., Martin, N.L. and Hancock, R.E.W. (1988) Interaction of macrophage cationic proteins with the outer membrane of *Pseudomonas aeruginosa. Infect. Immun.* 56:693-698.

675. Hancock, R.E.W., Piers, K., Brown, M., Falla, T., Gough, M., Wu, M. and Fidai, S. (1996) Cationic peptides: A class of antibiotics able to access the self-promoted uptake pathway across the *Pseudomondas aeruginosa* outer membrane. In *Molecular Biology of Pseudomondas,* (ed. Nakazawa, N.) pp. 441-450. ASM Press, Washington.

676. Shai, Y. and Oren, Z. (2001) From "carpet" mechanism to de-novo designed diastereomeric cell-selective antimicrobial peptides. *Peptides.* 22:1629-1641.

677. Tossi, A., Tarantino, C. and Romeo, D. (1997) Design of synthetic antimicrobial peptides based on sequence analogy and amphipathicity. *Eur. J. Biochem.* 250:549-558.

678. Szabo, G. (1974) Dual mechanism for the action of cholesterol on membrane permeability. *Nature.* 252:47-49.

679. Urbina, J.A., Pekerar, S., Le, H., Patterson, J., Montez, B. and Oldfield, E. (1995) Molecular order and dynamics of phosphatidylcholine bilayer membranes in the presence of cholesterol, ergosterol and lanosterol: A comparative study using ^{2}H-, ^{13}C- and ^{31}P-NMR spectroscopy. *Biochim. Biophys. Acta.* 1238:163-176.

680. Tytler, E.M., Anantharamaiah, G.M., Walker, D.E., Mishra, V.K., Palgunachari, M.N. and Segrest, J.P. (1995) Molecular basis for prokaryotic specificity of magainin-induced lysis. *Biochem.* 34:4393-4401.

681. Matsuzaki, K., Sugishita, K., Fujii, N. and Miyajima, K. (1995) Molecular basis for membrane selectivity of an antimicrobial peptide, magainin 2. *Biochem.* 34:3423-3429.

682. Stankowski, S., Schwartz, U.D. and Schwartz, G. (1988) Voltage-dependent pore activity of the peptide alamethicin correlated with incorporation in the membrane: Salt and cholesterol effects. *Biochim. Biophys. Acta.* 941:11-18.

683. Mattila, K., Kinder, R. and Bechinger, B. (1999) The alignment of a voltage-sensing peptide in dodecylphosphocholine micelles and in oriented lipid bilayers by nuclear magnetic resonance and molecular modeling. *Biophys. J.* 77:2102-2113.

684. Kagan, B.L., Selsted, M.E., Ganz, T. and Lehrer, R.I. (1990) Antimicrobial defensin peptides form voltage-dependent ion-permeable channels in planar lipid bilayer membranes. *Proc. Natl. Acad. Sci.* 87:210-214.

685. Cruciani, R.A., Barker, J.L., Zasloff, M., Chen, H. and Colamonici, O. (1991) Antibiotic magainins exert cytolytic activity against transformed cell lines through channel formation. *Proc. Natl. Acad. Sci.* 88:3792-3796.

686. Utsugi, T., Schroit, A.J., Connor, J., Bucana, C.D. and Fidler, I.J. (1991) Elevated expression of phosphatidylserine in the outer membrane leaflet of human tumor cells and recognition by activated human blood monocytes. *Cancer Res.* 51:3062-3066.

687. Pathak, N., Salasauvert, R., Ruche, G., Janna, M.H., McCarthy, D. and Harrison, R.G. (1995) Comparison of the effects of hydrophobicity, amphiphilicity, and alpha-helicity on the activities of antimicrobial peptides. *Proteins: Struct. Funct. Genet.* 22:182-186.

688. Andreu, D. and Merrifield, R.B. (1985) N-terminal analogues of cecropin A: Synthesis, antibacterial activity, and conformational properties. *Biochem.* 24:1683-1688.

689. Chen, H., Brown, J.H., Morell, J.L. and Huang, C.M. (1988) Synthetic magainin analogues with improved antimicrobial activity. *FEBS Lett.* 236:462-466.

690. Blondelle, S.E., Takahashi, S., Dinh, K.T. and Houghten, R.A. (1988) The antimicrobial activity of hexapeptides derived from synthetic combinatorial libraries. *J. Appl. Bacteriol.* 78.

691. Blondelle, S.E. and Houghten, R.A. (1991) Hemolytic and antimicrobial activities of the twenty-four individual omission analogs of melittin. *Biochem.* 30:4671-4678.

692. Wieprecht, T., Dathe, M., Schumann, M., Krause, E., Beyermann, M. and Bienert, M. (1996) Conformational and functional study of magainin 2 in model membrane environments using the new approach of systematic double-D-amino acid replacement. *Biochem.* 35:10844-10853.

693. Dathe, M., Schumann, M., Wieprecht, T., Winkler, A., Beyermann, M., Krause, E., Matsuzaki, K., Murase, O. and Bienert, M. (1996) Peptide helicity and membrane surface charge modulate the balance of electrostatic and hydrophobic interactions with lipid bilayers and biological membranes. *Biochem.* 35:12612-12622.

694. Bikshapathy, E., Sitaram, N. and Nagaraj, R. (1999) Addition and omission analogs of the 13-residue antibacterial and hemolytic peptide PKLLKTFLSKWIG: Structural preferences, model membrane binding and biological activities. *J. Pept. Res.* 53:47-55.

695. Shai, Y. and Oren, Z. (1996) Diastereomers of cytolysins, a novel class of potent antibacterial peptides. *J. Biol. Chem.* 271:7305-7308.

696. Holak, T.A., Engstrom, A., Kraulis, P.J., Lindeberg, G., Bennich, H., Jones, T.A., Gronenborn, A.M. and Clore, G.M. (1988) The solution conformation of the antibacterial peptide cecropin A: A nuclear magnetic resonance and dynamical simulated annealing study. *Biochem.* 27:7620-7629.

697. Pastore, A., Harvey, T.S., Dempsey, C.E. and Campbell, I.D. (1989) The dynamic properties of melittin in solution. *Eur. J. Biochem.* 16:363-367.

698. Woolfson, D.N. and Williams, D.H. (1990) The influence of proline residues on α-helical structure. *FEBS Lett.* 277:185-188.

699. Hancock, R.E.W., Falla, T. and Brown, F. (1995) Cationic bactericidal peptides. In *Advanced Microbial Physiology,* (ed. Poole, R.) pp. 135-175. Academic Press, London.

700. Shin, S.Y., Kang, J.H., Jang, S.Y., Kim, Y., Kim, K.L. and Hahm, K. (2000) Effects of the hinge region of cecropin A(1-8)-magainin 2(1-12), a synthetic antimicrobial peptide, on liposomes, bacterial and tumor cells. *Biochim. Biophys. Acta.* 1463:209-218.

701. Oh, D., Shin, S.Y., Kang, J.H., Hahm, K., Kim, K.L. and Kim, Y. (1999) NMR structural characterization of cecropin A(1-8) - magainin 2(1-12) and cecropin A(1-8) - melittin (1-12) hybrid peptides. *J. Pept. Res.* 53:578-589.

702. Eisenberg, D. (1984) Three-dimensional structure of membrane and surface proteins. *Annu. Rev. Biochem.* 53:595-623.

703. Eisenberg, D., Wesson, M. and Wilcox, W. (1989) Hydrophobic moments as tools for analyzing protein sequences and structures. In *Prediction of Protein Structure and Principles of Protein Conformation,* (ed. Fasman, G.) pp. 635-646. Plenum Press, New York.

704. Wieprecht, T., Dathe, M., Beyermann, M., Krause, E., Maloy, W.L., MacDonald, D.L. and Bienert, M. (1997) Peptide hydrophobicity controls the activity and selectivity of magainin 2 amide in interaction with membranes. *Biochem.* 36:6133-6140.

705. Kwon, M.Y., Hong, S.Y. and Lee, K.H. (1998) Stucture-activity analysis of brevinin 1E amide, an antimicrobial peptide from *Rana esculenta. Biochim. Biophys. Acta.* 1378:239-248.

706. Javadpour, M.M., Juban, M.M., Lo, W.C., Bishop, S.M., Alberty, J.B., Cowell, S.M., Becker, C.L. and McLaughlin, M.L. (1996) *De novo* antimicrobial peptides with low mammalian cell toxicity. *J. Med. Chem.* 39:3107-3113.

707. Kiyota, T., Lee, S. and Sugihara, G. (1996) Design and synthesis of amphiphilic α-helical model peptides with systematically varied hydrophobic-hydrophilic balance and their interaction with lipid- and bio-membranes. *Biochem.* 35:13196-13204.

708. Eisenberg, D., Weiss, R.M. and Terwilliger, T.C. (1982) The helical hydrophobic moment: A measure of the amphiphilicity of a helix. *Nature.* 299:371-374.

709. Blondelle, S.E. and Houghten, R.A. (1992) Design of model amphipathic peptides having potent antimicrobial activities. *Biochem.* 31:12688-12694.

710. Subbalakshmi, C., Nagaraj, R. and Sitaram, N. (1999) Biological activities of C-terminal 15-residue synthetic fragment of melittin: Design of an analog with improved antibacterial activity. *FEBS Lett.* 448:62-66.

711. Wieprecht, T., Dathe, M., Krause, E., Beyermann, M., Maloy, W.L., MacDonald, D.L. and Bienert, M. (1997) Modulation of membrane activity of amphipathic, antibacterial peptides by slight modifications of the hydrophobic moment. *FEBS Lett.* 417:135-140.

712. Pérez-Payá, E., Houghten, R.A. and Blondelle, S.E. (1995) The role of amphipathicity in the folding, self-association and biological activity of multiple subunit small proteins. *J. Biol. Chem.* 270:1048-1056.

713. Brasseur, R., Pillot, T., Lins, L., Vandekerckhove, J. and Rosseneu, M. (1997) Peptides in membranes: Tipping the balance of membrane stability. *Trends Biochem. Sci.* 22:167-171.

714. Wieprecht, T., Dathe, M., Epand, R.M., Beyermann, M., Krause, E., Maloy, W.L., MacDonald, D.L. and Bienert, M. (1997) Influence of the angle subtended by the positively charged helix face on the membrane activity of amphipathic, antibacterial peptides. *Biochem.* 36:12869-12880.
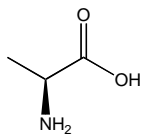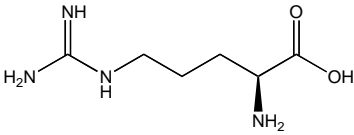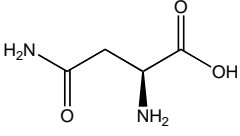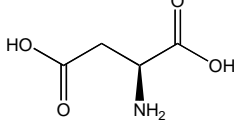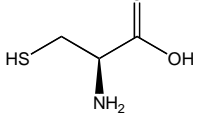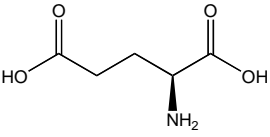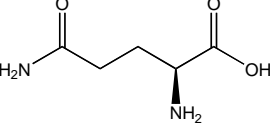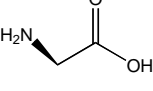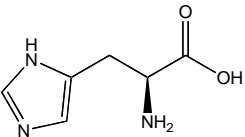
715. Uematsu, N. and Matsuzaki, K. (2000) Polar angle as a determinant of amphipathic α-helix-lipid interaction: A model peptide study. *Biophys. J.* 79:2975-2083.

716. Dathe, M., Wieprecht, T., Nikolenko, H., Handel, L., Maloy, W.L., MacDonald, D.L., Beyermann, M. and Bienert, M. (1997) Hydrophobicity, hydrophobic moment and angle subtended by charged residues modulate antibacterial and haemolytic activity of amphipathic helical peptides. *FEBS Lett.* 403:208-212.

717. Thennarasu, S. and Nagaraj, R. (1995) Design of 16-residue peptides possessing antimicrobial and hemolytic activities or only antimicrobial activity from an inactive peptide. *Int. J. Peptide Protein Res.* 46:480-486.

718. Bechinger, B. (1996) Towards membrane protein design - pH-sensitive topology of histidine-containing polypeptides. *J. Mol. Biol.* 263:768-775.

719. Csordas, A. and Michl, H. (1969) Primary structure of two oligopeptides of the toxin of *Bombina variegata* L. *Toxicon.* 7:103-108.

720. Marcotte, I., Wegener, K.L., Lam, Y., Chia, B.C.S., de Planque, M.R.R., Bowie, J.H., Auger, M. and Separovic, F. (2003) Interaction of antimicrobial peptides from Australian amphibians with lipid membranes. *Chem. Phys. Lipids.* 122:107-120.

721. Chia, B.C.S., Carver, J.A., Mulhern, T.D. and Bowie, J.H. (2000) Maculatin 1.1, an anti-microbial peptide from the Australian tree frog, *Litoria genimaculata* - Solution structure and biological activity. *Eur. J. Biochem.* 267:1894-1908.

722. Brock, T.D. (1984) *Biology of Microorganisms. 4th ed.* Prentice-Hall Inc., Englewood Cliffs.

723. Struppe, J., Whiles, J.A. and Vold, R.R. (2000) Acidic phospholipid bicelles: A versatile model membrane system. *Biophys. J.* 78:281-289.

724. Bonev, B.B., Lam, Y., Anderluh, G., Watts, A., Norton, R.S. and Separovic, F. (2003) Effects of the eukaryotic pore-forming cytolysin equinatoxin II on lipid membranes and the role of sphingomyelin. *Biophys. J.* 84:2382-2392.

725. Seelig, J. and Niederberger, W. (1974) Deuterium-labelled lipids as structural probes in liquid crystalline bilayers. A deuterium magnetic resonance study. *J. Am. Chem. Soc.* 96:2069-2072.

726. Shoji, A., Ozaki, T., Fujito, T., Deguchi, K. and Ando, I. (1987) High-resolution ^{15}N NMR study of solid homopolypeptides by the CP MAS method: Conformation-dependent ^{15}N chemical shift characteristics of the α-helix and β-sheet forms. *Macromolecules.* 20:2441-2445.

727. Shoji, A., Ozaki, T., Fujito, T., Deguchi, K., Ando, S. and Ando, I. (1989) Nitrogen-15 NMR chemical shift tensors and conformation of some nitrogen-15-labeled polypeptides in the solid state. *Macromolecules.* 22:2860-2863.

728. Shoji, A., Ozaki, T., Fujito, T., Deguchi, K., Ando, S. and Ando, I. (1990) ^{15}N chemical shift tensors and conformation of solid polypeptides containing ^{15}N-labeled L-alanine residues by ^{15}N NMR. 2. Secondary structure reflection in σ_{22}. *J. Am. Chem. Soc.* 112:4693-4697.
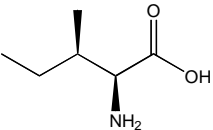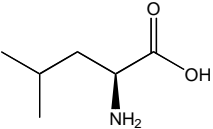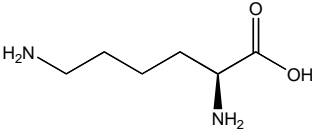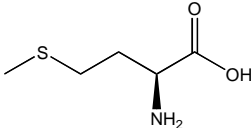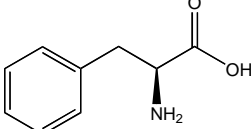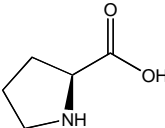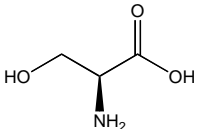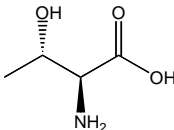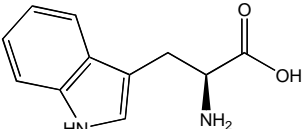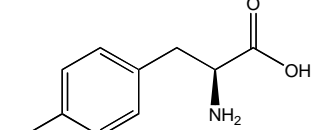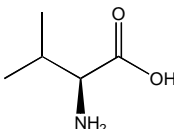
729. Bechinger, B., Zasloff, M. and Opella, S.J. (1998) Structure and dynamics of the antibiotic peptide PGLa in membranes by solution and solid-state nuclear magnetic resonance spectroscopy. *Biophys. J.* 74:981-987.

730. Smith, R., Separovic, F., Bennett, F.C. and Cornell, B.A. (1992) Melittin-induced changes in lipid multilayers. *Biophys. J.* 63:469-474.

731. Hori, Y., Demura, M., Niidome, T., Aoyagi, H. and Asakura, T. (1999) Orientational behaviour of phospholipid membranes with mastoparan studied by ^{31}P solid state NMR. *FEBS Lett.* 455:228-232.

732. Koenig, B.W., Ferretti, J.A. and Gawrisch, K. (1999) Site-specific deuterium order parameters and membrane-bound behaviour of a peptide fragment from the intracellular domain of HIV-1 gp41. *Biochem.* 38:6327-6334.

733. Strandberg, E. and Ulrich, A.S. (2004) NMR methods for studying membrane-active antimicrobial peptides. *Concepts Mag. Res. A.* 23:89-120.

734. Dufourc, E.J., Smith, I.C.P. and Dufourcq, J. (1986) Molecular details of melittin-induced lysis of phospholipid membranes as revealed by deuterium and phosphorus NMR. *Biochem.* 25:6448-6455.

735. Chia, B.C.S., Torres, J., Cooper, M.A., Arkin, I.T. and Bowie, J.H. (2002) The orientation of the antibiotic peptide maculatin 1.1 in DMPG and DMPC lipid bilayers. Support for a pore forming mechanism. *FEBS Lett.* 512:47-51.

736. Matsuzaki, K., Sugishita, K. and Miyajima, K. (1999) Interactions of an antimicrobial peptide, magainin 2, with lipopolysaccharide-containing liposomes as a model for outer membranes of Gram-negative bacteria. *FEBS Lett.* 449:221-224.

737. Whittall, K.P., Sternin, E., Bloom, M. and Mackay, A.L. (1989) Time- and frequency-domain "dePakeing" using inverse theory. *J. Mag. Reson.* 84:64-71.

738. Wullschleger, B., Kuhn-Nentwig, L., Tromp, J., Kampfer, U., Schaller, J., Schurch, S. and Nentwig, W. (2004) CSTX-13, a highly synergistically acting two-chain neurotoxic enhancer in the venom of the spider *Cupiennius salei* (Ctenidae). *Proc. Natl. Acad. Sci.* 101:11251-11256.

739. Haeberli, S., Kuhn-Nentwig, L., Schaller, J. and Nentwig, W. (2000) Characterisation of antibacterial activity of peptides isolated from the venom of the spider *Cupiennius salei* (Araneae: Ctenidae). *Toxicon.* 38:373-380.

740. Wullschleger, B., Nentwig, W. and Kuhn-Nentwig, L. (2005) Spider venom: Enhancement of venom efficacy mediated by different synergistic strategies in *Cupiennius salei*. *J. Exp. Biol.* 208:2115-2121.

741. Kuhn-Nentwig, L., Dathe, M., Walz, A., Schaller, J. and Nentwig, W. (2002) Cupiennin 1d*: The cytolytic activity depends on the hydrophobic N-terminus and is modulated by the polar C-terminus. *FEBS Lett.* 527:193-198.

742. Monne, M., Nilsson, I., Elofsson, A. and von Heijne, G. (1999) Turns in transmembrane helices: Determination of the minimal length of a 'helical hairpin' and derivation of a fine-grained turn propensity scale. *J. Mol. Biol.* 293:807-814.

743. Garnier, J., Gibrat, J.F. and Robson, B. (1996) GOR secondary structure prediction method version IV. *Methods Enzymol.* 266:540-553.

744. Yamaguchi, S., Huster, D., Waring, A., Lehrer, R.I., Kearney, W., Tack, B.F. and Hong, M. (2001) Orientation and dynamics of an antimicrobial peptide in the lipid bilayer by solid-state NMR spectroscopy. *Biophys. J.* 81:2203-2214.

745. Klee, C.B. and Vanaman, T.C. (1982) Calmodulin. *Adv. Protein Chem.* 35:213-321.

746. Morita, H., Yoshikawa, H., Sakata, R., Nagata, Y. and Tanaka, H. (1997) Synthesis of nitric oxide from the two equivalent guanidino nitrogens of L-arginine by *Lactobacillus fermentum*. *J. Bacteriol.* 179:7812-7815.

747. Choi, W.S., Chang, M.S., Han, J.W., Hong, S.Y. and Lee, H.W. (1997) Identification of NOS in *Staphylococcus aureus*. *Biochem. Biophys. Res. Commun.* 237:554-558.

~ APPENDIX A ~

The 20 Common Amino Acids

Amino Acid	Structure	Resuide Nominal Mass
Alanine Ala A		71
Arginine Arg R		156
Asparagine Asn N		114
Aspartic Acid Asp D		115
Cysteine Cys C		103
Glutamic Acid Glu E		129
Glutamine Gln Q		128
Glycine Gly G		57
Histidine His H		137

Amino Acid	Structure	Residue Nominal Mass
Isoleucine Ile I		113
Leucine Leu L		113
Lysine Lys K		128
Methionine Met M		131
Phenylalanine Phe F		147
Proline Pro P		97
Serine Ser S		87
Threonine Thr T		101
Tryptophan Trp W		186
Tyrosine Tyr Y		163
Valine Val V		99

~ APPENDIX B ~

Mass Spectral Sequencing Data

All masses given are nominal masses, i.e. equal to the sum of the integral masses of the amino acid constituents. Where Lys/Gln or Leu/Ile are present, the correct residue is always shown in the text.

Caerin 1.1 – GLLSVLGSVAKHVLPHVVPVIAEHL-NH$_2$

Fraction	MH$^+$	Sequence Data	
J	**2582**	B ions	*m/z* 2565, 2452, 2315, 2186, 2115, 2002, 1806, 1707, 1608, 1374, 1261
			Leu (Pro His) Val Val (Pro Val) Ile Ala Glu His Leu-NH$_2$
		Y+2 ions	*m/z* 1558, 1421, 1322, 1209, 1112, 876, 777
			His Val Leu Pro (His Val) Val
Lys-C	**1043**	B ions	*m/z* 1025, 897, 727, 640, 583, 470, 371, 284, 171
			(Gly Leu) Leu Ser Val Leu Gly Ser (Val Ala) Lys-OH
		Y+2 ions	*m/z* 873, 760, 673, 574, 461, 404, 317, 218, 147
			(Gly Leu) Leu Ser Val Leu Gly Ser Val Ala Lys-OH
	1558	B ions	*m/z* 1541, 1428, 1291, 1162, 1091, 978, 879, 782, 683, 584, 447, 350, 237, 138
			His Val Leu Pro His Val Val Pro Val Ile Ala Glu His Leu-NH$_2$
		Y+2 ions	*m/z* 1421, 1322, 1209, 1112, 975, 876, 777, 581, 468, 397, 268
			His Val Leu Pro His Val Val (Pro Val) Ile Ala Glu (His Leu)-NH$_2$

Caerin 1.6 – GLFSVLGAVAKHVLPHVVPVIAEKL-NH$_2$

Fraction	MH$^+$	Sequence Data	
I	**2591**	B ions	*m/z* 2574, 2461, 2333, 2204, 2133, 2020, 1824, 1725, 1626, 1392, 1279, 1180, 915, 745,
			(Val Ala) (Lys His) Val Leu (Pro His) Val Val (Pro Val) Ile Ala Glu Lys Leu-NH$_2$
		Y+2 ions	*m/z* 1748, 1677, 1549, 1313, 1200, 1103, 867, 768, 671, 572, 459, 388 259
			Ala Lys (His Val) Leu Pro (His Val) Val Pro Val Ile Ala Glu (Lys Leu-NH$_2$)
Lys-C	**1061**	B ions	*m/z* 1043, 915, 745, 617, 504, 405, 318, 171
			(Gly Leu) Phe Ser Val Leu (Gly Ala) (Val Ala) Lys-OH
		Y+2 ions	*m/z* 891, 744, 657, 558, 445, 388, 317, 218
			(Gly Leu) Phe Ser Val Leu Gly Ala Val (Ala Lys-OH)
	1549	B ions	*m/z* 1532, 1419, 1162, 978, 683, 584, 350, 237
			(His Val) Leu (Pro His) Val (Val Pro Val) (Ile Ala) (Glu Lys) Leu-NH$_2$
		Y+2 ions	*m/z* 768, 671, 572
			Pro Val

Caerin 1.10 – GLLSVLGSVAKHVLPHVVPVIAEKL-NH$_2$

Fraction	MH$^+$	Sequence Data	
K	**2573**	B ions	*m/z* 2556, 2443, 2315, 2186, 2115, 2002, 1903, 1806, 1707, 1608, 1374, 1261, 1025
			(His Val) Leu (Pro His) Val Val Pro Val Ile Ala Glu Lys Leu-NH$_2$
		Y+2 ions	*m/z* 1748, 1677, 1549, 1412, 1313, 1200, 1103, 867, 768
			Ala Lys His Val Leu Pro (His Val) Val
Lys-C	**1043**	B ions	*m/z* 1025, 897, 727, 640, 583, 470, 371, 284, 171
			(Gly Leu) Leu Ser Val Leu Gly Ser (Val Ala) Lys-OH
		Y+2 ions	*m/z* 873, 760, 673, 461, 404, 317, 218, 147
			(Gly Leu) Leu Ser (Val Leu) Gly Ser Val Ala Lys-OH
	1549	B ions	*m/z* 1532, 1419, 1291, 1162, 1091, 978, 782, 683, 350, 237
			(His Val) Leu (Pro His Val) Val (Pro Val) Ile Ala Glu Lys Leu-NH$_2$
		Y+2 ions	*m/z* 259, 131
			Lys Leu-NH$_2$

Caerin 1.20 – GLFGILGSVAKHVLPHVIPVVAEHL-NH₂

Fraction	MH⁺	Sequence Data	
G	**2600**	B ions	*m/z* 2583, 2470, 2333, 2204, 2133, 2034, 1838, 1725, 1626, 1392, 1279, 1043, 915, 844, 745, 601, 488, 375
			Ile Leu (Gly Ser) Val Ala Lys (His Val) Leu (Pro His) Val Ile (Pro Val) Val Ala Glu His Leu-NH₂
		Y+2 ions	*m/z* 2283, 2226, 2113, 2000, 1943, 1856, 1757, 1686, 1558, 1421, 1322, 1209, 1112, 975, 876, 763
			Gly Ile Leu Gly Ser Val Ala Lys His Val Leu Pro His Val Ile
Lys-C	**1061**	B ions	*m/z* 1043, 915, 844, 745, 658, 601, 488, 375, 318, 171
			(Gly Leu) Phe Gly Ile Leu Gly Ser Val Ala Lys-OH
		Y+2 ions	*m/z* 1004, 891, 744, 687, 574, 461, 404, 317, 218, 147
			Gly Leu Phe Gly Ile Leu Gly Ser Val Ala Lys-OH
	1558	B ions	*m/z* 1541, 1428, 1291, 1162, 1091, 992, 893, 796, 683, 584, 447, 350, 237, 138
			His Val Leu Pro His Val Ile Pro Val Val Ala Glu His Leu-NH₂
		Y+2 ions	*m/z* 1421, 1322, 1209, 1112, 975, 876, 763, 666, 567, 468, 397, 268
			His Val Leu Pro His Val Ile Pro Val Val Ala Glu (His Leu-NH₂)

Caerin 2.2 – GLVSSIGRALGGLLADVVKSKEQPA-OH

Fraction	MH⁺	Sequence Data	
F2	**2464**	B ions	*m/z* 2446, 2375, 2278, 2150, 2021, 1893, 1806, 1678, 1579, 1480, 1365, 1294, 1181, 1068, 1011, 954, 841, 770, 557, 444, 357, 270, 171
			(Gly Leu) Val Ser Ser Ile (Gly Arg) Ala Leu Gly Gly Leu Leu Ala Asp Val Val Lys Ser Lys Glu Gln Pro Ala-OH
		Y+2 ions	*m/z* 2108, 2021, 1908, 1851, 1695, 1511, 1454, 1171, 1100, 985, 886, 659, 572, 444, 315, 187
			Ser Ile Gly Arg (Ala Leu) Gly (Gly Leu Leu) Ala Asp Val (Val Lys) Ser Lys Glu Gln (Pro Ala-OH)
Lys-C	**659**	B ions	*m/z* 641, 570, 473, 345, 216, 88
			Ser Lys Glu Gln Pro Ala-OH
		Y+2 ions	*m/z* 572, 444, 315, 187, 90
			Ser Lys Glu Gln Pro Ala-OH
	1824	B ions	*m/z* 1806, 1678, 1579, 1480, 1365, 1294, 1181, 1068, 1011, 954, 841, 770, 614, 444, 357, 270, 171
			(Gly Leu) Val Ser Ser (Ile Gly) Arg Ala Leu Gly Gly Leu Leu Ala Asp Val Val Lys-OH
		Y+2 ions	*m/z* 1654, 1555, 1468, 1381, 1268, 1211, 984, 871, 814, 644, 531, 460, 345, 246, 147
			(Gly Leu) Val Ser Ser Ile Gly (Arg Ala) Leu Gly (Gly Leu) Leu Ala Asp Val Val Lys-OH

Caerin 3.1 – GLWQKIKDKASELVSGIVEGVK-NH$_2$

Fraction	MH$^+$	Sequence Data	
D	2382	B ions	*m/z* 2365, 2237, 2138, 2081, 1952, 1853, 1683, 1596, 1497, 1384, 1255, 1168, 1097, 969, 854, 726, 613, 485, 357
			Gln Lys Ile Lys Asp Lys Ala Ser Glu Leu Val Ser (Gly Ile) Val Glu Gly Val Lys-NH$_2$
		Y+2 ions	*m/z* 1898, 1770, 1657, 1529, 1414, 1286, 1215, 999, 886, 787, 700, 643, 530, 431, 302, 146
			Lys Ile Lys Asp Lys Ala (Ser Glu) Leu Val Ser Gly Ile Val Glu (Gly Val) Lys-NH$_2$
Lys-C	631	B ions	*m/z* 613, 485, 357, 171
			(Gly Leu) Trp Gln Lys-OH
		Y+2 ions	*m/z* 574, 461, 275, 147
			Gly Leu Trp Gln Lys-OH
	1287	B ions	*m/z* 1269, 1141, 985, 856, 757, 644, 587, 500, 401, 288, 159, 72
			Ala Ser Glu Leu Val Ser Gly Ile Val Glu (Gly Val) Lys-OH
		Y+2 ions	*m/z* 1216, 1129, 1000, 887, 788, 701, 644, 531, 432, 303, 246, 147
			Ala Ser Glu Leu Val Ser Gly Ile Val Glu Gly Val Lys-OH

Caerin 3.5 – GLWEKVKEKANELVSGIVEGVK-NH$_2$

Fraction	MH$^+$	Sequence Data	
B	2410	B ions	*m/z* 2393, 2265, 2166, 2109, 1980, 1881, 1711, 1624, 1525, 1412, 1283, 1169, 1098, 970, 841, 713, 614, 486, 357,
			Glu Lys Val Lys Glu Lys Ala Asn Glu Leu Val Ser (Gly Ile) Val Glu Gly Val Lys-NH$_2$
		Y+2 ions	*m/z* 2240, 2054, 1797, 1698, 1570, 1441, 1313, 1242, 999, 886, 787, 700, 643, 530, 431, 302, 146
			(Gly Leu) Trp (Glu Lys) Val Lys Glu Lys Ala (Asn Glu) Leu Val Ser Gly Ile Val Glu (Gly Val) Lys-NH$_2$
Lys-C	632	B ions	*m/z* 614, 486, 357, 171
			(Gly Leu) Trp Glu Lys-OH
		Y+2 ions	*m/z* 575, 462, 276, 147
			Gly Leu Trp Glu Lys-OH
	1313	B ions	*m/z* 1296, 1168, 1069, 1012, 883, 784, 671, 614, 527, 428, 315, 186
			(Ala Asn) Glu Leu Val Ser Gly Ile Val Glu Gly Val Lys-NH$_2$
		Y+2 ions	*m/z* 1128, 999, 886, 787, 700, 643, 530, 431, 302, 245, 146
			(Ala Asn) Glu Leu Val Ser Gly Ile Val Glu Gly Val Lys- NH$_2$

Caerin 4.2 – GLWQKIKSAAGDLASGIVEAIKS-NH$_2$

Fraction	MH$^+$	Sequence Data	
H	**2340**	B ions	*m/z* 2323, 2236, 2108, 1995, 1924, 1795, 1696, 1583, 1526, 1439, 1368, 1255, 1140, 1083, 1012, 941, 854, 726, 613, 485, 357
			Gln Lys Ile Lys Ser Ala Ala Gly Asp Leu Ala Ser Gly Ile Val Glu Ala Ile Lys Ser-NH$_2$
		Y+2 ions	*m/z* 1856, 1728, 1615, 1487, 1400, 1329, 1258, 1086, 973, 902, 815, 645, 546, 417, 346, 233
			Lys Ile Lys Ser Ala Ala (Gly Asp) Leu Ala Ser (Gly Ile) Val Glu Ala Ile (Lys Ser-NH$_2$)
Lys-C	**631**	B ions	*m/z* 613, 485, 357, 171
			(Gly Leu) Trp Gln Lys-OH
		Y+2 ions	*m/z* 574, 461, 275, 147
			Gly Leu Trp Gln Lys-OH
	872	B ions	*m/z* 854, 726, 613, 485, 357, 171
			(Gly Leu) Trp Gln Lys Ile Lys-OH
		Y+2 ions	*m/z* 702, 516, 388, 260, 147
			(Gly Leu) Trp Gln Lys Ile Lys-OH
	1401	B ions	*m/z* 1383, 1255, 1142, 1071, 942, 843, 730, 673, 586, 515, 402, 287, 230, 159,
			(Ser Ala) Ala Gly Asp Leu Ala Ser Gly Ile Val Glu Ala Ile Lys-OH
		Y+2 ions	*m/z* 1314, 1243, 1172, 1115, 1000, 887, 816, 729, 672, 559, 460, 331, 260, 147
			Ser Ala Ala Gly Asp Leu Ala Ser Gly Ile Val Glu Ala Ile Lys-OH

Caerulin – pEQDY(SO$_3$)TGWMDF-NH$_2$

Fraction	MH$^+$	Sequence Data	
A	**1272***	B ions	*m/z* 1272, 1255, 1108, 993, 862, 676, 619, 518, 355
			Tyr Thr Gly Trp Met Asp Phe-NH$_2$
		Y+2 ions	*m/z* 1033, 918, 755, 654, 597, 411
			(pGlu Gln) Asp Tyr(SO$_3$) Thr Gly Trp

Lys-C - No digestion by Lys-C

* The SO$_3$ functionality is cleaved from Tyr in the acidic conditions encountered during positive ion spectra acquisition, accounting for the observed MH$^+$ ion at *m/z* 1272. The presence of a sulfated Tyr residue is justified by negative ion spectra which show a [M-H]$^-$ peak at *m/z* 1350 and [(M-H)-SO$_3$]$^-$ peak at *m/z* 1270.

Caeridin 1 – GLLDGLLGTLGL-NH₂

Fraction	MH⁺	Sequence Data	
I	**1140**	B ions	*m/z* 1123, 1010, 953, 840, 739, 682, 569, 456, 399, 284, 171
			(Gly Leu) Leu Asp Gly Leu Leu Gly Thr Leu Gly Leu-NH₂
		Y+2 ions	*m/z* 742, 685, 572, 459, 402, 188
			Gly Leu Leu Gly (Thr Gly)

Lys-C - No digestion by Lys-C

Caeridin 5 – GLLGMVGSLLGGLGL-NH₂

Fraction	MH⁺	Sequence Data	
O	**1355**	B ions	*m/z* 1337, 1225, 1168, 1055, 998, 941, 828, 715, 628, 571, 472, 341, 284
			(Gly Leu Leu) Gly Met Val Gly Ser Leu Leu Gly Gly Leu Gly Leu-NH₂
		Y+2 ions	*m/z* 884, 785, 728, 641, 528, 415, 301, 188
			Val Gly Ser Leu Leu (Gly Gly) Leu

Lys-C - No digestion by Lys-C

333

~ PUBLICATIONS ~

Journal Articles Related to Ph. D. Thesis

Host-defence peptides of Australian anurans: Structure, mechanism of action and evolutionary significance. Apponyi, M.A., Pukala, T.L., Brinkworth, C.S., Maselli, V.M., Bowie, J.H., Tyler, M.J., Booker, G.W., Wallace, J.C., Carver, J.A., Separovic, F., Doyle, J. and Llewellyn, L.E. (2004) *Peptides* 25(6):1035-1054.

Host-defence peptides from the glandular secretions of amphibians: Structure and activity. Pukala, T.L., Bowie, J.H., Maselli, V.M., Musgrave, I.F. and Tyler, M.J. (2006) *Nat. Prod. Rep.* 23(3):368-393.

Host-defence peptide profiles of the skin secretions of interspecific hybrid tree frogs and their parents, female *Litoria splendida* and male *Litoria caerulea*. Pukala, T.L., Bertozzi, T., Donnellan, S.C., Bowie, J.H., Surinya-Johnson, K.H., Liu, Y., Jackway, R.J., Doyle, J.R., Llewellyn, L.E. and Tyler, M.J. (2006) *FEBS J.* 273(15): 3511-3519.

Additional Journal Articles

Investigating the importance of the flexible hinge in caerin 1.1: Solution structures and activity of two synthetically modified caerin peptides. Pukala, T.L., Brinkworth, C.S., Carver, J.A. and Bowie, J.H. (2004) *Biochem.* 43:937-944.

Host defence peptides from the skin glands of Australian amphibians. Caerulein neuropeptides and antimicrobial, anticancer and nNOS inhibiting citropins from the glandular frog *Litoria subglandulosa*. Brinkworth, C.S., Pukala, T.L., Bowie, J.H. and Tyler, M.J. (2004) *Aust. J. Chem.* 57:693-701.